

Microwave Electronics

**DESIGN AND DEVELOPMENT OF RECONFIGURABLE
COMPACT CROSS PATCH ANTENNA FOR
SWITCHABLE POLARIZATION**

A thesis submitted by

NISHAMOL M.S.

in partial fulfillment of the requirements for the degree of

DOCTOR OF PHILOSOPHY

Under the guidance of

Prof. K.VASUDEVAN



**DEPARTMENT OF ELECTRONICS
FACULTY OF TECHNOLOGY
COCHIN UNIVERSITY OF SCIENCE AND TECHNOLOGY
COCHIN-22, INDIA**

January 2012

*Dedicated to the Almighty,
Parents, Teachers and Dear ones...*





**DEPARTMENT OF ELECTRONICS
COCHIN UNIVERSITY OF SCIENCE AND TECHNOLOGY,
COCHIN – 682 022**

Certificate

Certified that this thesis entitled “DESIGN AND DEVELOPMENT OF RECONFIGURABLE COMPACT CROSS PATCH ANTENNA FOR SWITCHABLE POLARIZATION” is a bonafide record of the research work done by Mrs. Nishamol M. S. under my supervision in the Centre for Research in ElectroMagnetics and Antennas, Department of Electronics, Cochin University of Science and Technology. The results presented in this thesis or parts of it have not been presented for the award of any other degree.

Cochin-22
04/01/2012

Prof. K. Vasudevan
Supervising Guide
Dean, Faculty of Technology
Professor, Department of Electronics
Cochin University of Science and Technology
Cochin-22

Declaration

I hereby declare that the work presented in this thesis entitled “DESIGN AND DEVELOPMENT OF RECONFIGURABLE COMPACT CROSS PATCH ANTENNA FOR SWITCHABLE POLARIZATION” is a bonafide record of the research work done by me under the supervision of Prof. K. Vasudevan, Department of Electronics, Cochin University of Science and Technology, India and that no part thereof has been presented for the award of any other degree.

Cochin-22

04/01/2012

Nishamol M. S.

Centre for Research in Electro Magnetics and Antennas (CREMA)

Department of Electronics

Cochin University of Science and Technology

Cochin-22

Acknowledgments

It is my pleasure and privilege to thank the many individuals who made this thesis possible. First and foremost I offer my sincere gratitude towards my supervisor, Prof. K. Vasudevan, Dean, Faculty of Technology, and Professor, Department of Electronics, Cochin University of Science and Technology, who has guided me through this work with his patience. The opportunities and exposure that he offered during the course of my research is invaluable to me. A gentleman personified, in true form and spirit, I consider it to be my good fortune to have been associated with him. His profound view points and extraordinary motivation enlightened me to shape my traits and career.

I am grateful to Prof. P. Mohanan, Professor, Department of Electronics, Cochin University of Science and Technology for his constant encouragement and care that he rendered to me during my research period. I also wish to thank him for his valuable suggestions and exposure that he offered during the course of my research work.

A special and sincere acknowledgement goes to Dr. C. K. Anandan, Professor, Department of Electronics, Cochin University of Science and Technology for his well-timed care in my research, valuable suggestions and constant encouragements to improve my work.

I thank Prof. P. R. S. Pillai, Professor and Head, Department of Electronics, Cochin University of Science and Technology, for all the help and assistance rendered to me during my research period.

My sincere thanks to Dr. K. G. Nair, former Head and founder of Electromagnetics and Antennas Research (CREMA) Laboratory in Department of Electronics, Cochin University of Science and Technology, for establishing full-fledged laboratory that enabled me to do my research work in a well reputed laboratory in the country.

Let me thank Dr. Tessamma Thomas, Dr. James Kurien, Dr. M.H. Supriya and all other faculty members of Department of Electronics for the help and assistance extended to me.

I thank all the non-teaching staff and technical staff at the Department of Electronics especially Mrs. Vineetha, Mr.Mohanan, Mr.Siraj, Mr.Noorudheenn, Mr.Ibrahim Kutty, Mr.Pradeep, Ms.Bindu and Ms.Sudha and the staff at the Administrative Section of CUSAT for their co-operation.

I thankfully bear in mind the inspiring words of Prof. K. C. Sankaranarayanan, Director, School of Management studies, M. E. S College, Marampally and former head, School of management studies, CUSAT for introducing me towards research.

Special thanks to Dr. S. Mridula, Dr. Binu Paul and Mrs. Anju Pradeep, School of Engineering, CUSAT for their whole hearted support and helps rendered to me.

My senior research scholars Dr. Deepu, Dr. Suma, Dr. Gijo Augustin, Dr. Bybi, Dr. Jitha, Dr. Gopikrishna and Dr. Deepti Das Krishna were always there with their support and encouragement. Their views and way of analysis had a strong impact on me.

Mere words are not enough to thank Sarin V. P., Laila D., Shameena V. A. and Sujith R. who have been my work associates at the Department for almost the entire period of my research here. We have been complimentary to each other in more ways than one and this enabled us to work together productively.

Special thanks to Tony D, Nijas, Dinesh, and Deepak U. for being at the beck and call to sort out all my hardware and software problems. I take this opportunity to thank Abdul Rasheed, Vinesh P.V, Lindo A.O., Ullas G.K., Sreejith M. Nair, Paulbert Thomas, Anju P. Mathews, Sarah Jacob, Sreenath S., and Ashkar Ali for their whole hearted support and encouragement. I am grateful to Cyriac M.O., Jaimon Yohanan, Deepa Shankar, Reji A. P., Prajas John, Jaison Peter, Adrine Correya and Sooraj at the Department of Electronics for all their support and for being such a fun to work with.

I thank the University Grants Commission (UGC), Govt. of India for supporting my research work financially under the Research Fellowship Scheme for Meritorious Students.

My deepest gratitude goes to my parents for their unflagging love and support throughout my life. I am really proud about my family for their prayers and encouragement which gave me the courage to persevere. Above all, I thank my husband Nassar for his deep love, support, care and patience. My kids-Althaf and Aathifa, thanks a lot for being so patient with their mother. I am lucky to enjoy my in-laws integrity, care and patience in taking care of us.

I wish to place on record my gratitude to my teachers, mentors and my friends at all stages of my education.

Finally, I would like to thank everybody who was important to the successful realization of the thesis, as well as expressing my apology that I could not mention personally one by one.

Above all there is the god almighty whose blessings and kindness helped a lot to tide over.

Nishamol M. S.

ABSTRACT

Antennas are necessary and vital components of communication and radar systems, but sometimes their inability to adjust to new operating scenarios can limit system performance. Reconfigurable antennas can adjust with changing system requirements or environmental conditions and provide additional levels of functionality that may result in wider instantaneous frequency bandwidths, more extensive scan volumes, and radiation patterns with more desirable side lobe distributions. Their agility and diversity created new horizons for different types of applications especially in cognitive radio, Multiple Input Multiple Output Systems, satellites and many other applications. Reconfigurable antennas satisfy the requirements for increased functionality, such as direction finding, beam steering, radar, control and command, within a confined volume.

The intelligence associated with the reconfigurable antennas revolved around switching mechanisms utilized. In the present work, we have investigated frequency reconfigurable polarization diversity antennas using two methods:

1. By using low-loss, high-isolation switches such as PIN diode, the antenna can be structurally reconfigured to maintain the elements near their resonant dimensions for different frequency bands and/or polarization.
2. Secondly, the incorporation of variable capacitors or varactors, to overcome many problems faced in using switches and their biasing.

The performances of these designs have been studied using standard simulation tools used in industry/academia and they have been experimentally verified. Antenna design guidelines are also deduced by accounting the resonances. One of the major contributions of the thesis lies in the analysis of the designed antennas using FDTD based numerical computation to validate their performance.

Contents

1. INTRODUCTION.....	1
1.1 Introduction	2
1.2 Microstrip antennas	4
1.3 Advantages and Disadvantages.....	6
1.4 Applications of microstrip antennas.....	8
1.5 Various microstrip antenna configurations	8
1.5.1 Microstrip patch antennas.....	8
1.5.2 Microstrip or printed dipoles.....	9
1.5.3 Printed slot antennas	9
1.5.4 Microstrip travelling-wave antennas	9
1.6 Feeding Techniques.....	10
1.6.1 Microstrip Line Feed.....	10
1.6.2 Coaxial Feed	11
1.6.3 Aperture Coupled Feed	12
1.6.4 Proximity Coupled Feed	13
1.6.5 Coplanar waveguide feed	14
1.7 Analysis of antennas.....	15
1.7.1 Transmission Line Model.....	16
1.7.2 Cavity model.....	17
1.7.3 Multiport Network Model	17
1.7.4 Method of Moments	18
1.7.5 Finite Element Method	18
1.7.6 Spectral Domain Technique	19
1.7.7 Finite Difference Time Domain method	19
1.8 Compact microstrip antennas.....	20
1.9 Compact circularly polarized microstrip antennas	22
1.10 Compact broadband microstrip antennas.....	22

1.11 Compact dual-frequency microstrip antennas.....	23
1.11.1 Multi-patch dual-frequency antennas.....	24
1.11.2 Reactively loaded dual-frequency antennas.....	24
1.11.3 Orthogonal mode dual frequency antennas.....	24
1.12 Compact reconfigurable antennas.....	24
1.12.1 Frequency reconfigurable antennas.....	25
1.12.2 Polarization reconfigurable antennas.....	26
1.12.3 Radiation pattern reconfigurable antennas.....	26
1.13 Reconfiguration mechanisms.....	27
1.13.1 Switches.....	27
1.13.2 Variable reactive loading.....	27
1.13.3 Structural/Mechanical Tuning.....	27
1.13.4 Material changes.....	28
1.14 Motivation and development of subject of research.....	29
1.15 Thesis organization.....	31
2. REVIEW OF LITERATURE AND METHODOLOGY.....	39
2.1 Microstrip antenna technology.....	40
2.2 Dual- frequency microstrip antennas.....	43
2.3 Reconfigurable antennas.....	49
2.3.1 Reconfigurability Concept.....	50
2.3.2 Frequency Reconfigurability.....	51
2.3.3 Radiation Pattern Reconfigurability.....	51
2.3.4 RF-MEMS Based Reconfigurable Antennas.....	52
2.4 Simulation and Optimization.....	56
2.5 Antenna fabrication.....	58
2.6 Excitation Technique.....	59
2.7 Antenna measurement facilities.....	60
2.7.1 HP 8510C Vector Network analyzer (VNA).....	61
2.7.2 Agilent E8362B Precision Network Analyzer.....	61

2.7.3 Anechoic chamber	62
2.7.4 Automated turntable assembly for far field measurement	63
2.7.5 Crema Soft: Automated antenna measurement.....	64
2.8 Measurement of Antenna characteristics.....	64
2.8.1 Reflection coefficient and VSWR.....	64
2.8.2 Antenna Gain	66
2.8.3 Radiation Pattern	66
3. INVESTIGATIONS ON FREQUENCY AND POLARIZATION RECONFIGURABLE	
MICROSTRIP ANTENNA USING PIN DIODES	81
3.1 Introduction	82
3.2 Design of the passive dual frequency dual polarized rectangular microstrip antenna	84
3.2.1 Parametric Analysis.....	92
3.2.1. a Effect of X- slot	94
3.2.1. b Effect of corner slit length	95
3.2.2 Design.....	98
3.2.3 Measurements	100
3.3 Frequency Reconfigurable microstrip antenna with switchable slots using PIN diodes	104
3.3.1 PIN diode switch	105
3.3.2 Bias-circuit / RF circuit isolation	106
3.3.3 Antenna geometry	106
3.4 Frequency reconfigurable polarization diversity microstrip antenna	114
3.4.1 Antenna geometry	114
3.4.2 Simulations	115
3.4.3 Measurements	123
3.5 Summarized conjecture at a glance.....	127
4. INVESTIGATIONS ON VARACTOR CONTROLLED FREQUENCY AND	
POLARIZATION RECONFIGURABLE MICROSTRIP ANTENNA	129
4.1 Introduction	130

4.2 Frequency reconfigurable microstrip antenna for tunable frequency ratio using capacitive loading	131
4.2.1 Antenna Geometry	131
4.2.2 Simulated and measured results	132
4.3 Frequency and polarization tuning of a microstrip antenna using capacitive loading	137
4.3.1 Antenna Geometry	138
4.3.2 Simulated and Measured results	139
4.4 Varactor controlled frequency reconfigurable microstrip antenna	147
4.4.1 Varactor diode	148
4.4.2 Antenna Geometry	149
4.4.3 Simulated and measured results	151
4.5 Frequency and polarization reconfigurable cross patch antenna using varactor	156
4.5.1 Antenna Geometry	157
4.5.2 Simulated and measured results	158
4.6 Summarized conjecture at a glance	167
5. THEORETICAL ANALYSIS OF CROSS PATCH ANTENNA	169
5.1 Finite Difference Time Domain Technique (FDTD)	170
5.1.1 Stability criteria	173
5.1.2 Numerical Dispersion	174
5.1.3 Absorbing Boundary Conditions	174
5.1.4 Source model	177
5.1.5 Staircase approximation	178
5.1.6 General flow chart of FDTD algorithm	179
5.1.7 Return loss calculation	180
5.2 Theoretical analysis of cross patch antenna	182
5.3 Theoretical analysis of cross patch antenna with X-slot	185
5.4 Theoretical analysis of Frequency reconfigurable polarization diversity antenna	187
5.5 Chapter summary	193

6. CONCLUSION AND FUTURE PERSPECTIVE.....	197
6.1 Thesis Summary.....	198
6.2 Inferences from PIN diode controlled frequency and polarization reconfigurable compact cross patch antenna.....	199
6.3 Inferences from capacitor/varactor controlled compact cross patch antenna for frequency and polarization diversity applications.....	200
6.4 Inferences from theoretical analysis of cross patch antenna	202
6.5 Suggestions for future work	202
APPENDIX A: DESIGN OF CIRCULARLY POLARIZED RECTANGULAR MICROSTRIP ANTENNA FOR GPS APPLICATIONS.....	205
APPENDIX B: DESIGN AND DEVELOPMENT OF BROADBAND MICROSTRIP ANTENNAS.....	239
<i>List of publications</i>	
<i>Resume of the author</i>	
<i>Index</i>	

LIST OF TABLES

<i>Table 1.1</i>	<i>Comparisons of MIC and MSA</i>	6
<i>Table 1.2</i>	<i>Comparison of various types of microstrip antennas</i>	10
<i>Table 1.3</i>	<i>Comparison of different feeding techniques</i>	16
<i>Table 2.1</i>	<i>Specifications of PNA</i>	62
<i>Table 3.1</i>	<i>Performance of the antenna for different slot dimensions</i>	99
<i>Table 3.2</i>	<i>Comparison between the computed and simulated resonances of the designed antennas.</i>	99
<i>Table 3.3</i>	<i>States of the external DC bias voltage and PIN diodes for different antenna prototypes.</i>	117
<i>Table 4.1</i>	<i>Impedance variation of the frequency reconfigurable cross patch antenna against various capacitances</i>	134
<i>Table 4.2</i>	<i>Performance of the frequency and polarization reconfigurable cross patch antenna against various capacitances</i>	142
<i>Table 4.3</i>	<i>Varactor details</i>	150
<i>Table 5.1</i>	<i>Comparison between Measured, Simulated and FDTD computed resonant frequency of Frequency reconfigurable polarization diversity microstrip antenna</i>	188
<i>Table A.1</i>	<i>Antenna Description</i>	216
<i>Table A.2</i>	<i>Parameters of the Antennas</i>	216
<i>Table A.3</i>	<i>Antenna Description</i>	228
<i>Table A.4</i>	<i>Parameters of the Antennas</i>	228
<i>Table A.5</i>	<i>Comparison of single and dual slot CP antenna</i>	230
<i>Table B.1.</i>	<i>Antenna details</i>	244

LIST OF FIGURES

Figure 1.1	Structure of a Microstrip antenna	5
Figure 1.2	Common shapes of microstrip patch elements	9
Figure 1.3	Microstrip Line Feed	11
Figure 1.4	Probe fed Rectangular Microstrip Patch Antenna	12
Figure 1.5	Aperture-coupled feed	13
Figure 1.6	Proximity-coupled Feed	14
Figure 1.7	Co-Planar Waveguide feed	15
Figure 2.1	Step by step procedure involved in photolithographic process	60
Figure 2.2	Measurement setup and PNA Specifications	62
Figure 2.3	Photograph of the anechoic chamber used for the antenna measurements	63
Figure 2.4	Radiation Pattern Measurement Setup	67
Figure 3.1	Geometry, Simulated and measured reflection characteristics and Simulated input impedance of electromagnetically coupled cross patch antenna	85-86
Figure 3.2	Simulated input impedance variation of the cross patch antenna with respect to the patch overlap distance S	87
Figure 3.3	Simulated surface current distribution of the cross patch antenna at 2.3GHz	88
Figure 3.4	Geometry, Simulated and measured reflection characteristics and Simulated input impedance of electromagnetically coupled dual-frequency dual-polarized cross patch antenna	89-90
Figure 3.5	Simulated surface current distribution of dual-frequency dual-polarized cross patch antenna at (a) 1.74GHz and (b) 2.3GHz	90
Figure 3.6	Measured transmission coefficient of dual-frequency dual-polarized cross patch antenna in two orthogonal planes for the two resonant modes	91

Figure 3.7	Geometry, Simulated and measured reflection characteristics and Simulated input impedance of electromagnetically coupled dual-frequency dual-polarized cross patch antenna with X-slot	92-93
Figure 3.8	The response of first and second resonant modes of dual-frequency dual-polarized compact cross patch antenna with respect to X-slot length	95
Figure 3.9	Effect of slit length on first and second resonant modes of the dual-frequency dual-polarized antenna (a) Reflection coefficient (b) Resonant frequency	96
Figure 3.10	Simulated current distribution and 3D radiation patterns of the dual-frequency dual-polarized compact cross patch antenna at (a) 1.1GHz and (b) 1.4GHz	97
Figure 3.11	Measured and simulated reflection coefficient of the dual-frequency dual-polarized microstrip antenna for the two resonant frequencies	101
Figure 3.12	Measured transmission coefficient of the antenna in two orthogonal planes for the two resonant frequencies	102
Figure 3.13	Measured far-field radiation patterns of the dual frequency dual polarized cross patch antenna with X-slot for (a) $f_1=1.1\text{GHz}$ and (b) $f_2=1.4\text{GHz}$	102-103
Figure 3.14	Prototype of the fabricated dual-frequency dual-polarized cross patch antenna with X-slot	103
Figure 3.15	Geometry of the reconfigurable dual-frequency dual polarized microstrip antenna controlled using PIN diodes	107
Figure 3.16	Measured reflection coefficient for the reconfigurable antenna for different diode positions (a) OFF state (b) ON state	108
Figure 3.17	Reconfigurable dual frequency combinations and frequency ratios for different diode positions (a) OFF state (b) ON state	109

Figure 3.18	Measured transmission coefficient of the reconfigurable dual frequency microstrip antenna with $P_D=14.5\text{mm}$ (a) OFF state (b) ON state	110-111
Figure 3.19	Radiation Patterns of the reconfigurable dual frequency dual polarized microstrip antenna controlled by PIN diodes (a) at $f_1=1.12\text{GHz}$ when PIN diodes are OFF (b) at $f_2=1.43\text{GHz}$ when PIN diodes are OFF (c) at $f_1=1.34\text{GHz}$ when PIN diodes are ON and (d) at $f_2=1.72\text{GHz}$ when PIN diodes are ON	111-113
Figure 3.20	Geometry of frequency reconfigurable microstrip antenna for polarization diversity using PIN diodes	116
Figure 3.21	Simulated surface current distribution of (a) antenna 1 at 1.48 GHz (b) antenna 2 at 1.53GHz and (c) antenna 3 at 1.53GHz	120
Figure 3.22	Simulated reflection characteristics of the frequency reconfigurable polarization diversity microstrip antenna	121
Figure 3.23	Simulated input impedance characteristics of the frequency reconfigurable polarization diversity microstrip antenna	121
Figure 3.24	Simulated 3D radiation patterns of (a) Antenna 1 (b) Antenna 2 and (c) Antenna 3	122
Figure 3.25	Effect of the chamfers in antenna 3	123
Figure 3.26	Simulated and measured reflection characteristics of the frequency reconfigurable polarization diversity microstrip antenna for different diode configuration	124
Figure 3.27	Prototype of the fabricated frequency reconfigurable polarization diversity microstrip antenna	124
Figure 3.28	Measured axial ratio of the frequency reconfigurable polarization diversity microstrip antenna	125
Figure 3.29	Radiation pattern of frequency reconfigurable polarization diversity microstrip antenna (a) antenna 1 at 1.48 GHz (b)	

	<i>antenna 2 at 1.53GHz and (c) antenna 3 in two orthogonal planes at 1.53GHz</i>	126
Figure 4.1	<i>Geometry of the frequency reconfigurable cross patch antenna</i>	132
Figure 4.2	<i>Reflection coefficient of the antenna without and with various capacitances</i>	135
Figure 4.3	<i>Variation of resonant modes and frequency ratio against various capacitances</i>	135
Figure 4.4	<i>Simulated surface current distribution and 3D radiation pattern of the frequency reconfigurable microstrip antenna (a) without capacitor at 1.13GHz (b) without capacitor at 1.43GHz (c) with C=10pF at 1.16GHz and (d) with C=10pF at 1.99GHz</i>	136-137
Figure 4.5	<i>Geometry of frequency and polarization reconfigurable cross patch antenna using chip capacitor</i>	138
Figure 4.6	<i>Measured reflection coefficient of the frequency and polarization reconfigurable cross patch antenna against different capacitance</i>	140
Figure 4.7	<i>Variation of resonant frequencies and frequency ratio of frequency and polarization reconfigurable cross patch antenna against different capacitance</i>	142
Figure 4.8	<i>Simulated surface current distribution and 3D radiation pattern of the frequency and polarization reconfigurable cross patch antenna for different capacitance values (a) at 1.1GHz without chip capacitor (b) at 1.4GHz without chip capacitor (c) at 1.448GHz with C=6.8pF (d) at 1.559GHz with C=6.8pF and (e) at 1.465GHz with C=15pF</i>	143-144
Figure 4.9	<i>Measured axial ratio of the frequency and polarization reconfigurable cross patch antenna when C=15pF</i>	144
Figure 4.10	<i>Measured radiation pattern of the frequency and polarization reconfigurable cross patch antenna with various capacitances (a)</i>	

	at 952MHz when $C=1\text{pF}$ (b) at 1.45GHz when $C=1\text{pF}$ (c) at 1.45GHz when $C=6.8\text{pF}$ and (d) at 1.56GHz when $C=6.8\text{pF}$	145-146
Figure 4.11	Geometry of frequency reconfigurable microstrip antenna using varactor diodes	150
Figure 4.12	Measured reflection coefficient of the dual frequency reconfigurable microstrip antenna	152
Figure 4.13	Variation of resonant frequencies against bias voltages (a) first resonant frequency (b) second resonant frequency	152-153
Figure 4.14	Simulated surface current distribution and 3D radiation pattern of the frequency reconfigurable cross patch antenna at (a) 1.03GHz and (b) 1.28GHz when biasing 0V	154
Figure 4.15	Measured radiation patterns of frequency reconfigurable cross patch antenna (a) at 1.03GHz when biasing 0V (b) at 1.28GHz when biasing 0V (c) at 1.3GHz when biasing 16V and (d) at 1.48GHz when biasing 16V	154-155
Figure 4.16	Geometry of frequency and polarization reconfigurable cross patch antenna	158
Figure 4.17	Effect of the corner notches in the frequency and polarization reconfigurable cross patch antenna	160
Figure 4.18	Simulated surface current distribution of the frequency and polarization reconfigurable cross patch antenna at 1.43GHz with 0V DC bias	160
Figure 4.19	Measured reflection coefficient of the frequency and polarization reconfigurable cross patch antenna for different bias voltages	162
Figure 4.20	Variation of resonant modes with respect to the bias voltage variation of frequency and polarization reconfigurable cross patch antenna	162

Figure 4.21	Radiation patterns of the frequency and polarization reconfigurable cross patch antenna measured at 1.43GHz for different bias voltages in (a) XZ-plane and (b) YZ-plane	164
Figure 4.22	Measured radiation patterns of frequency and polarization reconfigurable cross patch antenna at 1.43GHz when biasing 0V (a) XZ-Plane (b) YZ-Plane	164
Figure 4.23	Measured radiation patterns of frequency and polarization reconfigurable cross patch antenna at 1.45GHz when biasing 10V (a) XZ-Plane and (b) YZ-Plane	165
Figure 4.24	Radiation patterns of frequency and polarization reconfigurable cross patch antenna measured with biasing 15V at (a) 1.43GHz and (b) 1.527GHz	166
Figure 4.25	Measured axial ratio of the frequency and polarization reconfigurable cross patch antenna for different bias voltages	166
Figure 4.26	A prototype of the frequency and polarization reconfigurable cross patch antenna	167
Figure 5.1	Yee Cell using in FDTD with Electric and Magnetic field components	
Figure 5.2	Central differencing with Leapfrog method (a) Discretization in space and time and (b) Leap frog time integration	173
Figure 5.3	Truncation of the domain by the exterior region in FDTD algorithm	175
Figure 5.4	Staircase meshing employed in the X-slot boundary	179
Figure 5.5	FDTD Staircase feed model for microstrip line in FDTD	179
Figure 5.6	Flow chart for the computation of return loss	181
Figure 5.7	2D view of the FDTD computation domain of microstrip line feed	183
Figure 5.8	2D view of the FDTD computation domain of cross patch antenna	183

Figure 5.9	Reflection characteristics of center fed cross patch antenna	183
Figure 5.10	FDTD computed Electric field distribution of the center fed cross patch at 2.3GHz	184
Figure 5.11	Reflection characteristics of dual-frequency dual-polarized cross patch antenna	184
Figure 5.12	FDTD computed Electric field distribution of the dual-frequency dual-polarized cross patch antenna	185
Figure 5.13	2D view of the FDTD computation domain of cross patch antenna with X-slot	186
Figure 5.14	Reflection characteristics of dual-frequency dual-polarized cross patch antenna with X-slot	186
Figure 5.15	FDTD computed Electric field distribution of the X-slot loaded cross patch antenna	187
Figure 5.16	2D view of the FDTD computation domain of Antenna 1	189
Figure 5.17	Reflection characteristics of Antenna 1	189
Figure 5.18	FDTD computed Electric field distribution of the Antenna 1	190
Figure 5.19	2D view of the FDTD computation domain of Antenna 2	190
Figure 5.20	Reflection characteristics of Antenna 2	191
Figure 5.21	FDTD computed Electric field distribution of the Antenna 2	191
Figure 5.22	2D view of the FDTD computation domain of Antenna 3	192
Figure 5.23	Reflection characteristics of Antenna 3	192
Figure 5.24	FDTD computed Electric field distribution of the Antenna 3	193
Figure A.1	Geometry of circularly polarized cross patch antenna (a) Front view (b) side view	210
Figure A.2	Simulated reflection coefficient and input impedance curve of circularly polarized cross patch antenna	210
Figure A.3	Simulated 3D radiation pattern of circularly polarized cross patch antenna at 1.57GHz	211

Figure A.4	Simulated 2D radiation pattern of circularly polarized cross patch antenna at 1.57GHz in (a) XZ-plane and (b) YZ- plane	211
Figure A.5	The influence of L_v on reflection characteristics of the antenna	212
Figure A.6	Reflection characteristics of the antenna for different α	213
Figure A.7	Effect of w_s on CP operation of the antenna	213
Figure A.8	Axial ratio of the antenna against W_v	214
Figure A.9	Simulated surface current distribution of circularly polarized cross patch antenna at 1.57GHz	215
Figure A.10	Simulated reflection characteristics of circularly polarized cross patch antenna for dielectric substrate	217
Figure A.11	Simulated reflection coefficient of the proposed antenna with substrate height h	217
Figure A.12	Simulated and measured reflection coefficient of circularly polarized cross patch antenna	218
Figure A.13	Prototype of the fabricated antenna	218
Figure A.14	Simulated and measured axial-ratio along the on-axis	219
Figure A.15	Measured gain of circularly polarized cross patch antenna	220
Figure A.16	Radiation patterns of circularly polarized cross patch antenna at 1.57GHz (a) XZ-plane and (b) YZ-plane	220
Figure A.17	2D view of the FDTD computation domain of circularly polarized cross patch antenna	221
Figure A.18	Reflection characteristics of circularly polarized cross patch antenna	222
Figure A.19	FDTD computed Electric field distribution of circularly polarized cross patch antenna	222
Figure A.20	Geometry of circularly polarized dual slot cross Patch antenna (a) Front view (b) side view	224
Figure A.21	Simulated reflection coefficient of single and dual slot antenna	225

Figure A.22	Simulated input impedance curve of dual slot loaded circularly polarized cross patch antenna	225
Figure A.23	3D radiation pattern and surface current distribution of dual slot loaded circularly polarized cross patch antenna at 1.46GHz	226
Figure A.24	Simulated reflection coefficient of dual slot loaded circularly polarized cross patch antenna for different substrate dielectric constant	227
Figure A.25	Simulated and measured reflection coefficient of dual slot loaded circularly polarized cross patch antenna	229
Figure A.26	Axial ratio of dual slot loaded circularly polarized cross patch antenna	229
Figure A.27	Radiation patterns of dual slot loaded circularly polarized cross patch antenna at 1.46GHz	230
Figure A.28	2D view of the FDTD computation domain of circularly polarized dual-slot cross patch antenna	231
Figure A.29	Reflection characteristics of circularly polarized dual-slot cross patch antenna	232
Figure A.30	FDTD computed Electric field distribution of circularly polarized dual-slot cross patch antenna	232
Figure B.1	Geometry of the broadband octagonal ring slot antenna (a) Front view (b) side view	243
Figure B.2.	Simulated return losses of the antenna for various L_v and W_v keeping $W_s=2\text{mm}$.	244
Figure B. 3	Simulated return losses of the antenna for various w_s	245
Figure B.4	Effect of corner slit length over the reflection characteristics, center frequency and bandwidth of broadband ring slot antenna	246
Figure B.5	Simulated 3D radiation pattern of broadband ring slot antenna at (a)5.2GHz (b)5.78GHz and (c) 6.78GHz	247

Figure B.6	Photograph of the ring slot loaded broadband cross patch antenna	248
Figure B.7	Simulated and measured reflection characteristics of ring slot loaded broadband cross patch antenna	248
Figure B.8	Measured radiation patterns (a) at 5.2GHz (b) at 5.78GHz and (c) at 6.78GHz	249
Figure B.9	Measured gain of the proposed antenna	250
Figure B.10	2D view of the FDTD computation domain of broadband octagonal ring slot antenna	251
Figure B.11	Theoretical, simulated and experimental reflection coefficient of the broadband octagonal ring slot antenna	251
Figure B.12	FDTD computed electric field distribution of the broadband octagonal ring slot antenna	252
Figure B.13	Geometry of the broadband cross patch antenna	254
Figure B.14	Simulated reflection coefficient of cross patch antenna with and without slot	255
Figure B.15	3D radiation pattern of the antenna simulated at (a) 3.75GHz (b) 5GHz and (c) 6.33GHz	256
Figure B.16	Input impedance of the antenna with and without slot (a) real part and (b) imaginary part	257
Figure B.17	Effect of V-slot gap V_g on the reflection characteristics of the antenna	258
Figure B.18	Variation of reflection characteristics with corner notch dimension L_s of the antenna	258
Figure B.19	Influence of tilt angle on the reflection coefficient of broadband cross patch antenna	259
Figure B.20	Influence of substrate parameters on the reflection coefficient of the broadband cross patch antenna (a) Substrate dielectric constant (b) substrate height	259-260

<i>Figure B.21</i>	<i>Measured and simulated reflection characteristics of the antenna</i>	261
<i>Figure B.22</i>	<i>Simulated surface current distribution of broadband cross patch antenna at (a) 3.82GHz (b) 4.2GHz(c) 5.29GHz and (d) 6.13GHz</i>	262
<i>Figure B.23</i>	<i>Measured radiation patterns (a) at 3.75 GHz (b) at 5GHz (c) at 6.33GHz</i>	263
<i>Figure B.24</i>	<i>Measured gain of the antenna</i>	264
<i>Figure B.25</i>	<i>2D view of the FDTD computation domain of broadband microstrip antenna</i>	265
<i>Figure B.26</i>	<i>Theoretical, measured and simulated reflection characteristics of broadband microstrip antenna</i>	265
<i>Figure B.27</i>	<i>FDTD computed electric field distribution of broadband microstrip antenna</i>	266

1.1	Introduction
1.2	Microstrip antennas
1.3	Advantages and Disadvantages
1.4	Applications of microstrip antennas
1.5	Various microstrip antenna configurations
1.6	Feeding Techniques
1.7	Analysis of antennas
1.8	Compact microstrip antennas
1.9	Compact circularly polarized microstrip antennas
1.10	Compact broadband microstrip antennas
1.11	Compact dual-frequency microstrip antennas
1.12	Compact reconfigurable antennas
1.13	Reconfiguration mechanisms
1.14	Motivation and development of subject of research
1.15	Thesis organization

Antennas are necessary and critical components of communication and radar systems. One of the breakthroughs is that a single system could support several applications on different frequency bands or polarizations and the system requires separate antennas in order to support different applications. Sometimes their inability to adjust to new operating scenarios can limit system performance. Making antennas reconfigurable so that their behavior can adjust with changing system requirements or environmental conditions eliminate these restrictions and provide additional levels of functionality for any system. In recent years, many problems like co-site interference, cost, maintainability, reliability, weight etc. arise since the number of systems on individual platforms grows. Therefore, the design of multifunctional antennas for newly developed systems is of practical interest.

This chapter serves to explore the historical advancements in the microstrip antenna technology. Literature overview of the state of art technologies is followed by the state of affairs that motivated the present investigations. The chapter concludes with a brief description of the organization of subsequent sections.

1.1 Introduction

Antennas are our electronic eyes and ears on the world. They are our links with space. They are an integral part of our civilization. Antennas have been around for a long time, millions of years, as the organ of touch. But in the last 100 years they have acquired a new significance as the connecting link between a radio system and the outside world.

In the year 1864, James Clerk Maxwell (1831-1879) proposed his “Dynamical Theory of the Electromagnetic Field”, wherein he observed theoretically that an electromagnetic disturbance travels in free space with the velocity of light. He then conjectured that light is a transverse electromagnetic wave. Although the idea of electromagnetic waves was hidden in the set of equations proposed by Maxwell, he had, in fact, said virtually nothing about electromagnetic waves other than light, nor did he propose any idea for generating such waves electromagnetically.

The first radio antennas were built by Heinrich Hertz, a professor at the Technical institute in Karlsruhe, Germany. In 1886, he assembled an apparatus we would now describe as a complete radio system operating at meter wavelength with an end-loaded dipole as the transmitting antenna and a resonant square-loop antenna as receiver. He also experimented with a parabolic reflector antenna.

Although Hertz was the pioneer and father of radio, his invention remained a laboratory curiosity until 20 years-old Guglielmo Marconi of Bologna, Italy, went on to add tuning circuits, big antenna and ground systems for longer wavelengths, and was able to signal over large distances. In mid-December 1901, he startled the world by receiving signals at St. Johns,

Newfoundland, from a transmitting station he had constructed at Poldhu in Cornwall, England. Marconi became the Wizard of wireless.

With the advent of radar during World War II, centimeter wavelengths became popular and the entire radio spectrum opened up to wide usage. Thousands of communication satellites bristling with antennas now circle the earth in low, medium and geostationary orbits. Our probes with their arrays of antennas have visited the planets of the solar system and beyond, responding to our commands and sending photographs and data at centimeter wavelengths [1].

Antennas are the essential communication link for aircrafts and ships. Arguably, nine different types of antennas have proliferated during the past 50 years in both wireless communication and radar systems. These nine varieties comprise dipoles/monopoles, loop antennas, slot/horn antennas, reflector antennas, microstrip antennas, log periodic antennas, helical antennas, dielectric/lens antennas and frequency-independent antennas. Each category possesses inherent benefits that make them more or less suitable for particular applications. When faced with a new system design, engineers change and adapt these basic antennas, using theoretical knowledge and general design guidelines as starting points to develop new structures that often produce acceptable results.

Antennas for cellular phones and all types of wireless devices link us to everyone and everything. With mankind's activities expanding into space, the need for antennas will grow to an unprecedented degree. Antennas will provide the vital links to and from everything out there. The future of antennas reaches to the stars.

1.2 Microstrip antennas

The concept of the planar antennas was first proposed by Deschamps in 1953 [2]. However, practical antennas were developed by Munson [3, 4] and Howell [5, 6] in the 1970s. The numerous advantages of microstrip antenna, such as its low weight, small volume, and ease of fabrication using printed-circuit technology, led to the design of several configurations for various applications. With increasing requirements for personal and mobile communications, the demand for smaller and low-profile antennas has brought the microstrip antenna to the forefront [7-11].

A microstrip antenna in its simplest form consists of a radiating patch on one side of a dielectric substrate and a ground plane on the other side as shown in figure 1.1. The patch is generally made of conducting material such as copper or gold and can take any possible shape, but regular shapes are used to simplify analysis and performance prediction. The radiating patch and the feed lines are usually photo etched on the dielectric substrate. Radiation from the microstrip antenna can occur from the fringing fields between the periphery of the patch and the ground plane. Rectangular and circular microstrip resonant patches have been used extensively in a variety of array configurations. A major contributing factor for recent advances of microstrip antennas is the current revolution in electronic circuit miniaturization brought about by developments in large scale integration. As conventional antennas are often bulky and costly part of an electronic system, microstrip antennas based on photolithographic technology are seen as an engineering breakthrough.

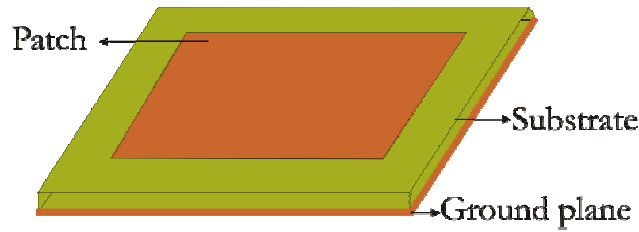


Figure 1.1 Structure of a Microstrip antenna

For a rectangular patch, the length L of the patch is usually $0.3333\lambda_0 < L < 0.5\lambda_0$, where λ_0 is the free-space wavelength. For the fundamental TM_{10} mode excitation, the patch length is slightly smaller than $\lambda/2$, where λ is the wavelength in the dielectric medium related to free-space wavelength λ_0 as λ_0/ϵ_{ef} and ϵ_{ef} is the effective dielectric constant of a microstrip line of width W . The value of ϵ_{ef} is slightly less than the dielectric constant ϵ_r of the substrate because the fringing fields from the patch to the ground plane are not confined in the dielectric only, but are also spread in the air. To enhance the fringing fields from the patch, which account for the radiation, the width W of the patch is increased. The fringing fields are also enhanced by decreasing ϵ_r or by increasing the substrate thickness h . Therefore, unlike the microwave integrated circuit (MIC) applications, microstrip antenna uses microstrip patches with larger width and substrates with lower ϵ_r and thicker h . For microstrip antenna applications in the microwave frequency band, the height h of the dielectric substrate is usually $0.003\lambda_0 \leq h \leq 0.05\lambda_0$. The patch is selected to be very thin such that $t \ll \lambda_0$ where t is the patch thickness. The dielectric constant of the substrate (ϵ_r) is typically in the range $2.2 \leq \epsilon_r \leq 12$. A typical comparison of microstrip antenna with MIC in the microwave frequency range is given in Table 1.1.

Table 1.1 Comparisons of MIC and MSA

Characteristics	MIC	Microstrip antenna
Height, h	≤ 0.159 cm	≥ 0.159 cm
Dielectric constant, ϵ_r	≥ 9.8	≤ 9.8
Width, W	Small	Large
Radiation	Minimized	Maximized

For good antenna performance, a thick dielectric substrate having low dielectric constant is desirable since this provides better efficiency, larger bandwidth and better radiation. However, such a configuration leads to a larger antenna size. In order to design a compact Microstrip antenna, substrates with higher dielectric constants must be used which are less efficient and result narrow bandwidth. Hence a trade-off must be realized between the antenna dimensions and antenna performance [12].

1.3 Advantages and Disadvantages

Microstrip antennas are increasing in popularity for use in wireless applications due to their low-profile structure. Therefore they are extremely compatible for embedded antennas in handheld wireless devices. The telemetry and communication antennas on missiles are often in the form of microstrip patch antennas. Another area where they have been used successfully is in Satellite communication. Some of their principal advantages are given below:

- Light weight and low volume.
- Low profile planar configuration which can be easily made conformal to host surface.
- Low fabrication cost, hence can be manufactured in large quantities.
- Supports both linear as well as circular polarization.

- Can be easily integrated with microwave integrated circuits (MICs).
- Capable of dual and triple frequency operations.
- Mechanically robust when mounted on rigid surfaces.

Microstrip antennas suffer from some drawbacks as compared to conventional antennas. They are:

- Narrow bandwidth.
- Low efficiency.
- Low Gain.
- Extraneous radiation from feeds and junctions.
- Poor end fire radiator except tapered slot antennas.
- Low power handling capacity.
- Surface wave excitation.

Microstrip antennas have a very high antenna quality factor (Q). It represents the losses associated with the antenna where a large Q leads to narrow bandwidth and low efficiency. Q can be reduced by increasing the thickness of the dielectric substrate. But as the thickness increases, an increasing fraction of the total power delivered by the source goes into a surface wave. This surface wave contribution can be counted as an unwanted power loss since it is ultimately scattered at the dielectric bends and causes degradation of the antenna characteristics. Other problems such as lower gain and lower power handling capacity can be overcome by using an array configuration for the elements [10, 12].

1.4 Applications of microstrip antennas

The advantages of microstrip antennas make them suitable for numerous applications. The telemetry and communications antennas on missiles are often microstrip antennas. Radar altimeters use small arrays of microstrip radiators. Other aircraft-related applications include antennas for telephone and satellite communications. Microstrip arrays have been used for satellite imaging systems. Patch antennas have been used on communication links between ships or buoys and satellites. Smart weapon systems use microstrip antennas because of their thin profile. The global system for mobile communication (GSM) and the global positioning system (GPS) are major users of microstrip antennas [7-10].

1.5 Various microstrip antenna configurations

Microstrip antennas can be divided into four basic categories: microstrip patch antennas, microstrip or printed dipoles, printed slot antennas and microstrip travelling-wave antennas.

1.5.1 Microstrip patch antennas

A microstrip patch antenna consists of a conducting patch of any planar or non planar geometry on one side of a dielectric substrate with a ground plane on the other side. The basic configurations used in practice are shown in figure 1.2. The radiation characteristics of microstrip patch antennas are similar to that of a dipole because they behave like a dipole. A patch antenna has a gain between 5 and 6dB typically and exhibits a 3dB beam width between 70° and 90° . Rectangular and circular patch antennas are widely used. Some of the other patch shapes are used for special applications.

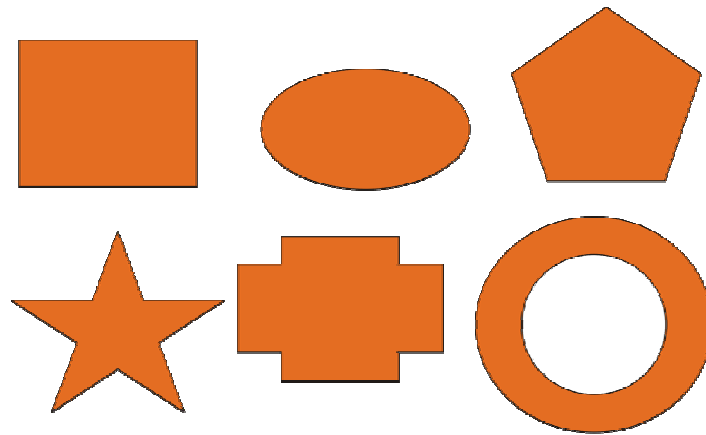


Figure 1.2 Common shapes of microstrip patch elements

1.5.2 Microstrip or printed dipoles

Microstrip dipoles differ geometrically from rectangular patch antennas in their length-to-width ratio. The width of a dipole is typically less than $0.05\lambda_0$. The radiation patterns of the dipole and patch are similar owing to similar longitudinal current distributions. However, the radiation resistance, bandwidth and cross-polar radiation differ widely. The dipoles are well suited for higher frequencies for which the substrate can be electrically thick.

1.5.3 Printed slot antennas

Printed slot antennas comprise a slot in the ground plane of a grounded substrate. The slot can have any shape. Slot antennas are generally bidirectional radiators so that they radiate on both sides of the slot. By using a reflector plate on one side of the slot a unidirectional pattern is obtained.

1.5.4 Microstrip travelling-wave antennas

A microstrip travelling-wave antenna consists of a chain shaped periodic conductors or a long microstrip line of sufficient width to support a TE mode. The other end of the travelling-wave antenna is terminated in a matched

resistive load to avoid the standing waves. Travelling-wave microstrip antennas are designed so that the main beam lies in any direction from broadside to end fire [10].

The characteristics of microstrip patch antennas, slot antennas and dipole antennas are compared in Table 1.2

Table 1.2 Comparison of various types of microstrip antennas

Characteristics	Patch antennas	Slot antennas	Dipole antennas
Profile	Thin	Thin	Thin
Fabrication	Very easy	Easy	Easy
Polarization	Both linear and circular	Both linear and circular	Linear
Dual-frequency operation	Possible	Possible	Possible
Shape flexibility	Any shape	Mostly rectangular and circular shapes	Rectangular and triangular shapes
Spurious radiation	Exists	Exists	Exists
Bandwidth	2-50%	5-30%	□30%

1.6 Feeding Techniques

Microstrip patch antennas can be fed by a variety of methods. These methods can be classified into two categories- contacting and non-contacting. In the contacting method, the RF power is fed directly to the radiating patch using a connecting element such as a microstrip line. In the non-contacting scheme, electromagnetic field coupling is done to transfer power between the microstrip line and the radiating patch. The four most popular feed techniques used are the microstrip line, coaxial probe (both contacting schemes), aperture coupling and proximity coupling (both non-contacting schemes) [9-10].

1.6.1 Microstrip Line Feed

In this type of feed technique, a conducting strip is connected directly to the edge of the Microstrip patch as shown in figure 1.3. The conducting strip is

smaller in width as compared to the patch and this kind of feed arrangement has the advantage that the feed can be etched on the same substrate to provide a planar structure.

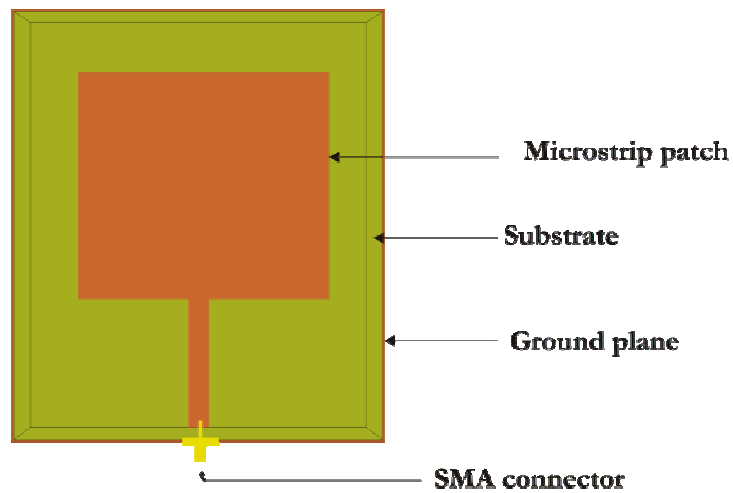


Figure 1.3 Microstrip Line Feed

This is an easy feeding scheme, since it provides ease of fabrication and simplicity in modeling as well as impedance matching. However as the thickness of the dielectric substrate being used increases, surface waves and spurious feed radiation also increases, which hampers the bandwidth of the antenna. The feed radiation also leads to undesired cross polarized radiation [7, 10 and 12-13].

1.6.2 Coaxial Feed

The Coaxial feed or probe feed is a very common technique used for feeding Microstrip patch antennas. As seen from figure 1.4, the inner conductor of the SMA connector extends through the dielectric and is soldered to the radiating patch, while the outer conductor is connected to the ground plane.

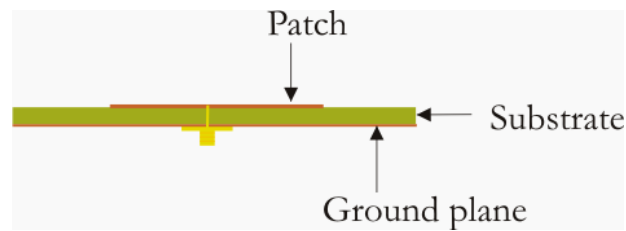


Figure 1.4 Probe fed Rectangular Microstrip Patch Antenna

The main advantage of this type of feeding scheme is that the feed can be placed at any desired location inside the patch in order to match with its input impedance. This feed method is easy to fabricate and has low spurious radiation. However, a major disadvantage is that it provides narrow bandwidth and is difficult to model since a hole has to be drilled in the substrate and the connector protrudes outside the ground plane, thus not making it completely planar for thick substrates ($h > 0.02\lambda_0$). Also, for thicker substrates, the increased probe length makes the input impedance more inductive, leading to matching problems. It is seen above that for a thick dielectric substrate, which provides broad bandwidth, the microstrip line feed and the coaxial feed suffer from numerous disadvantages. The non-contacting feed techniques which have been discussed below, solve these issues [7, 10].

1.6.3 Aperture Coupled Feed

In this type of feed technique, the radiating patch and the microstrip feed line are separated by the ground plane as shown in figure 1.5. Coupling between the patch and the feed line is made through a slot or an aperture in the ground plane. The coupling aperture is usually centered under the patch, leading to lower cross-polarization due to symmetry of the configuration. The amount of coupling from the feed line to the patch is determined by the shape, size and location of the aperture. Since the ground plane separates the patch and the feed line, spurious radiation is minimized. Generally, a high dielectric material is

used for bottom substrate and a thick, low dielectric constant material is used for the top substrate to optimize radiation from the patch. The major disadvantage of this feed technique is that it is difficult to fabricate due to multiple layers, which also increases the antenna thickness. This feeding scheme also provides narrow bandwidth [10-12 and 16-20].

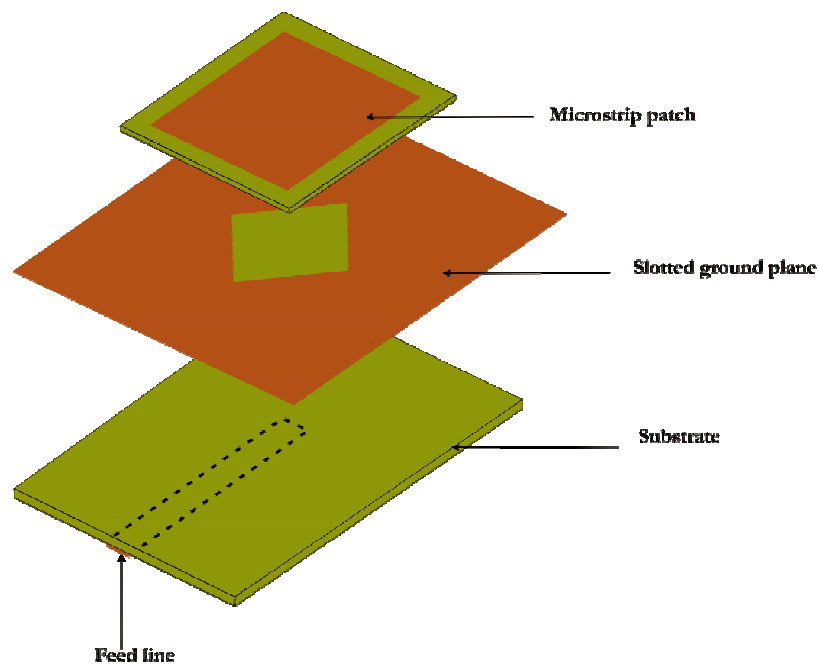


Figure 1.5 Aperture-coupled feed

1.6.4 Proximity Coupled Feed

This type of feed technique is also called as the electromagnetic coupling scheme. As shown in figure 1.6, two dielectric substrates are used such that the feed line is between the two substrates and the radiating patch is on top of the upper substrate. The main advantage of this feed technique is that it eliminates spurious feed radiation and provides very high bandwidth (as high as 13%), due to overall increase in the thickness of the microstrip patch antenna. This scheme also provides choices between two different dielectric media, one for the patch and one for the feed line to optimize the individual performances [21-22].

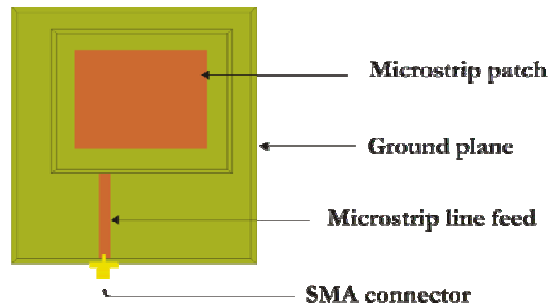


Figure 1.6 Proximity-coupled Feed

Matching can be achieved by controlling the length of the feed line and the width to-line ratio of the patch. The major disadvantage of this feed scheme is that it is difficult to fabricate because of the two dielectric layers which need proper alignment. Also, there is an increase in the overall thickness of the antenna.

1.6.5 Coplanar waveguide feed

A coplanar waveguide (CPW) is the preferred transmission line for microwave monolithic integrated circuits. The configuration of a CPW is shown in figure 1.7. Coupling is accomplished via a slot. This coupling arrangement is somewhat similar to the aperture coupling. An advantage of CPW feed is that the radiation from the feed structure is negligible because the coplanar waveguide is excited in the odd mode of the coupled slot line. Due to this mode, the equivalent magnetic currents on both the CPW slots radiate almost out of phase, contributing negligibly to the feed radiation. This feature of a CPW feed is useful in the design of antenna arrays since mutual coupling between adjacent lines is minimized [23-24]. Table 1.3 below summarizes the characteristics of the different feed techniques.

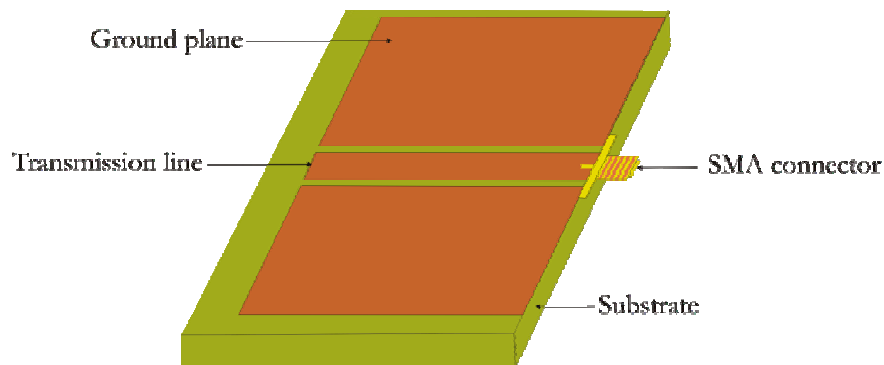


Figure 1.7 Co-Planar Waveguide feed

1.7 Analysis of antennas

The microstrip antenna generally has a radiating patch on a thin dielectric substrate and is considered as a two-dimensional planar component for analysis purposes. The analysis methods for microstrip antennas are broadly divided into two groups. In the first group, the methods are based on equivalent magnetic current distribution around the patch edges. The popular analytical techniques are:

- The transmission line model
- The cavity model
- The Multiport Network Model (MNM).

In the second group, the methods are based on the electric current distribution on the patch conductor and the ground plane. The numerical methods for analyzing microstrip antennas are listed as follows:

- The method of moments (MoM)
- The finite-element method (FEM)
- The spectral domain technique (SDT)
- The finite-difference time domain (FDTD) method.

Table 1.3 Comparison of different feeding techniques

Characteristics	Microstrip Line Feed	Coaxial Feed	Aperture coupled Feed	Proximity coupled Feed	CPW feed
Spurious feed radiation	More	More	Less	Minimum	Less
Reliability	Better	Poor due to soldering	Good	Good	Good
Ease of Fabrication	Easy	Soldering and drilling needed	Alignment required	Alignment required	Alignment required
Impedance Matching	Easy	Easy	Easy	Easy	Easy
Bandwidth (achieved with impedance matching)	2-5%	2-5%	2-5%	13%	3%

1.7.1 Transmission Line Model

The transmission line model was the first technique and is very simple and helpful in understanding the basic performance of a microstrip antenna. The microstrip radiator element is viewed as a transmission line resonator with no transverse field variations (the field only varies along the length), and the radiation occurs mainly from the fringing fields at the open circuited ends. The patch is represented by two slots that are spaced by the length of the resonator. This model was originally developed for rectangular patches but has been extended for generalized patch shapes. Although the transmission line model is easy to use, all types of configurations cannot be analyzed using this model since it does not take care of variation of field in the orthogonal direction to the direction of propagation [23-25].

1.7.2 Cavity model

In the cavity model, the region between the patch and the ground plane is treated as a cavity that is surrounded by magnetic walls around the periphery and by electric walls from the top and bottom sides. Since thin substrates are used, the field inside the cavity is uniform along the thickness of the substrate. The fields underneath the patch for regular shapes such as rectangular, circular, triangular, and sectoral can be expressed as a summation of the various resonant modes of the two-dimensional resonator.

The fringing fields around the periphery are taken care of by extending the patch boundary outward so that the effective dimensions are larger than the physical dimensions of the patch. The effect of the radiation from the antenna and the conductor loss are accounted for by adding these losses to the loss tangent of the dielectric substrate. The far field and radiated power are computed from the equivalent magnetic current around the periphery [26-27].

An alternate way of incorporating the radiation effect in the cavity model is by introducing an impedance boundary condition at the walls of the cavity. The fringing fields and the radiated power are not included inside the cavity but are localized at the edges of the cavity. However, the solution for the far field, with admittance walls is difficult to evaluate.

1.7.3 Multiport Network Model

The Multiport Network Model (MNM) for analyzing the microstrip antenna is an extension of the cavity model. In this method, the electromagnetic fields underneath the patch and outside the patch are modeled separately. The patch is analyzed as a two-dimensional planar network, with a multiple number of ports located around the periphery. The multiport impedance matrix of the

patch is obtained from its two-dimensional Green's function. The fringing fields along the periphery and the radiated fields are incorporated by adding an equivalent edge admittance network. The segmentation method is then used to find the overall impedance matrix. The radiated fields are obtained from the voltage distribution around the periphery [10-11 and 28-29].

The above three analytical methods offer both simplicity and physical insight. In the latter two methods, the radiation from the microstrip antenna is calculated from the equivalent magnetic current distribution around the periphery of the radiating patch, which is obtained from the corresponding voltage distribution. Thus, the microstrip antenna analysis problem reduces to that of finding the edge voltage distribution for a given excitation and for a specified mode. These methods are accurate for regular patch geometries. For complex geometries, the numerical techniques described below are employed.

1.7.4 Method of Moments

In the Method of Moments (MoM) the surface currents are used to model the microstrip patch and polarization currents in the dielectric slab are used to model the fields in the dielectric slab. An integral equation is formulated for the unknown currents on the microstrip patches, feed lines and their images in the ground plane. The integral equations are transformed into algebraic equations that can be easily solved using a computer. This method takes into account the fringing fields outside the physical boundary of the two-dimensional patch, thus providing a more exact solution [30].

1.7.5 Finite Element Method

The Finite Element Method (FEM), unlike the MoM, is suitable for volumetric configurations. In this method, the region of interest is divided into a

number of finite surfaces or volume elements depending upon the planar or volumetric structures to be analyzed. These discretized units, generally referred to as finite elements, can be any well-defined geometrical shapes such as triangular elements for planar configurations and tetrahedral and prismatic elements for three-dimensional configurations, which are suitable even for curved geometry. It involves the integration of certain basis functions over the entire conducting patch, which is divided into a number of subsections. The problem of solving wave equations with inhomogeneous boundary conditions is tackled by decomposing it into two boundary value problems, one with Laplace's equation with an inhomogeneous boundary and the other corresponding to an inhomogeneous wave equation with a homogeneous boundary condition [31].

1.7.6 Spectral Domain Technique

In the Spectral Domain Technique (SDT), a two-dimensional Fourier transform along the two orthogonal directions of the patch in the plane of substrate is employed. Boundary conditions are applied in Fourier transform plane. The current distribution on the conducting patch is expanded in terms of chosen basis functions, and the resulting matrix equation is solved to evaluate the electric current distribution on the conducting patch and the equivalent magnetic current distribution on the surrounding substrate surface. The various parameters of the antennas are then evaluated [32].

1.7.7 Finite Difference Time Domain method

The Finite Difference Time Domain (FDTD) method is well-suited for microstrip antennas, as it can conveniently model numerous structural inhomogeneities encountered in these configurations. It can also predict the response of the microstrip antenna over the wide bandwidth with a single

simulation. In this technique, spatial as well as time grid for the electric and magnetic fields are generated over which the solution is required. The spatial discretizations along three Cartesian coordinates are taken to be same. The E-cell edges are aligned with the boundary of the configuration and H-fields are assumed to be located at the center of each E-cell. Each cell contains information about material characteristics. The cells containing the sources are excited with a suitable excitation function, which propagates along the structure. The discretized time variations of the fields are determined at desired locations. Using a line integral of the electric field, the voltage across the two locations can be obtained. The current is computed by a loop integral of the magnetic field surrounding the conductor, where the Fourier transform yields a frequency response.

The above numerical techniques, which are based on the electric current distribution on the patch conductor and the ground plane, give results for any arbitrarily shaped antenna with good accuracy, but they are time consuming. These methods can be used to plot current distributions on patches but otherwise provide little of the physical insight required for antenna design [33-36].

1.8 Compact microstrip antennas

In general, microstrip antennas are half-wavelength structures and are operated at the fundamental resonant mode TM_{01} or TM_{10} . Many techniques have been reported to reduce the size of microstrip antennas at a fixed operating frequency. It is found that the radiating patch of the microstrip antenna has a resonant length approximately proportional to $1/\sqrt{\epsilon_r}$. The use of a microwave substrate with a larger permittivity result in a smaller physical antenna length at a fixed operating frequency. The use of an edge-shortened patch for size reduction is also well known and makes a microstrip antenna act as a quarter wavelength

structure and thus can reduce the antenna's physical length by half at a fixed operating frequency. When a shorting plate (also called a partial shorting wall) or a shorting pin is used instead of a shorting wall, the antenna's fundamental resonant frequency can be further lowered and further size reduction can be obtained. In this case, the diameter of a shorting-pin-loaded circular microstrip patch or the linear dimension of a shorting-pin-loaded rectangular microstrip patch can be as small as one-third of that of the corresponding microstrip patch without a shorting pin at the same operating frequency [13 and 37-39].

Meandering the excited surface current paths in the antenna's radiating patch is also an effective method for achieving a lowered fundamental resonant frequency for the microstrip antenna [40-43]. For the case of a rectangular radiating patch, the meandering can be achieved by inserting several narrow slits at the patch's non-radiating edges. The excited patch's surface currents are effectively meandered, leading to a greatly lengthened current path for a fixed patch linear dimension. This behavior results in a greatly lowered antenna fundamental resonant frequency, and thus a large antenna size reduction at a fixed operating frequency can be obtained.

By embedding suitable slots in the radiating patch, compact operation of microstrip antennas can be obtained. This kind of slotted patch causes meandering of the patch surface current path in two orthogonal directions and is suitable for achieving compact circularly polarized radiation [44-45] or compact dual-frequency operation with orthogonal polarizations. The microstrip-line-fed planar inverted-L (PIL) patch antenna is a good candidate for compact operation. The PIL patch antenna is a quarter-wavelength structure, and has the same broadside radiation characteristics as conventional half-wavelength microstrip antennas. The antenna's ground plane is meandered by inserting several meandering slits at its edges. Moreover, probably because the

meandering slits in the antenna's ground plane can effectively reduce the quality factor of the microstrip structure, the obtained impedance bandwidth for a compact design with a meandered ground plane can be greater than that of the corresponding conventional microstrip antenna.

1.9 Compact circularly polarized microstrip antennas

Antennas produce circularly polarized waves when two orthogonal field components with equal amplitude but in phase quadrature are radiated. Various printed antennas are capable of satisfying these requirements. They are classified as resonator and travelling-wave types. A resonator type antenna consists of a single patch that is capable of simultaneously supporting two orthogonal modes in phase quadrature or an array of linearly polarized resonating patches with proper orientations. A travelling-wave type of antenna is usually constructed from a microstrip transmission line. It generates circular polarization by radiating orthogonal field components along discontinuities in the travelling-wave line [10].

Various novel designs have been reported in literature to achieve compact circularly polarized (CP) radiation with microstrip antennas. Compact CP designs can be achieved by embedding suitable slots or slits in the radiating patch or the antenna's ground plane. Two types of feeding schemes can be accomplished. The first type is a dual-orthogonal feed which employs an external power divider network. The other is a single-point feed for which an external power divider is not required.

1.10 Compact broadband microstrip antennas

With a size reduction at a fixed operating frequency, the impedance bandwidth of a microstrip antenna is usually decreased. To obtain an enhanced

impedance bandwidth, one can simply increase the antenna's substrate thickness to compensate for the decreased electrical thickness of the substrate due to the lowered operating frequency, or one can use a meandering ground plane or a slotted ground plane. These design methods lower the quality factor of compact microstrip antennas and result in an enhanced impedance bandwidth [46].

By embedding suitable slots in a radiating patch, compact operation with an enhanced impedance bandwidth can be obtained. However, the obtained impedance bandwidth for such a design is equal to or less than 2.0 times that of the corresponding conventional microstrip antenna. To achieve a much greater impedance bandwidth with a reduction in antenna size, one can use compact designs with chip-resistor loading or stacked shorted patches. However, due to the introduced ohmic loss of the chip-resistor loading, the antenna gain is decreased, and is estimated to be about 2 dBi, compared to a shorted patch antenna with a shorting pin. For the latter design with stacked shorted patches, an impedance bandwidth of greater than 10% can be obtained. For this design, of course, the total antenna volume or height is increased [47].

1.11 Compact dual-frequency microstrip antennas

Compact dual-frequency design is very suitable for applications in handset antennas of mobile communication units. Dual frequency antennas exhibit a dual resonant behavior in a single radiating structure. The two operating frequencies can have the same polarization planes or orthogonal polarization planes. Most of the dual-frequency antennas found in the literature can be subdivided into three major categories namely multi-patch, reactively loaded and orthogonal mode antennas.

1.11.1 Multi-patch dual-frequency antennas

Multi-patch dual-frequency antennas can be obtained by printing more resonators on the same substrate. These antennas can operate with same polarization at the two frequencies as well as with an orthogonal polarization [48-50].

1.11.2 Reactively loaded dual-frequency antennas

In these structures, an adjustable stub is connected to one of the radiating edge of the patch, in such a way that, this stub introduces an additional resonant length that is responsible for the second operating frequency [51]. Different kinds of reactive loads like notches, pins, capacitors and slots are used for dual frequency generation.

1.11.3 Orthogonal mode dual frequency antennas

Dual-polarized operation has been an important subject in microstrip antenna design and finds application in wireless communication systems that require frequency reuse or polarization diversity. Microstrip antennas capable of performing dual-polarized operation can combat multipath effects in wireless communications and enhance system performance. A simple rectangular patch can be regarded as a cavity with magnetic walls on the radiating edges. The simplest way to operate at dual frequencies is to use the first resonance of the two orthogonal dimensions of the rectangular patch, i.e, the TM_{10} and TM_{01} modes [52-53].

1.12 Compact reconfigurable antennas

Reconfigurability, when used in the context of antennas, is the capacity to change an individual radiator's fundamental operating characteristics through

electrical, mechanical, or other means. Ideally, reconfigurable antennas should be able to alter their operating frequencies, impedance bandwidths, polarizations, and radiation patterns independently to accommodate changing operating requirements. However, the development of these antennas poses significant challenges to both antenna and system designers. These challenges lie not only in obtaining the desired levels of antenna functionality but also in integrating this functionality into complete systems to arrive at efficient and cost-effective solutions. As in many cases of technology development, most of the system cost will come not from the antenna but the surrounding technologies that enable reconfigurability.

1.12.1 Frequency reconfigurable antennas

Frequency reconfigurable antennas are also called tunable antennas. They are classified into two categories: Continuous and switched. Continuous frequency tunable antennas allow smooth transition within or between operating bands without jumps. Switched tunable antennas, on the other hand, use some kind of switching mechanism to operate at distinct and/or separated frequency bands. Both kinds of these antennas in general share a common theory of operation and reconfiguration.

Many common antennas including microstrip antennas, loop antennas and slot antennas are usually operated in resonance. The effective electrical length of the antenna determines the operating frequency, its associated bandwidth and the current distribution on the antenna dictates its radiation pattern. In this case, if one wants the antenna to operate at a particular frequency, the antenna structure is simply be modified to the correct length corresponding to a half wavelength at the new frequency. A number of mechanisms can be used to change the effective length of resonant antennas,

although some of these are more effective than others in maintaining the radiation characteristics of the original configuration. The development efforts include the use of switches, variable reactive loading, mechanical tuning and material changes [54].

1.12.2 Polarization reconfigurable antennas

Antenna polarization reconfiguration provide immunity to interfering signals in varying environments as well as provide an additional degree of freedom to improve link quality as a form of switched antenna diversity. The direction of current flow on the antenna translates directly into the polarization of the electric field in the far field of the antenna [55]. To achieve polarization reconfigurability, the antenna structure, material properties, and/or feed configuration have to change that alter the way of current flows on the antenna. Polarization reconfigurations take place between different kinds of linear polarization, between right- and left-handed circular polarizations, or between linear and circular polarizations. The mechanisms to achieve these modifications (switches, structural changes etc.) are largely the same as those described for frequency reconfiguration, although their implementations are different. The main difficulty of this kind of reconfigurability is that this must be accomplished without significant changes in impedance or frequency characteristics.

1.12.3 Radiation pattern reconfigurable antennas

The arrangement of currents, either electric or magnetic, on an antenna structure directly determines the spatial distribution of radiation from the structure. This relationship between the source currents and the resulting radiation makes pattern reconfigurability to achieve without significant changes in operating frequency. Manipulation of an antenna radiation pattern can be

used to avoid noise sources or intentional jamming, improve security by directing signals only towards intended users and serves as a switched diversity system [54].

1.13 Reconfiguration mechanisms

1.13.1 Switches

The effective length of the antenna, and hence its operating frequency, can be changed by adding or removing a part of the antenna length through electronic, optical, mechanical or other means. The different kinds of switches include optical switches, PIN diodes, FETs and radio frequency microelectromechanical (RF-MEMS). When the switch is open, currents must flow around the slot. When the switch is closed, the current can follow the shorter path created by the closed switch [56].

1.13.2 Variable reactive loading

The use of variable reactive loading has much in common with the switched reconfigurability. The only real difference between the two is that, the change in effective antenna length is achieved with devices or mechanisms that can take on a continuous range of values (typically capacitance) that allows smooth rather than discrete changes in antennas operating frequency band [54].

1.13.3 Structural/Mechanical Tuning

Mechanical rather than electrical changes in antenna structure can deliver large frequency shifts. The main challenges of these antennas lie in the physical design of the antenna, the actuation mechanism and the maintenance of other characteristics with respect to the significant structural changes. The reconfigurable antennas developed were all make use of shorting pins, stubs or

air-gaps. Schaubert *et al.* first introduced the shorting pin concept for tuning the resonant frequency of the patch. The shorting pins are introduced in between the ground plane and patch metallization [57].

Printed or co-axial transmission line stubs connected to the antenna are used for tuning the resonant frequency by varying its length mechanically. The two-stub approach is more common and tuning is only possible from a lower frequency to a higher frequency owing to the destructive nature of trimming.

Dahele and Lee proposed another method of tuning which involves an adjustable air-gap between the substrate and ground plane [58]. The effective dielectric constant varies with respect to the thickness of the air gap thereby varying the resonant frequency of the patch. Another example of continuous frequency changes enabled by mechanical changes is a magnetically actuated microstrip antenna. Here, a microstrip antenna is covered with a thin layer of magnetic material and released from the substrate. Application of an external DC magnetic field causes plastic deformation of the antenna at the boundary where it is attached to the feed. Small changes at which the structure resides results in changes in operating frequency that preserve radiation characteristics, whereas larger changes result in frequency shifts accompanied by significant changes in the antenna radiation pattern.

1.13.4 Material changes

Although changes to conductors predominate in reconfigurable antenna designs, changes in the material characteristics also promise the ability to tune antennas operating frequency. An applied static electric field can be used to change the relative permittivity of a ferroelectric material and an applied static magnetic field can be used to change the relative permeability of a ferrite. The changes in relative permittivity or permeability can then be used to change the

effective electrical length of antennas resulting in shifts in operating frequency [54].

1.14 Motivation and development of subject of research

Wireless communication technologies have been growing rapidly in recent years. One of the breakthroughs is that a single system could support several applications like satellite communications, cellular phones (GSM, PCS, 3G), wireless local area networks, WiMax etc. These applications do not utilize the same frequency bands or polarizations and the system requires separate antennas in order to support different applications. In recent years, many problems arise since the number of systems on individual platforms grows, such as: co-site interference, cost, maintainability, reliability and weight. Therefore, the design of multifunctional antennas for newly developed systems is of practical interest.

The reconfigurable antennas are foreseen to be a booster for the future high rate wireless communications, both for the benefits in terms of performance and for the capacity gains. The goal of a reconfigurable antenna is to reduce the complexity of an antenna system operating over a wide frequency band, and to reduce the need of multiple antennas to perform a specific task, providing a relatively large bandwidth and achieving a dynamical reconfiguration within a few microseconds. Reconfigurable antennas have recently received much attention for their applications in wireless communications, electronic surveillance and countermeasures, by adapting their properties to achieve selectivity in frequency, bandwidth, polarization and gain. Instead of wide-band antennas, tunable narrow-band antennas provide frequency selectivity which relaxes the requirement of receiver filters. Also, reconfigurable microstrip antennas offer the advantages of compact size,

frequency selectivity and similar radiation pattern and gain for all designed frequency bands.

Frequency agile systems must be able to receive signals over a large frequency range and therefore, requires either wide-band or tunable antennas. However, conventional microstrip patch antennas have disadvantage of narrow bandwidth and the instantaneous bandwidth of efficient antennas is limited as they become small with respect to the wavelength. Hence, tunable narrow-band antennas can be advantageous if small efficient antennas are required to cover a large frequency range. In addition, tunable narrow-band antennas provide frequency selectivity which relaxes the requirement of the receiver filters. Frequency and polarization reconfigurable antennas extend the flexibility of a system even further.

Frequency Hopping Spread Spectrum systems switch between many different frequencies at a high rate to provide immunity to jamming, narrow-band interferers and multi-path fading. Software defined radios can be reconfigured to communicate many different protocols at different frequencies and polarizations. In Cognitive Radios, the frequency and data rate are automatically determined depending on the available spectrum at runtime. Reconfigurable antennas with stable radiation characteristics at different frequencies and polarizations offer several degrees of freedom to antenna designers. In microwave tagging systems polarization diversity antenna provides a powerful modulation scheme such as the circular polarization modulation. Therefore the main objective of this research work is to devise and analyze compact electronically reconfigurable microstrip antenna with polarization switching using simple and efficient tuning mechanisms.

1.15 Thesis organization

This thesis presents the design, fabrication and characterization of a reconfigurable compact cross patch antenna to be used at different operating frequencies and polarizations, thus reducing the complexity of implementing several antennas and circuitry for different applications. PIN diodes and varactors are used for switching. A brief introduction on microstrip antenna technology, feeding techniques, analysis and reconfiguration mechanisms are explained in Chapter 1. The motivation of the work is also included in this chapter.

Chapter 2 gives a brief review of recent developments in the field of printed antennas in a historical perspective. A comprehensive survey of the state of microstrip antenna technology is covered in the first section. A review of various dual-frequency dual-polarized microstrip antenna design techniques is given in the second section. The third section covers reconfigurable antenna techniques employed in modern communication systems, with an emphasis to frequency and polarization reconfigurable antennas using PIN diodes and varactors. Fabrication method adopted for the manufacturing of antennas is discussed in the following section. The experimental techniques used to measure the fabricated antennas are also mentioned. Electromagnetic modeling of frequency and polarization reconfigurable cross patch antennas using FEM based Ansoft's HFSS is depicted in detail.

In Chapter 3, all the experimental and theoretical investigations carried out for the analysis of frequency and polarization reconfigurable compact cross patch antenna using PIN diodes are portrayed in detail. A semi empirical design equation for the vital passive antenna structure is also discussed. The details for fabrication challenges of the antenna structure are also presented.

Chapter 4 highlights the control of the operating frequency and polarization of a cross patch antenna using reactive loading. The method consists of placing chip capacitor/varactor diodes at appropriate locations and then biasing the diodes for frequency and polarization diversity applications. The detailed experimental studies and parametric analysis are employed for the characterization of the antenna.

The step by step procedure to analyze a cross patch antenna using FDTD based numerical computation is discussed in chapter 5. The staircase approximation is employed to derive the slant edges of the X-slot. Various steps involved in the extraction of antenna parameters along with the assumptions taken in the implementation of the algorithm are also described. The predicted results are experimentally verified by fabricating and testing different printed cross patch antennas.

In the last chapter the conclusions are drawn and some recommendations are made for future designs. Design of a circularly polarized compact cross patch antenna is discussed in Appendix A. Appendix B presents design and development of broadband cross patch antenna for IEEE 802.11. a/WiMax/HiperLAN2 applications.

References

1. J. D. Kraus, *Antennas: Our Electronic eyes and ears*, Microwave journal, January 1989.
2. G. A. Deschamps, *Microstrip Microwave Antennas*, Proc. 3rd USAF Symposium on Antennas, 1953.
3. R. E. Munson, *Single Slot Cavity Antennas Assembly*, U.S. Patent No. 3713162, January 23, 1973.
4. R. E. Munson, *Conformal Microstrip Antennas and Microstrip Phased Arrays*, IEEE Trans. Antennas Propagation, Vol. AP-22, 74–78, 1974.
5. J. Q. Howell, *Microstrip antennas*, Dig. International symposium antennas propagation Society, Williamsburg, VA, 177-180, 1972.
6. J. Q. Howell, *Microstrip Antennas*, IEEE Trans. Antennas Propagation, Vol. AP-23, 90–93, 1975.
7. I. J. Bahl, and P. Bhartia, *Microstrip Antennas*, Dedham, MA: Artech House, 1980.
8. David M. Pozar, *Microstrip Antennas*, Proceedings of IEEE, vol. 80, No.1, 1992.
9. K. R. Carver and J. M. Mink, *Microstrip antenna technology*, IEEE Antennas and Propagation, Vol.29, No.1, 1981.
10. Ramesh Garg, P. Bhartia, I. J. Bhal and A. Ittipiboon, *Microstrip antenna design handbook*, Artech house, 2001.
11. J. R. James, P. S. Hall and C. Wood, *Microstrip antenna theory and design*, Peter Petergrins, 1981.
12. G. Kumar and K. P Ray, *Broadband microstrip antennas*, Artech house, 2003.

13. K. L Wong, *Compact and broadband microstrip antennas*, John wiley & sons, 2002.
14. D. M. Pozar, *A microstrip antenna aperture coupled to a microstrip line*, *Electronic Letters*, Vol-21, 49-50. 1985.
15. G. Gronau and I. Wolff, *Aperture coupling of a rectangular microstrip resonator*, *Electronic Letters*, Vol-22, 554-556, 1986.
16. D. M. Pozar, and S. D. Targonski, *Improved Coupling for Aperture-Coupled Microstrip Antennas*, *Electronics Letters*, Vol. 27, No. 13, 1129–1131, 1991.
17. V. Rathi, G. Kumar, and K. P. Ray, *Improved Coupling for Aperture-Coupled Microstrip Antennas*, *IEEE Trans. Antennas Propagation*, Vol. AP-44, No. 8, 1196–1198, 1996,.
18. J. C. MacKinchan et al., *A Wide Bandwidth Microstrip Sub-Array for Array Antenna Application Using Aperture Coupling*, *IEEE AP-S Int. Symp. Digest*, 878–881, 1989.
19. D. M. Pozar and B. Kaufman, *Increasing bandwidth of a microstrip antenna by proximity coupling*, *Electronic Letters*, Vol-23, 368-369, 1987.
20. J. S. Roy et al., *Some Experimental Investigations on Electromagnetically Coupled Microstrip Antennas on Two Layer Substrate*, *Microwave Optical Tech. Letters*, Vol. 4, No. 9, 236–238, 1991.
21. W. Menzel and W. Grabherr, *Microstrip Patch Antenna with Coplanar Feed Line*, *IEEE Microwave and Guided Wave Letters*, Vol. 1, No. 11, 340–342, 1991.
22. R. L. Smith and J. T. Williams, *Coplanar Waveguide Feed for Microstrip Patch Antenna*, *Electronics Letters*, Vol. 28, No. 25, 2272–2274, 1992.

23. A. K. Bhattacharya and R. Garg, *Generalized Transmission Line Model for Microstrip Patches*, IEE Proc. Microwaves, Antennas Propagation, Pt. H, Vol. 132, No. 2, 93–98, 1985.
24. G. Dubost and G. Beauquet, *Linear Transmission Line Model Analysis of a Circular Patch Antenna*, Electronics Letters, Vol. 22, 1174–1176, 1986.
25. S. Babu, I. Singh, and G. Kumar, *Improved Linear Transmission Line Model for Rectangular, Circular and Triangular Microstrip Antennas*, IEEE AP-S Int. Symp. Digest, 614–617, 1997.
26. Y. T. Lo, D. Solomon and W. F. Richards, *Theory and experiments on microstrip antennas*, IEEE Transactions on Antennas and propagation, Vol-AP-27, 137-145, 1979.
27. W. F. Richards, Y. T. Lo and D. Solomon, *An improved theory for microstrip antennas and applications*, IEEE Transactions on Antennas and propagation, Vol-AP-29, 38-46, 1981.
28. T. Okoshi and T. Miyoshi, *The Planar Circuit—An Approach to Microwave Integrated Circuitry*, IEEE Trans. Microwave Theory Tech., Vol. 20, 245–252, 1972.
29. K. C. Gupta and P. C. Sharma, *Segmentation and Desegmentation Techniques for the Analysis of Two Dimensional Microstrip Antennas*, IEEE AP-S Int. Symp.Digest, 19–22, 1981.
30. E. H. Newman and P. Tulyathan, *Analysis of Microstrip Antennas Using Method of Moments*, IEEE Trans. Antennas Propagation, Vol. AP-29, 47–53, 1981.
31. P. Silvester, *Finite Element Analysis of Planar Microwave Network*, IEEE Trans.Microwave Theory Tech., Vol. MTT-21, 104–108, 1973.

32. T. Itoh and W. Menzel, *A Full-Wave Analysis Method for Open Microstrip Structure*, IEEE Trans. Antennas Propagation, Vol. AP-29, 63–68, 1981.
33. D. M. Pozar, *Radiation and scattering from a microstrip patch on a uniaxial substrate*, IEEE Transactions on antennas and propagation, Vol-AP-35, 613-621, 1987.
34. M. D. Deshpande and M. C. Bailey, *Input impedance of microstrip antennas*, IEEE Transactions on antennas and propagation, Vol-AP-30, 645-650, 1982.
35. J. R. Mosig and F. E. Gardiol, *A dynamic radiation model for microstrip structures*, Advances in electronics and electron physics, Vol-59, 139-234, 1982.
36. A. Taflove, *Computational electrodynamics, Finite difference time domain method*, Artech house, MA, 1995.
37. R. Waterhouse, *Small microstrip patch antenna*, Electron. Lett. 31, 604–605, 1995.
38. S. Dey and R. Mittra, *Compact microstrip patch antenna*, Microwave Opt. Technol. Lett. 13, 12–14, 1996.
39. K. L. Wong and S. C. Pan, *Compact triangular microstrip antenna*, Electron. Lett. 33, 433–434, 1997.
40. K. L. Wong, C. L. Tang, and H. T. Chen, *A compact meandered circular microstrip antenna with a shorting pin*, Microwave Opt. Technol. Lett. 15, 147–149, 1997.
41. C. K. Wu, K. L. Wong, and W. S. Chen, *Slot-coupled meandered microstrip antenna for compact dual-frequency operation*, Electron. Lett. 34, 1047–1048, 1998.

42. J. H. Lu and K. L. Wong, *Slot-loaded, meandered rectangular microstrip antenna with compact dual-frequency operation*, Electron. Lett. 34, 1048–1050, 1998.
43. J. George, M. Deepukumar, C. K. Aanandan, P. Mohanan, and K. G. Nair, *New compact microstrip antenna*, Electron. Lett. 32, 508–509, 1996.
44. H. Iwasaki, *A circularly polarized small-size microstrip antenna with a cross slot*, IEEE Trans. Antennas Propagat. 44, 1399–1401, 1996.
45. K. L. Wong and Y. F. Lin, *Circularly polarized microstrip antenna with a tuning stub*, Electron. Lett. 34, 831–832, 1998.
46. J. S. Kuo and K. L. Wong, *A compact microstrip antenna with meandering slots in the ground plane*, Microwave Opt. Technol. Lett. 29, 95–97, 2001.
47. K. L. Wong and Y. F. Lin, *Small broadband rectangular microstrip antenna with chip resistor loading*, Electron. Lett. 33, 1593–1594, 1997.
48. S. A. Long and M. D. Walton, *A dual frequency stacked circular disc antenna*, IEEE Trans. Antennas Propag., Vol. AP-27, 1281-1285, 1979.
49. J. S. Dahele, K. F. Lee and D. P. Wong, *Dual frequency stacked annular ring microstrip antenna*, IEEE Trans. Antennas Propag., Vol. AP-35, 137-145, 1987.
50. J. Wang, R. Fralich, C. Wu and L. Litva, *Multifunctional aperture coupled stack antenna*, Electronics Letters, 26, 2067-2068, 1990.
51. W. F. Richards, S. E. Davidson and S. A. Long, *Dual band reactively loaded microstrip antenna*, IEEE Trans. Antennas Propag., Vol. AP-33, 556-560, 1985.

52. S. Maci and G. Biffi Gentili, *Dual-frequency patch antennas*, IEEE Antennas Propagat. Mag. 39, 13–20, 1997.
53. J. S. Chen and K. L. Wong, *A single-layer dual-frequency rectangular microstrip patch antenna using a single probe feed*, Microwave Opt. Technol. Lett. 11, 83–84, 1996.
54. J. T. Bernhard, *Reconfigurable antennas*, Morgan and Claypool, 2007.
55. Boti, M., Dussopt, L., and Laheurte, J.-M., *Circularly polarized antenna with switchable polarization sense*, Electronics Letters, vol. 36, 1518–1519, 2000.
56. F. Yang and Y. Rahmat-Samii, *Patch antennas with switchable slots (PASS) in wireless communications: Concepts, designs, and applications*, IEEE Antennas and Propagation Magazine, vol. 47, 13–29, 2005.
57. D. H. Schaubert et al, *Microstrip antennas with frequency agility and polarization diversity*, IEEE Trans. Antennas Propag., Vol. AP-29, 118–121, 1981.
58. J. S. Dahele and K. F. Lee, *Theory and experiment on microstrip antennas with air gaps*, IEE proc., Vol.132, 455-460, 1985.



REVIEW OF LITERATURE AND METHODOLOGY

Contents

- 2.1 Microstrip antenna technology
 - 2.2 Dual- frequency microstrip antennas
 - 2.3 Reconfigurable antennas
 - 2.5 Antenna fabrication
 - 2.6 Excitation Technique
 - 2.7 Antenna measurement facilities
 - 2.8 Measurement of Antenna characteristics
-

This chapter presents the results of previous investigative works, as well as the literature of the antenna structure in a historical perspective. A comprehensive survey of the state of microstrip antenna technology is covered in the first section. A review of various reconfigurable antenna techniques employed in modern communication systems, with an emphasis to frequency and polarization reconfigurable antennas using PIN diodes and varactors are discussed in the following section. The simulation, fabrication and measurement procedures utilized for characterizing the antennas are discussed in the next section. The antenna simulation studies and parametric analysis are carried out using Ansoft High Frequency Structure Simulator (HFSS). The prototype of the different antenna geometries were fabricated using photolithographic process and measurements are carried out at our test facility consisting of vector network analyzer and anechoic chamber. The chapter concludes with a concise description of the measurement techniques employed to analyze the experimental results.

2.1 Microstrip antenna technology

The present research in printed antenna technology points to the development of antennas which cater the need of low profile, compact communication gadgets. The antenna designers around the world are concentrated in the design of compact antennas with efficient radiation characteristics. The following modules provide a comprehensive survey about the developments in the state of art printed antenna technology around the world. This section provides a comprehensive survey of the state of microstrip antenna technology.

Even though G. A. Deschamps, USA first proposed the concept of a microstrip radiator in 1953 [1], Gutton and Baissinot in France [2] acquired a patent in 1955. However, work was not reported in the literature until the early 1970s, when a conducting strip radiator separated from a ground plane by a dielectric substrate was described by Byron [3]. The first practical antennas were developed by Howell [4]. Yoshimura *et al.* proposed a microstrip line slot antenna and a two-dimensional Dolph-Chebyshev slot-array antenna at X-band frequency [5]. Microstrip line slot antennas appear to be quite useful in various fields of application because of their savings in cost, size and weight. Microstrip antennas constitute a new class of omni-directional antenna for missiles and satellites. These antennas are capable of producing nearly perfect omni-directional coverage. A new low- cost low profile flat microstrip arrays by Munson [6-8] has 90-percent aperture efficiency. Design procedures for both linear and circular polarized antennas from UHF through C band were published by Howell [9].

Derneryd derived an equivalent network for square and rectangular shaped microstrip radiating elements [10]. The resonant frequency in analytical

form for a planar, circular disc antenna which is etched on a printed-circuit board so that the low-profile antenna is separated from the ground plane only by a thin layer of dielectric material was derived by L. C Shen *et al.* [11]. The formula is found to have an error of less than 25 percent when compared with experimental data. James *et al.* proposed a new design technique for linear microstrip microwave arrays [12]. Open-circuit terminations on half-wavelength stubs form the radiating elements. The usefulness of the new design technique has been demonstrated for both resonant and travelling-wave elements and ancillary problems, involving radomes, corporate feeds and the novelty of being able to direct the beam to broadside in the travelling-wave antenna. Another method to analyze a microstrip antenna is presented by Pradeep *et al.* [13]. It involves representing the antenna by a fine wire grid immersed in a dielectric medium and then using Richmond's reaction formulation to evaluate the piecewise sinusoidal currents on the wire grid segments. The calculated results are then modified to account for the finite dielectric discontinuity. A comparison of calculated and measured results was presented. This technique will serve as an excellent tool to design microstrip antennas. Theoretical and experimental works on the radiation characteristics of microstrip antennas have been done at microwave frequencies by Chatterjee *et al.* [14] and Lewin [15]. A method for altering the resonant length of a square microstrip antenna was described by Chowdhury *et al.* [16].

The relevant analysis and computations have been carried out to propose a possibility of realizing a microstrip antenna having comparatively smaller dimensions and larger bandwidth. The theoretical modeling of the microstrip antennas was carried out by Derneryd [17]. The input impedance as a function of the feed point is calculated by considering the element as a line resonator with the open-circuited terminations modeled as an RC network. From a

radiation point of view the element is treated as two narrow slots, one at each end of the line resonator. The interaction between the two slots is considered by defining a mutual conductance. From the far fields, the directivity of a patch and the mutual conductance between patches are calculated. The analysis of the pattern and impedance loci of microstrip antennas developed by Richards *et al.* yields a theory that is simple and inexpensive to apply [18]. This is achieved by lumping all antenna losses into an effective dielectric loss tangent and then analysing the microstrip antenna as a lossy cavity. It is found that the resulting expression for impedance of the microstrip antenna is in good agreement with measured results for all modes and feed locations.

Krali *et al.* developed an omni microstrip antenna which is a microstrip-shorted quarter-wave resonator that is wrapped around a cylinder [19]. It is an electrically short antenna, and it can be made to radiate an omnidirectional pattern normal to the axis of the cylinder. Equations governing the design of the antenna are given along with a method of excitation. Lo *et al.* in 1979 developed a simple theory based on the cavity model to analyze microstrip antennas [20]. In general the theoretically predicted radiation patterns and impedance loci closely agree with those measured for many antennas of various shapes and dimensions investigated. In fact, this theory enables the computation of both patterns and impedance loci with little effort. The input admittance locus generally follows a circle of nearly constant conductance, but its center is shifted to the inductive region in the Smith chart plot. Peculiar properties for the case with degenerate or slightly degenerate eigen values are discussed. An accurate formula for determining the resonant frequency of a rectangular microstrip antenna is also given. Many variations of this method have been used to analyze the microstrip antenna [21-23].

The numerous advantages of microstrip antenna, such as its low weight, small volume, and ease of fabrication using printed-circuit technology, led to the design of several configurations for various applications [24-25]. With increasing requirements for personal and mobile communications, the demand for smaller and low-profile antennas has brought the microstrip antenna to the forefront. Microstrip antennas have narrow bandwidth, typically 1–5%, which is the major limiting factor for the widespread application of these antennas. Increasing the bandwidth of microstrip antennas has been the major thrust of research in this field [26-32]. The microstrip antenna can be excited directly either by a coaxial probe or by a microstrip line. It can also be excited indirectly using electromagnetic coupling or aperture coupling and a coplanar waveguide feed, in which case there is no direct metallic contact between the feed line and the patch [33-36]. Feeding technique influences the input impedance and characteristics of the antenna, and is an important design parameter.

The regular microstrip antenna configurations, such as rectangular and circular patches have been modified to rectangular ring [42] and circular ring [43], respectively, to enhance the bandwidth. The larger bandwidth is because of a reduction in the quality factor Q of the patch resonator, which is due to less energy stored beneath the patch and higher radiation. When a U-shaped slot is cut inside the rectangular patch, it gives a bandwidth of approximately 40% for $VSWR \leq 2$ [44]. Similar results are obtained when a U-slot is cut inside a circular or a triangular microstrip antenna [45-46].

2.2 Dual- frequency microstrip antennas

Dual-frequency planar antennas should operate with similar features, both in terms of radiation and impedance matching, at two separate frequencies. Obtaining these features by using planar technologies is not a straightforward

matter, particularly when the intrinsic structural and technological simplicity of patch antennas is to be preserved. Dual-frequency patch antennas may provide an alternative to large-bandwidth planar antennas, in applications in which large bandwidth is really needed for operating at two separate transmit-receive bands. When the two operating frequencies are far apart, a dual-frequency patch structure can be conceived to avoid the use of separate antennas. Dual-frequency antennas exhibit a dual-resonant behavior in a single radiating structure.

Modern communication systems, such as GPS, vehicular, as well as emerging applications such as wireless local networks (WLAN), often require antennas with compactness and low-cost, thus rendering planar technology useful, and sometimes unavoidable. Furthermore, thanks to their lightness, patch antennas are well suitable for systems to be mounted on airborne platforms, like synthetic-aperture radar (SAR) and scatterometers. From these applications, a new motivation is given for research on innovative solutions that overcome the bandwidth limitations of patch antennas. In applications in which the increased bandwidth is needed for operating at two separate sub-bands, a valid alternative to the broadening of total bandwidth is represented by dual-frequency patch antennas. Despite the convenience that they may provide in terms of space and cost, little attention has been given to dual-frequency patch antennas. This is probably due to the relative complexity of the feeding network which is required, in particular for array applications. An excellent review of dual frequency microstrip antennas was given by S. Maci and Biffi Gentili in the year 1997 [47-48].

Wang and Lo were the first to use shorting pins and slots in a rectangular microstrip patch to generate dual frequency operation. The upper and lower frequencies showed similar broadside radiation characteristics. In 1987, J. S.

Dahele *et al.* presented experimental results of a dual-frequency microstrip antenna [49] consisting of two stacked annular rings of outer radii 5 cm and inner radii 2.5 cm fabricated on a duroid substrate with relative permittivity 2.32 and thickness 0.159 cm. The separations of the two resonant frequencies range from 6.30-9.36 percent for the first three modes. The frequency separations can be altered by means of an adjustable air gap between the lower ring and the upper substrate. A novel microstrip antenna has been proposed by C. S. Lee *et al.* to operate at dual frequencies [50]. The non-radiating edges of a microstrip patch are closed with a conducting foil. Resonant frequencies are altered by varying the air gap under the patch. The separation of the resonant frequencies can be nearly zero and has no upper limit in principle. The input impedance is easily matched by shifting the air gap. The radiation patterns are not affected by modification for dual-frequency operation.

If two orthogonal polarizations at separate frequencies are required, the simplest antenna for this is a rectangular patch fed at the diagonal for exciting the (1, 0) and (0, 1) modes. The frequencies of these modes are determined by the respective lengths of the patch. Impedance matching for these two resonant frequencies can be easily achieved with a single feed. Salvador *et al.* [51], proposed a new configuration of dual frequency planar antenna operating at S and X bands. They used a cross patch sub array and the geometry had two symmetric planes to provide radiation in double-linear polarization by using a proper feeding system. Dual-frequency operation of a triangular microstrip antenna is proposed by S. C. Pan *et al.* using a shorting pin and fed by a single probe feed [52]. By varying the shorting-pin position in the microstrip patch, such a design can provide a large tunable frequency ratio of about 2.5–4.9 for the two operating frequencies. K. L. Wong and G. B. Hsieh [53] suggested a dual frequency circular microstrip antenna with a pair of arc shaped slots

excited with a single co-axial feed. Frequency ratio ranging from 1.38 to 1.58 were implemented and studied. A slot loaded bow-tie microstrip antenna for dual frequency operation was proposed by K. L. Wong and W. S. Chen [54]. Frequency ratios within the range 2 to 3 were obtained with a single probe feed. A single probe fed dual frequency rectangular microstrip antenna with a square slot at its center is demonstrated by Chen [55]. This was one of the simplest methods of dual frequency generation in a rectangular patch with linear orthogonal polarization. A compact dual band dual polarization microstrip patch antenna for terrestrial cellular communication and satellite mobile was developed by E. Lee *et al.* [56]. The two operating frequencies showed different polarization with bandwidths of 2 and 4% respectively. J. H. Lu demonstrated a rectangular microstrip patch antenna [57] with embedded spur lines and an equilateral triangular microstrip antenna [58] for dual frequency operation. The two operating frequencies had the same polarization planes and frequency ratios 1.1 to 1.6 were achieved with a single feed.

A dual band slot loaded short circuited patch antenna was proposed by Guo *et al.* [59]. By controlling the shorting plane width, the two resonant frequencies can be significantly reduced and the frequency ratio was tunable in the range 1.6 to 2.2. J. H. Lu [60] proposed a slot loaded dual frequency rectangular microstrip antenna with a single feed. By varying the angle and the horizontal length of the bent slots, the frequency ratio was tunable in a range from 1.28 to about 1.79. M. Yang *et al.* analyzed and optimized the electric performance of a U-shaped dual-frequency single feeding port planar inverted-F microstrip antenna [61-62] for mobile communication applications in both the GSM and DCS 1800 systems by means of the generalized non-uniform finite-difference time-domain (NU-FDTD) Maxwell's solver.

G. S. Binoy *et al.* [63] proposed a slot coupled chip capacitor loaded square microstrip patch antenna for dual frequency operation. This design provides an enhanced area reduction of 64% and 36% respectively, for the two operating frequencies with good cross polarization levels. A dual-frequency electric–magnetic– electric (EME) microstrip [64] exhibiting two leaky-wave regions of similar radiation characteristics like the microstrip patch is proposed by Y. C. Chen *et al.* The EME microstrip incorporates a photonic band gap (PBG) structure, which is a two-dimensional array consisting of unit cell made of coupled coils connected by via. The PBG structure employed in the EME prototype conducts at dc and shows the first stop band between 8.8–12.4 GHz, thus rendering the so-called magnetic surface. The EME microstrip is essentially made by substituting the PBG cells for the metal strip of a conventional microstrip. The finite-element method (FEM) analyses of the PBG structure show that the first and second modes are TM-like and TEM-like, respectively. The latter is leaky between 12.4–12.9 GHz and is found to be responsible for the second leaky region of the EME microstrip. The dispersion characteristics of the EME microstrip are obtained by two theoretical methods, namely, the matrix-pencil method and the FEM. Both show excellent agreement in the two leaky regions.

Jen-Yea Jan demonstrated a novel dual-frequency design of a single-layer single-feed circular microstrip antenna with an offset open-ring slot [65]. By selecting a suitable radius of the circular patch enclosed by this offset open-ring slot, a dual-frequency operation with its two operating modes excited with the same polarization planes is obtained. The frequency ratio of the two frequencies is within a range of about 1.22 to 2.17. The measured results show that similar broadside radiation patterns are obtained and the variations of antenna gain are small for frequencies within the two resonant modes. Since the

Global Positioning System (GPS) has been launched, significant progress has been made in GPS receiver technology but the multipath error remains unsolved. As solutions based on signal processing are not adequate, the most effective approach to discriminate between direct and multipath waves is to specify new and more restrictive criteria in the design of the receiving antenna. An innovative low profile, lightweight dual band GPS radiator with a high multipath-rejection capability is presented by L. Boccia *et al.* The proposed solution has been realized by two stacked shorted annular elliptical patch antennas [66]. J. Anguera *et al.* proposed a triple-frequency antenna combining a dual-band and a single band antenna with broadside radiation patterns [67]. The dual-band antenna is inspired in the Sierpinski fractal. Such a dual-band antenna is stacked over a single band antenna. The antenna presents a broadband behavior at each band thanks to parasitic patches. The antenna has been designed using a MoM commercial code and has been experimentally tested, obtaining three bands with a broad bandwidth, high efficiency, and similar radiation patterns.

Yahya Rahmat-Samii developed a novel compact and light-weight dual-frequency, dual linearly polarized, high-efficiency, stacked-patch microstrip-array antenna for use in standalone aircraft-based remote sensing applications [68]. The sixteen-element stacked-patch array antenna optimized for center frequencies of 1.26 GHz and 1.413 GHz with 10 MHz and 25 MHz bandwidths in each band, respectively. Due to the large number of design parameters and demanding design requirements of beam-efficiency, side lobe levels, and polarization characteristics, particle-swarm optimization (PSO) and Finite-Difference Time-Domain (FDTD) simulations were used for synthesis and analysis. Cancellation techniques, based on symmetry, were applied to the antenna ports, with a custom-built feed network to reduce cross polarization.

Simulations and measurement results from a spherical near-field test facility confirmed excellent performance of the array configuration, with a beam efficiency of greater than 90%, isolation better than -35 dB, and cross polarization in the main beam of the array better than -40 dB.

Xiulong Bao *et al.* [69] used a single layer annular slot antenna to achieve dual-frequency and dual-sense circular-polarization by adjustment of the key antenna parameters, which are the inner and outer radii of annular-slot, the length of the four additional linear slots spurred from the annular slot and the length of microstrip feed line. The proposed antenna can provide broad impedance bandwidth and axial-ratio bandwidth. The right-hand circular polarization and left-hand circular polarization performance is realized simultaneously, for the first and second frequency, respectively. The proposed slot antenna can find useful application in indoor wireless communication systems and in satellite navigation systems.

2.3 Reconfigurable antennas

Reconfigurable antennas have become more attractive with the increased demand for multiband antennas. They provide more levels of functionality to a system by eliminating the need for complicated wideband antenna solutions. Common antenna designs not involving reconfigurability impose restrictions on the system performance because of their fixed structure. Reconfiguring antennas can enhance their performance by providing the ability to adapt to new operating scenarios.

There are several methods that rely on geometry reconfiguration for the tuning of the operating frequency of a particular antenna design, including varactor and PIN diodes, and the use of optically activated switches by fiber optic cables [70-73]. Many antennas have been designed to maintain their

radiation characteristics by using self-similar structures, while changing the aperture dimensions for a different operating frequency [71]. Other design consists of using a linear dipole antenna that is shortened to a specific length to operate at a higher frequency [72]. In the reconfigurable dipole case the radiation pattern stays the same because the antenna current distribution will be the same relative to the wavelength of the resonant frequency. Some reconfigurable antenna applications change the radiation pattern but maintain the same resonant frequency [73]. This concept can enhance a system's ability to null jamming, or undesirable noise sources by directing the energy to the intended user.

The challenge faced by antenna designers is that the reconfiguration of one property, for example, frequency response, will have an impact on radiation characteristics. Likewise, reconfigurations that result in radiation pattern changes will also alter the antenna's frequency response. This linkage is not desirable among antenna developers, which usually prefer the characteristics to be separable.

2.3.1 Reconfigurability Concept

The concept of reconfigurable antennas refers to a change in the frequency characteristics, radiation pattern, impedance bandwidth, and/or polarization of an antenna by changing its aperture dimensions or geometry through electrical or mechanical means. By tuning the operating frequency, the antenna could be used to filter signals interfering with the communication or simply to change operating frequency band [74].

2.3.2 Frequency Reconfigurability

Antennas with reconfigurable frequency response (also known as tunable antennas) can either switch abruptly from one frequency band to another or continuously perform this task. The frequency response reconfigurability is achieved by actively controlling the effective electrical length of the antenna thus enabling the antenna to operate in different frequency bands. This is usually done by adding or removing a part or parts of the antenna through electrical, mechanical, optical, or other means [71-76]. The antenna resonant frequency can also be altered by maintaining the antenna footprint but changing the radiating current path [77].

2.3.3 Radiation Pattern Reconfigurability

The radiation pattern reconfigurability is needed to steer the radiation pattern away from noise sources or to reduce interference. To reconfigure the radiation pattern, some researchers have used shorting pins and in-line open tuning elements [78]. Possible applications for this type of antennas are in phased antenna arrays in wide-angle scanning. There are methods to change radiation patterns independently from frequency behavior. One of these methods is the use of electrically tuned or switched parasitic elements. This method provides isolation of the driven element from the tuned element or elements, potentially wide frequency bandwidth, and a range of available topologies and functionalities [70]. This technique relies on the mutual coupling between closely spaced driven and parasitic elements, resulting in effective array behavior from a single feed point. Therefore, changes in radiation patterns are achieved through changes in the coupling between the elements, which, in turn, changes the effective source currents on both the driven and parasitic elements.

2.3.4 RF-MEMS Based Reconfigurable Antennas

The concept of reconfigurable RF MEMS based antenna systems was first introduced in 1998 by E. R. Brown [79] and many researchers have enthusiastically studied this area since then. In the past, the resonant frequency of the microstrip patch antenna was tuned by adjusting the effective length of the patch using varactor diodes [80]. RF MEMS switches have replaced FETs and diodes in certain applications. They have been fabricated, tested and measured against these solid state devices and were found to have few advantages for low and medium power handling applications [79, 81]. Nevertheless, the integration of RF MEMS switches hasn't been demonstrated and/or explained in depth.

Anagnostou *et al.* demonstrated the concept of reconfigurable antenna design and fabrication with self-similar fractal antennas [82]. In their design, they started by characterizing a single antenna element and then improving their design and fabrication process for achieving a multiple-frequency antenna. These antennas have the advantage of radiating similar patterns in a variety of frequency bands. Their design, feed, and performance as well as the structure and the biasing network of the used RF-MEMS switches were the primary objective of the research. They also presented the functionality of a new type of RF-MEMS based reconfigurable multiband antenna consisting on a self-similar design, and introduced an analytical procedure to be used in their antenna design. Even though their antenna design had good characteristics, its performance showed relatively shallow resonances, with respect to a return loss $S_{11} = -10$ dB, which they improved later.

The Sierpinski multiband fractal antenna was introduced in 1998 [75]. This antenna is described by an infinite number of iterations with an infinite

number of frequency bands resulting in a very complex antenna structure. Their approach was to apply low pass filters between the triangle interconnections to suppress any side-lobes that may exist after the first resonance. Most of the research regarding Sierpinski antennas has been done for a low relative permittivity structure etched on thin dielectric materials, thus approximating the free space environment. Anagnostou *et al.* also followed the principles of the Sierpinski antenna to design their own RF MEMS-based reconfigurable Sierpinski [76]. They implemented three sets of RF MEMS switches with different actuation voltages to sequentially activate and deactivate parts of a multiband Sierpinski fractal antenna. The direct actuation of the electrostatic MEMS switches was done through the RF feeding line. The antenna was fabricated over a liquid crystal polymer substrate and operates at several different frequencies between 2.4 and 18 GHz. It was the first RF MEMS reconfigurable antenna on a flexible organic polymer substrate for multiband antenna applications.

Gabriel M. Rebeiz studied the use of RF MEMS switches in microstrip patch antennas and feed structures for developing reconfigurable multiband antennas [81]. He named the design reconfigurable patch module (RPM). The RPM consists of a 3x3 array of patches connected together using MEMS switches. However, the real MEMS switches were not implemented since they were not available. Instead, they simulated the MEMS switches using ideal open and closed circuits. Their contribution is that they were able to achieve 12% impedance bandwidth for the L-band configuration and greater than 7% bandwidth at X-band, demonstrating that with the RPM the frequency was reconfigured from one band to another. Rebeiz also talks about the integration of RF MEMS switches as ideal elements for reconfigurable antennas in his

book [83]. He does a slight comparison of them against their solid state devices counterparts, FET switches and P-I-N diodes.

Jennifer T. Bernhard from University of Illinois at Urbana Champaign also performed much research on this field, implementing the concept of integrating packaged RF MEMS switches into a square spiral antenna by surface mounting techniques [84]. In their research, they modified the switch to reduce the impedance mismatch, as well as the antenna to physically and electrically accommodate the switch. An electrically active single stub matching network is included in their design, but only in one of the antenna configurations. Concurrent with this previous work, a research group from University of California at Irvine, supported by DARPA and NSF, presented a reconfigurable rectangular spiral antenna with a set of MEMS switches, which were monolithically integrated and packaged onto the same substrate [85]. This system was based on a single-arm rectangular spiral antenna, capable of changing its radiation pattern. C. W Jung *et al.* considered their design “the first truly reconfigurable printed antenna design using MEMS devices as active elements integrated in the same low loss substrate”. The effort of the proposed system was to emphasize the feasibility of MEMS switches integration into the same substrate for antenna applications

Another interesting writing from a research group at Auburn University in Alabama deals with a MEMS-based electrostatically tunable circular microstrip patch antenna [86]. They designed a tunable circular microstrip patch antenna, fabricated by using printed circuit processing techniques. The microstrip patch antenna was patterned on the top side of a Kapton polyimide film, suspended above the ground plane. The patch was inductively coupled to a coplanar waveguide feed line via a slot in the ground plane. The only drawback to this work was that for a tuning range of 270 MHz, they needed an actuation

voltage of 165V. Previously, they were able to achieve a higher frequency range using 268V [87]. This is considered a high voltage since there are many products in the market with actuation voltages below 100 V and with similar characteristics [88]. Because the substrate used was not compatible for fabricating MEMS switches they needed to treat them as packaged lumped components, and use surface mounting techniques.

A novel design of a reconfigurable slot aperture antenna consists of interleaved crossed-slot elements for dual-polarized and broadband array operation without grating lobes [89]. The dimensions of the array elements can be reconfigured by using radiofrequency switches, such as RF-MEMS switches or P-I-N diodes. The array elements along with the switches are integrated into the top layer of a multilayered composite structure consisting of passive, resistively loaded frequency selective surface (FSS) elements that form a broadband ground plane system. The analysis of the FSS slot array configuration and measurements that could serve as a reference in future developments of the FSS layered arrays was emphasized. The private industry has also seen the need for the design of reconfigurable antennas in order to reduce the complexity of an antenna system for performance over a wide frequency band [90]. A work presented in 2001 describes a reflective antenna array approach that can perform time delay beam steering by using cascaded RF-MEMS switches/coplanar strip transmission line sections. They measured the RF-MEMS switches characteristics in coplanar strip transmission line and modeled a reflected phase of five cascaded switch transmission line sections. The true-time delay switched beams were created by placing the RF-MEMS switches along the transmission lines behind the flared notch elements, where RF-MEMS switches were proposed to be the reflective elements [91]. The switches were characterized as coplanar strip elements by designing test

substrates fabricated with switches placed in both shunt and series configurations, as they used coplanar strip transmission lines to eliminate the need for a balun to microstrip line.

The MEMS switches are being researched for better radiation performance for specific applications in antenna designs. A research group in University of California at Irvine designed an air bridged RF-MEMS capacitive series switches in single pole single throw (SPST) transmission lines for reconfigurable antenna applications [92]. In their design, they analyzed the RF characteristics of the capacitive series switches, measured, and compared with coplanar waveguide and microstrip line structures. They fabricated the series switches monolithically on a glass wafer with a spiral antenna that operates at 11 GHz in order to measure the radiation characteristics of the antenna. They concluded that the use of RF-MEMS series switch shows better performance for electric field radiation of reconfigurable antenna applications. Other researchers have designed integrated systems of antennas and MEMS on the same substrate as well [85]. The main difference between [76] and [93] is the substrate used. They have proved the feasibility of RF-MEMS-based reconfigurable antennas for many applications and the research to be done in order to fulfill future communication needs.

2.4 Simulation and Optimization

The use of simulation software is essential in order to achieve our goals. The software used should facilitate the calculation of the location of the antenna's feed point, as well as the theoretical behavior of such structure. The simulation models of the investigated antennas are developed in Ansoft High Frequency Structure Simulator (HFSS). HFSS is a commercial Finite Element Method (FEM) solver for electromagnetic structures from Ansoft Corporation.

It is one of the most popular and powerful applications used for the complex RF electronic circuit elements and filters. It integrates simulation, modeling, visualization and automation in an easy to learn environment. With adaptive meshing and brilliant graphics the HFSS gives an unparalleled performance and complete insight to the actual radiation phenomenon in the antenna. With HFSS one can extract the parameters such as S, Y, and Z, visualize 3D electromagnetic fields (near- and far-field), and optimize design performance. An important and useful feature of this simulation engine is the availability of different kinds of port schemes. It provides lumped port, wave port, incident wave scheme etc. The accurate simulation of coplanar waveguides and microstrip lines can be done using wave port. The parametric set up available with HFSS is highly suitable for Antenna engineer to optimize the desired dimensions [94].

The first step in simulating a system in HFSS is to define the geometry of the system by giving the material properties and boundaries for 3D or 2D elements available in HFSS window. The suitable port excitation scheme is then given. A radiation boundary filled with air is then defined surrounding the structure to be simulated. Now, the simulation engine can be invoked by giving the proper frequency of operations and the number of frequency points. Finally the simulation results such as scattering parameters, current distributions and far field radiation pattern can be displayed. The optimization tool available with HFSS is very useful for antenna engineers to optimize the antenna parameters very accurately. There are many kinds of boundary schemes and excitation techniques available in HFSS. Radiation boundary and PEC boundary are widely used in this work. The vector as well as scalar representation of E, H and J values of the device under simulation gives a good insight in to the problem under simulation.

2.5 Antenna fabrication

Printed antennas are usually fabricated on microwave substrate materials using standard photolithographic techniques or chemical etching methods. Selection of proper substrate material is the essential part in antenna design. The dielectric constant, loss tangent, homogeneity, isotropicity and dimensional strength of the substrate all are of importance. High loss tangent substrate adversely affects the efficiency of the antenna especially at high frequencies. The selection of dielectric constant of the substrate depends on the application of the antenna and the radiation characteristics specifications. High Dielectric constant substrates cause surface wave excitation and low bandwidth performance. After the proper selection of the substrate material a computer aided design of the geometry is initially made and a negative mask of the geometry to be generated is printed on a butter paper. A single side copper cladded substrate of suitable dimension is properly cleaned using acetone and dried in order to avoid the discontinuity caused by the impurities. Any disparity in the etched structure will shift the resonant frequency from the predicted values, especially when the operating frequency is very high. A thin layer of negative photo resist material is coated using spinning technique on copper surfaces and it is dried. The mask is placed onto the photo resist and exposed to UV light. After the proper UV exposure the layer of photo-resist material in the exposed portions hardens which is then immersed in developer solution for few minutes. The hardened portions will not be washed out by the developer. The board is then dipped in the dye solution in order to clearly view the hardened photo resist portions on the copper coating. After developing phase the unwanted copper portions are etched off using Ferric Chloride (FeCl_3) solution to get the required antenna geometry on the substrate. The etched board is rinsed in running water to remove any etchant. FeCl_3 dissolves the copper parts

except underneath the hardened photo resist layer after few minutes. The laminate is then cleaned carefully to remove the hardened photo resist using acetone solution. The various steps involved in the fabrication process is illustrated in figure 2.1

To implement frequency and polarization reconfigurable microstrip antennas, a few non-linear smd components need to be integrated into the surface of the fabricated antenna. For this a high precision soldering station with temperature control is used.

2.6 Excitation Technique

To excite the resonant modes with good matching, the matching point inside the patch can be easily achieved by a proximity coupling from a microstrip feed line, which is slightly displaced from the two principal axes of the patch. The width of the microstrip line is designed for 50Ω characteristic impedance using HP AppCAD software. The optimum matching location can be easily determined by sliding the patch along the surface of the feed line. Since the characteristic impedance Z_0 is determined by the width of the microstrip line W_f and the dielectric constant of the substrate over which the feed line is fabricated. The standard design equations are

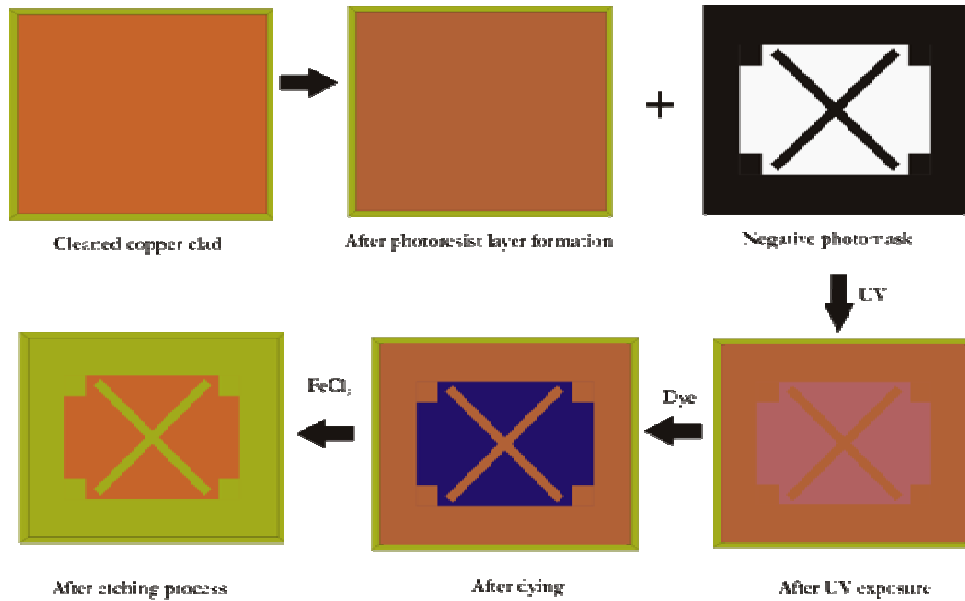


Figure 2.1 Step by step procedure involved in photolithographic process

$$Z_0 = \frac{Z}{2\pi\sqrt{\epsilon_{eff}}} \ln\left(\frac{8h}{wf} + \frac{wf}{4h}\right) \Omega \text{ when } \frac{wf}{h} \leq 1$$

$$\text{For } \frac{wf}{h} \geq 1,$$

$$Z_0 = \frac{Z}{\sqrt{\epsilon_{eff}}} \left(\frac{wf}{h} + 1.393 + 0.667 \ln\left(\frac{wf}{h} + 1.444\right) \right) \Omega$$

Where Z is the characteristic impedance of free space and h is the substrate thickness. The substrate used for the fabrication of all antennas is FR-4 substrate of dielectric constant 4.4 with height 1.6mm. For this substrate, the width W_f of the feed line corresponding to characteristic impedance 50Ω is found to be 3mm.

2.7 Antenna measurement facilities

A brief description of equipments and facilities used for the measurements of antenna characteristics is presented in this section with details of the measurement procedure.

2.7.1 HP 8510C Vector Network analyzer (VNA)

HP8510C is sophisticated equipment capable of making rapid and accurate measurements in frequency and time domain [95]. The network analyzer can measure the magnitude and phase of the S parameters. 32 bit microcontroller MC68000 based system can measure two port network parameters such as S_{11} , S_{12} , S_{22} , S_{21} and it's built in signal processor analyses the transmit and receive data and displays the results in many plot formats. The network analyzer consists of source, S parameter test set, signal processor and display unit. The synthesized sweep generator HP 83651B uses an open loop YIG tuned element to generate the RF stimulus. It can synthesize frequencies from 10 MHz to 50 GHz. The frequencies can be set in step mode or ramp mode depending on the required measurement accuracy. The antenna under test is connected to the two port S parameter test set unit, HP8514B and incident and reflected wave at the port are then down converted to an intermediate frequency of 20MHz and fed to the detector. These signals are suitably processed to display the magnitude and phase information in the required format. These constituent modules are interconnected through GPIB system bus. An in-house developed MATLAB based data acquisition system coordinates the measurements and saves the data in the text format. HP 8510C VNA is mainly used for the antenna radiation pattern measurements.

2.7.2 Agilent E8362B Precision Network Analyzer

The Agilent E8362B vector network analyzer is a member of the PNA Series network analyzer platform and provides the combination of speed and precision for the demanding needs of today's high frequency, high-performance component test requirements. The PNA Series meets these testing challenges by providing the right combination of fast sweep speeds, wide dynamic range, low trace noise and flexible connectivity. The operating frequency of the system is

from 10 MHz to 20 GHz. It has 16, 001 points per channel with < 26 μsec/point measurement speed. This analyzer is used for the reflection coefficient studies and the measurement setup along with the specifications of the PNA is depicted in figure 2.2.

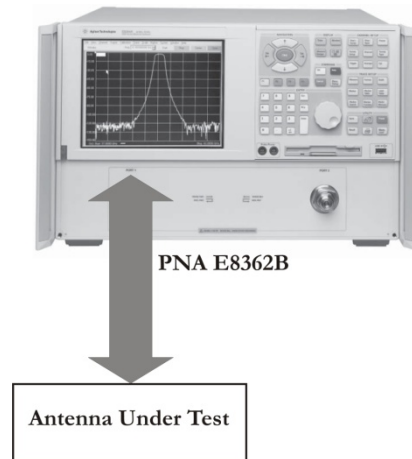


Figure 2.2 Measurement setup and PNA Specifications

Table 2.1 Specifications of PNA

Operating Band	10MHz to 10 GHz
IF Bandwidth	1Hz to 40KHz
RF Connector	3.5mm, 50 Ω
CPU	Intel Pentium 1.1 GHz
I/O ports	USB, LAN, GPIB
O/S	Windows XP
Measurement Automation Software	CREMA Soft

2.7.3 Anechoic chamber

The Anechoic chamber is an acoustic free room used to measure the antenna characteristics accurately. The room consists of microwave absorbers fixed on the walls, roof and floor to avoid EM reflections as shown in figure

2.3. High quality low foam impregnated with dielectrically / magnetically lossy medium is used to make the microwave absorber. The tapered shapes of the absorber provide good impedance matching for the microwave power impinges upon it. Aluminium sheets are used to shield the chamber to avoid electromagnetic interference from surroundings.

2.7.4 Automated turntable assembly for far field measurement

The turn table assembly kept at distance greater than $2D^2/\lambda$ consists of a stepper motor driven rotating platform for mounting the Antenna under Test (AUT). An indigenously developed microcontroller based antenna positioner STIC 310C is used for radiation pattern measurement. The AUT is used as the receiver and a standard wideband ridged horn (1-18GHz) is used as transmitting antenna for radiation pattern measurements. The main lobe tracking for gain measurement and radiation pattern measurement is done using this setup. Antenna positioner is interfaced to the computer and with the in-house developed software 'Crema Soft' automatic measurements can be carried out.



Figure 2.3 Photograph of the anechoic chamber used for the antenna measurements

2.7.5 Crema Soft: Automated antenna measurement

The user friendly software CremaSoft is built in MATLAB™ environment. The powerful instrument control toolbox of the package is used for communicating with the stepper motor control and Network Analyzer using the GPIB interface. This automated software can be used for calibration, antenna measurements and material characterization of the substrate used for the antenna design.

2.8 Measurement of Antenna characteristics

The antennas, in general, are characterized by parameters like input impedance, efficiency, gain, effective area, radiation pattern, and polarization properties [96]. The experimental procedures followed to determine the antenna characteristics are discussed in the following sections. Power is fed to the antenna from the S parameter test set of antenna through different cables and connectors. The connectors and cables will have its losses associated at higher microwave bands. Hence the instrument should be calibrated with known standards of open, short and matched loads to get accurate scattering parameters. There are many calibration procedures available in the network analyzer. Single port, full two port and TRL calibration methods are usually used. The two port passive or active device scattering parameters can be accurately measured using TRL calibration method. Return loss, VSWR and input impedance can be characterized using single port calibration method.

2.8.1 Reflection coefficient and VSWR

The reflection coefficient (Γ) at the antenna input is the ratio of the reflected voltage (current) to the incident voltage (current) and is same as the S_{11} when the antenna is connected at the port 1 of the network analyzer. It is a

measure of the impedance mismatch between the antenna and the source line. The degree of mismatch is usually described in terms of input VSWR or the return loss. The return loss (RL) is the ratio of the reflected power to the incident power, expressed in dB as

$$RL = -20\log (|\Gamma|) = -20\log (|S_{11}|) = -|S_{11}|(\text{dB})$$

The return loss characteristic of the antenna is obtained by connecting the antenna to any one of the network analyzer port and operating the VNA in S_{11}/S_{22} mode. The calibration of the port is done for the frequency range of interest using the standard open, short and matched load. The calibrated instrument including the port cable is now connected to the device under test. The frequency vs reflection parameter (S_{11}/S_{22}) values is then stored on a computer using the 'Crema Soft' automation software.

The frequency corresponding to return loss minimum is taken as resonant frequency of the antenna. The range of frequencies for which the return loss value is within the -10dB points is usually treated as the bandwidth of the antenna. The antenna bandwidth is usually expressed as percentage of bandwidth, which is defined as

$$\%Bandwidth = \frac{bandwidth}{centre\ frequency} * 100$$

The voltage standing wave ratio (V SWR) is the ratio of the voltage maximum to minimum of the standing wave existing on the antenna input terminals. A well-matched condition will have return loss of 15dB or more. A VSWR equal to 2 gives a return loss of $\approx 10\text{dB}$ and it is set as the reasonable limits for a matched antenna.

2.8.2 Antenna Gain

Antenna gain is the ratio of the intensity of an antenna's radiation in the direction of strongest to that of a reference antenna when both the antennas are fed by the same input power. If the reference antenna is an isotropic antenna, the gain is often expressed in units of dBi. The gain of the antenna is a passive phenomenon - power is not added by the antenna, but redistributed to provide more radiated power in certain directions than would be transmitted by an isotropic antenna.

The gain of the antenna under test is measured using the gain transfer method [96-97]. This method uses two standard wide band ridged horn antennas and the AUT. One of the antennas whose gain chart is available is chosen as the reference antenna (G_{ref} (dBi)). The reference antenna is placed in the antenna positioner and boresighted. THRU calibration is made for the frequency range of interest. Standard antenna is then replaced by the AUT and the transmission coefficient S_{21} (dB) is recorded. Note that the AUT should be aligned so that the gain in the main beam direction is measured. This is the relative gain of the antenna with respect to the reference antenna. The absolute gain of the antenna is obtained by adding this relative gain to the original gain of the standard antenna, provided by the manufacturer.

2.8.3 Radiation Pattern

The measurement set up is illustrated in figure 2.4. The radiation pattern of an antenna is graphical representation of its radiation properties as a function of the space coordinates. This assumes a three dimensional (3-D) pattern. Because of the limits set by the practical measurement setup for measuring the 3-D pattern, usually patterns are measured in the two principal coordinate planes (YZ and XZ) for antennas with omni-directional patterns. The far field

patterns are measured at a distance $d > 2D^2/\lambda$, where D is the largest dimension of the antenna and λ is the smallest operating wavelength.

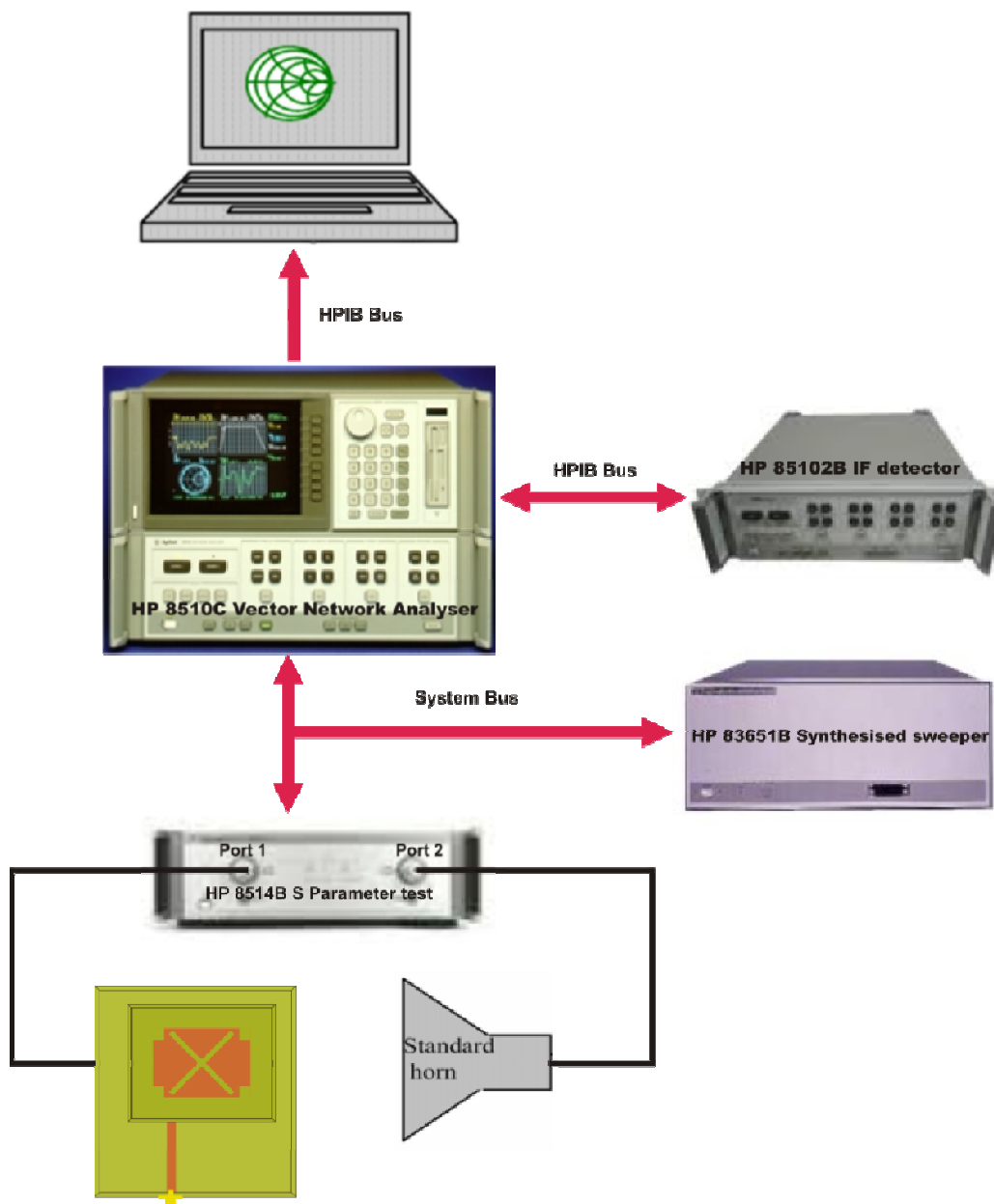


Figure 2.4 Radiation Pattern Measurement Setup

The measurement of far field radiation pattern is conducted in an anechoic chamber or using the time gating facility of Vector Network Analyzer HP8510C to ensure a reflection free environment. The AUT is placed in the quiet zone of the chamber on a turn table and connected to one port of the network analyzer. A wideband horn is used as a transmitter and connected to the other port of the network analyzer. The turn table is controlled by a STIC positioner controller. The automated radiation pattern measurement process is coordinated by the '*Crema Soft*' software in the remote computer.

In order to measure the radiation pattern, the network analyzer is kept in S_{21}/S_{12} mode with the frequency range within the -10dB return loss bandwidth. The number of frequency points is set according to the convenience. The start angle, stop angle and step angle of the motor is also configured in the '*Crema Soft*'. The antenna positioner is boresighted manually. Now the THRU calibration is performed for the frequency band specified and saved in the CAL set. Suitable gate parameters are provided in the time domain to avoid spurious radiations if any. The *Crema Soft* will automatically perform the radiation pattern measurement and store it as a text file.

References

1. G.A Deschamps, *Microstrip microwave antennas*, 3rd USAF Symposium on Antennas, 1953.
2. H. Gutton and G. Baissinot, *Flat aerial for Ultra high frequencies*, French patent, No. 70313, 1955.
3. E. V Byron, *A New flush mounted antenna element for phased array applications*, Proceedings of phased array antenna symposium, 1970, pp. 187-192.
4. J. Q. Howell, *Microstrip antennas*, IEEE AP-S International Symposium Digest, 1972, pp. 177-180.
5. Y. Yoshimura, *A micristrip line slot antenna*, IEEE Transactions on Microwave theory and techniques, November 1972, pp. 760-762.
6. R.E. Munson, *Single slot cavity antennas assembly*, US patent No. 3713162, January 23, 1973.
7. R.E. Munson, *Conformal Microstrip antennas and microstrip phased arrays*, IEEE Trans. On Antennas and propagation, Vol. Ap-22, 1974, pp. 74-78.
8. C. W. Garwin, R. E. Munson, L. T. Ostwald and K. G. Schroder, *Low profile electrically small missile base mounted microstrip antennas*, int. symposium Antennas propagation society, Urbana, IL, June, 1975, pp.244-247.
9. J. Q. Howell, *Microstrip antennas*, IEEE Tran. On antennas and propagation, January 1975, pp.90-93.
10. A. G. Derneryd, *Linearly polarized microstrip antennas*, IEEE Tran. On antennas and propagation, November 1976, pp. 846-851.

11. L. C Shen, S. A. Long, M. R. Allerdind and M. D. Walton, *Resonant frequency of a circular disc, printed circuit antenna*, IEEE Tran. On antennas and propagation, July 1977, 595-596.
12. J. R. James and P. S. Hall, *Microstrip antennas and arrays: new array design technique*, Microwaves, optics and acoustics, September 1977, Vol. 1, No. 5.
13. Pradeep K. Agarwal and M. C. Bailey, *An analysis technique for microstrip antennas*, IEEE Tran. On antennas and propagation, Vol. AP-25, No.6 November 1977.
14. R. Chatterjee and Nethaji S. Ganesan, *Microstrip antennas at microwave frequencies*, IEE-IERE proceedings, India, May-june 1977, pp. 103-110.
15. L. Lewin, *Spurious radiation from microstrip*, Proceedings of IEE, Vol.125, No.7, July 1978.
16. S. K. Chowdhury, A. K. Bandyopadhyay, T. Bhattacharyya and M. N. Roy, *Resonant length of a linearly polarized microstrip radiator*, Electronic letters, August 1978, No.18, pp. 594-595.
17. A. G. Derneryd, *A theoretical investigation of the rectangular microstrip antenna element*, IEEE Transactions on antennas and propagation, Vol. AP-26, No.4, July 1978, pp.532-535.
18. W. F. Richards, Y. T. Lo and D. D. Harrison, *Improved theory for microstrip antennas*, Electronic letters, January 1979, Vol.15, No.2, pp. 42-44.
19. A. D. Krali, J. M. McCorkle, J. F. Scarzello and A. M. Syeles, *The omni microstrip antenna: A new small antenna*, IEEE transactions on antennas and propagation, Vol. Ap-27, No.6, November 1979, pp.850-853.

20. Y. T. Lo, D. Solomon and W. F. Richards, *Theory and experiment on microstrip antennas*, IEEE transactions on antennas and propagation, Vol. AP-27, No.2, March 1979, pp.137-145.
21. A. K. Bhattacharya, and R. Garg, *Generalized Transmission Line Model for Microstrip Patches*, IEE Proc. Microwaves, Antennas Propagation, Pt. H, Vol. 132, No. 2, 1985, pp. 93–98.
22. G. Dubost, and G. Beauquet, *Linear Transmission Line Model Analysis of a Circular Patch Antenna*, Electronics Letters, Vol. 22, October 1986, pp. 1174–1176.
23. S. Babu, I. Singh, and G. Kumar, *Improved Linear Transmission Line Model for Rectangular, Circular and Triangular Microstrip Antennas*, IEEE AP-S Int. Symp. Digest, July 1997, pp. 614–617.
24. I. J. Bahl and P. Bhartia, *Microstrip antennas*, Artech house, Dedham, MA, 1980.
25. K. R. Carver, and J. W. Mink, *Microstrip Antenna Technology*, IEEE Trans.Antennas Propagation, Vol. AP-29, January 1981, pp. 2–24.
26. J. R. James, P. S. Hall and C. Wood, *Microstrip antennas: Theory and design*, Peter Peregrinus, London, UK, 1981.
27. J. R. James, P. S. Hall, C. Wood and A. Henderson, *Some recent developments in microstrip antenna design*, IEEE transactions on antennas and propagation, Vol. Ap-29, No.1, January 1981, pp. 124-128.
28. M. Malkomes and A. Quitmann, *microstrip circular segment antenna*, Electronic letters, March 1981, Vol. 17, No.5, pp. 198-200.
29. N. Das and J. S. Chatterjee, *Quarterwave microstrip antenna on a ferromagnetic substrate*, Electronic letters, June 1981, Vol. 17, No.13, pp. 441-442.

30. D. M. Pozar, *Microstrip Antenna Aperture-Coupled to a Microstrip Line*, Electronics Letters, Vol. 21, No. 2, 1985, pp. 49–50.
31. D. M. Pozar, and B. Kaufman, *Increasing the Bandwidth of a Microstrip Antenna by Proximity Coupling*, Electronics Letters, Vol. 23, No. 8, 1987, pp. 368–369.
32. J. R. James and P. S. Hall, *Handbook of Microstrip Antennas*, Vol. 1, London: Peter Peregrinus Ltd., 1989.
33. J. S. Roy, et al., *Some Experimental Investigations on Electromagnetically Coupled Microstrip Antennas on Two Layer Substrate*, Microwave Optical Tech. Letters, Vol. 4, No. 9, 1991, pp. 236–238.
34. D. M. Pozar, and S. D. Targonski, *Improved Coupling for Aperture-Coupled Microstrip Antennas*, Electronics Letters, Vol. 27, No. 13, 1991, pp. 1129–1131.
35. W. Menzel and W. Grabherr, *Microstrip Patch Antenna with Coplanar Feed Line*, IEEE Microwave and Guided Wave Letters, Vol. 1, No. 11, 1991, pp. 340–342.
36. R. L. Smith, and J. T. Williams, *Coplanar Waveguide Feed for Microstrip Patch Antenna*, Electronics Letters, Vol. 28, No. 25, 1992, pp. 2272–2274.
37. D. M. Pozar, *Microstrip antennas*. Proc. IEEE, Vol.80, 1992, pp.79-91.
38. V. Rathi, G. Kumar, and K. P. Ray, *Improved Coupling for Aperture-Coupled Microstrip Antennas*, IEEE Trans. Antennas Propagation, Vol. AP-44, No. 8, 1996, pp. 1196–1198.
39. R. A. Sainati, *CAD of Microstrip Antennas for Wireless Applications*, Norwood, MA: Artech House, 1996.

40. H. F. Lee, and W. Chen, *Advances in Microstrip and Printed Antennas*, New York: John Wiley & Sons, 1997.
41. C.A. Balanis, *Antenna Theory; Analysis and design*, 2nd edition, John Wiley, New York, 1997, Chap. 14.
42. Palanisamy, V., and R. Garg, *Rectangular Ring and H-Shaped Microstrip Antennas Alternative to Rectangular Patch Antennas*, Electronics Letters, Vol. 21, No. 19, 1985, pp. 874–876.
43. Chew, W. C., *A Broadband Annular Ring Microstrip Antenna*, IEEE Trans. Antennas Propagation, Vol. AP-30, September 1982, pp. 918–922.
44. Huynh, T., and K. F. Lee, *Single-Layer Single-Patch Wideband Microstrip Antenna*, Electronics Letters, Vol. 31, No. 16, 1995, pp. 1310–1312.
45. Luk, K. M., K. F. Lee, and W. L. Tam, *Circular U-Slot Patch with Dielectric Superstrate*, Electronics Letters, Vol. 33, No. 12, 1997, pp. 1001–1002.
46. Wong, K. L., and Hsu W. H., *Broadband Triangular Microstrip Antenna with U-Shaped Slot*, Electronics Letters, Vol. 33, No. 25, 1997, pp. 2085–2087.
47. S. Maci and G. Biffi Gentili, *Dual-Frequency Patch Antennas*, IEEE Antennas and Propagation Magazine, Vol. 39, No. 6, December 1997, pp.13-20.
48. B. F. Yang and Y. T Lo, *Microstrip antennas for dual-frequency operation*, IEEE Transactions on Antennas and Propagation, vol.32, May 1984, pp.938-943.

49. J. S. Dahele, K. F. Lee and D. P. Wong, *Dual-frequency stacked annular ring microstrip antenna*, IEEE Transactions on Antennas and Propagation, Vol. Ap-35, No.11, November 1987, pp. 1281-1285.
50. C. S. Lee and V. Nalbandian, *Impedance matching of a dual-frequency microstrip antenna with an air gap*, IEEE Transactions on Antennas and Propagation, Vol. 41, No.5, May 1993, pp. 680-682.
51. C. Salvador, L. Boreselli, A. Falciani and S. Maci, *Dual frequency planar antenna at S and X bands*, Electronic letters, vol.31, no.20, 1995, pp.1706-1707.
52. Shaa-Cheng. Pan and Kin-Lu Wong, *Dual frequency Triangular microstrip antenna with a shorting pin*, IEEE Transactions on Antennas and Propagation, Vol45, No.12, December 1997, pp. 1889-1891.
53. K. L. Wong and G. B. Hsieh, *Dual frequency circular microstrip antenna with a pair of arc shaped slots*, Microwave and optical technology letters, vol.19, no.5, December 1998, pp. 410-412.
54. K. L. Wong and W. S. Chen, *Slot loaded Bow-tie microstrip antenna for dual frequency operation*, Electronics Letters, vol.34, no.18, 1998, pp. 1713-1714.
55. W. Chen, *Single feed dual frequency rectangular microstrip antenna with square slot*, Electronic letters, vol.34, no.3, 1998, pp.231-232.
56. E. Lee, P.S. Hall and P. Gardner, *Compact dual band dual polarization microstrip patch antenna*, Electronic Letters, vol. 35, no. 13, 1999, pp. 1034-1036.
57. J. H. Lu and K. L. Wong, *Dual frequency rectangular microstrip antenna with embedded spur lines and integral reactive loading*, Microwave and optical technology letters, vol. 21, no. 4, 1999, pp. 272-275.

58. Jui-Han Lu, *Novel dual frequency design of single feed equilateral triangular microstrip antenna*, Microwave and optical technology letters, vol. 22, no. 2, 1999, pp. 133-136.
59. Y. X. Guo, K. M. Luk and K. F. Lee, *Dual band slot loaded short circuited patch antenna*, Electronic Letters, vol.36, no.4, 2000, pp.289-291.
60. J. H. Lu, *Slot loaded rectangular microstrip antenna for dual frequency operation*, Microwave and optical technology letters, vol.24, no.4, February 2000, pp. 235-237.
61. M. Yang and Y. Chen, *A novel U-shaped planar microstrip antenna for dual-frequency mobile telephone communications*, IEEE Transactions on Antennas and Propagation, Vol49, No. 6, June 2001, pp. 1002-1004.
62. Ming-Sze Tong, M. Yang, Y. Chen and R. Mittra, *Finite-Difference Time-Domain Analysis of a Stacked Dual-Frequency Microstrip Planar Inverted-F Antenna for Mobile Telephone Handsets*, IEEE transactions on antennas and propagation, vol. 49, no. 3, March 2001, pp.367-376.
63. G.S.Binoy, C.K. Aanandan, P. Mohanan and K. Vasudevan, *Slot coupled square microstrip antenna for compact dual frequency operation*, Microwave and optical technology letters, vol.32, no.1, January 2002, pp 7-9.
64. Yu-Chiao Chen, Ching-Kuo Wu, and Ching-Kuang C. Tzuang, *Dual-Frequency Electric–Magnetic–Electric Microstrip Leaky-Mode Antenna of a Single Fan Beam*, IEEE transactions on microwave theory and techniques, vol. 50, no. 12, December 2002, pp. 2713- 2720.
65. Jen-Yea Jan, *Single-Layer Single-Feed Dual-Frequency Circular Microstrip Antenna With an Offset Open-Ring Slot*, IEEE transactions on antennas and propagation, vol. 51, no. 10, October 2003, pp.3010-3012.

66. L. Boccia, G. Amendola, and G. Di Massa, *A Dual Frequency Microstrip Patch Antenna for High-Precision GPS Applications*, IEEE antennas and wireless propagation letters, vol. 3, 2004, pp.157-160.
67. Jaume Anguera, Enrique Martínez-Ortigosa, Carles Puente, Carmen Borja and Jordi Soler, *Broadband Triple-Frequency Microstrip Patch Radiator Combining a Dual-Band Modified Sierpinski Fractal and a Monoband Antenna*, IEEE transactions on antennas and propagation, vol. 54, no. 11, November 2006, pp.3367-3372.
68. Yahya Rahmat-Samii, Keerti S. Kona, Majid Manteghi, Simon Yueh, William J. Wilson, J Steve Dinardo, and Don Hunter, *A Novel Lightweight Dual-Frequency Dual-Polarized Sixteen-Element Stacked Patch Microstrip Array Antenna for Soil-Moisture and Sea-Surface-Salinity Missions*, IEEE Antennas and Propagation Magazine, Vol. 48, No. 6, December 2006, pp.33-46.
69. Xiulong Bao and M. J. Ammann, *Dual-Frequency Dual-Sense Circularly-Polarized Slot Antenna Fed by Microstrip Line*, IEEE transactions on antennas and propagation, vol. 56, no. 3, March 2008, pp.645-649.
70. J. T. Bernhard (University of Illinois at Urbana Champaign), *Reconfigurable Antennas*, Morgan & Claypool Publisher, pp. 5, 2007.
71. T. Kolsrud, M.-Y. Li, and K. Chang, *Dual-frequency electronically tunable CPW-fed CPS dipole antenna*, Electronics Letters, vol. 34, pp. 609-611, 1998.
72. Luxey, L. Dussopt, J.-L. Le Sonm, and J.-M. Laheurte, *Dual-frequency operation of CPW-fed antenna controlled by pin diodes*, Electron Letters., Vol. 36, pp. 2–3, 2000.

73. Panagamuwa, A. Chauraya, J. Vardaxoglou, *Frequency and Beam Reconfigurable Antenna Using Photoconducting Switches*, IEEE Transactions on Antennas and Propagation, Vol. 54, No. 2, pp. 449-454, February 2006.
74. D. E. Anagnostou, G. Zheng, L. Feldner, M. T. Chryssomallis, J. C. Lyke, J. Papapolymerou, and C. G. Christodoulou, *Silicon-etched reconfigurable self-similar antenna with RF-MEMS switches*, in Proc. Antennas and Propagation Society Symposium, vol. 2, pp. 1804–1807, Jun. 20–25, 2004.
75. C. Puente-Baliarda, J. Romeu, R. Pous, and A. Cardama, *On the behavior of the Sierpinski multiband fractal antenna*, IEEE Transactions on Antennas and Propagation, vol. 46, no. 4, pp. 517–524, Apr. 1998.
76. D. E. Anagnostou, *et al.*, *Design, fabrication, and measurements of an RF-MEMS-Based self similar reconfigurable antenna*, IEEE Transactions on Antennas and Propagation, Vol. 54, No. 2, February 2006.
77. J. A. Zamrni, A. Muscat, *A small tunable antenna using multiple shorting posts and varactor diodes*, 2008 International Symposium on Communications, Control and Signal Processing, pp. 83-86, March 2008.
78. G. H. Huff, J. Feng, S. Zhang, J. T. Bernhard, *A Novel Radiation Pattern and Frequency Reconfigurable Single Turn Square Spiral Microstrip Antenna*, IEEE Microwave and Wireless Components Letters, Vol. 13, No. 2, pp. 57-59, February 2003.
79. E. R. Brown, *RF-MEMS switches for reconfigurable integrated circuits*, IEEE Transactions on Microwave Theory and Techniques, vol. 46, no. 11, pp. 1868–1880, Nov. 1998.

80. A. S. Daryoush, K. Bontzos, P.R. Hercsfeld, *Optically tuned patch antenna for phased array applications*, IEEE Antennas and Propagation International Symposium, pp. 361–364.
81. G. Rebeiz, W. H. Weedon, W. J. Payne, *MEMS-Switched Reconfigurable Antennas*, IEEE Antennas and Propagation Society International Symposium, Boston, MA, Volume: 3, pp. 654-657, July 8-13, 2001.
82. D. E. Anagnostou, G. Zheng, L. Feldner, M. T. Chryssomallis, J. C. Lyke, J. Papapolymerou, and C. G. Christodoulou, *Silicon-etched reconfigurable self-similar antenna with RF-MEMS switches*, in Proc. Antennas and Propagation Society Symposium, vol. 2, pp. 1804–1807, Jun. 20–25, 2004.
83. G. M. Rebeiz, *RF MEMS: Theory, Design, and Technology*, Chapter 13, N.J. 2003.
84. G. H. Huff, J. T. Bernhard, *Integration of Packaged RF MEMS Switches With Radiation Pattern Reconfigurable Square Spiral Microstrip Antennas*, IEEE Transactions on Antennas and Propagation, Vol. 54, No. 2, February 2006.
85. Chang won Jung, Ming-jer Lee, G. P. Li, and Franco De Flaviis, *Reconfigurable Scan-Beam Single-Arm Spiral Antenna Integrated With RFMEMS Switches*, IEEE Transactions on Antennas and Propagation, Vol.54, No. 2, pp. 455- 463, February 2006.
86. R. Jackson Jr., R. Ramadoss, *A MEMS-based electrostatically tunable circular microstrip patch antenna*, Journal of Micromechanics and Microengineering, 2007, Vol. 17, pp. 1-8.

87. R. Jackson, *et al.*, *MEMS based electrostatically tunable microstrip patch antenna fabricated using printed circuit processing techniques*, IEEE Antennas Wireless Propagation Letters, pp. 228-30, 2006.
88. S. Majumder, J. Lampen, R. Morrison, J. Maciel, *MEMS Switches*, IEEE Instrumentation & Measurement Magazine, March 2003.
89. Y. E. Erdemli, R. A. Gilbert, J. L. Volakis, *A Reconfigurable Slot Aperture Design Over a Broad-Band Substrate/Feed Structure*, IEEE Transactions on Antennas and Propagation, Vol. 52, No. 11, November 2004, pp. 2860-2870.
90. J. H. Schaffner, D. F. Sievenpiper, R. Y. Loo, J. J. Lee, S. W. Livingston, *A Wideband Beam Switching Antenna Using RF MEMS Switches*, special session SS-3 MEMS For Antenna Applications, IEEE Antennas and Propagation Society International Symposium 2001, Vol. 3, pp. 658-661.
91. J. H. Schaffner, *et al.*, *Reconfigurable Aperture Antennas Using RF MEMS Switches for Multi-Octave Tunability and Beam Steering*, Proceedings 2000 IEEE Antennas and Propagation Symposium, Salt Lake City, pp. 321-324.
92. Chang won Jung, *et al.*, *RF-MEMS Capacitive Series Switches of CPW & MSL Configurations for Reconfigurable Antenna Application*, EMC Europe Workshop 2005, Rome, Italy.
93. Wang, B. Z., Xiao, S., and Wang, J., *Reconfigurable patch-antenna design for wideband wireless communication systems*, IET Microwaves, Antennas & Propagation, Vol. 1, No. 2, pp. 414–419, April 2007.
94. HFSS User's manual, version 10, Ansoft Corporation, July 2005

95. HP8510C Network Analyzer operating and programming manual, Hewlett Packard, 1988.
96. C. A. Balanis, “Antenna Theory: Analysis and Design”, Second Edition, John Wiley & Sons Inc. 1982.
97. John D. Kraus, “Antennas”, Mc. Graw Hill International, second edition, 1988.



Chapter 3

INVESTIGATIONS ON FREQUENCY AND POLARIZATION RECONFIGURABLE MICROSTRIP ANTENNA USING PIN DIODES

Contents

- 3.1 Introduction
 - 3.2 Design of the passive dual frequency dual polarized rectangular microstrip antenna
 - 3.3 Frequency Reconfigurable microstrip antenna with switchable slots using PIN diodes
 - 3.4 Frequency reconfigurable polarization diversity microstrip antenna
 - 3.5 Summarized conjecture at a glance
-

This chapter describes the detailed design and experimental investigations on frequency and polarization reconfigurable rectangular microstrip antennas. The aim is to develop single feed compact electronically reconfigurable microstrip antennas with switchable polarizations. The chapter begins with the design of passive dual frequency dual polarized rectangular microstrip antenna with a single feed excitation. It is followed by a detailed study regarding the effect of slot dimensions on the operating frequencies of the antenna. The chapter concludes with the development of an electronic control mechanism of frequency and polarization using PIN diodes.

3.1 Introduction

Historically from a systems standpoint, antennas have been viewed as static devices with time-constant characteristics. Once an antenna design is finalized, its operational characteristics remain unchanged during system use. However, the recent advent of RF switching components into microwave and millimeter wave applications has opened new and novel avenues of antenna technology development. High quality, miniature RF switches provide the antenna designer with a new tool for creating dynamic radiating structures that can be reconfigured during operation. In the near future the antenna will evolve as a component that will offer intelligence which alters itself to meet operational goals. This development is similar to the introduction of viable field programmable gate arrays for integrated circuit logic in the late 1980s.

While the method of antenna operation is evolving, its role in communication systems still remains the same. An antenna must perform fundamentally as a radiator and thus the metrics by which antennas operate are still intact. Gain, bandwidth, polarization, antenna size, etc. are still the realizable quantities of interest. Only now the introduction of dynamic radiating structures has given the antenna designer an additional degree of freedom to meet these design goals.

The ability of reconfigurable antennas to tune resonances, change polarization and modify their radiation patterns, made their development imperative in modern telecommunication systems. Their agility and diversity created new horizons for different types of applications especially in cognitive radio, Multiple Input Multiple Output (MIMO) Systems, satellites and many other applications. Reconfigurable antennas satisfy the requirements for increased functionality, such as direction finding, beam steering, radar, control and command, within a confined volume.

Reconfigurable antennas have made use of many reconfiguration techniques for last few decades. Compared to broadband antennas,

reconfigurable antennas offer the efficient use of the electromagnetic spectrum and frequency selectivity useful for reducing the adverse effects of co-site interference and jamming. The most common techniques utilized revolved around switching mechanisms. By combining low-loss, high-isolation switches such as MEMS or PIN diode switches with compatible antenna elements, we can physically reconfigure antennas and their feed structures providing frequency and polarization diversity. Other techniques such as the incorporation of variable capacitors, inductors and physical structure alteration surfaced recently to overcome many problems faced in using switches and their biasing.

To make the transformation from fixed element operation to reconfigurable antenna design requires a suitable conversion in design methodology. Three broad methodologies have been identified for achieving reconfigurable antenna designs and operation: total geometry morphing, matching network morphing and smart geometry reconfiguration.

The total geometry morphing method achieves reconfigurable operation by switching a large array of interconnected sub-elements. The sub-elements are connected together via RF switches and are typically less than $\lambda/20$ in size. Because the sub-elements are much less than a wavelength in size they do not form efficient radiating elements individually. However, switching together multiple adjacent sub-elements results in an aggregate structure that forms the desired radiator. This sub-element arraying allows considerable flexibility in forming the radiator. The geometry of the aggregate radiating structure can take a wide variety of forms depending on the desired application. The reconfigurable antennas designed via this method are distributed radiators because the total radiating structure is distributed over many smaller structures.

The matching network morphing method represents the simplest of the three techniques for achieving reconfigurable antenna operation. In this method, the actual radiating structure remains constant and only the feed or impedance matching section of the antenna is reconfigured. Like the total geometry

method, this method is often employed with microstrip geometries because of the relative ease in placing RF switches on planar structures.

The final identified method of reconfigurable antenna design is smart geometry reconfiguration. Falling between total geometry morphing and the matching network morphing method in both the amount of achievable parameter control and system complexity, this method modifies only critical parameters of the antenna radiating structure to achieve the desired reconfigurable performance. It can be implemented with considerably fewer control elements than the total geometry method and thus has the advantage of reduced design complexity. However, with a thorough understanding of the underlying antenna design and careful design consideration it can yield a high level of reconfigurability and antenna parameter control. The primary disadvantage of this method is that the underlying physics of the particular antenna must be known in order to take advantage of minor geometry modifications to achieve the reconfigurable goal. Additionally, the amount of reconfigurability is ultimately limited by the electrical characteristics of the antenna geometry. The reconfigurable antennas presented in this thesis make use of smart geometry reconfiguration method to tune the operating frequency and polarization using PIN diodes and varactors.

3.2 Design of the passive dual frequency dual polarized rectangular microstrip antenna

The basic passive antenna design is vital in order to take the advantage of minor geometry modifications to devise frequency and polarization diversity microstrip antennas with single feed. Moreover, the patch design must include appropriate slot geometries in order to include RF switching components such as PIN diodes. Keeping these things in mind, the patch is designed.

The microstrip patch can assume any shape such as square, ring, cross shape etc. The cross shape is selected as the shape of the patch which is excited by a proximity feed. Although the feed line can be selected anywhere along the

patch width, the feed line is centered with respect to the width of the patch so that the TM_{10} mode of the patch is excited at 2.3GHz. The electromagnetically coupled cross patch antenna given in figure 3.1(a) achieves the 2:1 VSWR bandwidth from 2.26GHz to 2.35GHz (90MHz). The reflection characteristics and the input impedance of cross patch are given in figure 3.1 (b) and 3.1(c) respectively. The measured and simulated reflection characteristics are in good agreement as shown in figure.

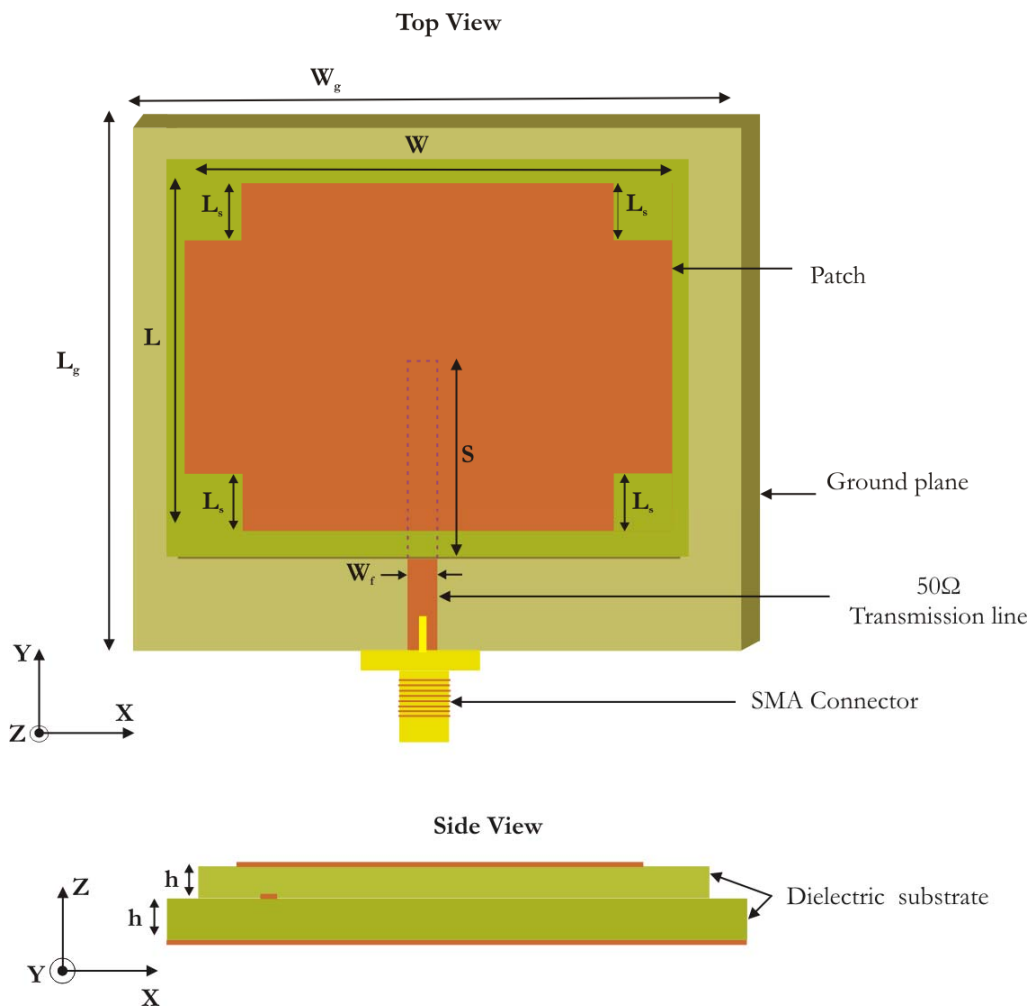


Figure 3.1(a) Geometry of electromagnetically coupled cross patch antenna
 ($L=30.9$, $W=43.5$, $L_s=5.1$, $S=34.5$, $L_g=W_g=75$, $W_f=3$, $h=1.6$
 (All are in mm) $\epsilon_r=4.4$)

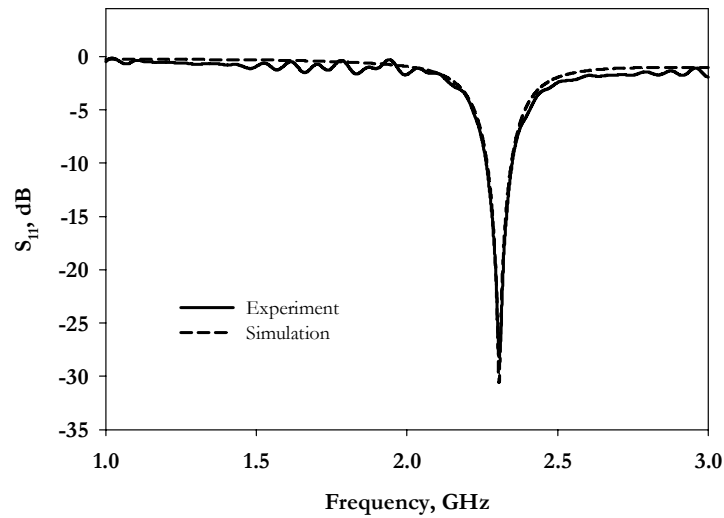


Figure 3. 1(b) Simulated and measured reflection characteristics of electromagnetically coupled cross patch antenna ($L=30.9$, $W=43.5$, $L_S=5.1$, $S=34.5$, $L_g=W_g=75$, $W_f=3$, $h=1.6$ (All are in mm) $\epsilon_r=4.4$)

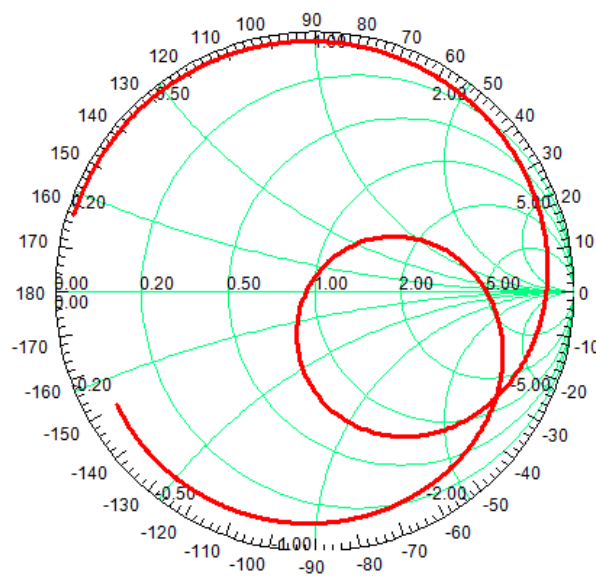


Figure 3. 1(c) Simulated input impedance of the cross patch antenna ($L=30.9$, $W=43.5$, $L_S=5.1$, $S=34.5$, $L_g=W_g=75$, $W_f=3$, $h=1.6$ (All are in mm) $\epsilon_r=4.4$)

The patch overlap distance (S) may be adjusted for best match or optimum impedance bandwidth. From figure 3.2, it is observed that the impedance locus shrinks in size as the patch overlap distance increases and shifted away from the edge of the patch. Once optimized, the two layers are bound using a bonding film. The simulated surface current distribution of the antenna in figure 3.3 reveals that the polarization is linear and directed along the resonating dimension. The fringing field along the non-radiating edges causes cross-polarization. These fields are oriented 90° with respect to the field at the radiating edges.

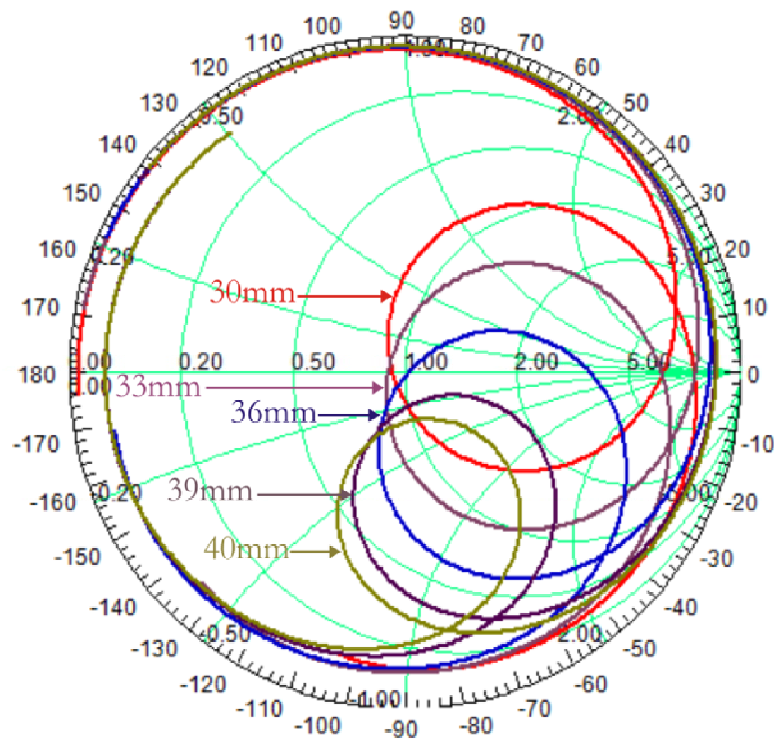


Figure 3. 2 Simulated input impedance variation of the cross patch antenna with respect to the patch overlap distance S ($L=30.9$, $W=43.5$, $L_S=5.1$, $L_g=W_g=75$, $W_f=3$, $h=1.6$ (All are in mm) $\epsilon_r=4.4$)

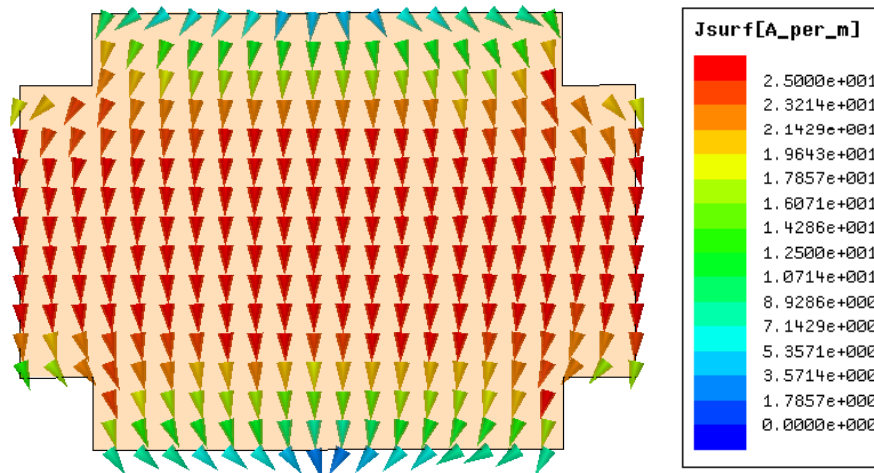


Figure 3. 3 Simulated surface current distribution of the cross patch antenna at 2.3GHz ($L=30.9$, $W=43.5$, $L_s=5.1$, $S=34.5$, $L_g=W_g=75$, $W_f=3$, $h=1.6$ (All are in mm) $\epsilon_r=4.4$)

A simple patch can be regarded as a cavity with magnetic walls on the radiating edges. The first three resonant modes of the patch are TM_{10} , TM_{20} and TM_{30} with same polarization. The simultaneous matching of these modes with a single feed is generally difficult in microstrip antennas. Thus the simplest way to operate at dual frequencies is to use the first resonance of the two orthogonal dimensions of the patch, i.e. TM_{10} and TM_{01} modes. Since dual-polarization is an increasingly important requirement of modern communication systems, the excitation of these orthogonal resonant modes with a single feed will be an interesting feature to be studied in detail. The geometry, reflection characteristics and the input impedance of the dual-frequency dual-polarized cross patch are given in figure 3.4 (a), 3.4 (b) and 3.4(c) respectively. The simulated surface current distribution of the antenna in figure 3.5 reveals that the polarization is linear and directed along X-direction at 1.74GHz and along Y-direction at 2.3GHz. The measured transmission coefficient of the dual-frequency dual-polarized cross patch antenna having cross-polar level better than 15dB, plotted in figure 3.6, reveals that the polarization planes in two resonant modes are orthogonal.

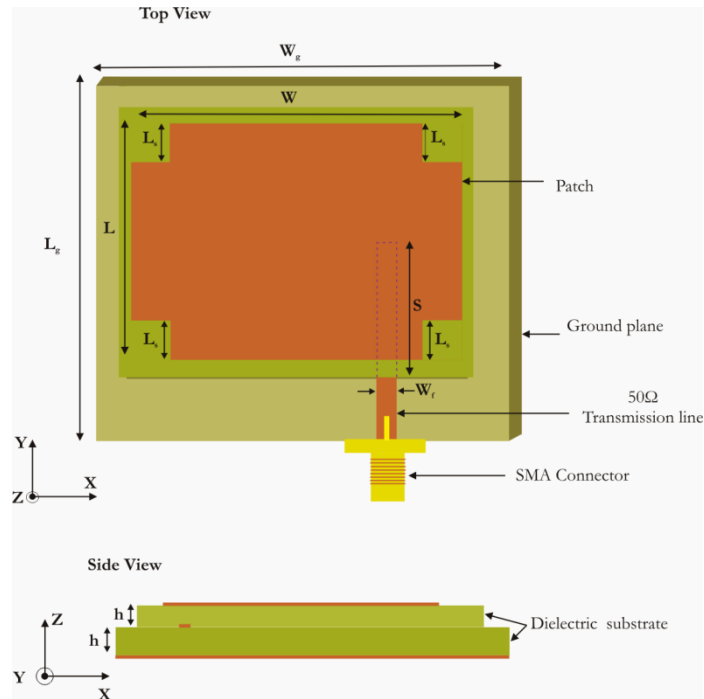


Figure 3.4(a) Geometry of electromagnetically coupled dual-frequency dual-polarized cross patch antenna ($L=30.9$, $W=43.5$, $L_S=5.1$, $S=34.5$, $L_g=W_g=75$, $W_f=3$, $h=1.6$ (All are in mm) $\epsilon_r=4.4$)

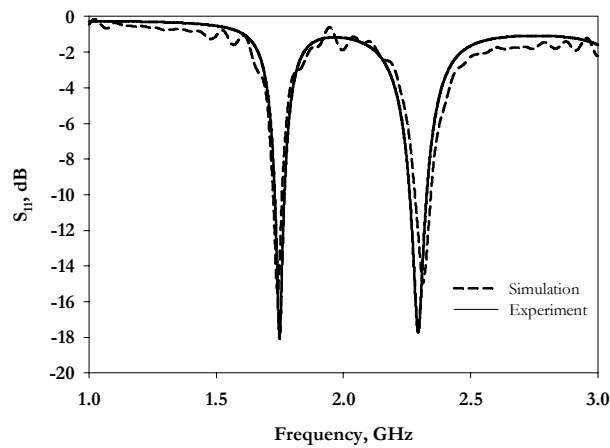


Figure 3. 4(b) Simulated and measured reflection characteristics of electromagnetically coupled dual-frequency dual-polarized cross patch antenna ($L=30.9$, $W=43.5$, $L_S=5.1$, $S=34.5$, $L_g=W_g=75$, $W_f=3$, $h=1.6$ (All are in mm) $\epsilon_r=4.4$)

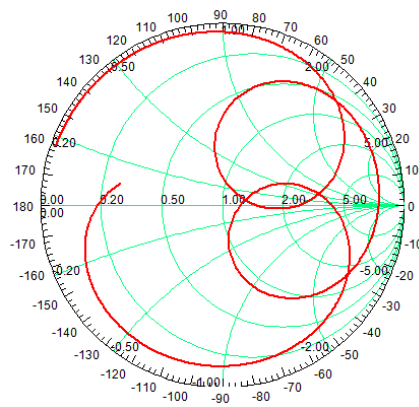
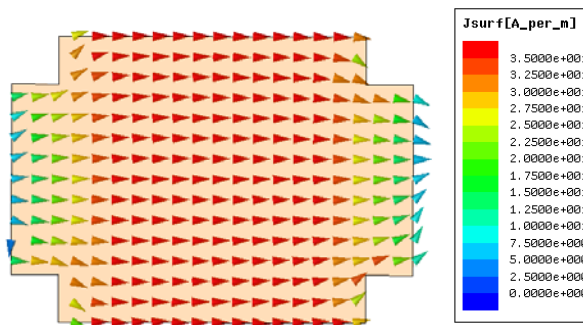
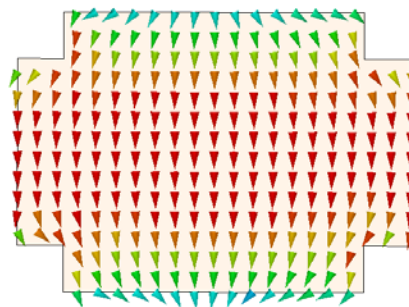


Figure 3. 4(c) Simulated input impedance of dual-frequency dual-polarized cross patch antenna ($L=30.9$, $W=43.5$, $L_S=5.1$, $S=34.5$, $L_g=W_g=75$, $W_f=3$, $h=1.6$ (All are in mm) $\epsilon_r=4.4$)



(a)



(b)

Figure 3.5 Simulated surface current distribution of dual-frequency dual-polarized cross patch antenna at (a) 1.74GHz and (b) 2.3GHz ($L=30.9$, $W=43.5$, $L_S=5.1$, $S=34.5$, $L_g=W_g=75$, $W_f=3$, $h=1.6$ (All are in mm) $\epsilon_r=4.4$)

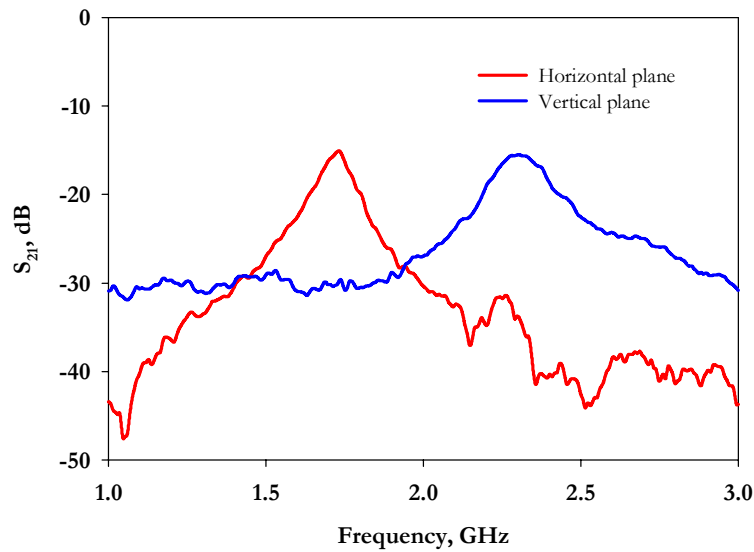


Figure 3.6 Measured transmission coefficient of dual-frequency dual-polarized cross patch antenna in two orthogonal planes for the two resonant modes ($L=30.9$, $W=43.5$, $L_s=5.1$, $S=34.5$, $L_g=W_g=75$, $W_f=3$, $h=1.6$ (All are in mm) $\epsilon_r=4.4$)

Furthermore, the compactness of the patch antenna can be enhanced by increasing the current density paths of the two orthogonal resonant modes, by adding symmetric slot structures in the center of the patch. Several slot geometries were considered and finally X-slot is selected and optimized the dimensions to induce symmetric current distributions and to achieve maximum reduction in area for the TM_{01} and TM_{10} modes. The compact dual frequency dual polarized microstrip antenna design is shown in figure 3.7(a). The antenna is fabricated on an Fr4 substrate of thickness h (1.6mm) and dielectric constant ϵ_r (4.4). In this design, a single proximity feed is used to obtain impedance matching for the two frequencies with orthogonal polarization. The resulting antenna gives greater reduction in area with good cross polarization levels and low frequency ratio. The design has been successfully implemented and the experimental results are in good agreement with the simulations using Ansoft HFSS. The optimum parameters of the antenna geometry are $L=30.9$ mm, $W=43.5$ mm, $L_s=5.1$ mm, $L_x=18.3$ mm and $W_x=2.3$ mm.

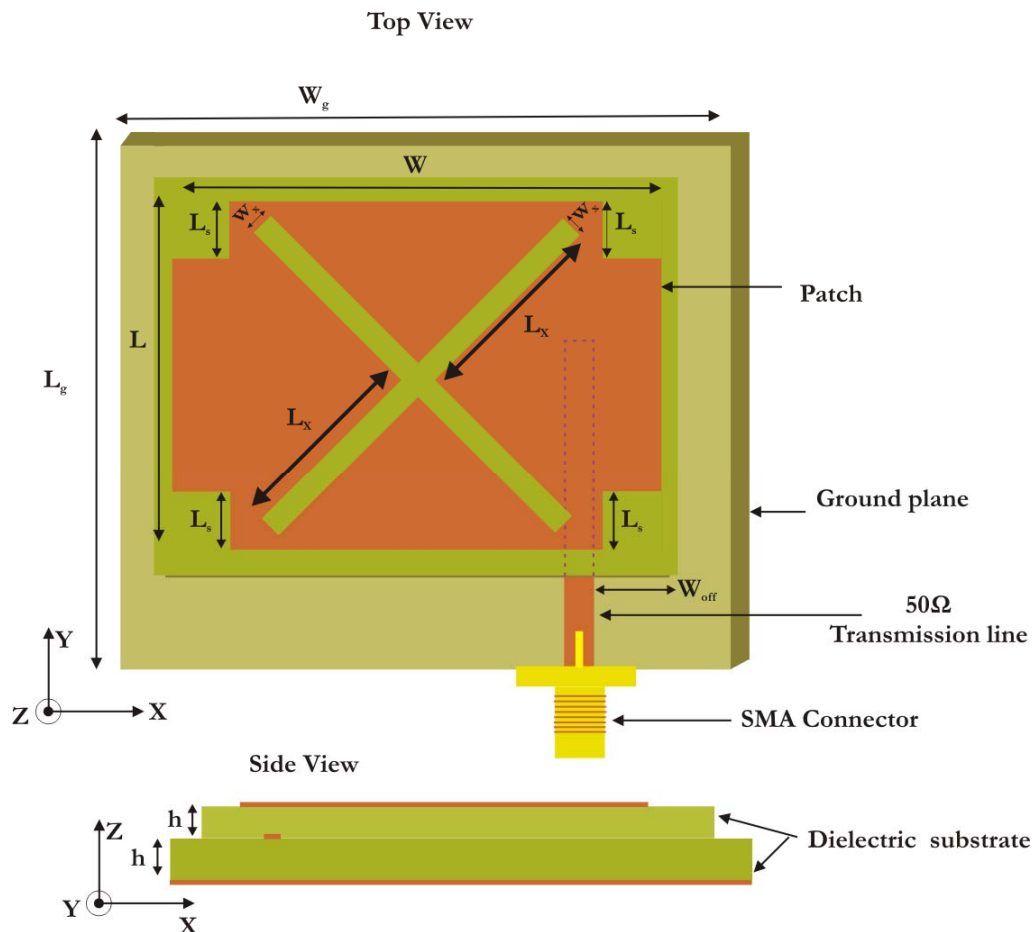


Figure 3.7(a) Geometry of electromagnetically coupled dual-frequency dual-polarized cross patch antenna with X-slot ($L=30.9\text{mm}$, $W=43.5$, $L_s=5.1$, $L_x=18.3$, $W_x=2.3$, $L_g=W_g=75$, $W_{\text{off}}=6.8$, $h=1.6$ (All are in mm) $\epsilon_r=4.4$)

3.2.1 Parametric Analysis

To investigate the effect of various antenna parameters over the antenna characteristics, a detailed parametric analysis is performed. The resonant frequencies of the cross patch depends on horizontal and vertical dimensions of the patch. The X-slot at the center of the cross patch modifies the effective horizontal and vertical electrical lengths of the patch so that the TM_{10} and TM_{01} modes of the cross patch are lowered to 1.1GHz and 1.4GHz from 1.74GHz and 2.3GHz respectively. This is clearly observed in the reflection coefficient of the antenna with and without slot plotted in figure 3.7(b). The study conducted

is the effect of structural parameters such as X-slot length (L_x); corner slit length (L_s) etc. The following sessions provide discussions on the effect of each parametric analysis and conclusions derived from the analysis.

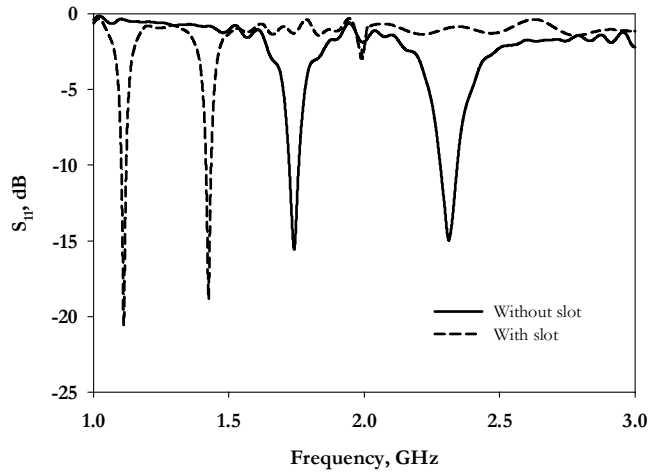


Figure 3.7(b) Simulated reflection characteristics of electromagnetically coupled dual-frequency dual-polarized cross patch antenna with and without X-slot ($L=30.9\text{mm}$, $W=43.5$, $L_s=5.1$, $L_x=18.3$, $W_x=2.3$, $L_g=W_g=75$, $W_{\text{off}}=6.8$, $h=1.6$ (All are in mm) $\epsilon_r=4.4$)

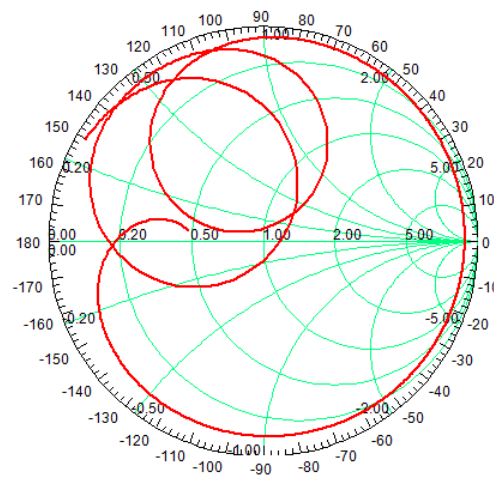


Figure 3.7 (c) Simulated input impedance of the passive dual-frequency dual-polarized compact microstrip antenna with X-slot ($L=30.9\text{mm}$, $W=43.5$, $L_s=5.1$, $L_x=18.3$, $W_x=2.3$, $L_g=W_g=75$, $W_{\text{off}}=6.8$, $h=1.6$ (All are in mm) $\epsilon_r=4.4$)

3.2.1. a Effect of X- slot

The fundamental resonant modes (TM_{10} and TM_{01}) of the cross shaped patch antenna without slot are at 1.74GHz and 2.3GHz with orthogonal polarizations. The proper selection of the X-slot size modifies the horizontal and vertical electrical lengths of the patch equally so that the two resonant frequencies are lowered to 1.1 GHz and 1.4 GHz. To get an insight on the effect of slot geometry on the antenna performance, the proposed antenna is designed with different slot sizes and the results are tabulated in Table 3.1. The X-slot length (L_x) modifies the first and second resonant modes equally while slight variations in resonant frequencies are observed when the width (W_x) is increased. But this change is found to be negligible compared to that of slot length. The change in the resonant frequencies with slot length shown in figure 3.8 establishes the frequency tuning mechanism of the proposed antenna by varying the slot dimensions. Besides the tuning effect, the increase in X-slot length also provides reduction in area for the two resonant modes compared to standard rectangular patches operating at the same frequencies. This is an added advantage of the proposed design. From Table 3.1, it is clear that the antenna gives an area reduction of 79% for the first frequency and 66% for the second frequency when $L_x=18.3\text{mm}$, as compared with a standard rectangular patch operating at the same frequencies. Bandwidth of 1.53% and 1.56% for the first and second resonant frequencies respectively with a frequency ratio of 1.29 is obtained.

Also, the change in length of the X-slot hardly affects the impedance matching of the two resonant frequencies so that the antenna gives good impedance matching for both the excited resonant modes. In other words, the antenna input impedance is not very sensitive to small changes in the length of the slot. This remarkable property of the proposed passive antenna design greatly simplifies the reconfigurable antenna design. The ratio of frequencies, f_2/f_1 is approximately equal to the ratio of effective resonant length of the

horizontal and vertical dimensions of the cross patch modified by the addition of X-slot. Since the X-slot modifies the TM_{10} and TM_{01} modes equally, the frequency ratio remains almost unchanged as shown in figure 3.8.

3.2.1.b Effect of corner slit length (L_s)

The length of the corner slit is varied from 3.1mm to 7.1mm and analyzed its effect over the resonant frequency. The variation of reflection characteristics with L_s is plotted in figure 3.9 (a). It is found that the slit length has feeble effect on the first resonant mode compared to that of the second resonant mode. For L_s less than 5.1 mm, the first resonant mode slightly shifted to lower frequency while the second resonant mode remains unaltered. For L_s greater than 5.1 mm, the second resonant mode slightly shifted to lower frequency while the first resonant mode remains unaltered.

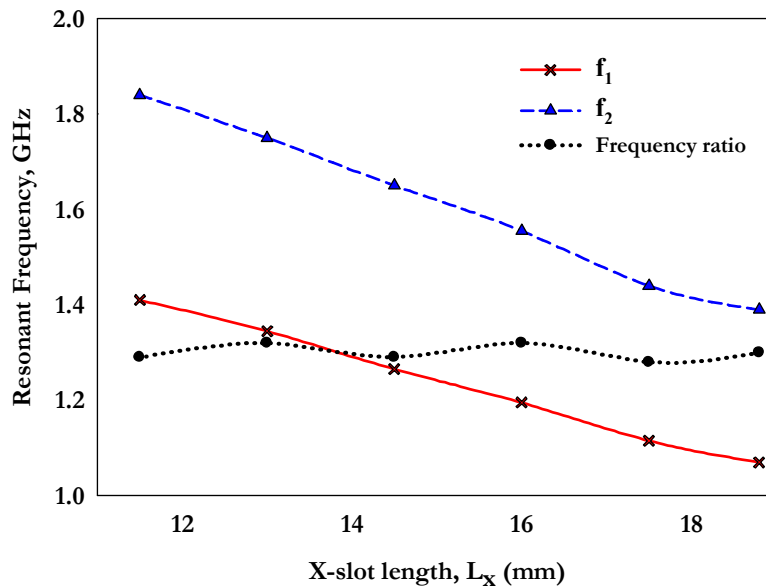


Figure 3.8 The response of first and second resonant modes of dual-frequency dual-polarized compact cross patch antenna with respect to X-slot length ($L=30.9\text{mm}$, $W=43.5$, $L_s=5.1$, $L_x=18.3$, $W_x=2.3$, $L_g=W_g=75$, $W_{\text{off}}=6.8$, $h=1.6$ (All are in mm) $\epsilon_r=4.4$)

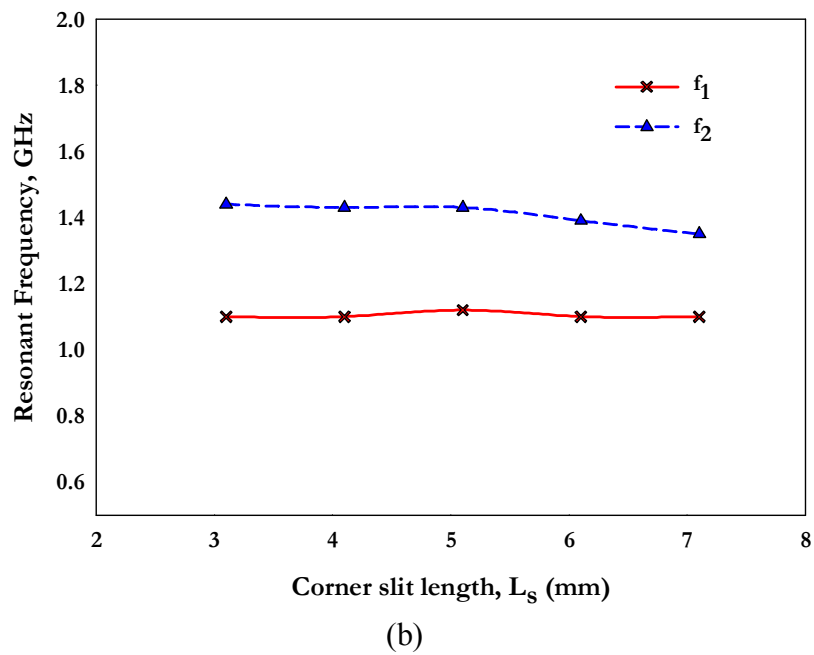
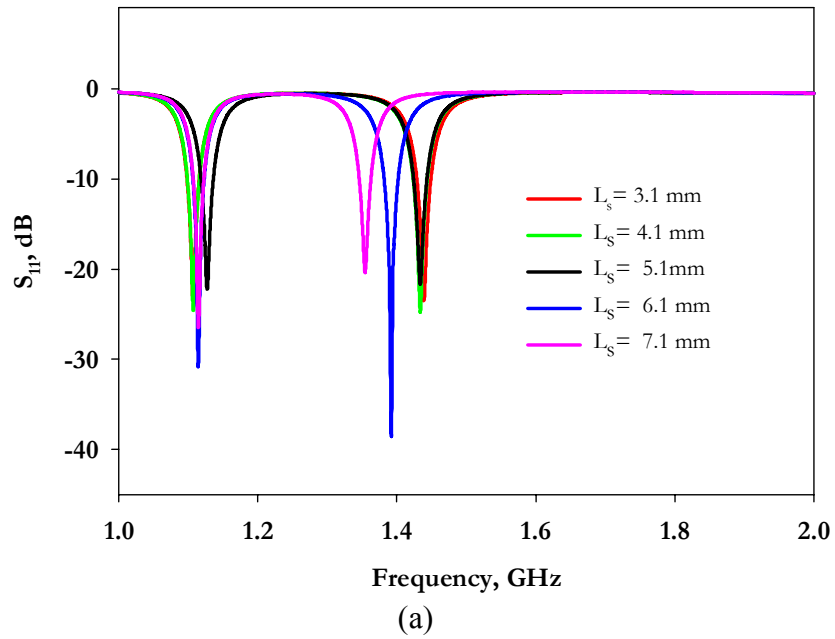


Figure 3.9 Effect of slit length on first and second resonant modes of the dual-frequency dual-polarized antenna (a) Reflection coefficient (b) Resonant frequency ($L=30.9\text{mm}$, $W=43.5$, $L_s=5.1$, $L_x=18.3$, $W_x=2.3$, $L_g=W_g=75$, $W_{off}=6.8$, $h=1.6$ (All are in mm) $\epsilon_r=4.4$)

The return loss or the input impedance can only describe the behavior of an antenna as a lumped load. The detailed EM behavior of the antenna is revealed by examining the surface current distributions and the radiation patterns. The surface current distribution of the antenna and their corresponding simulated 3D radiation patterns are plotted at their resonant frequencies in figure 3.10 (a) and (b) respectively. The surface current is following along the slot edges and a half-wave variation in current is observed at two resonant modes. This gives an indication about the dependence of antenna geometry on the resonant frequencies.

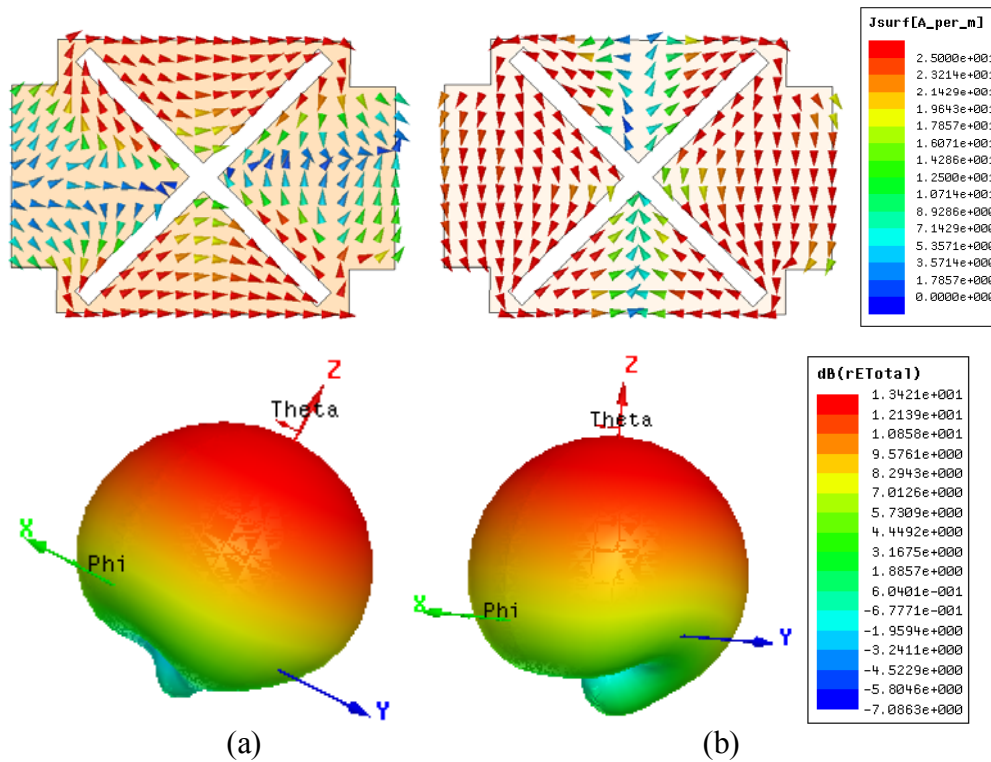


Figure 3.10 Simulated current distribution and 3D radiation patterns of the dual-frequency dual-polarized compact cross patch antenna at (a) 1.1GHz and (b) 1.4GHz ($L=30.9\text{mm}$, $W=43.5$, $L_s=5.1$, $L_x=18.3$, $W_x=2.3$, $L_g=W_g=75$, $W_{\text{off}}=6.8$, $h=1.6$ (All are in mm) $\epsilon_r=4.4$)

3.2.2 Design

Based on the above observations, equations for designing the antenna are summarized as follows:

- (i) *Substrate and feed lines*: Choose the width of the microstrip feed line W_f for 50Ω impedance on a substrate with permittivity ϵ_r and thickness h .
- (ii) *Patch length and width*: For the desired dual frequencies of operation, calculate the dimensions of the rectangular patch corresponding to f_{r10} and f_{r01} . Due to fringing, the patch antenna look electronically wider compared to its physical dimensions. The effect of fringing fields along the width and length direction of the patch is ΔL_{10} and ΔL_{01} respectively. This line extension lengths as well as the addition of X-slot modifies the patch dimensions as

$$W = \frac{c}{2f_{r10}\sqrt{\epsilon_{re}}} - 2\Delta L_{10} - \frac{c}{9.02f_{r10}} \quad (5.1)$$

$$L = \frac{c}{2f_{r01}\sqrt{\epsilon_{re}}} - 2\Delta L_{01} - \frac{c}{8.13f_{r01}} \quad (5.2)$$

Where ϵ_{re} is the effective dielectric constant. The last term account for the effect of X-Slot.

- (iii) *Slot Geometry*: The dimensions of the slot is deduced in terms of guided wavelength as follows,

$$\lambda_{g10} = \frac{\lambda_{10}}{\sqrt{\epsilon_{re}}} \text{ and } \lambda_{g01} = \frac{\lambda_{01}}{\sqrt{\epsilon_{re}}}$$

$$L_s = \frac{\lambda_{g10}}{29} \quad (5.3)$$

$$L_x = 0.12\lambda_{g10} \quad (5.4)$$

and

$$W_x = 0.019\lambda_{g01} \quad (5.5)$$

The above design equations of the antenna are validated on different substrates and the computed dimensions are simulated using Ansoft HFSS. The antenna parameters along with their resonances are tabulated in Table 3.2.

Table 3.1 Performance of the antenna for different slot dimensions

L _x (mm)	W _x (mm)	TM ₁₀ (GHz)	TM ₀₁ (GHz)	Input impedance, Ω				Freq. Ratio		% impedance bandwidth		% area reduction	
				TM ₁₀		TM ₀₁		TM ₁₀	TM ₀₁	TM ₁₀	TM ₀₁		
				Re.	Im.	Re.	Im.						
18.8	3.3	1.07	1.39	51	-15	56	1	1.3	1.57	1.57	82.45	69.9	
18.3	2.3	1.13	1.44	63	-10	53	-2	1.29	1.53	1.56	79.59	65.89	
17.5	1.3	1.18	1.48	52	-6	56	-12	1.28	1.6	1.62	75.79	60.2	
15.8	3.3	1.2	1.6	54	-8	46	-7	1.32	1.65	1.75	76	58.3	
15.3	2.3	1.26	1.65	54	-8	39	-2	1.3	1.74	1.85	73	54	
14.8	1.3	1.31	1.7	51	-12	37	-6	1.29	2.28	1.76	69.15	48.46	
12.8	3.3	1.37	1.8	50	-8	42	-0.5	1.32	1.93	2.15	68.69	45.14	
12.5	2.3	1.41	1.84	42	-3	42	-2.5	1.3	1.86	2.17	65.63	41.18	
11.8	1.3	1.46	1.89	45	0.6	43	-0.125	1.29	2.02	2.3	61.5	35.3	

Table 3.2 Comparison between the computed and simulated resonances of the designed antennas.

Antenna	ε _r	h (mm)	W _r (mm)	W (mm)	L (mm)	L _s (mm)	L _x (mm)	W _x (mm)	f ₁₀ , GHz		f ₀₁ , GHz	
									Computed	Simulated	Computed	Simulated
1	4.4	1.6	3	43.5	30.9	5.1	18.3	2.3	1.12	1.12	1.44	1.44
2	3.8	1.6	3.3	46.5	33.3	5.35	19.05	2.38	1.12	1.14	1.44	1.42
3	3.38	1.57	3.5	50.4	36.3	5.62	20	2.5	1.12	1.11	1.44	1.43
4	2.65	1.59	4.35	58.8	42.8	6.21	22.09	2.77	1.12	1.13	1.44	1.41
5	2.32	1.6	4.7	63.8	46.7	6.56	23.3	2.9	1.12	1.1	1.44	1.40

3.2.3 Measurements

A prototype of the antenna was fabricated on a substrate of $\epsilon_r=4.4$ and $h=1.6\text{mm}$ with the parameters $L=30.9\text{mm}$, $W=43.5\text{mm}$, $L_S=5.1\text{mm}$, $L_X=18.3\text{mm}$ and $W_X=2.3\text{mm}$. The measured reflection coefficient (S_{11}) of the antenna tested using HP8510C network analyzer along with its simulated ones is given in figure 3.11. The experimental and simulated results are matching very well. The proposed dual-frequency cross patch antenna excites two resonant modes, TM_{10} and TM_{01} which are orthogonal to each other. The transmission coefficient (S_{21}) of the antenna given in figure 3.12 reveals that the polarization planes of these two operating frequencies are in orthogonal planes. Also, high cross-polar level is obtained for the two resonances. A wide band standard horn antenna is used to measure the received cross polar power levels in both bands. The antenna resonates at two frequencies with orthogonal polarization and the obtained impedance bandwidth decreases similar to the related compact designs of slot loaded microstrip antennas, which is mainly due to the reduced antenna size at a fixed operating frequency. In order to have better understanding of the cross polar isolation of the antenna it is better to look at the 2D radiation patterns. The simulated and measured 2D radiation patterns of the antenna is given in figure 3.13 A and B respectively show broad beam characteristics in E-plane and H-plane for the two resonant frequencies. A stable radiation characteristic with 3dB beam width of more than 100° and the cross-polar isolation better than 15dB is obtained in both the principal planes. Gain of the antenna is measured using gain comparison method with a double ridged horn antenna as the reference. The gain is measured to be 2.45 dBi at the first resonant frequency and 3.57 dBi at the second resonant frequency. The low gain values are due to the reduction in radiating area of the cross patch with X-slot. Also, the opposing currents on either side of the slot cause field cancellation along

the on-axis at the far-field so that the peak gain of antenna is reduced at the resonance frequency. The photograph of the antenna is shown in figure 3.14.

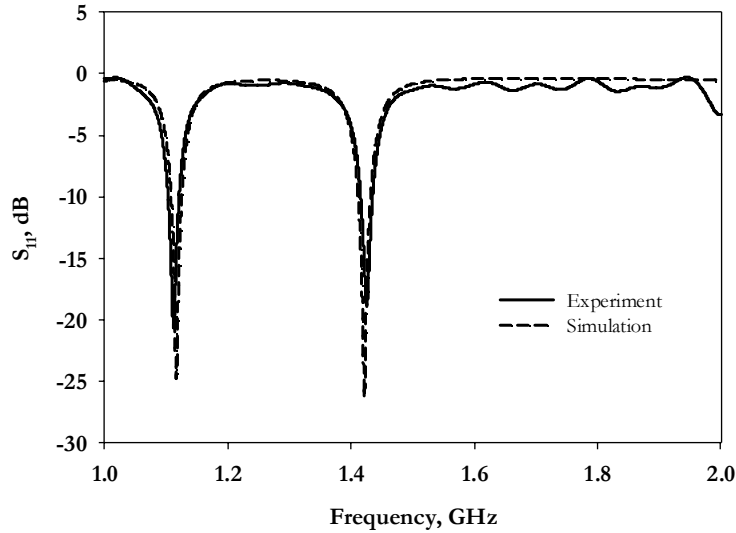


Figure 3.11 Measured and simulated reflection coefficient of the dual-frequency dual-polarized microstrip antenna for the two resonant frequencies ($L=30.9\text{mm}$, $W=43.5$, $L_s=5.1$, $L_x=18.3$, $W_x=2.3$, $L_g=W_g=75$, $W_{\text{off}}=6.8$, $h=1.6$ (All are in mm) $\epsilon_r=4.4$)

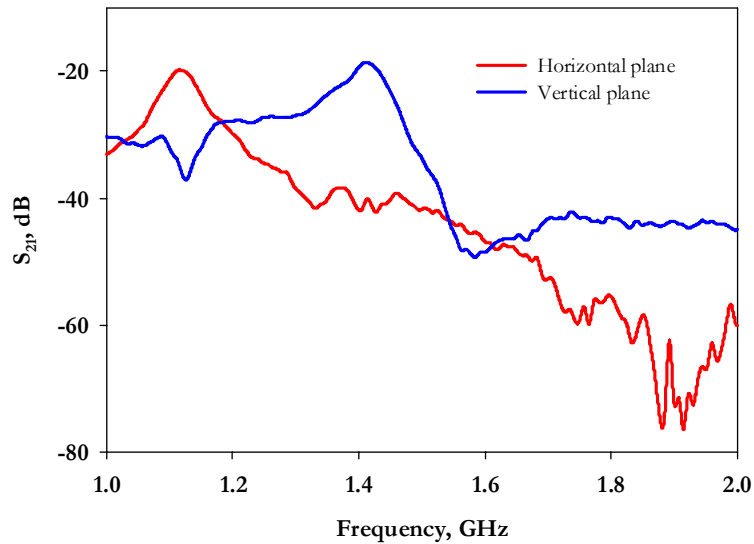


Figure 3.12 Measured transmission coefficient of the antenna in two orthogonal planes for the two resonant frequencies ($L=30.9\text{mm}$, $W=43.5$, $L_s=5.1$, $L_x=18.3$, $W_x=2.3$, $L_g=W_g=75$, $W_{\text{off}}=6.8$, $h=1.6$ (All are in mm) $\epsilon_r=4.4$)

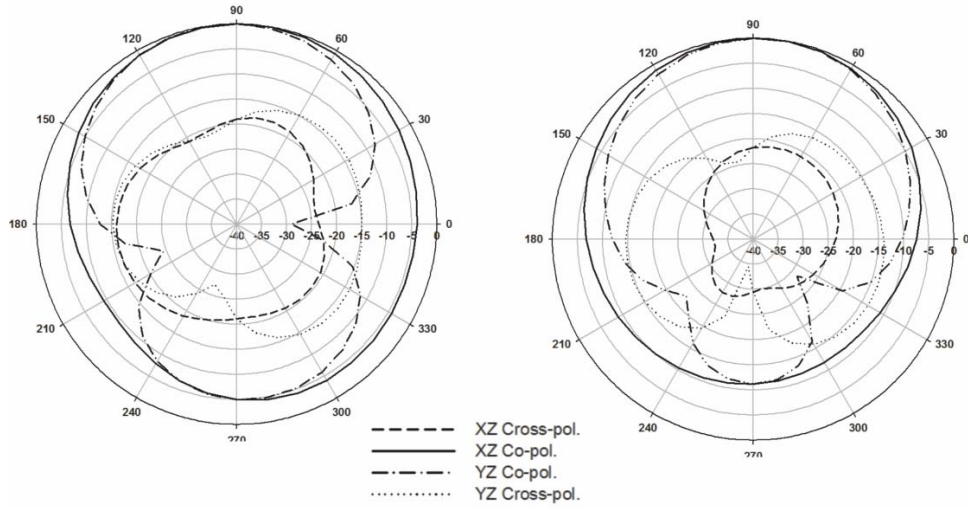
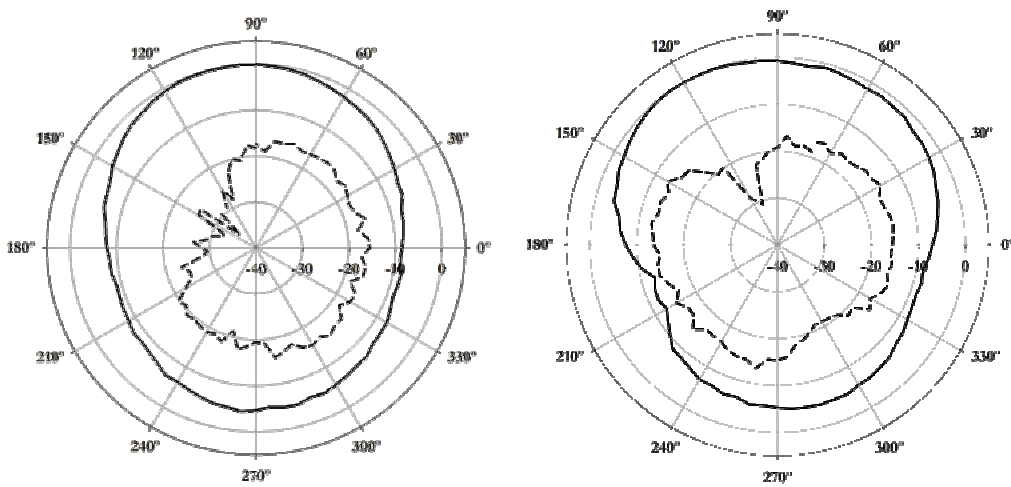


Figure 3.13 A Simulated 2D radiation pattern of dual frequency dual polarized cross patch antenna with X-slot for (i) $f_1=1.1\text{GHz}$ (ii) 1.4GHz



(a)

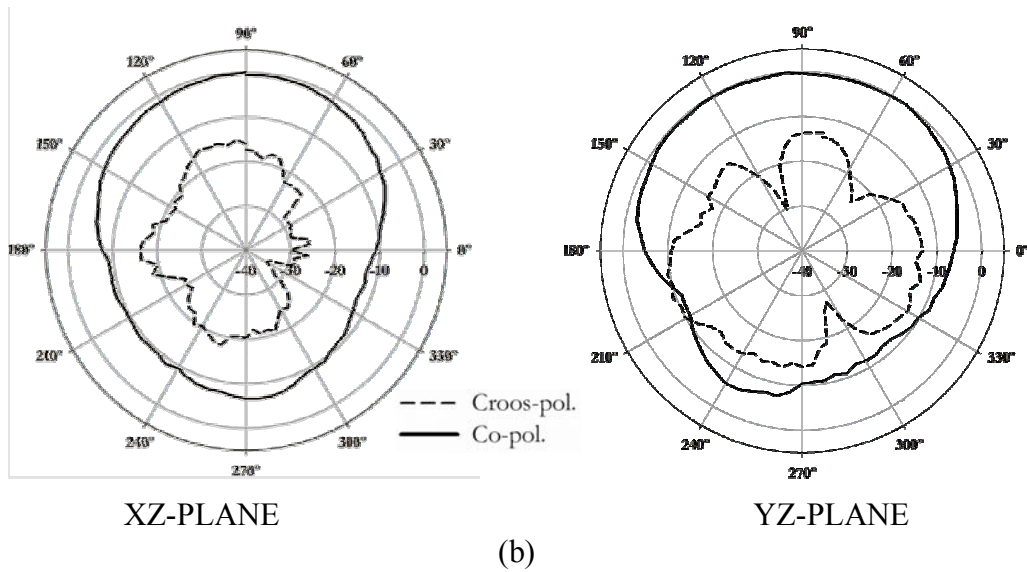


Figure 3.13B Measured far-field radiation patterns of the dual frequency dual polarized cross patch antenna with X-slot for (a) $f_1=1.1\text{GHz}$ and (b) $f_2=1.4\text{GHz}$ ($L=30.9\text{mm}$, $W=43.5$, $L_s=5.1$, $L_x=18.3$, $W_x=2.3$, $L_g=W_g=75$, $W_{\text{off}}=6.8$, $h=1.6$ (All are in mm) $\epsilon_r=4.4$)



Figure 3.14 Prototype of the fabricated dual-frequency dual-polarized cross patch antenna with X-slot ($L=30.9\text{mm}$, $W=43.5$, $L_s=5.1$, $L_x=18.3$, $W_x=2.3$, $L_g=W_g=75$, $W_{\text{off}}=6.8$, $h=1.6$ (All are in mm) $\epsilon_r=4.4$)

The area of the dual-frequency, dual polarized microstrip patch antenna with an X- slot is compared with a standard rectangular patch resonating at designed frequency. Reduction in area of 79% and 66% for the two operating frequencies can be achieved compared to rectangular microstrip resonating at the same frequency. Also, the two operating frequencies have orthogonal polarization with good cross polar level and low frequency ratio. The antenna exhibits fairly good radiation characteristics and has moderate gain in both the operating frequencies so that it can function as a good radiator.

In modern telecommunication systems, the dynamic radiating structures have given an additional degree of freedom due to their ability to tune resonances, change polarization and modify their radiation pattern. Their agility and diversity created new horizons for different types of applications. A compact patch antenna capable of reconfigurable dual frequency orthogonal polarization operation with the integration of PIN diodes is discussed in the following section. The proposed antenna can radiate four frequencies with stable radiation characteristics and considerable bandwidth and low operating frequency ratio in OFF and ON states of the PIN diodes. The antenna offers frequency shift of 190MHz for the first resonant frequency and 280MHz for the second resonant frequency.

3.3 Frequency Reconfigurable microstrip antenna with switchable slots using PIN diodes

Reconfigurable antennas extend the functional possibilities of regular antennas by changing their configurations upon request. The reconfiguration of such antennas is achieved through an intentional redistribution of the currents or, equivalently, the electromagnetic fields of the antenna effective aperture, resulting in reversible changes in the antenna impedance and/or radiation

properties. Reconfigurable antennas find applications in many areas especially when multiple radiation properties are required from a single element. These include Cognitive radio, Plug and play reconfigurable satellites, Multiple Input Multiple Output (MIMO) communication systems, Cellular and personal communication systems and Military applications.

The reconfiguration of an antenna may be achieved through many techniques. Some designers resort to circuit elements while others rely on mechanical alteration of the structure. Yet other approaches bias different antenna parts at different times, reconfigure the feeding networks or appropriately excite the antenna arrays. All such approaches have significantly contributed to the evolution of reconfigurable antennas during the last decade. More recently, antenna designers have used electrically-actuated switches such as p-i-n diodes and RF MEMS and variable capacitors in order to achieve reconfiguration. A reconfigurable dual frequency microstrip antenna using PIN diodes is discussed in this section.

3.3.1 PIN diode switch

The studies carried out in section 3.2 convincingly proved that the two resonant frequencies depend on the length of the X-slot and it can be easily tuned by changing the electrical length. This may be readily accomplished by introducing a short circuit at a specific location on the slot. Thus, the horizontal and vertical electrical lengths are modified so that the antenna will resonate at a different frequency. To implement electronic reconfigurability, the ideal short may be replaced by PIN diodes. The reliability, compactness, high switching speed, very small resistance and capacitance in the ON and OFF states makes it appropriate for the switching applications. BAR 64 PIN diodes from the Infineon Technologies are utilized for the frequency reconfigurable antenna discussed in this section and its characteristics are listed in Table 3.3A.

A PIN diode is a semiconductor device that operates as a variable resistor at RF and microwave frequencies, with a resistance value that can be varied over a range of approximately 1 W to 10 KW through the use of a DC or low frequency control current. The performance of the PIN diode primarily depends on chip geometry and the nature of the semiconductor material in the finished diode, particularly in the I-region. The forward biased PIN diode is a current controlled resistor, consists of a series combination of the series resistance (R_S) and a small Inductance (L_S) as shown in figure 3.15A(i). Figure 3.15A(ii) shows the Reverse Bias Equivalent Circuit of the PIN diode which consists of Capacitance (C_T), a shunt loss element, (R_P), and the parasitic Inductance (L_S). At lower microwave frequencies, $f < 2$ GHz, the PIN diode (including package parasitic) appears to be a very small impedance under forward bias and a very large impedance under reverse bias. It is the difference in performance between forward and reverse bias states upon which switch operation relies. The maximum isolation obtainable depends on the diode's Capacitance (C_T). The Insertion Loss and Power Dissipation depend on the diode's forward biased Series Resistance (R_S).

3.3.2 Bias-circuit / RF circuit isolation

It is necessary to provide some degree of isolation between the low-frequency dc bias circuit and the RF circuit. Otherwise, RF current can flow into the power supply's output impedance, causing effects that are detrimental to the efficient operation of the power control circuit. The dc bias supply is isolated from the RF circuits by inserting a low-pass filter structure between the bias supply and the RF control circuit. An RF inductor, in series with the bias line, and a n RF by-pass capacitor, in shunt with the power supply output impedance, will provide 20 dB or more of dc /RF isolation. If higher values of isolation are needed, more complex low-pass filter structures are necessary.

Low-pass filters may significantly increase the switching time of the PIN diode. It is well known that the implementation of PIN diode with microstrip antenna needs to incorporate blocking capacitors and choke inductors as shown in figure 3.15A (iii). This will reduce the gain and cross-polarization level of linearly polarized radiation obtained without PIN diodes.

Table 3.3 A. PIN diode details

Parameter	Values		Unit
	Min.	Max.	
Forward voltage, V_F	-	1.1	V
Diode Capacitance, C_T	-	0.17	pF
Reverse parallel resistance, R_P	-	3	K Ω
Forward resistance, R_S	0.85	1.35	Ω
Insertion loss	-	0.16	dB
Isolation	-	17	dB
Breakdown voltage, V_{BR}	150	-	V

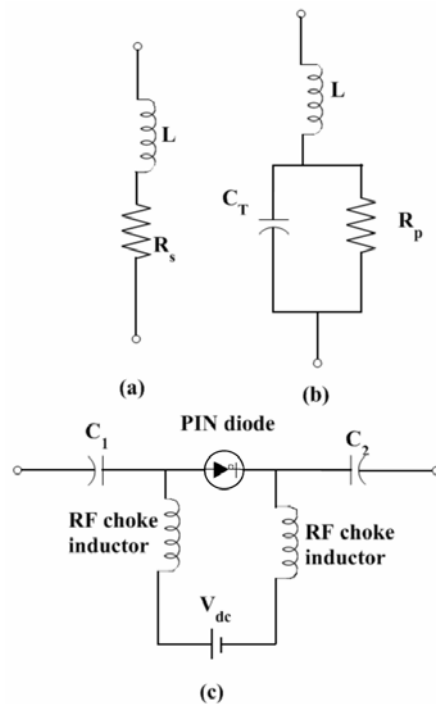


Figure 3.15A (i) Forward bias equivalent circuit (ii) Reverse bias equivalent circuit and (iii) PIN diode bias circuit

3.3.3 Antenna geometry

The configuration of the proposed reconfigurable dual frequency microstrip antenna is illustrated in figure 3.15B. The initial cross patch is obtained by removing the four square regions of side L_S mm from the corners of a rectangular patch of size $L \times W$ mm² fabricated on a substrate of thickness h (1.6 mm) and relative permittivity ϵ_r (4.4). An X-slot of arm length L_X mm and width W_X mm is then carved at the center of the cross patch. The antenna is electromagnetically coupled using a 50 Ω microstrip feed line fabricated using the same substrate. PIN diodes (D_1 , D_2 , D_3 and D_4) are positioned into the slot arms in such a way that each slot arm contains a PIN diode at equal distance P_D mm from the X-slot edge. For the proper biasing of the diodes, narrow slot lines are carved at the edge of the slot arms in the patch. Four small smd capacitors C_1 , C_2 , C_3 and C_4 are soldered at these slot lines which block the dc bias current as well as provide good RF continuity. The PIN diode requires a bias voltage of 1.1V which is supplied from a battery through chip inductors. The dc bias circuit is used to control the ON/OFF state of diodes. The feed line is kept unchanged even though the PIN diode position is varied for achieving reconfigurable dual frequency combinations.

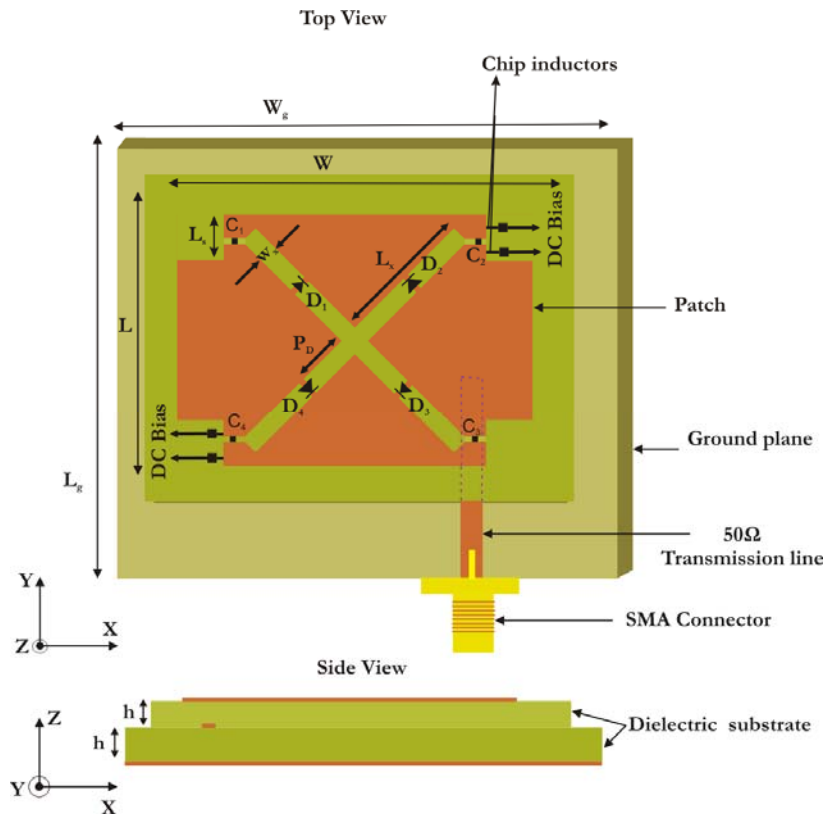


Figure 3.15 B Geometry of the reconfigurable dual-frequency dual polarized microstrip antenna controlled using PIN diodes. ($L= 30.9$ mm, $W= 43.5$ mm, $L_s= 5.1$ mm, $L_x= 17.6$ mm, $W_x= 2.3$ mm, $P_D=14.5$ mm, $C_1= C_2= 33$ pF, $h=1.6$ mm and $\epsilon_r= 4.4$)

When the PIN diode is ON, it essentially behave as equivalent short circuit, thus driving the currents on the patch directly through it. This reduces the effective length of the slot thereby increasing the resonant frequency of the patch. When the diode is switched OFF, the currents have to flow through the capacitor C_D . This increases the effective current path resulting in the shifting of resonant frequencies towards the lower frequency. Figure 3.16 (a) and (b) shows the measured reflection coefficient for the reconfigurable microstrip antenna for different diode positions in OFF and ON state respectively. The PIN diode positions principally determine the switchable resonant frequencies. Thus, different dual frequency combinations can be selected by changing the

PIN diode positions along the X-slot arm as shown in figure 3.17. The proposed antenna gives good impedance matching for all resonances even when the positions of the diodes are altered to achieve frequency tuning.

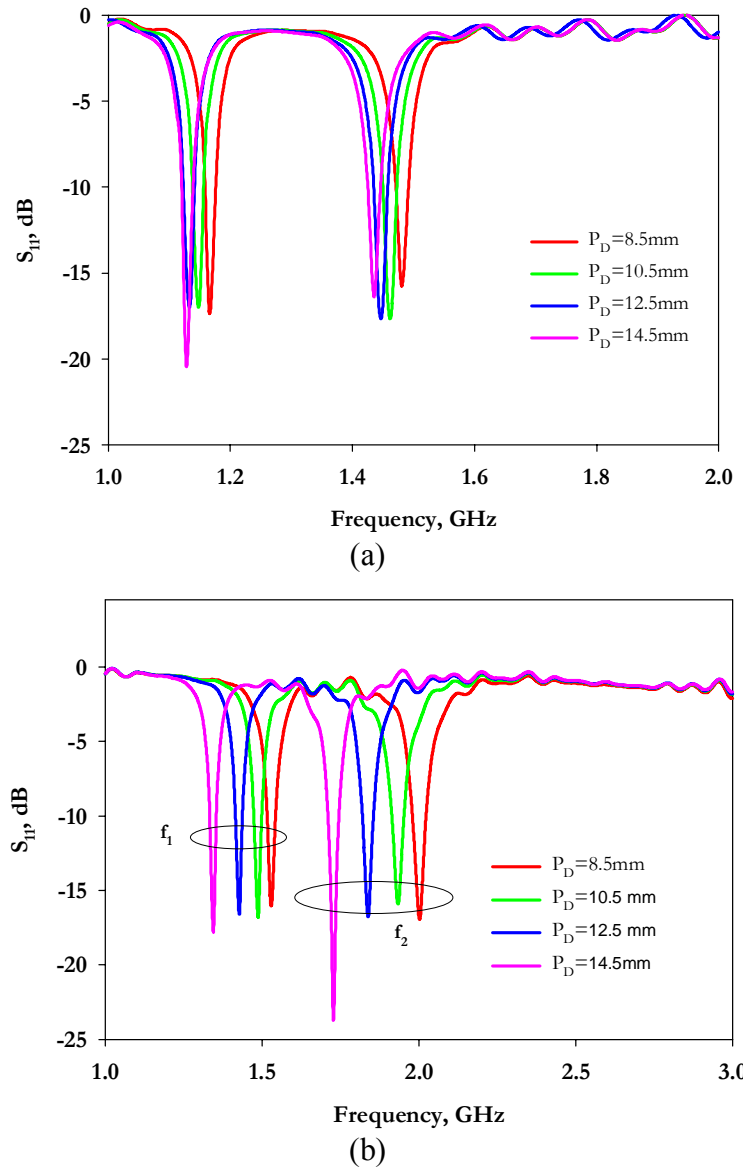
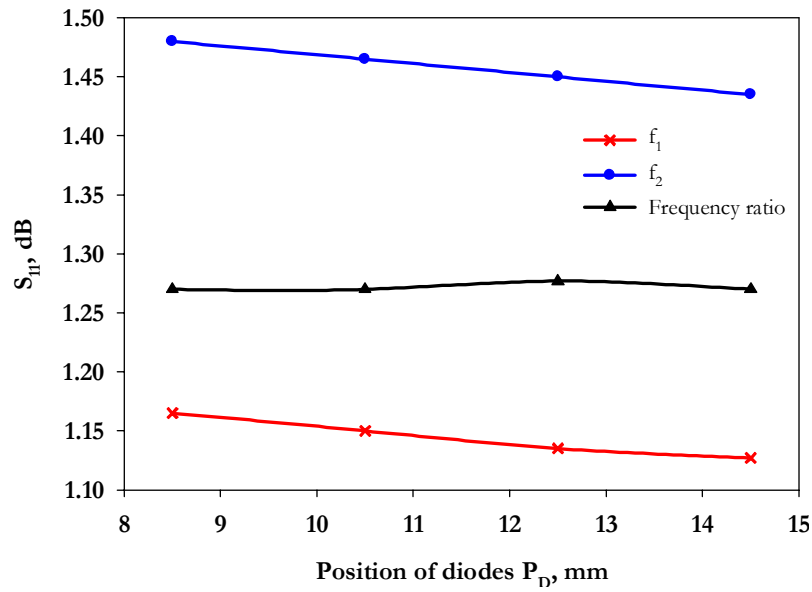
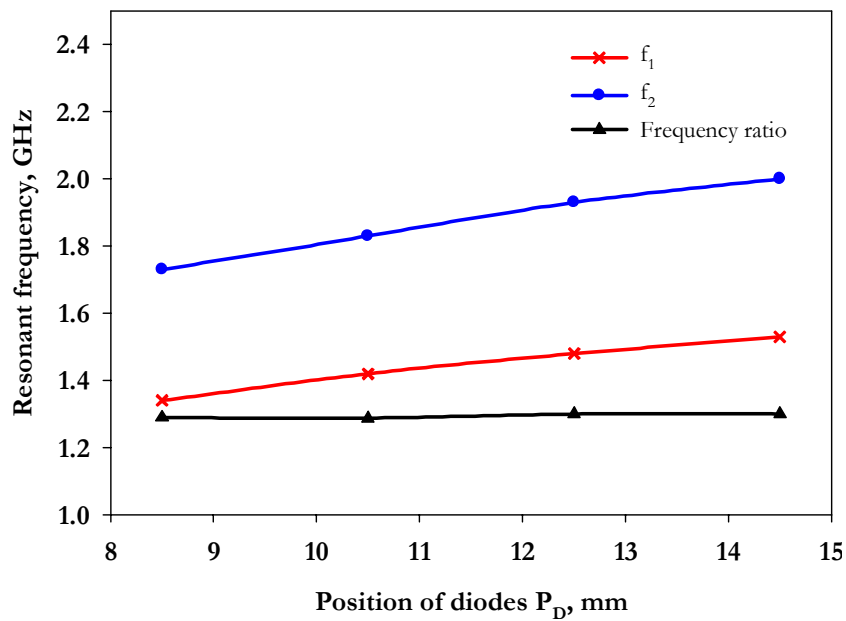


Figure 3.16 Measured reflection coefficient for the reconfigurable antenna for different diode positions (a) OFF state (b) ON state ($L = 30.9$ mm, $W = 43.5$ mm, $L_S = 5.1$ mm, $L_X = 17.6$ mm, $W_X = 2.3$ mm, $C_1 = C_2 = 33$ pF, $h = 1.6$ mm and $\epsilon_r = 4.4$)



(a)

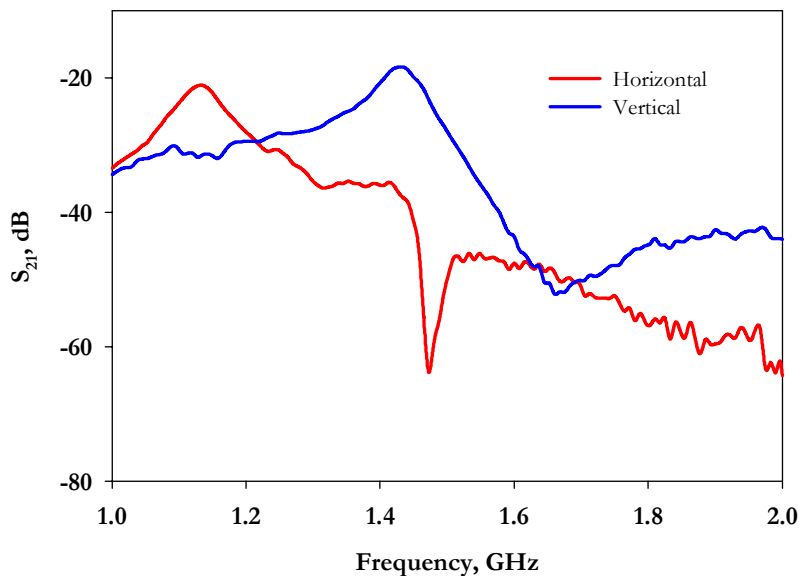


(b)

Figure 3.17 Reconfigurable dual frequency combinations and frequency ratios for different diode positions (a) OFF state (b) ON state. ($L=30.9$ mm, $W=43.5$ mm, $L_S=5.1$ mm, $L_X=17.6$ mm, $W_X=2.3$ mm, $C_1=C_2=33$ pF, $h=1.6$ mm and $\epsilon_r=4.4$)

It has been observed that the matching level of the operating frequencies deteriorates due to the forward resistance of the PIN diode in the ON state. However, this effect is insignificant in the experiment and good matching levels better than -15dB is observed for the dual resonant frequencies. Thus it is concluded that no matching network is required for the frequency switching. The transmission coefficient of the reconfigurable dual frequency microstrip antenna are measured for OFF and ON states and plotted in figure 3.18 (a) and (b) respectively. It can be seen that the polarization planes of the two resonant frequencies are mutually orthogonal in both OFF and ON states of the PIN diodes.

The normalized radiation patterns of the antenna for co-polarization and cross-polarization in the XZ- and YZ-plane are measured for the OFF and ON states of the diodes when the PIN diodes are placed at 14.5mm from the edge of the slot ($P_D=14.5\text{mm}$). The patterns resemble the broadside radiation characteristics of X-slot loaded dual-frequency dual-polarized cross patch antenna with a half power beam width of 100° for different diode states as shown in figure 3.19.



(a)

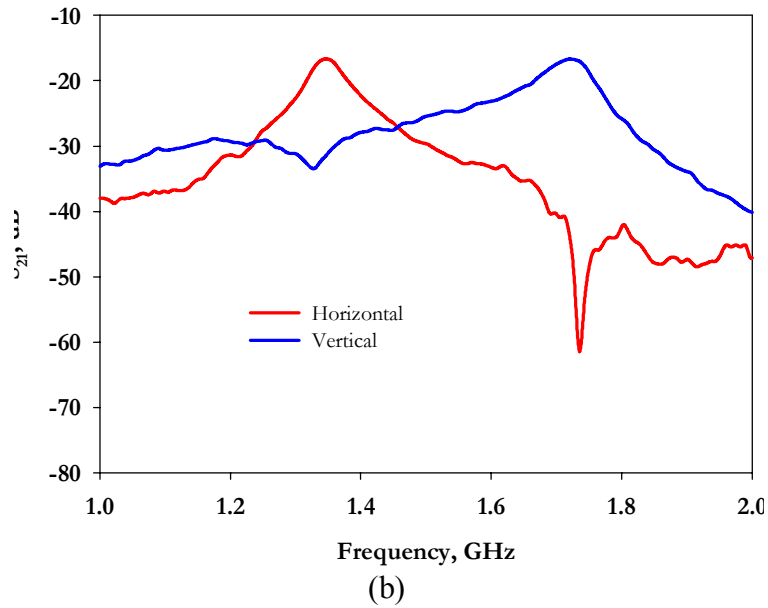


Figure 3.18 Measured transmission coefficient of the reconfigurable dual frequency microstrip antenna with $P_D=14.5\text{mm}$ (a) OFF state (b) ON state ($L= 30.9\text{ mm}$, $W= 43.5\text{ mm}$, $L_S= 5.1\text{mm}$, $L_X= 17.6\text{ mm}$, $W_X= 2.3\text{ mm}$, $P_D=14.5\text{mm}$, $C_1= C_2= 33\text{ pF}$, $h=1.6\text{ mm}$ and $\epsilon_r= 4.4$)

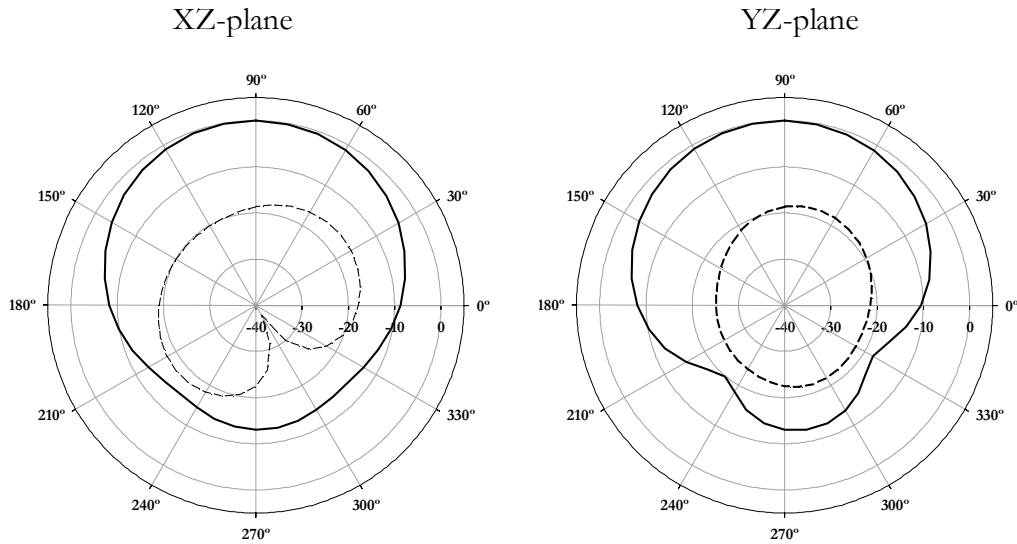


Figure 3.19(a) Radiation Patterns of the reconfigurable dual frequency dual polarized microstrip antenna controlled by PIN diodes at $f_1=1.12\text{GHz}$ when PIN diodes are OFF

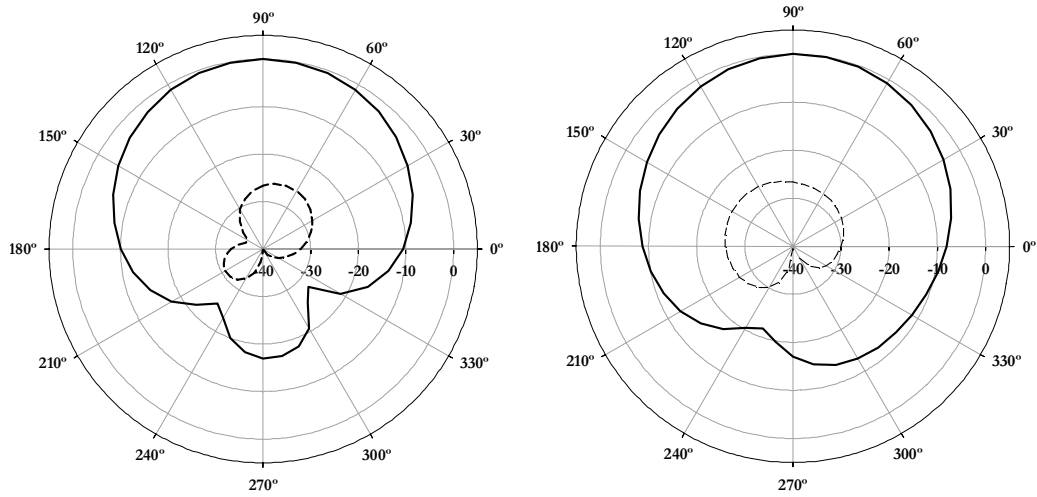


Figure 3.19(b) Radiation Patterns of the reconfigurable dual frequency dual polarized microstrip antenna controlled by PIN diodes at $f_2=1.43\text{GHz}$ when PIN diodes are OFF

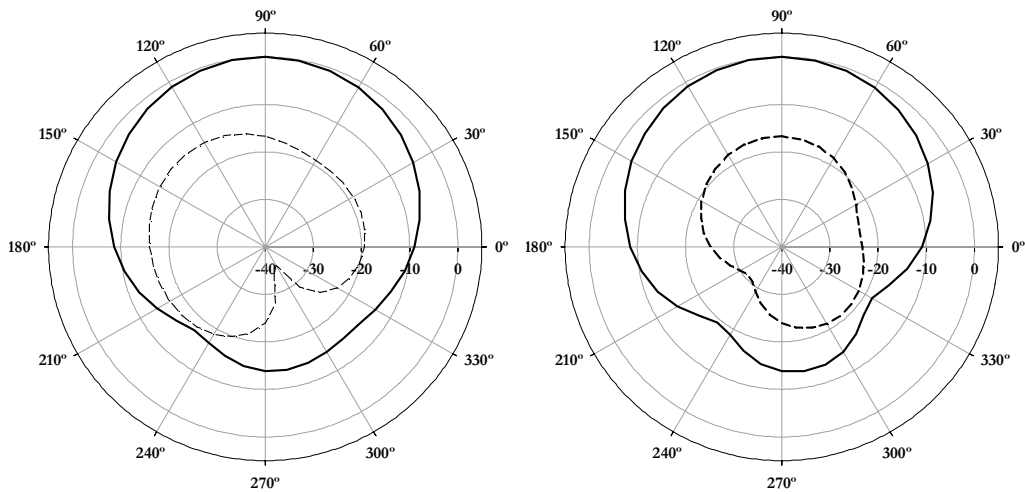


Figure 3.19(c) Radiation Patterns of the reconfigurable dual frequency dual polarized microstrip antenna controlled by PIN diodes at $f_1=1.34\text{GHz}$ when PIN diodes are ON

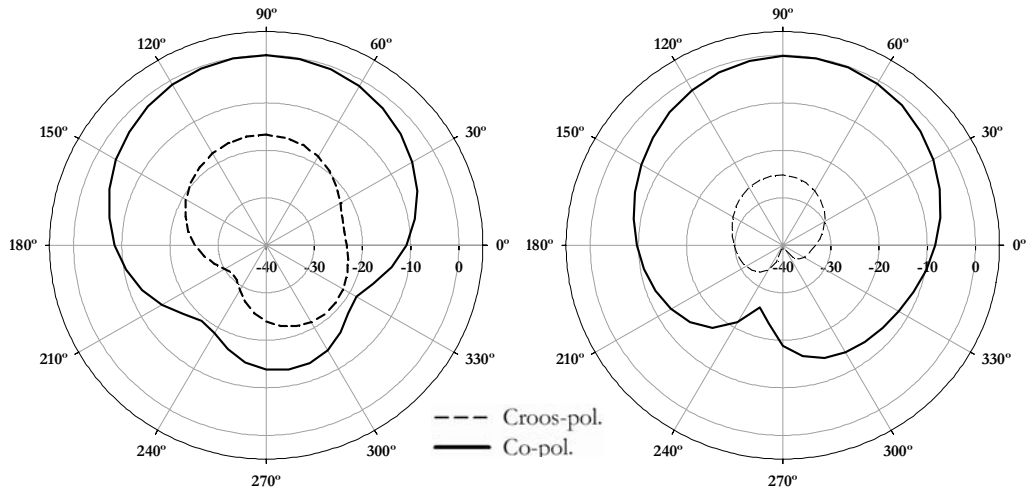


Figure 3.19 (d) Radiation Patterns of the reconfigurable dual frequency dual polarized microstrip antenna controlled by PIN diodes at $f_2=1.72\text{GHz}$ when PIN diodes are ON ($L=30.9\text{ mm}$, $W=43.5\text{ mm}$, $L_S=5.1\text{ mm}$, $L_X=17.6\text{ mm}$, $W_X=2.3\text{ mm}$, $P_D=14.5\text{ mm}$, $C_1=C_2=33\text{ pF}$, $h=1.6\text{ mm}$ and $\epsilon_r=4.4$)

The antenna presented here offers frequency shift of 190MHz for the first resonant frequency and 280MHz for the second resonant frequency with the integration of PIN diodes. The design of multifunction antennas, which could incorporate different radiation characteristics in a single antenna element, has become an important research area for antenna engineers. A polarization diversity antenna, which is an example of multifunction antennas, allows the user to roam any existing network and use only a single handset to access a great number of services. Therefore, these antennas can be utilized to realize frequency reuse. Microstrip antennas are usually designed for a single-mode operation that radiates mainly linear polarization. However, in some applications, such as satellite communications, a circularly polarized system is more suitable than a linearly polarized system because of its insensitivity to transmitter and receiver orientations. A frequency reconfigurable polarization

diversity design derived from the compact cross patch antenna with X-slot is discussed in the next section.

3.4 Frequency reconfigurable polarization diversity microstrip antenna

Circular polarized operation and polarization diversity are becoming major design considerations for practical applications of microstrip antennas. Reconfigurable antennas, with the ability to radiate more than one pattern, at different frequencies, and with various polarizations offer several degrees of freedom to antenna designers. Based on similar concept, a novel patch antenna allowing polarization switching is proposed and carefully examined in this section. A cross shaped microstrip antenna with an X-slot constitutes the fundamental structure. Two PIN diodes are inserted into the center of the X-slot in which D_1 is oriented parallel to the feed line and D_2 is oriented normal to the feed. The polarization is switchable between linear polarization and circular polarization by controlling their status. The validity of this concept is demonstrated by simulated and measured results, which show low cross polarized level for linear polarization and good axial ratio for circular polarization. Because the antenna structure is simple and compact, this antenna can be easily constructed.

3.4.1 Antenna geometry

The geometry of the proposed antenna is shown in figure 3.20. The initial cross patch is obtained by removing the four square regions of side L_s mm from the corners of a rectangular patch of size $L \times W$ mm². An X-slot of arm length L_x mm and width W_x mm is then carved at the center of the cross

patch. The antenna is electromagnetically coupled using a 50Ω microstrip line fabricated using the same substrate material. Two PIN diodes are inserted into the center of the slot in which D_1 is oriented parallel to the feed line and D_2 is oriented normal to the feed line. There is a printed crossed section in the center of the X-slot that connects both the diodes to the patch. For the proper biasing of the diodes, three narrow slot lines are carved in the patch. Three small smd capacitors C_1 , C_2 and C_3 are soldered at these slot lines which block the dc bias current as well as provide good RF continuity. The PIN diode (BAR 64-04) requires a bias voltage of 1.1V which is supplied from a battery through chip inductors. The dc bias circuit used to control the ON/OFF state of diodes is located on the right edge of the patch.

3.4.2 Simulations

The fundamental resonant modes (TM_{10} and TM_{01}) of the unslotted cross shaped patch are at 1.74 GHz and 2.3 GHz with orthogonal polarizations. The proper selection of the slot size modifies the horizontal and vertical electrical lengths of the patch equally so that the two resonant frequencies are lowered to 1.12GHz and 1.44GHz. It is well evident that the insertion of the slot increases the current path thereby lowering the resonant frequency. The X-slot length is optimized to achieve maximum area reduction using Ansoft HFSS. The antenna exhibits good radiation characteristics for both resonant frequencies with an area reduction of 79% and 66% for the first and second frequency respectively when compared to a standard rectangular patch operating at the same frequencies.

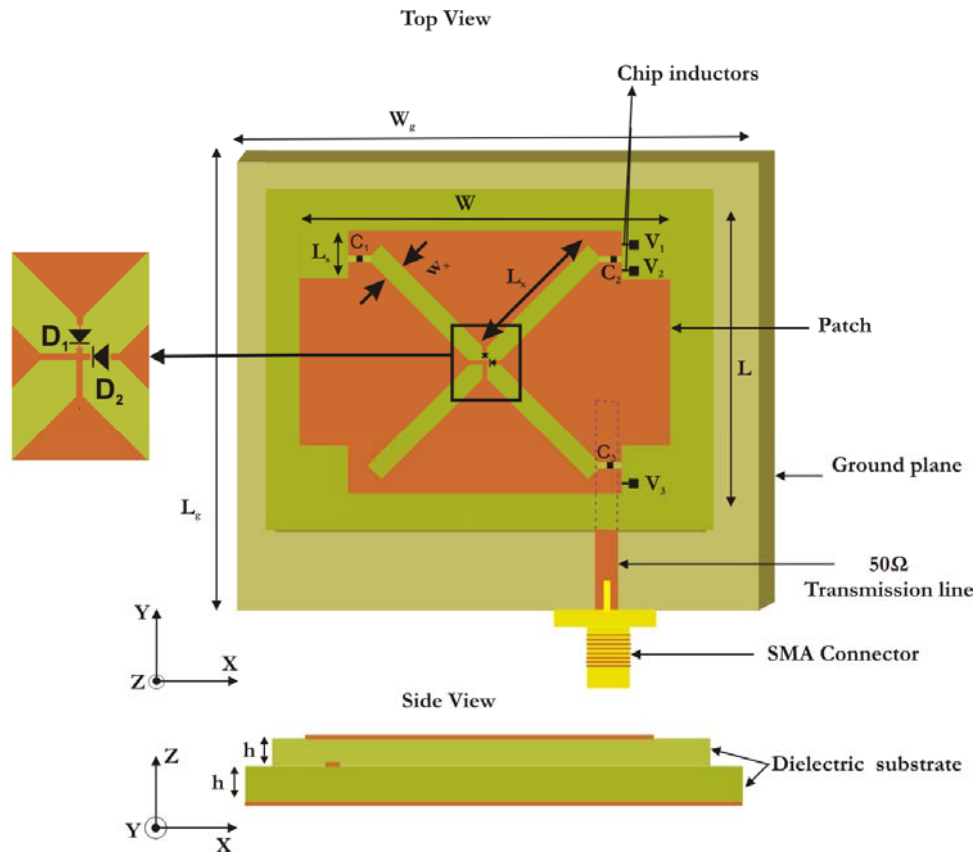


Figure 3.20 Geometry of frequency reconfigurable microstrip antenna for polarization diversity using PIN diodes ($L=30.9$ mm, $W=43.5$ mm, $L_s=5.1$ mm, $L_x=17.6$ mm, $W_x=2.3$ mm, $C_1=C_2=33$ pF, $h=1.6$ mm and $\epsilon_r=4.4$)

Two PIN diodes are inserted at the center of the X-slot to achieve the reconfigurable polarization capability. The orthogonally polarized dual frequency cross patch antenna can be reconfigured for different polarization with respect to the bias voltage applied to the diodes. The bias circuit consists of three dc block capacitors, RF chokes, two switches and input voltage. The dc bias lines are connected to the patch through RF chokes. The ON state of the diode is represented by a series resistor, $R=1.35\Omega$, while the OFF state is represented by a capacitor of $C=0.35\text{pF}$. Three dc block capacitors of $C=33\text{pF}$ are chosen to isolate the RF components from the dc signal and RF choke

inductor isolate the RF signal from flowing into the dc signal. The ON/OFF state of the diodes are controlled with respect to the potential applied to the terminals V_1 , V_2 and V_3 , which is described in Table 3.3 B.

Table 3.3 B States of the external DC bias voltage and PIN diodes for different antenna prototypes.

Antenna	V_1 (v)	V_2 (v)	V_3 (v)	D_1	D_2
1	+	+	-	ON	ON
2	-	-	+	OFF	OFF
3	-	+	-	OFF	ON
4	+	-	-	ON	OFF

To radiate linearly polarized waves, both PIN diodes on the cross patch should be biased either in the “ON state” (Antenna 1) or in the “OFF state” (Antenna 2). When the two diodes are in “ON state”, they act as electrically short circuits (1.35Ω). Hence, the shape of the X slot is modified with a cross shape at the center. From the simulated surface current distribution in figure 3.21(a), it is clear that the new slot shape forces the currents on the patch to flow directly through it so that the effective current path is shortened. Therefore, the antenna excites TM_{10} mode at 1.48GHz and TM_{01} mode at 1.95GHz. Thus antenna 1 is linearly polarized along X-direction with 2:1 VSWR bandwidth of 25MHz at 1.48GHz.

When both the PIN diodes are in the “OFF state”, they act as electrically open circuits. Hence, the shape of the slot is modified with a printed short circuit from left to bottom and open circuit from right to top at the X-slot center which makes the structure asymmetric with respect to the horizontal central line. Therefore, the currents flow through the center of the X-slot and along the

edges of the patch is asymmetric as shown in figure 3.21(b). This increased current path shifts the TM_{01} mode towards the lower frequency region. Hence, an “X” slot loaded cross patch antenna excites linearly polarized radiation along Y-direction at 1.53GHz with 2:1 VSWR bandwidth of 33 MHz.

To radiate circularly polarized waves, one of the diodes on the patch (D_2) should be in the “ON state” while the other should be in the “OFF state” (antenna 3). In this case, the X-slot shape is changed to two V slot connected back- to- back. As shown in figure 3.21(c), this new slot shapes forces the currents to flow through the center of the X-slot as well as along the edges of one of the slot arm. This behaviour results in the splitting of the current into two near orthogonal resonant modes at 1.5GHz and 1.535GHz respectively. The surface current distribution is along Y-direction at 1.5GHz and is along X-direction at 1.535GHz. Also, the input reactance of lower mode is inductive ($39+j4.3\Omega$) while that of the other mode is capacitive ($30-j3.9\Omega$) in nature for the two resonant modes. The 2:1 VSWR bandwidth of antenna 3 is measured to be 65 MHz (4.3%) with respect to the center frequency of 1.495GHz with 1.18% CP (3-dB axial ratio) bandwidth. Its narrow axial-ratio bandwidth is the consequence of imperfect excitation due to a single feed. However, the attractiveness of single-feed circularly polarized (SFCP) antenna is that it requires no polarizer for CP generation and makes the overall system compact.

When D_1 is in the “ON state” and D_2 in the “OFF state” (antenna 4), the antenna excites TM_{10} mode at 1.27GHz and TM_{01} mode at 1.95GHz. This case is not considered on later discussion since this condition is not in the range where frequency and polarization switching is obtained.

From the simulated current distribution it can be inferred that the proper biasing of the PIN diodes result in redistribution of currents which in turn provide the polarization diversity characteristics. The simulated reflection coefficient of the antenna for different diode configuration in Table 3.3 is plotted in figure 3.22. In order to identify the antenna resonance characteristics, its input impedance is plotted against frequency in figure 3.23. The input impedance is not very sensitive to the change in antenna configuration and good matching is realized with respect to the PIN diode biasing. Thus simplified frequency reconfigurable polarization diversity microstrip antenna design is possible without any matching networks.

The return loss or the input impedance can only describe the behavior of an antenna as a lumped load at the end of a feeding line. The detailed EM behavior of the antenna is revealed by examining the radiation patterns. The 3D radiation patterns plotted in figure 3.24 show similar broadside radiation characteristics for the different PIN diode states. Thus the frequency reconfigurable polarization diversity microstrip antenna devoid of matching networks and stable radiation characteristics makes the proposed design more attractive.

Extensive parametric analysis is conducted to optimize the functions of four corner notches of the rectangular patch. In antenna 1 or antenna 2, the corner notches cause a small shift in resonances. The effects of corner notches are significant in antenna 3 than that of antenna 1 or antenna 2. Figure 3.25 shows those $L_S=5.1\text{mm}$ is a good selection in antenna 3 to achieve two near orthogonal resonant modes.

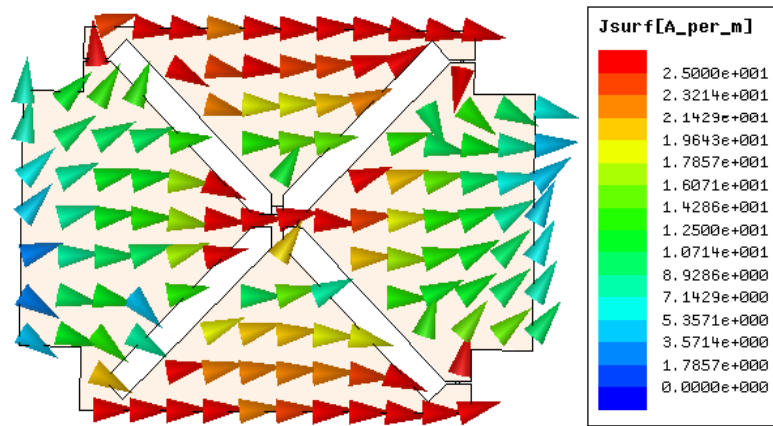


Figure 3.21 (a) Simulated surface current distribution of antenna 1 at 1.48 GHz

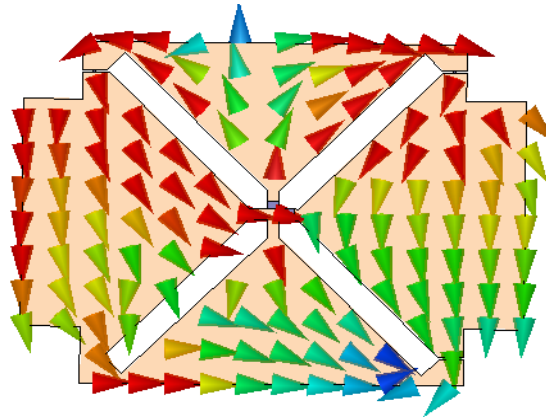


Figure 3.21 (b) Simulated surface current distribution of antenna 2 at 1.53GHz

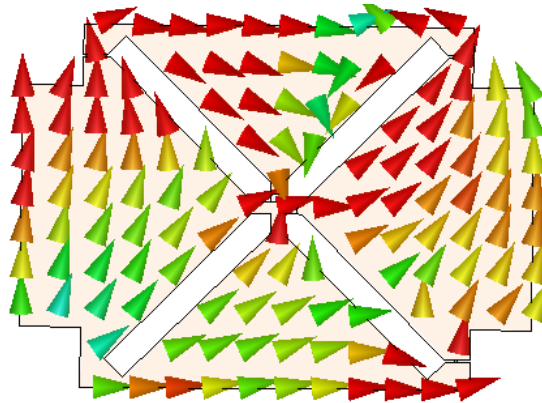


Figure 3. 21(c) Simulated surface current distribution of antenna 3 at 1.53GHz ($L= 30.9$ mm, $W= 43.5$ mm, $L_S= 5.1$ mm, $L_X= 17.6$ mm, $W_X= 2.3$ mm, $C_1= C_2= 33$ pF, $h=1.6$ mm and $\epsilon_r= 4.4$)

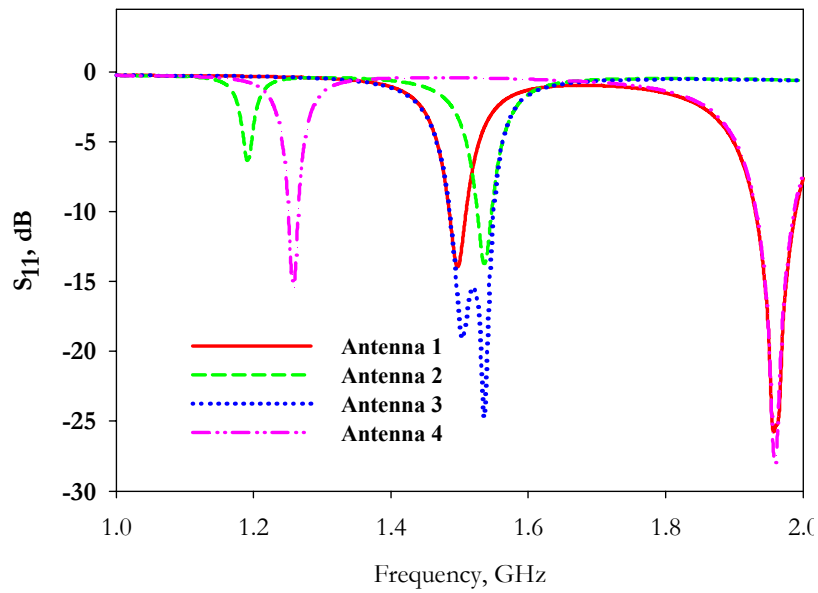


Figure 3.22 Simulated reflection characteristics of the frequency reconfigurable polarization diversity microstrip antenna ($L=30.9$ mm, $W=43.5$ mm, $L_S=5.1$ mm, $L_X=17.6$ mm, $W_X=2.3$ mm, $C_1=C_2=33$ pF, $h=1.6$ mm and $\epsilon_r=4.4$)

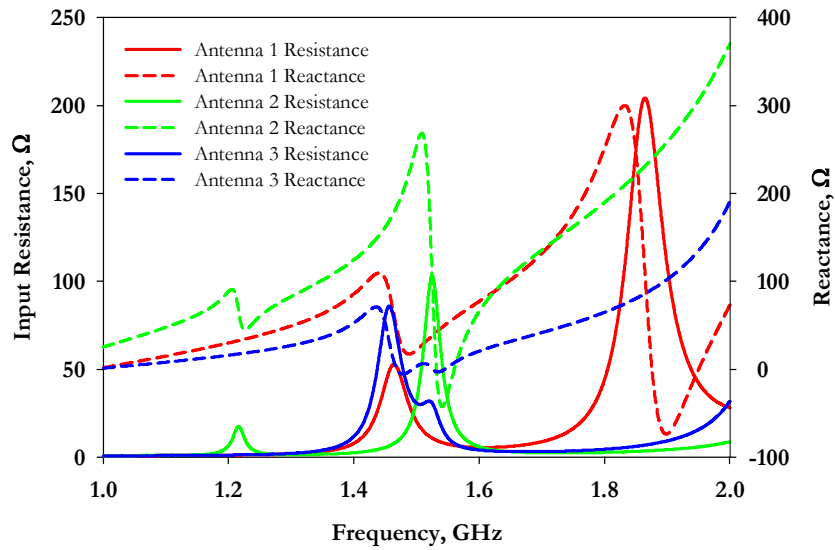


Figure 3.23 Simulated input impedance characteristics of the frequency reconfigurable polarization diversity microstrip antenna ($L=30.9$ mm, $W=43.5$ mm, $L_S=5.1$ mm, $L_X=17.6$ mm, $W_X=2.3$ mm, $C_1=C_2=33$ pF, $h=1.6$ mm and $\epsilon_r=4.4$)

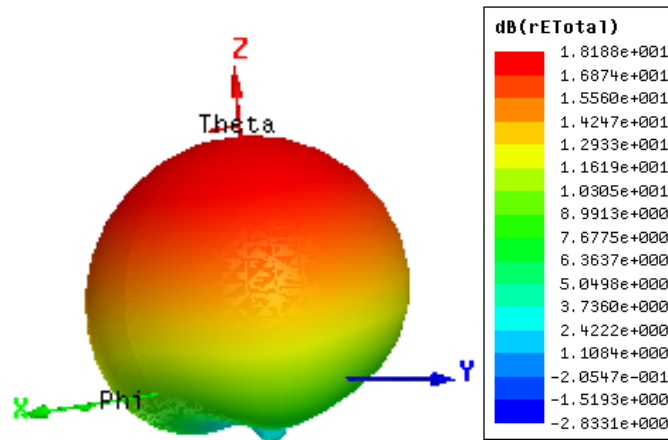


Figure 3.24 (a) Simulated 3D radiation patterns of Antenna 1

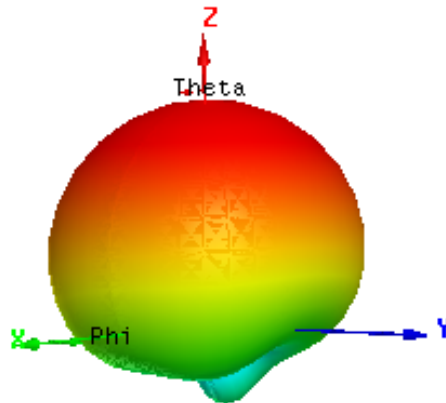


Figure 3.24(b) Simulated 3D radiation patterns of Antenna 2

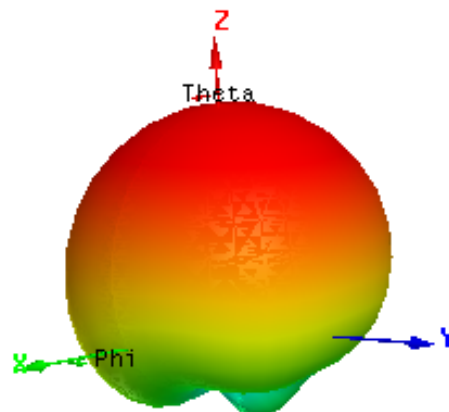


Figure 3.24(c) Simulated 3D radiation patterns of Antenna 3 ($L= 30.9$ mm, $W= 43.5$ mm, $L_S= 5.1$ mm, $L_X= 17.6$ mm, $W_X= 2.3$ mm, $C_1= C_2= 33$ pF, $h=1.6$ mm and $\epsilon_r= 4.4$)

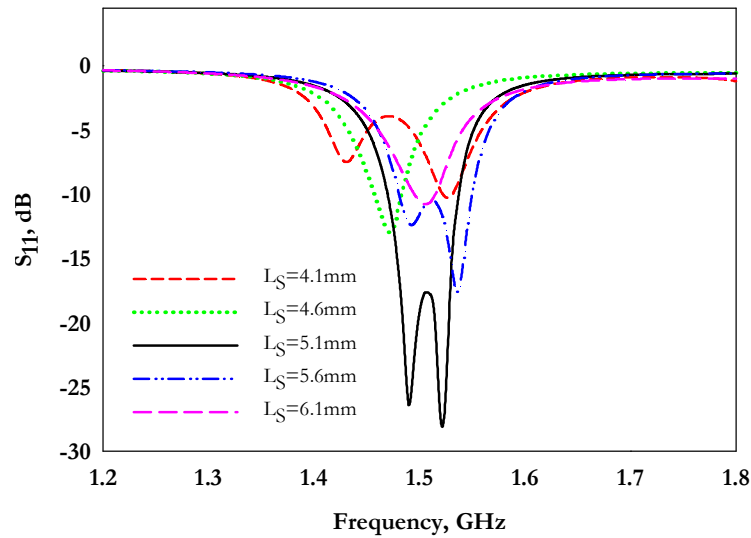


Figure 3.25 Effect of the chamfers in antenna 3 ($L= 30.9$ mm, $W= 43.5$ mm, $l_x= 17.6$ mm, and $W_x= 2.3$ mm)

3.4.3 Measurements

A prototype of the proposed antenna is fabricated with $L= 30.9$ mm, $W= 43.5$ mm, $L_S= 5.1$ mm, $L_X= 17.6$ mm and $W_X= 2.3$ mm. The simulated and measured reflection coefficients (S_{11}) of the antenna are given in figure 3.26. The agreement between simulation and measurement are good as the non-ideal characteristics of the diodes were taken into account. The prototype of the fabricated antenna is shown in figure 3.27.

The axial ratio graph of antenna 3 is plotted in figure 3.28. The best CP performance in the broadside direction is achieved at 1.53GHz with 1.18% CP bandwidth. Figure 3.29(a) and (b) shows the measured radiation patterns at 1.48GHz and 1.53GHz respectively for the LP states. The radiation pattern at 1.53GHz in $\varphi=0^0$ and $\varphi=90^0$ planes for the CP state is given in figure 3.29 (c). The level of cross-polarization (i.e., the left-hand circular polarization, LHCP) is lower than -15dB over the main beam direction. All the radiation patterns are broadside in nature with good LP and CP characteristics at the respective resonant frequency.

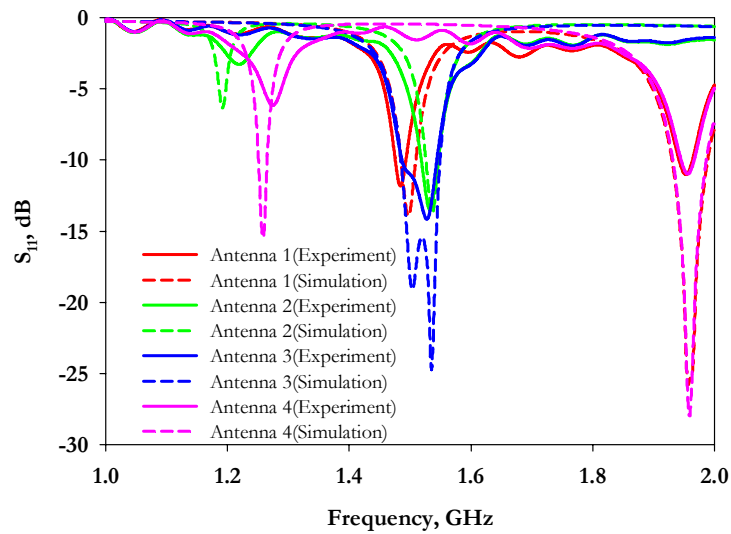


Figure 3. 26 Simulated and measured reflection characteristics of the frequency reconfigurable polarization diversity microstrip antenna for different diode configuration ($L= 30.9$ mm, $W= 43.5$ mm, $L_S= 5.1$ mm, $L_X= 17.6$ mm, $W_X= 2.3$ mm, $C_1= C_2= 33$ pF, $h=1.6$ mm and $\epsilon_r= 4.4$)

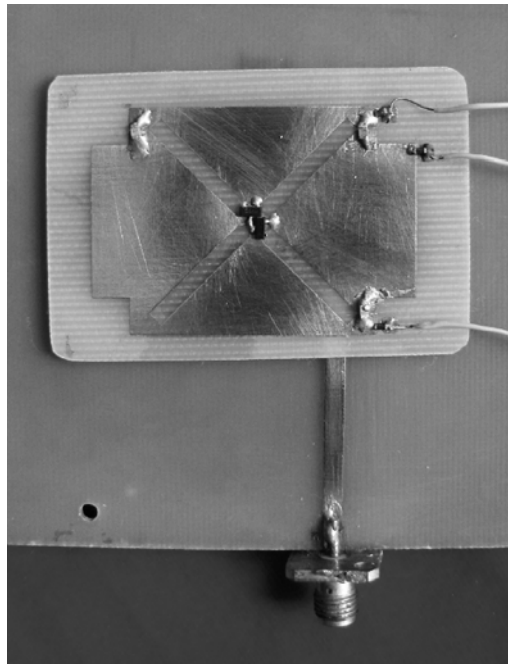


Figure 3. 27 Prototype of the fabricated frequency reconfigurable polarization diversity microstrip antenna

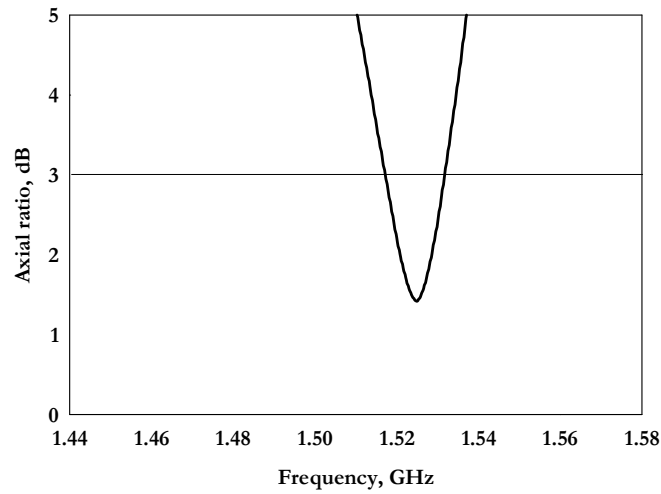


Figure 3. 28 Measured axial ratio of the frequency reconfigurable polarization diversity microstrip antenna ($L= 30.9$ mm, $W= 43.5$ mm, $L_S= 5.1$ mm, $L_X= 17.6$ mm, $W_X= 2.3$ mm, $C_1= C_2= 33$ pF, $h=1.6$ mm and $\epsilon_r= 4.4$)

The gain of the proposed antenna is measured using a double-ridged horn as reference. Antenna 1 follows a direct path through the center of the X-slot, which provides peak gain of 2.55dBi for TM_{10} mode. Since both the diodes are OFF at 1.54GHz the currents have to flow around the edges of the slot. The opposing currents on either side of the slot cause field cancellation along the on-axis at the far-field. So the peak gain of antenna 2 is reduced to 1.97dBi at the resonance frequency. Antenna 3 provides a maximum gain of 2.62dBi at 1.52GHz for the CP state. The average efficiency of the antenna is 52.7% for antenna 1, 47.8% for antenna 2 and 54.8% for antenna 3.

A single feed electronically reconfigurable microstrip antenna with switchable slots for frequency and polarization diversities has been presented. The antenna can produce linear and circular polarization by controlling the bias conditions of two PIN diodes. A good impedance matching performance for all polarization states is observed without any matching networks. The proposed design achieves a cross polar level better than -10dB in linear polarization and

0.85% CP bandwidth in circular polarization state with broadside radiation characteristics and moderate gain. In addition, the antenna is simple and compact because it uses only a few active and passive components and requires less area to occupy the patch and dc-bias circuit compared to conventional polarization diversity antennas. The frequency and polarization diversities of this design provide some potential applications for wireless communications.

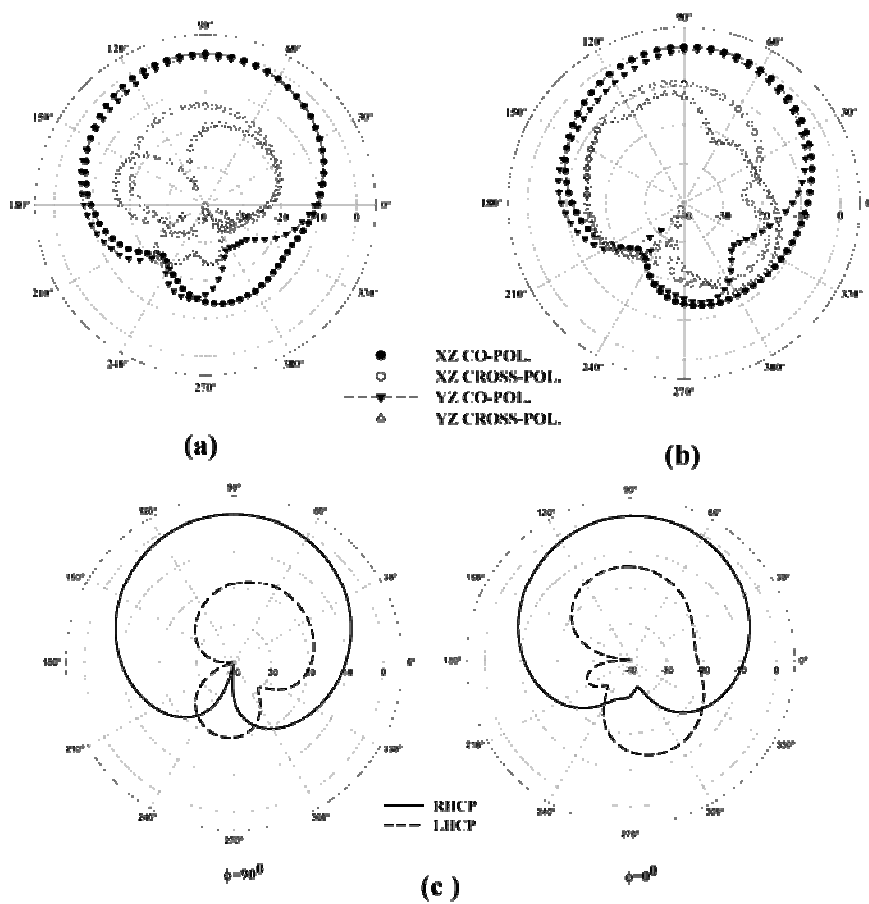


Figure 3. 29 Radiation pattern of frequency reconfigurable polarization diversity microstrip antenna (a) antenna 1 at 1.48 GHz (b) antenna 2 at 1.53GHz and (c) antenna 3 in two orthogonal planes at 1.53GHz ($L=30.9$ mm, $W=43.5$ mm, $L_s=5.1$ mm, $L_x=17.6$ mm, $W_x=2.3$ mm, $C_1=C_2=33$ pF, $h=1.6$ mm and $\epsilon_r=4.4$)

3.5 Summarized conjecture at a glance

Main inferences obtained from the investigation of compact cross shaped microstrip antenna with X-slot can be summarized as below.

- (i) A compact cross patch antenna with an embedded X-slot in the center excites compact orthogonal resonant modes.
- (ii) Mechanical tuning of the two orthogonal resonant modes can be varied by varying the length of the X-slot.
- (iii) The X-slot induces symmetric current distributions for the orthogonal resonant modes and can be easily modified to reconfigurable antenna with greater area reduction.
- (iv) Electronic control of both the operating frequencies and the frequency ratio between two orthogonal resonant modes can be achieved with PIN diode switches along the X-slot arms.
- (v) Frequency reconfigurable polarization diversity operation is possible with two PIN diodes at the center of the X-slot.
- (vi) Electronically reconfigurable cross patch operate either in linear polarization or in circular polarization state with respect to the proper biasing of the PIN diodes at the center of the X-slot is achieved.
- (vii) Implementation of PIN diodes and its associated biasing circuits introduces insertion loss which reduces the gain and cross-polarization level of linearly polarized radiation.



INVESTIGATIONS ON VARACTOR CONTROLLED FREQUENCY AND POLARIZATION RECONFIGURABLE MICROSTRIP ANTENNA

- 4.1 Introduction
- 4.2 Frequency reconfigurable microstrip antenna for tunable frequency ratio using capacitive loading
- 4.3 Frequency and polarization tuning of a microstrip antenna using capacitive loading
- 4.4 Varactor controlled frequency reconfigurable microstrip antenna
- 4.5 Frequency and polarization reconfigurable cross patch antenna using varactor
- 4.6 Summarized conjecture at a glance

This chapter highlights the control of operating frequency and polarization of a rectangular microstrip antenna using reactive loading. The method consists of placing chip capacitor/varactor diodes at appropriate locations provide narrow instantaneous bandwidths that are dynamically selectable at higher efficiency than in conventional antennas. The chapter begins with the mechanical tuning of the operating frequencies and polarizations by inserting different capacitor values at the center of the slot. The chapter concludes with the electronic control of frequency and polarization using varactors.

4.1 Introduction

Microstrip antennas have the attractive features of low profile, small size and conformability to mounting hosts. However, the size of conventional microstrip antenna is still large at the lower microwave regime, especially those used for mobile applications. Therefore compact broadband techniques have recently attracted much attention among researchers. The size of conventional microstrip antenna can be reduced in different ways such as: the use of high dielectric substrate, the use of reactive loading, the shaping of conventional patch structures by cutting slots or slits in the radiating patch or any combination of these techniques. Generally, small size antennas suffer from bandwidth limitations. Bandwidth can be increased by adding lossy elements but, they significantly affect the efficiency of the antenna. One method to solve the low bandwidth is to use the tunable antenna concept. Tunable antenna concept is based on tuning the antenna to the desired band. Therefore such an antenna would not cover all the bands simultaneously, but provides narrow instantaneous bandwidths that are dynamically selectable at higher efficiency than in conventional antennas.

Microstrip antenna is a resonant element and its resonance frequency can be determined by its lumped element equivalent. Therefore any reactive loading of the patch leads to a change in its resonance frequency. Such loading can be performed either mechanically or electronically. Pins, posts, stubs, adjusting the thickness of dielectric layer and use of chip capacitor enable mechanical tuning, whereas varactor and switching diodes embedded in the patch and optical control of PIN diode impedance can be used for electronic tuning of the patch antenna. This chapter begins with an investigation on cross patch antenna with X-slot to study the impact of antenna geometry on its frequency and polarization tuning characteristics using chip capacitor loading. Further, we modify the antenna configuration to attain an electronic control of the operating frequency and polarization with embedded varactor diodes.

4.2 Frequency reconfigurable microstrip antenna for tunable frequency ratio using capacitive loading

Frequency agile systems must be able to receive signals over a large frequency range and therefore, require either wide-band or tunable antennas. However, the instantaneous bandwidth of microstrip antennas is limited as they become small with respect to the wavelength. Hence, tunable narrow-band antennas can be advantageous if small efficient antennas are required to cover a large frequency range. In addition, tunable narrow-band antennas provide frequency selectivity which relaxes the requirement of the receiver filters. Frequency and polarization reconfigurable antennas extend the flexibility of a system even further. A single feed reconfigurable dual-frequency dual-polarized operation of an X-slot loaded microstrip antenna by embedding a chip capacitor is discussed in this section.

4.2.1 Antenna Geometry

As shown in figure 4.1, the proposed antenna is fabricated on a substrate of thickness h (1.6 mm) and relative permittivity ϵ_r (4.4). The antenna structure is obtained by removing the four square regions of side dimension L_S mm from the corners of a rectangular patch of size $L \times W$ mm². An X-slot of arm length L_X mm and width W_X mm is then carved at the centre of the cross patch and the antenna is electromagnetically coupled using a 50Ω microstrip line fabricated using the same substrate. A chip capacitor C inserted at the center of the slot is oriented parallel to the feed line.

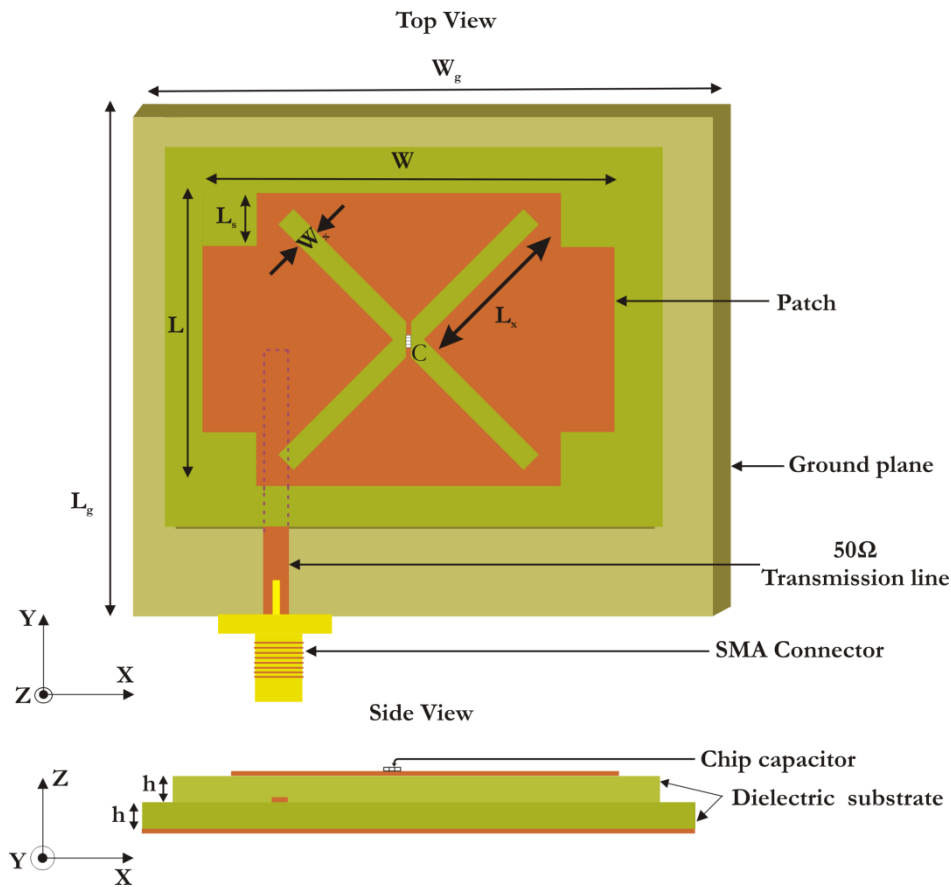


Figure 4.1 Geometry of the frequency reconfigurable cross patch antenna ($L=30.9\text{mm}$, $W=43.5\text{mm}$, $L_s=5.1\text{mm}$, $L_x=18.3\text{mm}$, $L_g=W_g=75\text{mm}$ and $W_x=2.3\text{mm}$.)

4.2.2 Simulated and measured results

The cross patch with an X-slot constitutes the fundamental structure for dual frequency dual polarized operation. The X shape is chosen to induce symmetric current distributions for TM_{10} and TM_{01} modes and can be easily modified to obtain a tunable antenna with greater area reduction. The proper selection of the X-slot size modifies the horizontal and vertical electrical lengths of the patch equally so that the two resonant frequencies are lowered to 1.12 GHz and 1.44 GHz from 1.74GHz and 2.3GHz respectively. By

embedding a chip capacitor at the center of the X-slot, the antenna can operate at a particular dual-frequency combination without changing the geometrical parameters of the antenna. The location of the capacitor is chosen parallel to the feed line which minimizes the variations of TM_{10} mode. While the TM_{01} mode of the patch is determined by the selected value of the chip capacitor.

The performance of the antenna against various capacitance values are listed in Table 4.1. It can be seen that the TM_{10} mode remains unaffected against the changes in capacitance values. The TM_{01} mode is lowered to 1.1GHz from 1.44GHz when a 1pF chip capacitor is soldered at the center of the X-slot. The effective resistance of this mode decreases drastically and is suppressed due to very low impedance ($3.2-j39.7\Omega$) by increasing the capacitor value to 4.7pF. At the same time, loading a chip capacitor generates an additional TM_{01} mode at higher frequency due to shortest electrical path through the capacitor along Y-direction. This additional resonant frequency is not matched for low C values due to high capacitive reactance and achieves impedance matching by increasing the value of C from 2.2pF onwards. In addition, increase in C offers tuning of 190MHz downwards to 1.95GHz from 2.14GHz and all the frequencies are well matched, except for $C=1\text{pF}$, with a linearly polarized radiation along Y-direction. The TM_{10} mode is well matched for all values of capacitance, which gives a linearly polarized radiation along X-direction. Hence, it is found that the capacitor inserted parallel to the feed line at the center of the X-slot modifies the TM_{01} mode and leaves the TM_{10} mode almost unchanged. This property of the antenna offers more flexibility in frequency tuning where the frequency ratio varies in a wider range from 1.84 to 1.68 when the capacitance is varied from 2.2pF to 82pF with linearly polarized radiation along Y-direction.

The reflection characteristics of the antenna measured for different capacitor values are shown in figure 4.2. Only a few variations are shown for brevity. The variation of resonant modes and frequency ratio against various capacitances is plotted in figure 4.3. From the graph it is clear that the proposed configuration can effectively tune the TM_{01} mode without affecting TM_{10} mode against the changes in capacitance values. The simulated surface current distribution and 3D radiation patterns of the antenna without capacitor and with $C=10\text{pF}$ are shown in figure 4.4. An additional shortest electrical length through the center of the X-slot is produced by embedding a capacitor vertically at the center of the X-slot as seen in figure 4.4 (d). This length varies against various capacitance values and determines the frequency ratio of the two operating frequencies.

Table 4.1 Impedance variation of the frequency reconfigurable cross patch antenna against various capacitances

Capacitance, pF	TM_{10} , GHz	TM_{01} , GHz	Input impedance, Ω			
			TM_{10}		TM_{01}	
			Real	Imaginary	Real	Imaginary
0	1.13	1.43	59.6	-3.73	60	13.58
1	1.15	1.1, 2.35	73.7	8.7	73.9, 60.5	23.57, -63.4
2.2	1.16	0.87, 2.14	44.45	-20	20.8, 98.9	-23.5, -8.38
3.3	1.16	0.74, 2.07	44.6	-19.95	38.9, 90.4	-29.8, -7.7
4.7	1.16	0.63, 2.04	44.7	-19.9	3.2, 83.6	-39.7, 8.09
6.8	1.16	2.01	44.7	-19.8	81.9	3.6
8.2	1.16	2	44.8	-19.8	80.8	4
10	1.16	1.99	44.8	-19.8	81	2.2
15	1.16	1.98	44.8	-19.7	77.2	7.14
22	1.16	1.97	44.8	-19.7	77.8	4.8
47	1.16	1.96	44.8	-19.7	76.8	5.28
82	1.16	1.95	44.8	-19.7	75.3	6.12

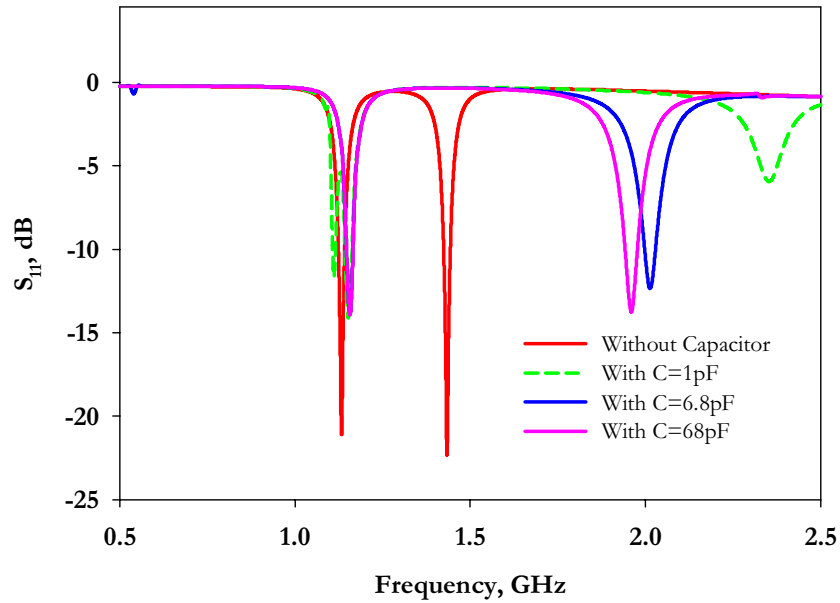


Figure 4.2 Reflection coefficient of the antenna without and with various capacitances ($L=30.9\text{mm}$, $W=43.5\text{mm}$, $L_s=5.1\text{mm}$, $L_x=18.3\text{mm}$ and $W_x=2.3\text{mm}$.)

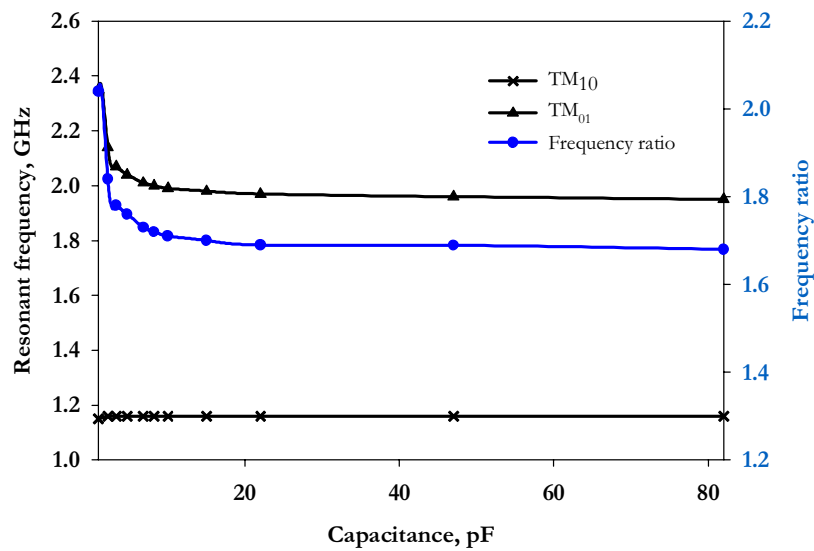


Figure 4.3 Variation of resonant modes and frequency ratio against various capacitances ($L=30.9\text{mm}$, $W=43.5\text{mm}$, $L_s=5.1\text{mm}$, $L_x=18.3\text{mm}$ and $W_x=2.3\text{mm}$.)

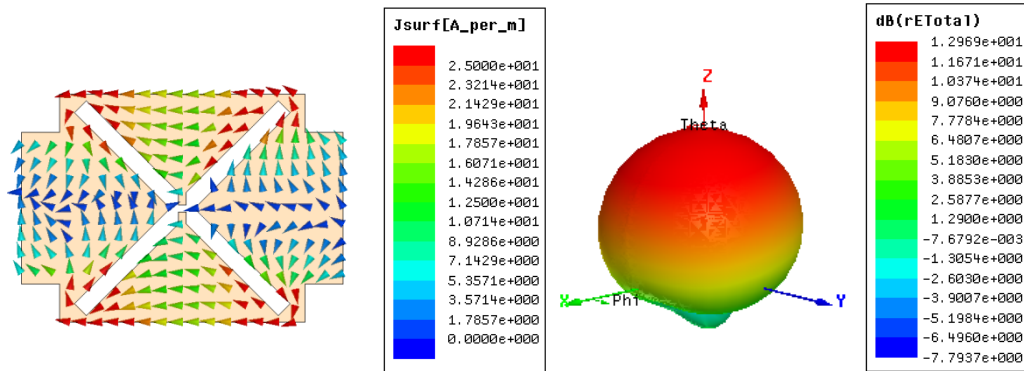


Figure 4.4 (a) Simulated surface current distribution and 3D radiation pattern of the frequency reconfigurable microstrip antenna without capacitor at 1.13GHz

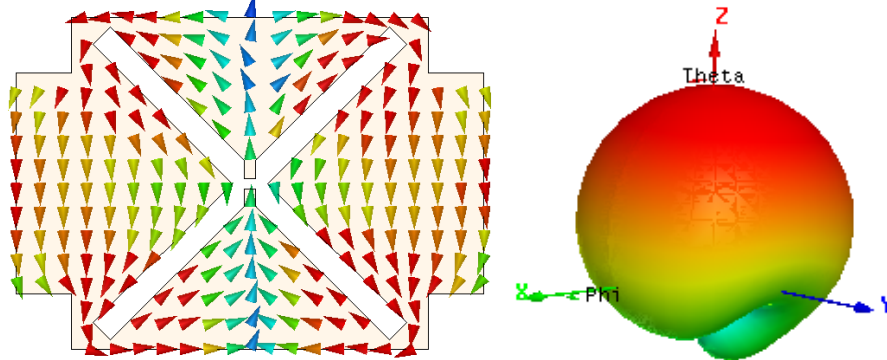


Figure 4.4 (b) Simulated surface current distribution and 3D radiation pattern of the frequency reconfigurable microstrip antenna without capacitor at 1.43GHz

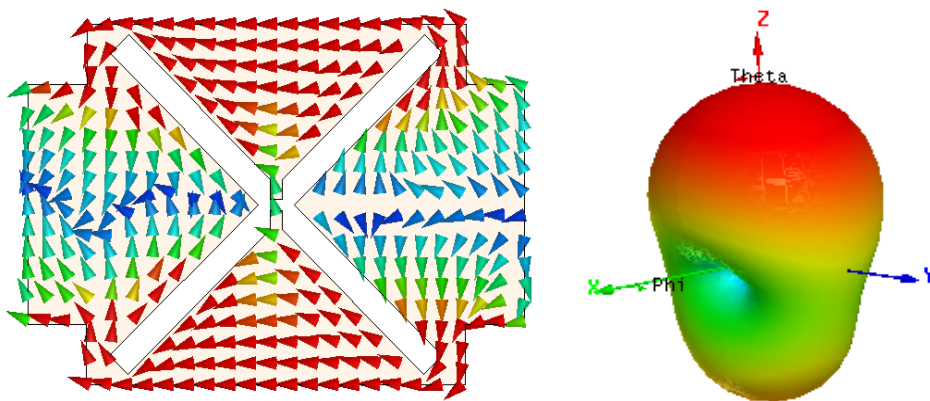


Figure 4.4(c) Simulated surface current distribution and 3D radiation pattern of the frequency reconfigurable microstrip antenna for tunable frequency ratio with C=10pF at 1.16GHz

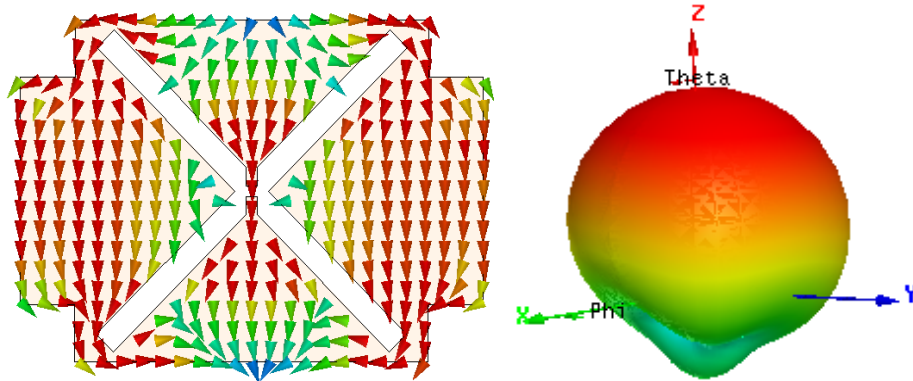


Figure 4.4 (d) Simulated surface current distribution and 3D radiation pattern of the frequency reconfigurable microstrip antenna for tunable frequency ratio with $C=10\text{pF}$ at 1.99GHz ($L=30.9\text{mm}$, $W=43.5\text{mm}$, $L_s=5.1\text{mm}$, $L_x=18.3\text{mm}$ and $W_x=2.3\text{mm}$.)

A single feed design of novel compact frequency reconfigurable microstrip antenna for tunable frequency ratio is proposed in this section. The concept is based on the tuning of embedded slot in the patch antenna using a chip capacitor. This property of the antenna offers more flexibility in frequency tuning where the frequency ratio varies in a wider range from 1.84 to 1.68 when the capacitance is varied from 2.2pF to 82pF with linearly polarized radiation along Y-direction. Furthermore the proposed antenna has an added advantage of size reduction, moderate gain and low levels of cross-polarized radiation keeping the radiation patterns of each frequency unchanged as the capacitor value is changed.

4.3 Frequency and polarization tuning of a microstrip antenna using capacitive loading

In this section, a novel compact microstrip antenna achieving frequency and polarization tunability is presented. A chip capacitor inserted normal to the feed line at the center of the X-slot is used to tune the operating frequency and polarization of the antenna. Polarization of the antenna is switchable between LP and CP by resoldering the right value for the lumped element without changing the geometrical parameters of the antenna. The frequency ratio can assume any value in the range $1.025 \leq f_r \leq 1.21$. The important aspect of this

design is that it provides an area reduction of 79% for the first frequency and 66% for the second frequency when compared with a standard rectangular patch operating at the same frequencies. The validity of this concept is demonstrated by simulated and measured results which show low cross polar level for linear polarization and good axial ratio for circular polarization.

4.3.1 Antenna Geometry

The proposed antenna configuration shown in figure 4.5 is same as that discussed in section 4.2.1 except for the orientation of the chip capacitor. Here, the chip capacitor is inserted horizontally to obtain a dual frequency antenna with adequate control over its frequency ratio.

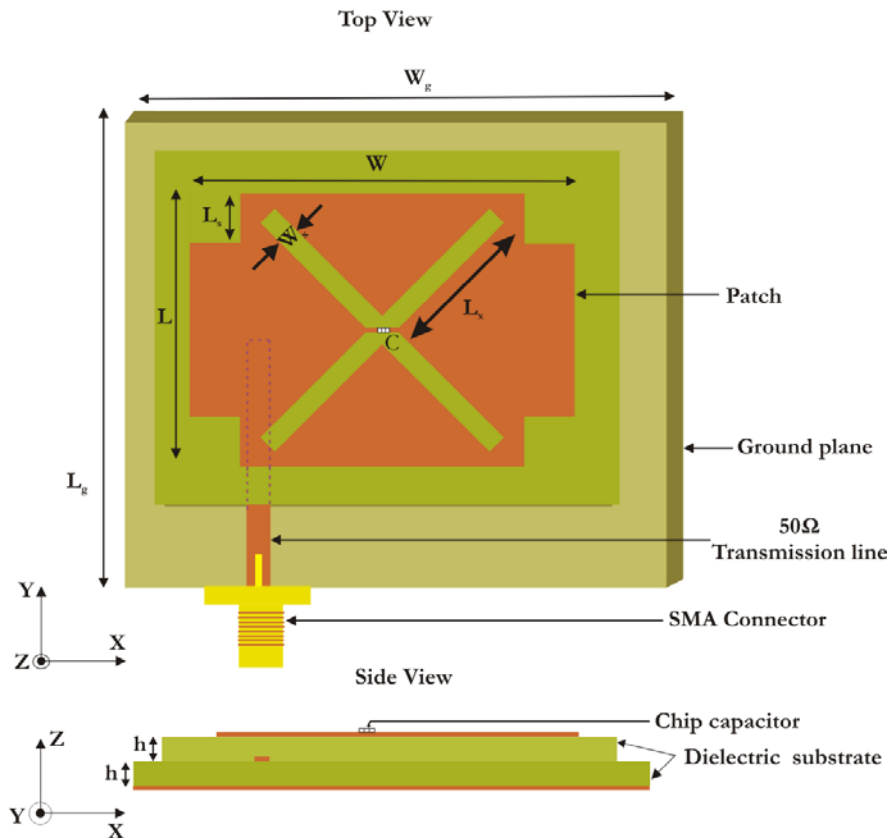


Figure 4.5 Geometry of frequency and polarization reconfigurable cross patch antenna using chip capacitor ($L=30.9\text{mm}$, $W=43.5\text{mm}$, $L_s=5.1\text{mm}$, $L_x=18.3\text{mm}$, $L_g=W_g=75\text{mm}$ and $W_x=2.3\text{mm}$)

4.3.2 Simulated and Measured results

A prototype of the antenna is fabricated on a substrate of $\epsilon_r= 4.4$ and $h=1.6\text{mm}$ with the parameters $L=30.9\text{mm}$, $W=43.5\text{mm}$, $L_s=5.1\text{mm}$, $L_x=18.3\text{mm}$ and $W_x=2.3\text{mm}$. The measurements of the antenna are done using HP8510C vector Network Analyzer. The resonant frequencies of the antenna can be reconfigured by loading a chip capacitor at the center of the X-slot. The location of the capacitor is chosen normal to the feed line that minimizes the variations of TM_{01} mode and at the same time TM_{10} mode can be tuned by changing the value of the capacitor to obtain a frequency and polarization tunable antenna with adequate control over its frequency ratio.

The reflection characteristics of the antenna for different capacitor values are shown in figure 4.6. Only a few variations are shown for brevity. The variation of resonant frequency for different values of chip capacitor is given in Table 4.2. It can be seen that the TM_{10} mode is tuned to 672 MHz from 1.118GHz with capacitor value $C=3.3\text{pF}$. The effective resistance of this mode decreases drastically and is suppressed due to very low impedance ($4.7-j2.5 \Omega$) by increasing the capacitor values from 10pF onwards. Also, loading a chip capacitor generates an additional TM_{10} mode at higher frequency due to shortest electrical path through the capacitor along X-direction. This third resonant frequency is not matched for low C values due to high inductive reactance ($68+j58 \Omega$) and achieves impedance matching by increasing the value of C from 2.2pF to 100pF. In addition, increase in C offers tuning to 1.594GHz from 1.748GHz and all the frequencies are well matched, except for $C=1\text{pF}$, with a linearly polarized radiation along x-direction.

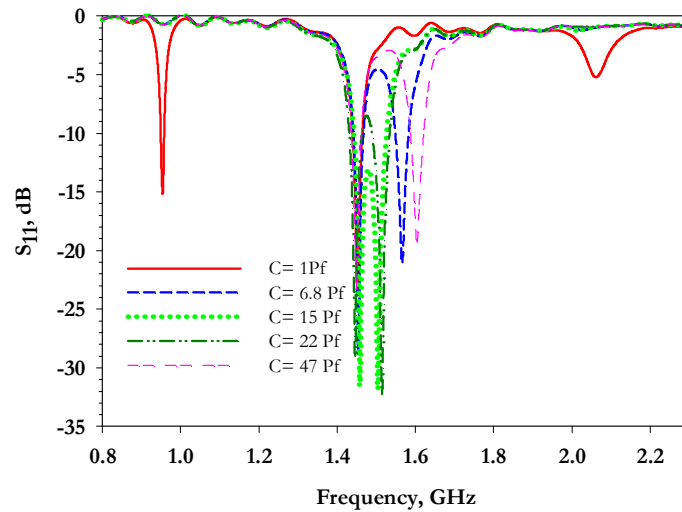


Figure 4.6 Measured reflection coefficient of the frequency and polarization reconfigurable cross patch antenna against different capacitance ($L=30.9\text{mm}$, $W=43.5\text{mm}$, $L_s=5.1\text{mm}$, $L_x=18.3\text{mm}$ and $W_x=2.3\text{mm}$).

The TM_{01} mode is well matched for all values of capacitance ranging from 1pF to 100pF , which gives a linearly polarized radiation along Y-direction. A slight variation is observed when the value of C is increased, but this change is negligible compared to that of third resonant frequency. Hence, it is found that the second resonance is determined by the cross patch antenna with X-slot while the first and third resonance is excited with respect to the chip capacitor value. Thus, the antenna offers a frequency ratio of 1.66 and 1.09 for first and second resonances with linearly polarized radiation along x-direction and y-direction respectively. With capacitor value equal to 15pF , the 2:1 VSWR bandwidth is measured to be 90 MHz , which amounts to 6% with respect to the centre frequency of 1.49 GHz . In addition, the second and third modes come close together which results a circularly polarized radiation at 1.465GHz . The measured resonant frequencies f_1 , f_2 and f_3 along with frequency ratio f_R (f_3/f_2) with various capacitances is shown in figure 4.7. The

simulated surface current distribution and 3D radiation patterns of the antenna without capacitor, with $C=6.8\text{pF}$ and 15pF are shown in figure 4.8. An additional shortest electrical length through the center of the X-slot is produced by embedding a capacitor horizontally at the center of the X-slot as seen in figure 4.8 (d). This length varies against various capacitance values and determines the frequency ratio of the two operating frequencies.

The measured axial ratio of the antenna when $C=15\text{pF}$ is plotted in figure 4.9. The best CP performance in the broadside direction is achieved at 1.465GHz with 3% CP bandwidth. The measured radiation patterns of the antenna for capacitor values 1pF , 6.8pF and 15pF are plotted in figure 4.10. It is observed that the antenna has similar radiation patterns at both the modes and the shape of the patterns remain unchanged as the capacitor value is changed. A broadside radiation characteristic in both XZ- and YZ-planes with more than 100° half power beam width are obtained in all linear polarization states. Furthermore, low cross polar levels are achieved. The cross-polarization levels are, however, larger at 952MHz due to smaller electrical dimensions of the antenna at this frequency.

The gain is also measured using a double ridged horn as a reference. The antenna shows a peak gain of 3.39dBi in the direction of maximum radiation. The lower gain of the antenna is a result of smaller electrical dimensions at lower frequencies that occurs due to capacitive loading.

Table 4.2 Performance of the frequency and polarization reconfigurable cross patch antenna against various capacitances

Capacitor (pF)	f ₁ (GHz), S11(-dB)	f ₂ (GHz), S11(-dB)	f ₃ (GHz), S11(-dB)	Input impedance (Ω)					
				f ₁		f ₂		f ₃	
				Re.	Im.	Re.	Im.	Re.	Im.
0	1.118, 23	1.44,20	56	+3.6	49.9	+9.5
1	0.953, 26	1.447, 21	2.07, 6.7	46	-2	49	+9	68	+58
2.2	0.772, 10.65	1.444, 18	1.748, 14	37.6	-9.8	52	+12	73	-7.5
3.3	0.672, 9.5	1.463, 18.5	1.639, 23	22.8	-3.5	62.7	+3.3	44.5	-3.8
4.7	0.596, 5	1.46, 23	1.617, 20	13	-4	56	+4	49	-10
6.8	0.505, 3	1.448, 19	1.559, 29	16.9	-13.3	57	+9	53	+1
8.2	0.453, 2.5	1.463, 17	1.552, 28.5	9.5	+28	64	+6.5	52	+3
10	0.419, 1.6	1.443, 17	1.538, 46	4.7	-2.5	54	+13	50.6	+0.3
15	1.445-1.535			57.5	-8	54.5	+3.4
22	...	1.442, 38	1.515, 21	50.9	+0.8	49.3	-9
47	...	1.444, 20	1.599, 26	60	+4.3	51.7	-4.7
100	...	1.489, 25	1.594, 32	50.5	-5.5	51.5	-2

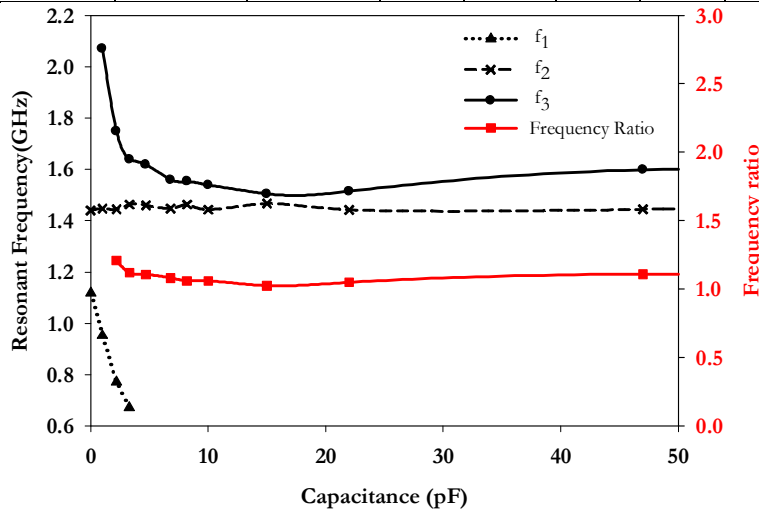
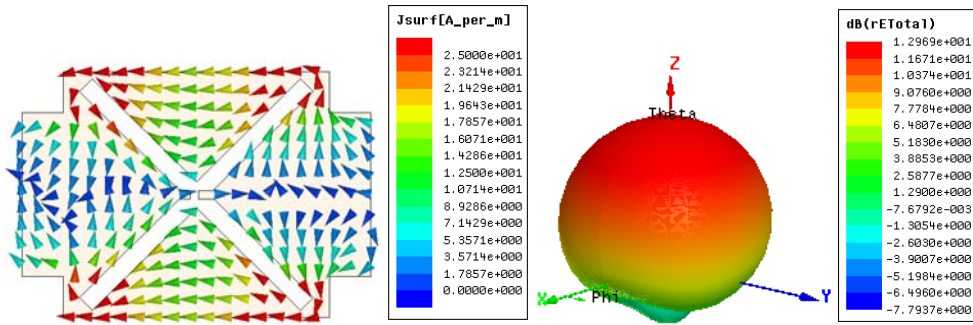
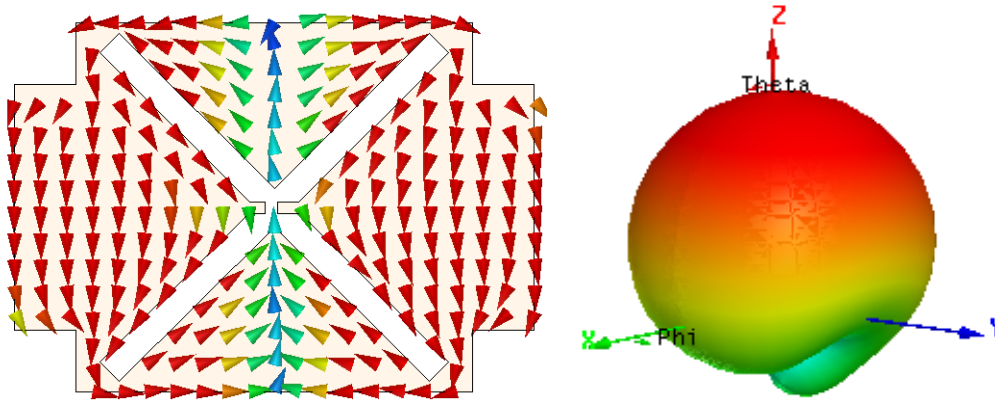


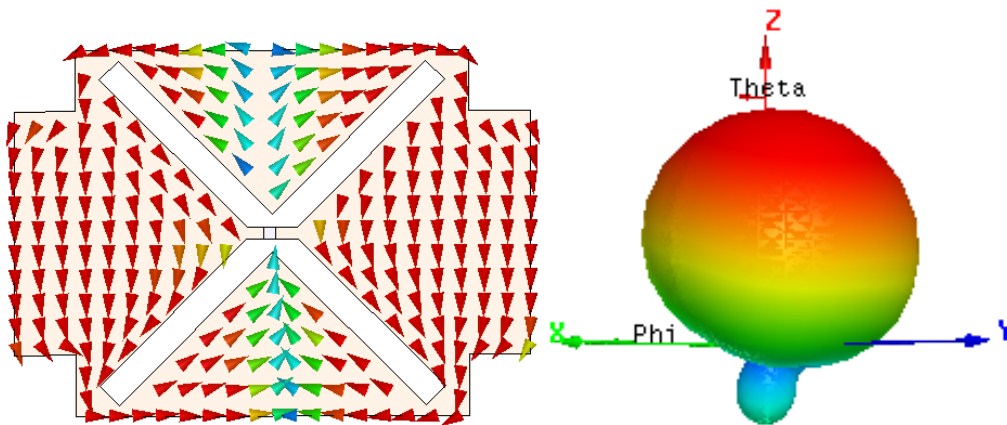
Figure 4.7 Variation of resonant frequencies and frequency ratio of frequency and polarization reconfigurable cross patch antenna against different capacitance (L=30.9mm, W=43.5mm, L_s=5.1mm, L_x=18.3mm and W_x=2.3mm).



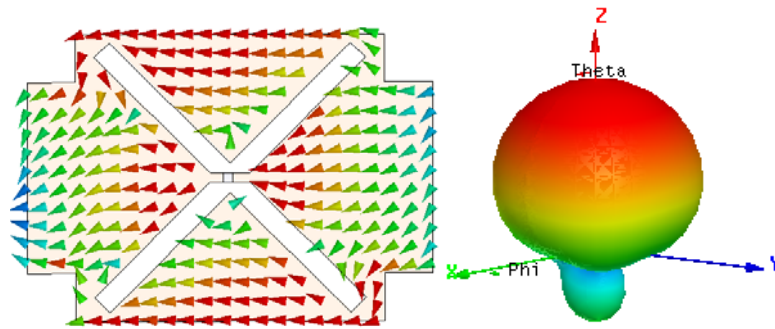
(a) at 1.1GHz without chip capacitor



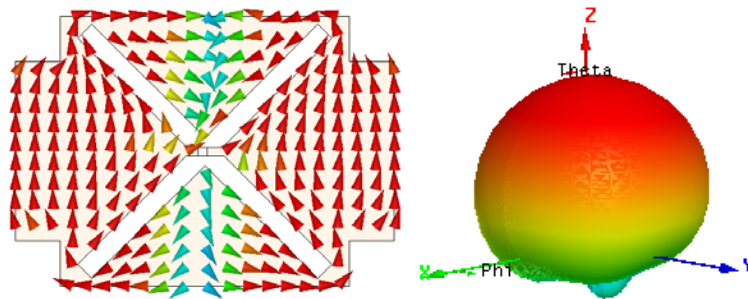
(b) at 1.4GHz without capacitor



(c) at 1.448GHz with C=6.8pF



(d) at 1.559GHz with $C=6.8\text{pF}$



(e) at 1.465GHz with $C=15\text{pF}$

Figure 4.8 Simulated surface current distribution and 3D radiation pattern of the frequency and polarization reconfigurable cross patch antenna for different capacitance values ($L=30.9\text{mm}$, $W=43.5\text{mm}$, $L_s=5.1\text{mm}$, $L_x=18.3\text{mm}$ and $W_x=2.3\text{mm}$).

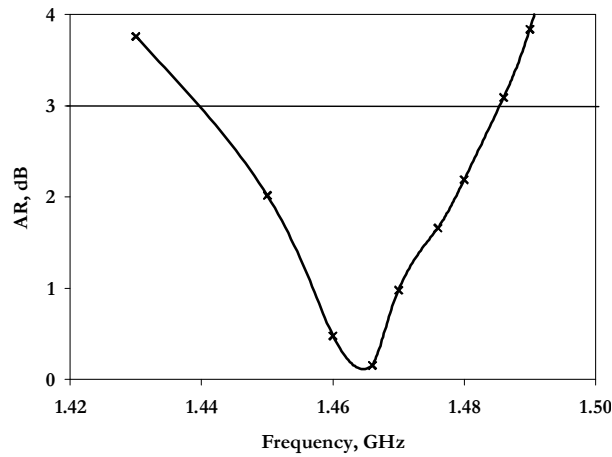


Figure 4.9 Measured axial ratio of the frequency and polarization reconfigurable cross patch antenna when $C=15\text{pF}$ ($L=30.9\text{mm}$, $W=43.5\text{mm}$, $L_s=5.1\text{mm}$, $L_x=18.3\text{mm}$ and $W_x=2.3\text{mm}$).

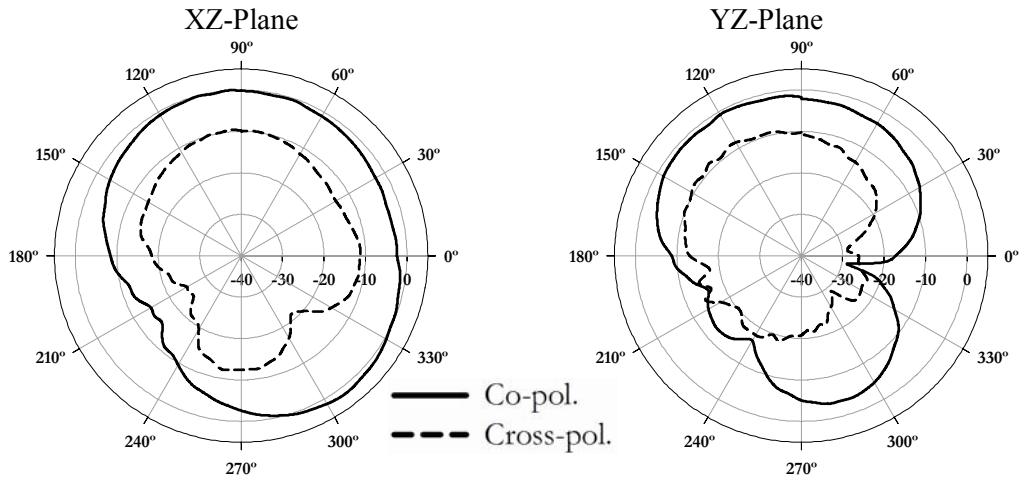
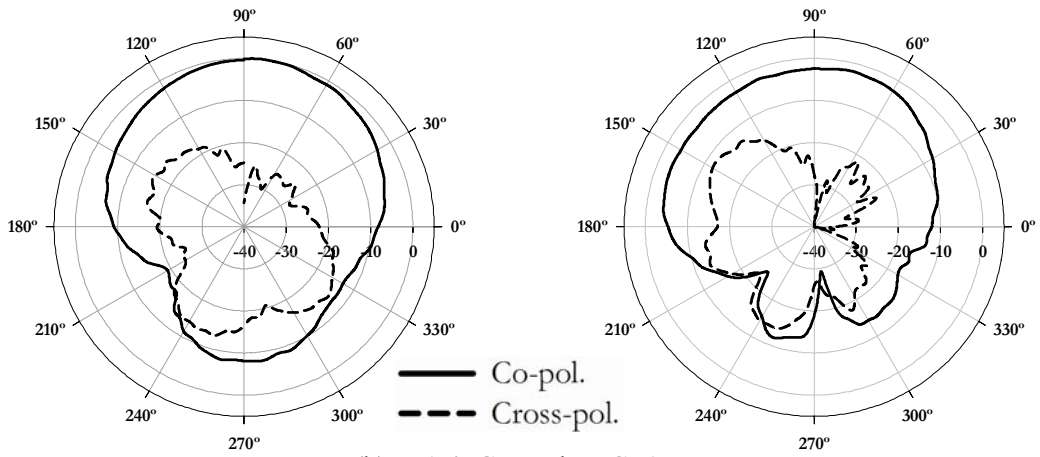
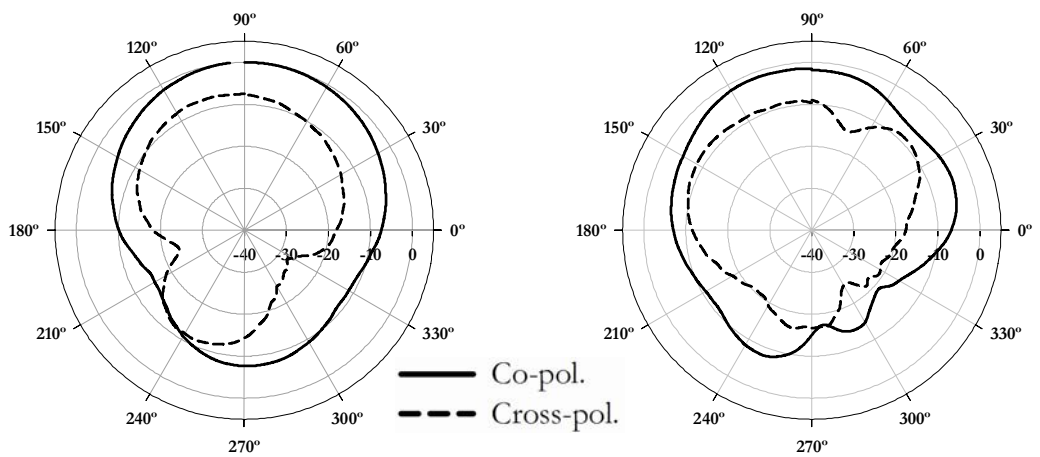


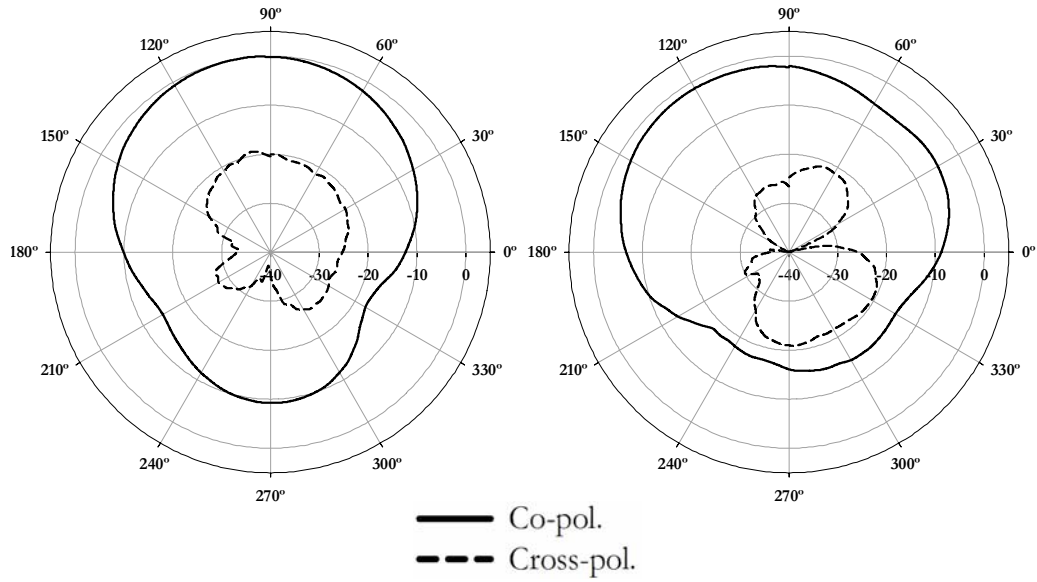
Figure 4. at 952MHz when C=1pF



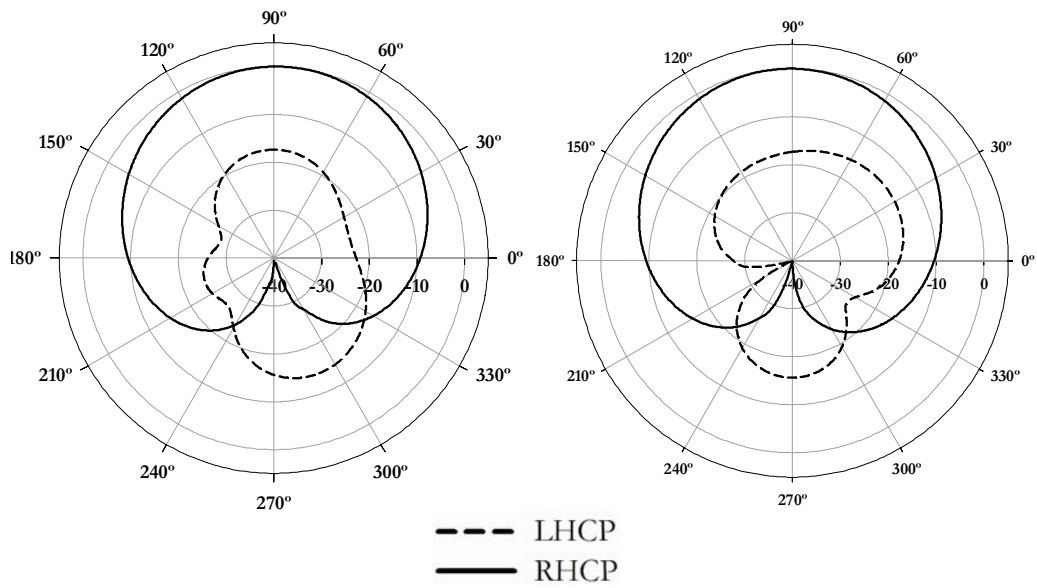
(b) at 1.45GHz when C=1pF



© at 1.45GHz when C=6.8pF



(d) at 1.56GHz when C=6.8pF



(e) at 1.465GHz when C=15pF

Figure 4.10 Measured radiation pattern of the frequency and polarization reconfigurable cross patch antenna with various capacitances ($L=30.9\text{mm}$, $W=43.5\text{mm}$, $L_s=5.1\text{mm}$, $L_x=18.3\text{mm}$ and $W_x=2.3\text{mm}$).

A single feed design of novel compact frequency and polarization tunable microstrip antenna proposed in this section is based on the tuning of embedded slots in the patch antenna using a chip capacitor. A high tuning range of 34.48% and 14.3% is achieved for the first and third resonant frequencies respectively by minimizing the variations of second resonant frequency. Measurement results of the antenna indicate that its frequency ratio can assume any value in the range $1.025 \leq f_R \leq 1.21$ with linear or circularly polarized radiation by changing the capacitor value from 1pF to 100pF. Furthermore the proposed antenna has an added advantage of size reduction, moderate gain, low levels of cross-polarized radiation and the radiation patterns of each frequency remain unchanged as the capacitor value is changed. By replacing the chip capacitor with a varactor diode the proposed design can be extended to frequency agile polarization diversity antenna.

4.4 Varactor controlled frequency reconfigurable microstrip antenna

One of the demands for future wireless communication systems is higher data rates to offer new services by the service providers. To achieve higher data rates the concept of MIMO (Multiple-Input Multiple-Output) systems has emerged. The basic principle behind MIMO is to use multiple antennas in contrast to the currently deployed systems mostly based on single antenna systems. The handheld devices need to be small and at the same time versatile due to the mobility of the user. To improve the overall performance following the MIMO paradigm, several antenna elements may be introduced on each handheld device. Requiring one feed chain per antenna element, this would result in a considerable increase in space, cost, and complexity and makes the implementation of large MIMO systems a difficult task. One way to overcome

the setbacks is the use of reconfigurable antennas. For a fixed number of antenna elements in an antenna array, the choice of reconfigurable elements will increase the number of possibilities. The reconfigurability is preferably achieved by integrating switches or varactors with the antenna to save space. A single tunable antenna would eliminate the need for multiple antennas operating in various frequency bands.

All the results and discussions stated in above sections convincingly proved the novel concept of tuning mechanism which can be used either to tune the frequency ratio or to reconfigure the frequency and polarization of the proposed dual frequency dual polarized single feed cross patch antenna. The important characteristic of frequency reconfigurable antenna is their flexibility in operation. That is, one can easily control their operating frequency electronically without changing the capacitors. This is accomplished by varactors integrated to the extended slot arms of the dual frequency dual polarized cross patch antenna.

4.4.1 Varactor diode

A varactor diode is a P-N junction diode that changes its capacitance and the series resistance as the bias applied to the diode is varied. The property of capacitance change is utilized to achieve a change in the frequency and/or the phase of an electrical circuit. The key electrical parameters guiding the selection and usage of a varactor diode are

- Reverse breakdown voltage and reverse leakage current.
- Capacitance value and the capacitance-voltage change behavior.

- Quality factor (also known as figure of merit), Q.

The junction capacitance of a varactor varies against the bias voltage and can be calculated from the applied bias voltage as,

$$C = \frac{C_0}{\left[1 - \frac{V}{V_{bi}}\right]^\gamma}$$

Where C_0 is the varactor capacitance at zero bias voltage, V is the applied bias voltage, V_{bi} is the built-in-potential and γ is a constant depending upon the doping profile of the p-n junction. From this equation it is clear that the capacitance value decreases with increase in reverse bias voltage of the varactor.

BB 152 diode from the Philips semiconductors are utilized for the frequency reconfigurable antenna discussed in this section and its characteristics are listed in Table 4.3. During simulation, the varactor is modeled as a lumped capacitor by selecting appropriate values for different bias voltages as provided in the data sheet. The incorporation of a varactor diode and its associated biasing circuitry introduces insertion loss. This will reduce the gain and cross-polarization level of linearly polarized radiation.

4.4.2 Antenna Geometry

The configuration of the proposed antenna is shown in figure 4.11. The antenna is fabricated on a substrate of thickness h (1.6 mm) and relative permittivity ϵ_r (4.4). The initial cross patch is obtained by removing the four square regions of side L_s mm from the corners of a rectangular patch of size $L \times W$ mm². An X-slot of arm length L_x mm and width W_x mm is then carved at the center of the cross patch. The antenna is electromagnetically coupled using a

50Ω microstrip line fabricated using the same substrate material. The dimension of the ground plane is 75 x 75 mm². Varactor diodes D₁, D₂, D₃ and D₄ are positioned at the extreme end of the slot arms in order to get maximum tuning range and better matching. DC bias voltage is supplied from a battery through chip inductors. The details of the varactor are listed in Table 4.3.

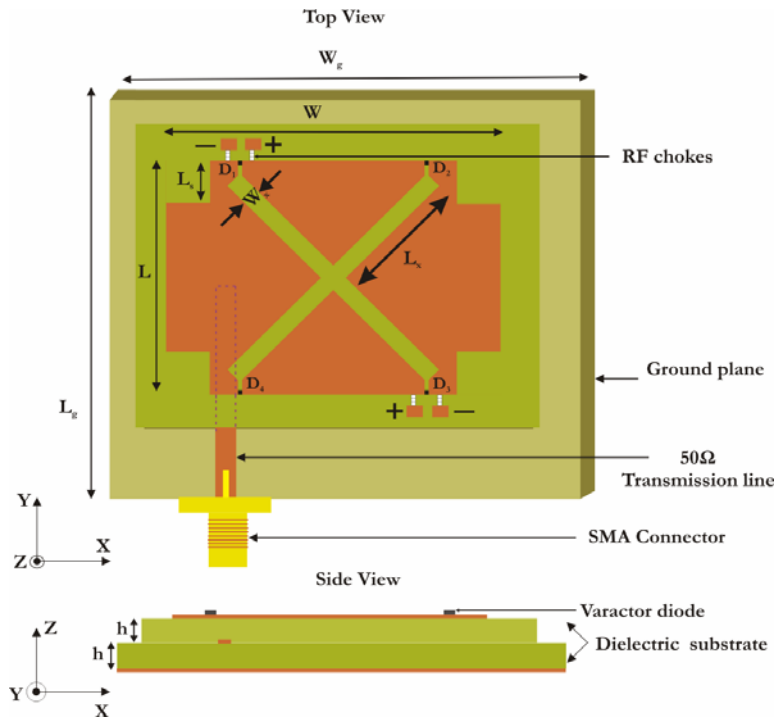


Figure 4.11 Geometry of frequency reconfigurable microstrip antenna using varactor diodes ($L=30.9\text{mm}$, $W=43.5\text{mm}$, $L_s=5.1\text{mm}$, $L_x=18.3\text{mm}$, $L_g=W_g=75\text{mm}$ and $W_x=2.3\text{mm}$).

Table 4.3 Varactor details

Type number	BB152
Package	SC-76
Version	SOD 323
Manufacturer	Philips semiconductors
Reverse voltage	32V
Diode series resistance	1Ω
Diode capacitance	2.48pF-62pF

4.4.3 Simulated and Measured results

To implement electronic reconfigurability, varactor diodes are directly integrated across the extended slot arms and DC bias is applied through two chip inductors. The junction capacitance of the varactors varies against the reverse bias voltage applied and these different capacitive loadings correspond to different electrical lengths and thus different resonant frequencies. The positions of the varactors are so selected to achieve maximum frequency tuning while less perturbing the antenna matching. The measured reflection coefficients of the antenna are shown in figure 4.12. When the reverse bias is OFF, the varactor loadings in all the slot arms correspond to high capacitance. Thus the resonant frequencies are lowered to 1.03 GHz and 1.28GHz with a frequency ratio of 1.279. It is observed that the varactors modify the electrical lengths of TM_{01} and TM_{10} modes of the patch which result an orthogonally polarized dual frequency reconfigurable antenna.

The reconfigurable antenna was then electronically tuned with a reverse DC voltage applied across the diodes. When the bias voltage is varied from 0 to 16 V, the tuning range for the first resonant frequency is found to be 26.3% or 279MHz upwards (from 1.02 to 1.299 GHz) and that of second resonant frequency is 15.3% or 197MHz upwards (from 1.305 to 1.502 GHz). At 16V the frequency ratio is found to be 1.156. The variation of first and second resonant frequencies (f_1 and f_2) with the applied varactor reverse bias voltage is measured and plotted in figure 4.13. The simulated surface current distribution and 3D radiation pattern of the antenna at 1.03GHz and 1.28GHz are given in figure 4.14. It is observed that the varactor loaded X-slot modifies the electrical lengths of TM_{01} and TM_{10} modes of the patch which result an orthogonally polarized dual frequency reconfigurable antenna.

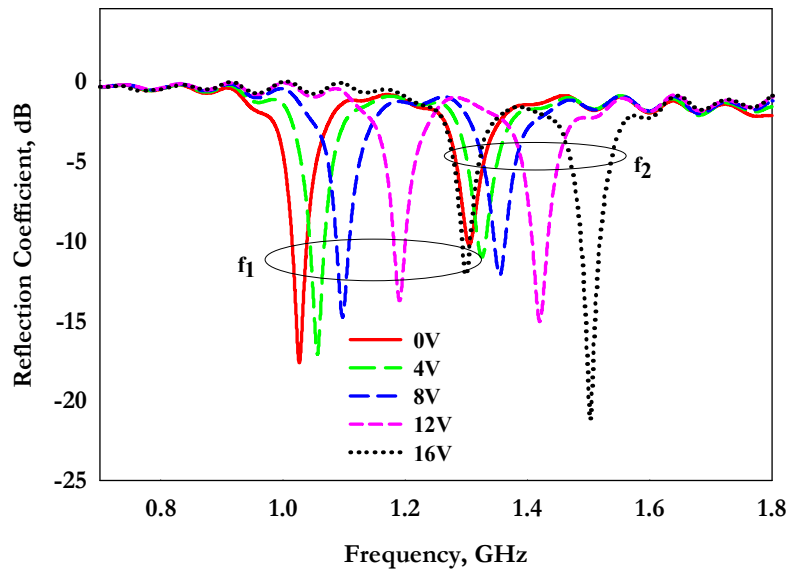
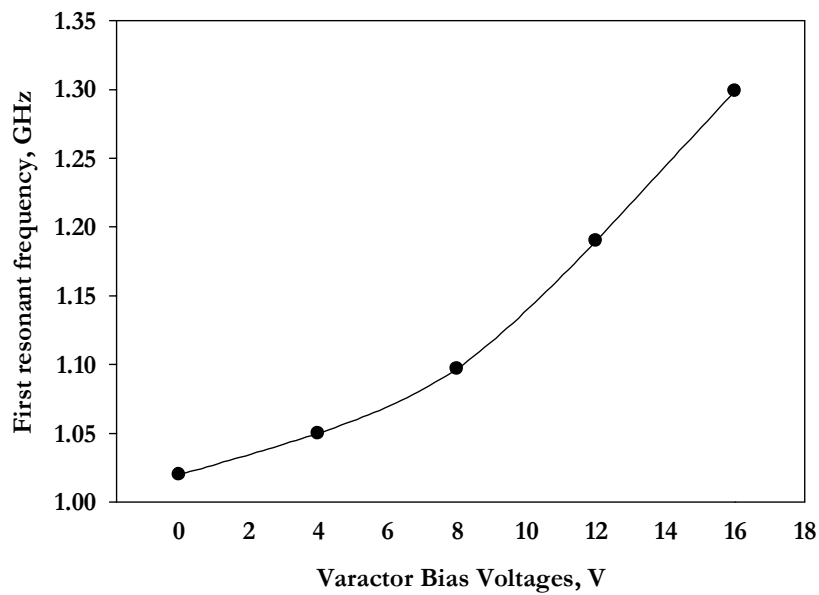


Figure 4.12 Measured reflection coefficient of the dual frequency reconfigurable microstrip antenna ($L=30.9\text{mm}$, $W=43.5\text{mm}$, $L_s=5.1\text{mm}$, $L_x=18.3\text{mm}$ and $W_x=2.3\text{mm}$).



(a)

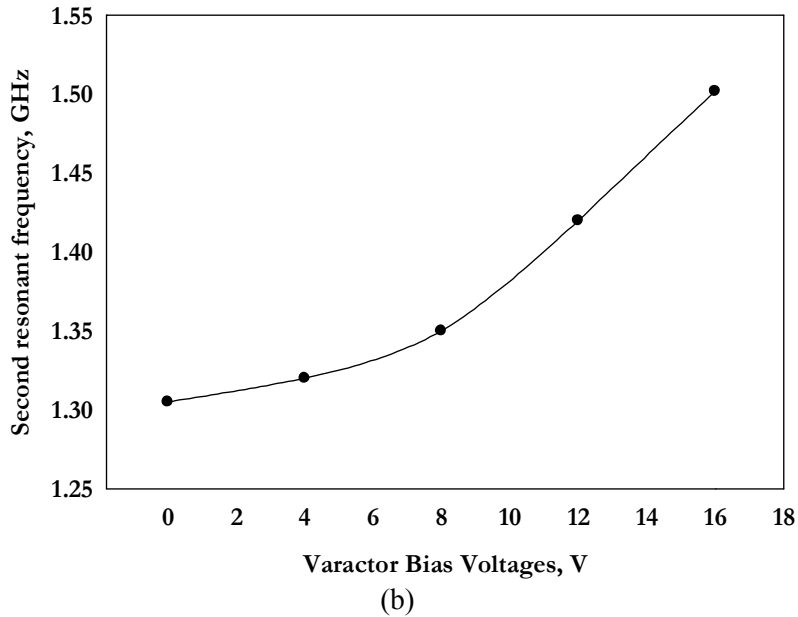


Figure 4.13 Variation of resonant frequencies against bias voltages (a) first resonant frequency (b) second resonant frequency ($L=30.9\text{mm}$, $W=43.5\text{mm}$, $L_s=5.1\text{mm}$, $L_x=18.3\text{mm}$ and $W_x=2.3\text{mm}$).

The E and H -plane radiation patterns of the reconfigurable antenna are measured for different bias voltages. All the patterns show similar broadside radiation characteristics with good cross polarization levels even when the operating frequencies are shifted greatly by applying reverse bias. Typical radiation patterns for the resonant frequencies of 1.03GHz and 1.28GHz for 0V and 1.3GHz and 1.48GHz for 16V are given figure 4.15(a), (b), (c) and (d) respectively. Bandwidths up to 2.26% and 2.36% respectively, have been obtained in the two modes. The polarization planes of the two resonant frequencies are mutually orthogonal in the entire tuning range. The gain is also measured using a double ridged horn as a reference. The peak gain of the reconfigurable antenna is found to be nearly 2.1 dB and 1.2 dB less for the first and second resonant frequencies respectively. The low gain values are due to the opposing currents on either side of the slot arm which cause field cancellation along the axis at the far-field.

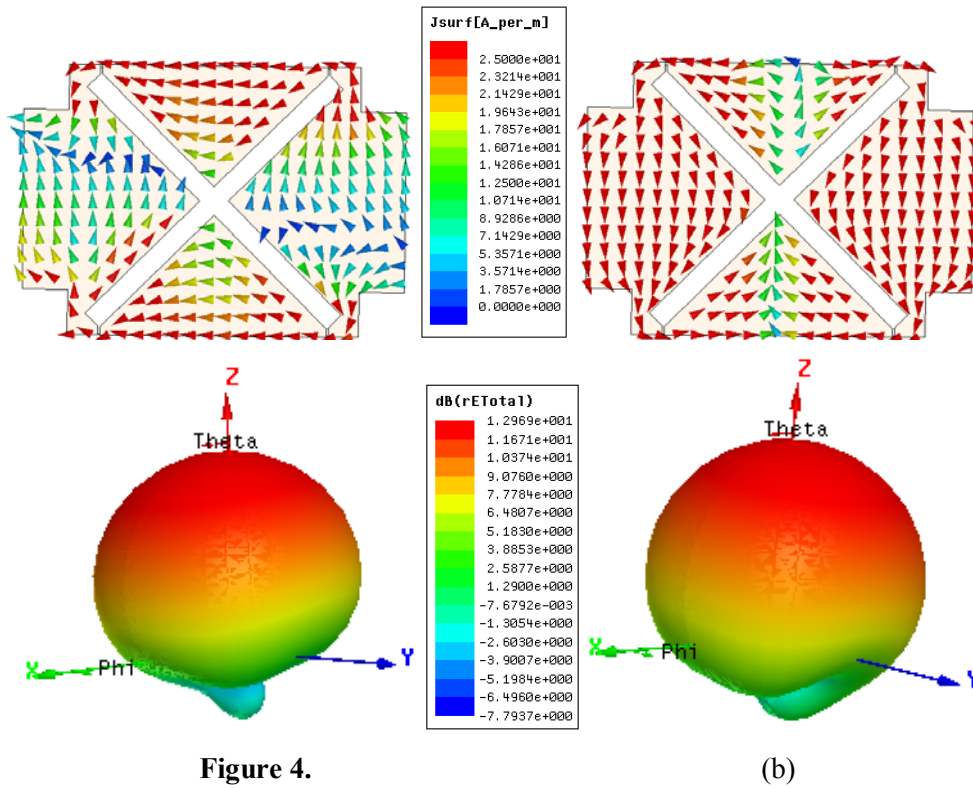


Figure 4.14 Simulated surface current distribution and 3D radiation pattern of the frequency reconfigurable cross patch antenna at (a) 1.03GHz and (b) 1.28GHz when biasing 0V ($L=30.9\text{mm}$, $W=43.5\text{mm}$, $L_s=5.1\text{mm}$, $L_x=18.3\text{mm}$ and $W_x=2.3\text{mm}$).

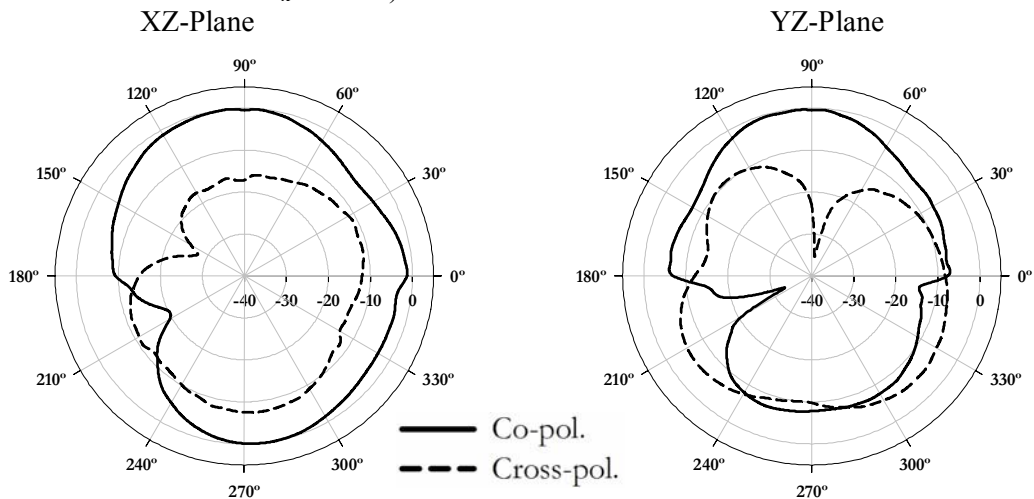


Figure 4. at 1.03GHz when biasing 0V

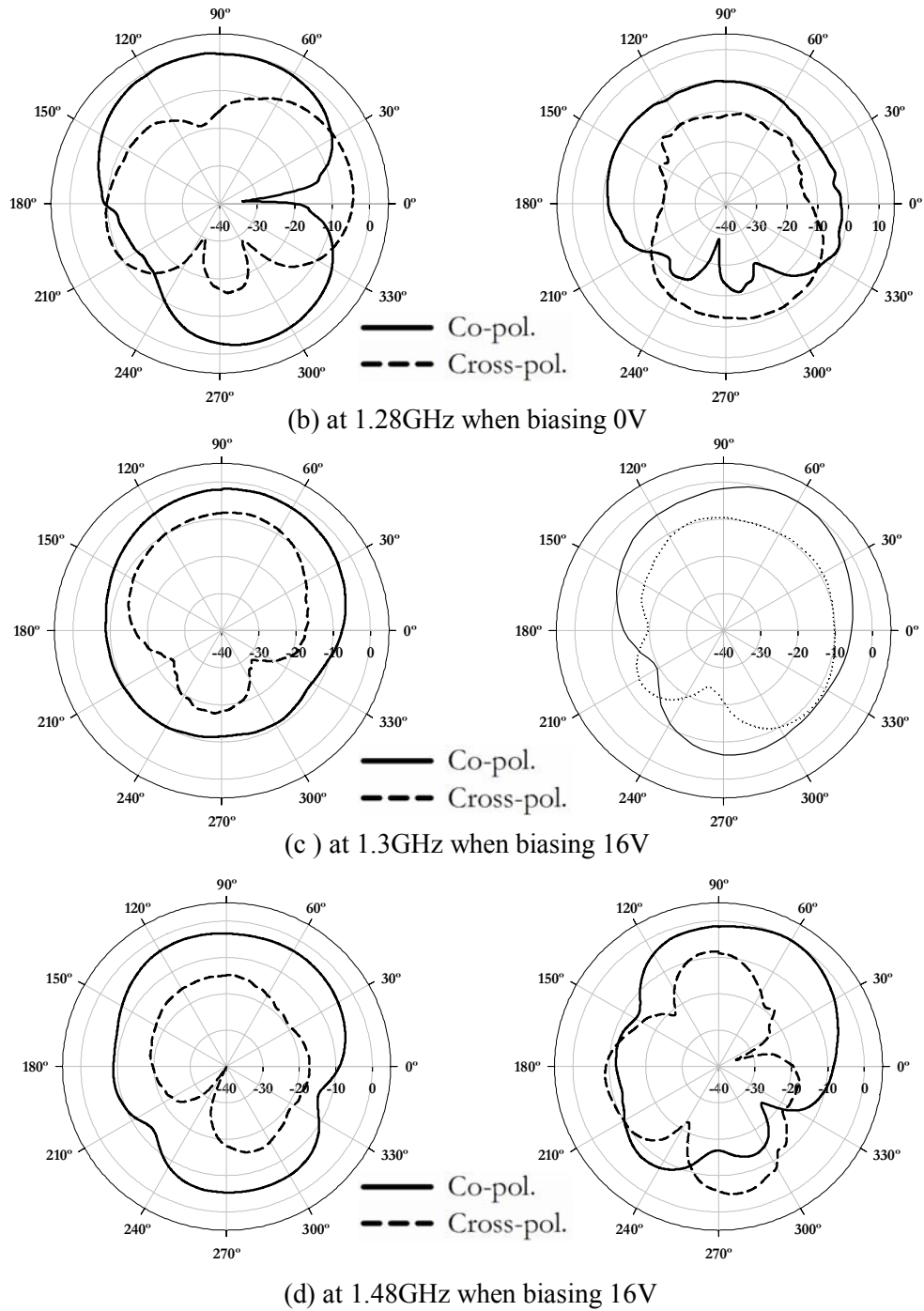


Figure 4.15 Measured radiation patterns of frequency reconfigurable cross patch antenna ($L=30.9\text{mm}$, $W=43.5\text{mm}$, $L_s=5.1\text{mm}$, $L_x=18.3\text{mm}$ and $W_x=2.3\text{mm}$).

A single feed design of compact, electronically reconfigurable dual frequency microstrip antennas is proposed in this section. The concept is based on the electronic tuning of embedded slots in the patch antenna using varactor diodes. A high tuning range of 26.3% (1.02–1.299 GHz) and 15.3% (1.305–1.502 GHz) is achieved for the two operating frequencies respectively, when the bias voltage is varied from 0 to 16V. The salient feature of this design is that it uses no matching networks even though the resonant frequencies are tuned in a wide range with good matching below -10 dB. The antenna has an added advantage of size reduction up to 77% and 64% for the two operating frequencies compared to conventional rectangular patches. Another feature of this antenna is that the radiation characteristic is remaining essentially unaffected by the frequency tuning.

4.5 Frequency and polarization reconfigurable cross patch antenna using varactor

MIMO systems introduce diversity at the mobile station allowing highly reliable communications compared to a corresponding SISO systems. One possibility to obtain diversity is to displace the antenna elements. This would give space diversity, meaning that the difference in paths for the two antennas is used. A different polarization at the antenna elements is another way of obtaining diversity. By having the possibility to change the receiving polarization the risk of losing information is reduced because of the incoming signal having a certain polarization. A third way of achieving diversity is to use antenna elements with different radiation patterns. By combining elements with different patterns, additional directions could be covered and the risk of losing information because of fading is reduced.

The frequency agility and polarization diversity provide added flexibility to the microstrip antenna. Furthermore, these features are obtained without sacrificing the thin conformal structure of the microstrip antenna and without increasing the complexity of the external microwave feed network. In this section, a simple compact frequency agile microstrip antenna achieving polarization diversity is presented. The proposed antenna reconfigures both frequency and polarization electronically without changing the geometrical parameters and devoid of any impedance matching circuitry. The radiation patterns are independent of tuning voltage which is highly desirable for reconfigurable microstrip antennas. In addition, the antenna requires only a single varactor and less area to occupy the patch and dc-bias circuit compared to conventional polarization diversity antennas available in literature.

4.5.1 Antenna Geometry

As shown in figure 4.16, the proposed antenna is fabricated on a substrate of thickness h (1.6 mm) and relative permittivity ϵ_r (4.4). The antenna consists of a rectangular patch ($L \times W$ mm²) with square slit of side L_s mm at the four corners. An X-slot of arm length L_x mm and width W_x mm is carved at the centre of the cross patch. The antenna is electromagnetically coupled using a microstrip line fabricated on the same substrate. The position of the feed line is optimized using Ansoft HFSS for 50 Ω impedance matching. The varactor diode inserted at the centre of the slot is oriented normal to the feed line. The detail of the varactor is listed in Table 4.3. The dc bias lines are connected to the top part of the patch containing dc block capacitors, RF choke and input voltage. Two dc block capacitors (C_1 and C_2) are chosen to isolate the RF components from the dc signal and the RF choke inductor isolate the RF signal from the dc signal.

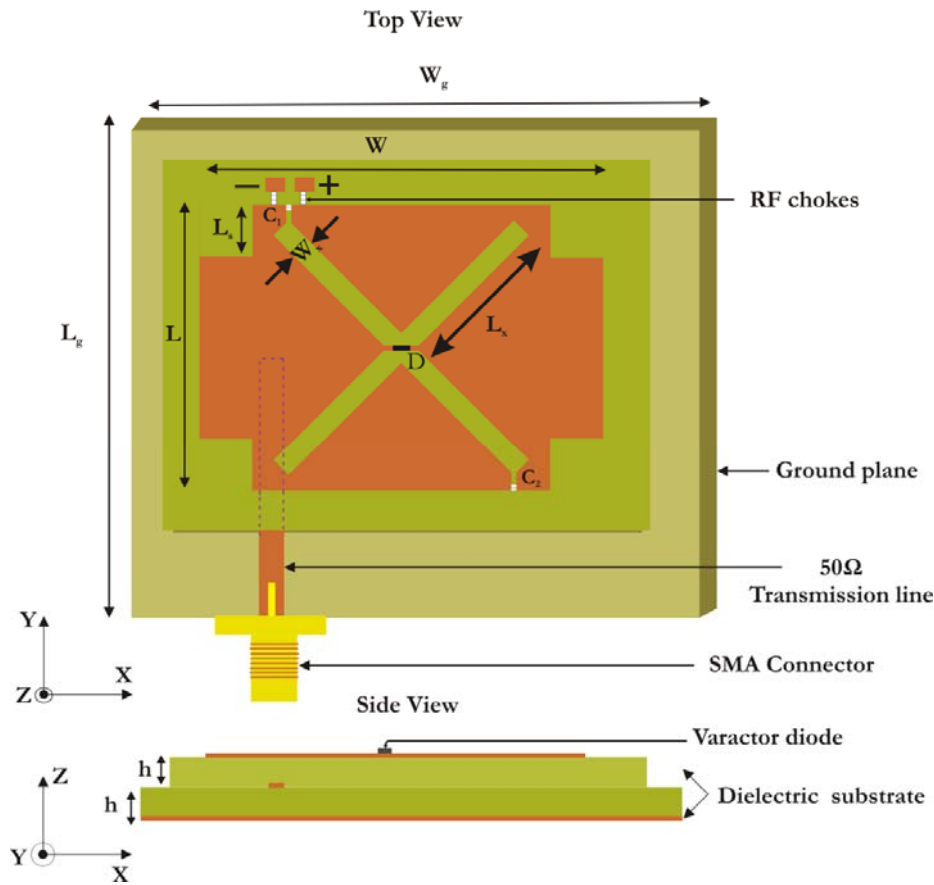


Figure 4.16 Geometry of frequency and polarization reconfigurable cross patch antenna ($L= 30.9\text{mm}$, $W= 43.5\text{mm}$, $L_x= 18.3\text{mm}$, $L_s=5.1\text{mm}$, $L_g=W_g=75\text{mm}$ and $W_x= 2.3\text{mm}$)

4.5.2 Simulated and Measured results

The fundamental resonant modes (TM_{10} and TM_{01}) of the unslotted cross shaped patch are at 1.74 GHz and 2.3 GHz with orthogonal polarizations. The proper selection of the slot size modifies the horizontal and vertical electrical lengths of the patch equally so that the two resonant frequencies are lowered to 1.13GHz and 1.44GHz. It is well evident that the insertion of the slot increases the current path thereby lowering the resonant frequency. The X-slot length is optimized using Ansoft HFSS to achieve maximum area reduction of 79% and 66% for the first and second frequency respectively when compared to a standard rectangular patch operating at the same frequencies.

A varactor diode inserted at the center of the X-slot is oriented normal to the feed line to achieve the reconfigurable polarization capability. The orthogonally polarized dual frequency cross patch antenna can be reconfigured for different polarization with respect to the bias voltage applied across the varactor. The bias circuit consists of two dc block capacitors, RF chokes and input voltage. The dc bias lines are connected to the top of the patch through RF chokes. Two dc block capacitors of $C_1=C_2=47\text{pF}$ are chosen to isolate the RF components from the dc signal and RF choke isolate the RF signal from flowing into the dc signal. The junction capacitance of the varactor diode varies against the reverse bias applied and these different capacitive loadings correspond to different electrical lengths along the X-direction. This behaviour results a strong effect on the TM_{01} mode but little on the TM_{10} mode of the patch with respect to the bias voltage. Thus, frequency and polarization agility is achieved electronically.

When the varactor inserted at the centre of the slot is oriented parallel to the feed line (vertical) the different capacitive loadings of the varactor correspond to different electrical lengths along the Y-direction with respect to the bias voltage. This behavior reconfigures the TM_{10} mode to higher frequency with the increase in bias voltage while keeping the TM_{01} mode unaffected.

Extensive parametric analysis is conducted to optimize the dimension of corner notches in the rectangular patch. From figure 4.17, it is observed that the impedance matching becomes poor when L_s is lowered. The increase in L_s causes the splitting of the resonance and $L_s=5.1\text{mm}$ is a good selection to achieve two near orthogonal resonant modes at 0V bias condition. The simulated surface current distribution of the antenna at 1.43GHz (biasing 0V) is shown in figure 4.18. A half-wave variation of current is observed through the center of the X-slot and another half wave variation around the edges of the X-slot arm. This behaviour results in the splitting of the current into two near orthogonal resonant modes.

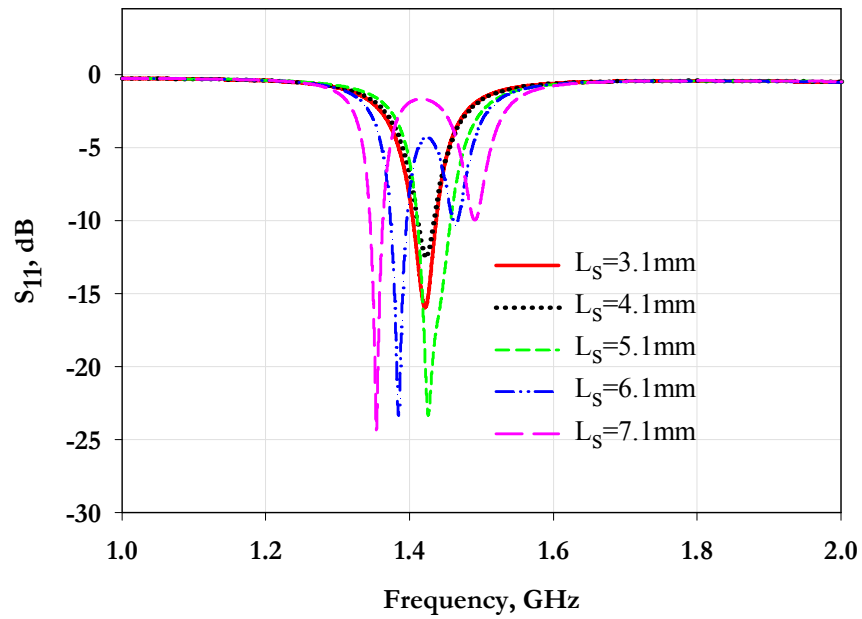


Figure 4.17 Effect of the corner notches in the frequency and polarization reconfigurable cross patch antenna ($L= 30.9\text{mm}$, $W= 43.5\text{mm}$, $L_x= 18.3\text{mm}$ and $W_x= 2.3\text{mm}$)

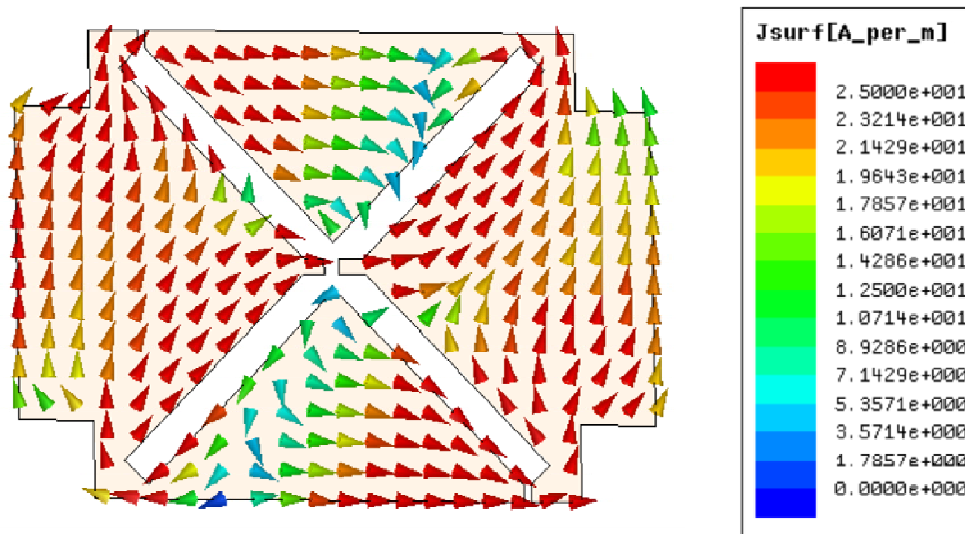


Figure 4.18 Simulated surface current distribution of the frequency and polarization reconfigurable cross patch antenna at 1.43GHz with 0V DC bias ($L=30.9\text{mm}$, $W=43.5\text{mm}$, $L_s=5.1\text{mm}$, $L_x=18.3\text{mm}$ and $W_x=2.3\text{mm}$).

The reflection characteristics of the antenna measured for different bias voltages are shown in figure 4.19. When the biasing voltage is held at 0V, the varactor offers very high reactance so that TM_{01} mode excited by the patch comes close together with the TM_{10} mode. Thus, the resonant frequency of one mode is slightly above the other yielding a circularly polarized (CP) radiation at 1.43GHz with 0.7% CP bandwidth. The antenna retains the CP performance up to 5V by reconfiguring its operating frequency. As the voltage applied across the varactor increases from 5 to 10V the junction capacitance decreases so that the coupling between the two adjacent modes decreases, yielding elliptical polarization. Further increase of bias voltage splits the adjacent modes into two orthogonal ones resulting in a dual frequency orthogonal polarized antenna in which the TM_{01} mode of the antenna can be reconfigured with respect to the bias voltage beyond 10V. A tunable frequency ratio of around 1.09 is achieved for TM_{01} mode against reverse bias applied from 10V to 25V. A slight variation is observed for TM_{10} mode but this change is negligible compared to that of TM_{01} mode. Hence, it is found that the first resonance is determined by the cross patch antenna with X-slot while the second resonance is tuned with respect to the bias voltage. The variation of resonant modes against bias voltage change is plotted in figure 4.20.

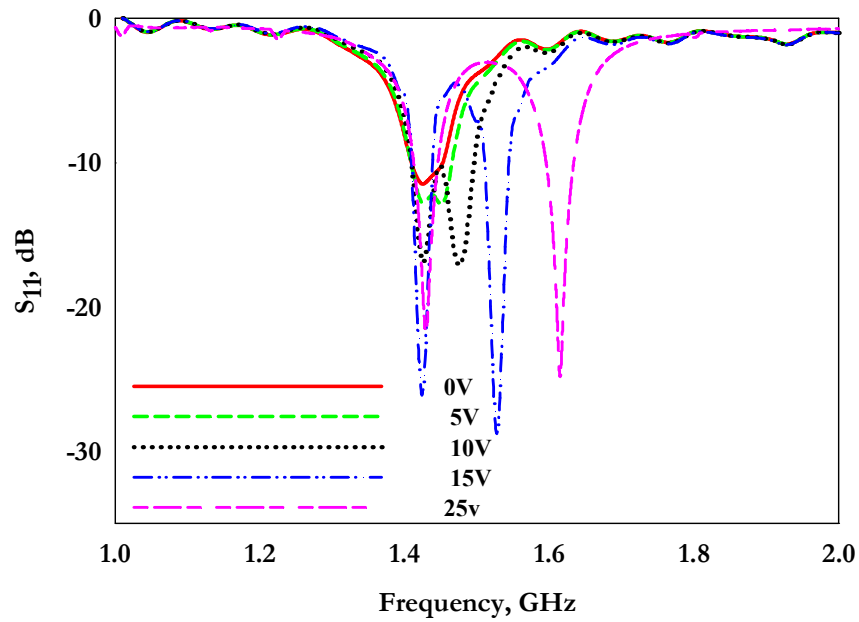


Figure 4.19 Measured reflection coefficient of the frequency and polarization reconfigurable cross patch antenna for different bias voltages ($L=30.9\text{mm}$, $W=43.5\text{mm}$, $L_s=5.1\text{mm}$, $L_x=18.3\text{mm}$ and $W_x=2.3\text{mm}$).

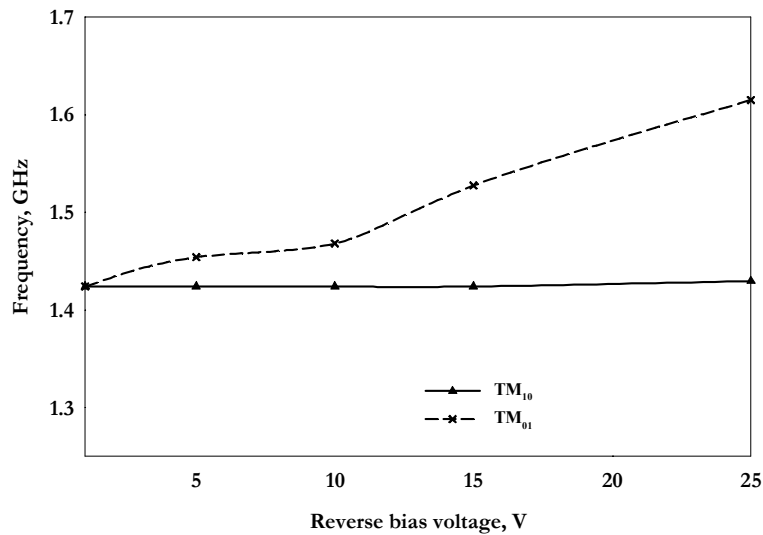


Figure 4.20 Variation of resonant modes with respect to the bias voltage variation of frequency and polarization reconfigurable cross patch antenna ($L=30.9\text{mm}$, $W=43.5\text{mm}$, $L_s=5.1\text{mm}$, $L_x=18.3\text{mm}$ and $W_x=2.3\text{mm}$).

The important aspect of this design is that it provides an area reduction of 79% for the first frequency and 66% for the second frequency when compared with a standard rectangular patch operating at the same frequencies. Thus, the antenna offers tuning from 1.43GHz to 1.615GHz with circular, elliptical and linear polarized radiation by varying the bias voltage from 0V to 25V.

The normalized co-polarization component measured at 1.43GHz in XZ- and YZ- planes for different bias voltages are plotted in figure 4.21(a) and (b) respectively. It is observed that the shape of the patterns are unaffected by electronic tuning which is highly desirable for reconfigurable microstrip antennas. Typical far-field radiation patterns of the antenna in two orthogonal planes of RHCP and LHCP mode plotted at 1.43GHz (0V) is given in figure 4.22. The best CP performance in the broadside direction is achieved with 10MHz axial ratio bandwidth.

The measured radiation patterns at 1.45GHz (biasing 10V) are plotted in figure 4.23. It is observed that the antenna is elliptically polarized at this frequency. A broadside radiation characteristic in both XZ- and YZ-planes with more than 100° half power beam width is obtained in all polarization states with a sufficient front-to-back ratio. The front-to-back ratio is determined by the ground plane size which is kept greater than that of the radiator since it strongly affects the radiation pattern and resonant frequency. Figure 4.24 shows the normalized patterns at 1.43GHz and 1.527GHz for the biasing of 15V. The antenna is linearly polarized with cross polar isolation of 8.9dB at 1.43GHz and 12dB at 1.527GHz. The current flowing around the edges of one of the slot arm cancels with that of the opposite arm. This degrades the polarization purity of the proposed antenna. Also, the antenna cross-polarization combines with the isolation of the switch/varactor giving place to a degradation of the polarization purity of the combined polarization diversity antenna.

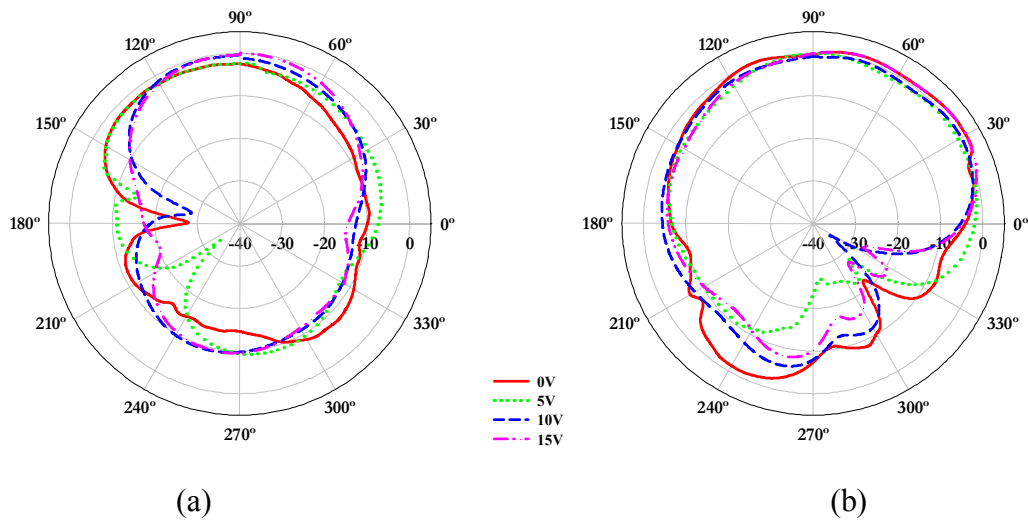


Figure 4.21 Radiation patterns of the frequency and polarization reconfigurable cross patch antenna measured at 1.43GHz for different bias voltages in (a) XZ-plane and (b) YZ-plane ($L=30.9\text{mm}$, $W=43.5\text{mm}$, $L_s=5.1\text{mm}$, $L_x=18.3\text{mm}$ and $W_x=2.3\text{mm}$).

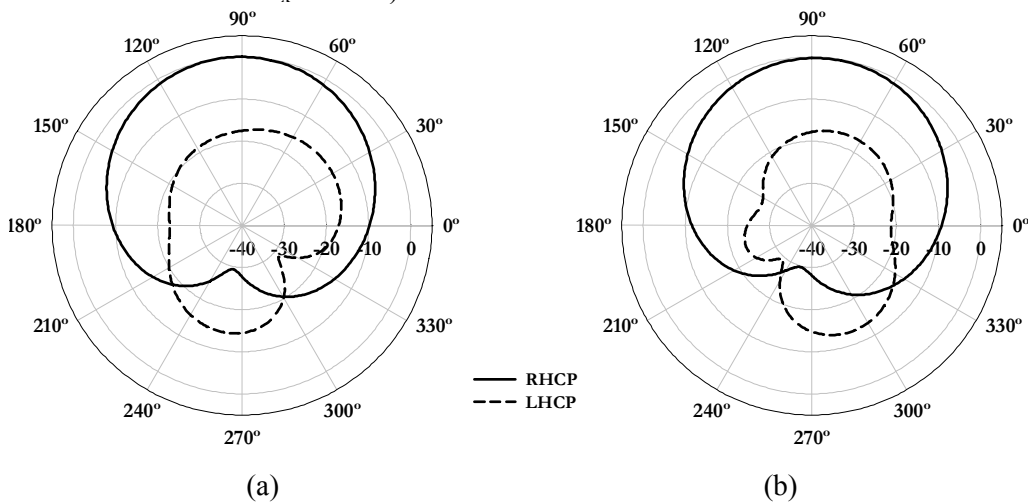


Figure 4.22 Measured radiation patterns of frequency and polarization reconfigurable cross patch antenna at 1.43GHz when biasing 0V (a) XZ-Plane (b) YZ-Plane ($L=30.9\text{mm}$, $W=43.5\text{mm}$, $L_s=5.1\text{mm}$, $L_x=18.3\text{mm}$ and $W_x=2.3\text{mm}$).

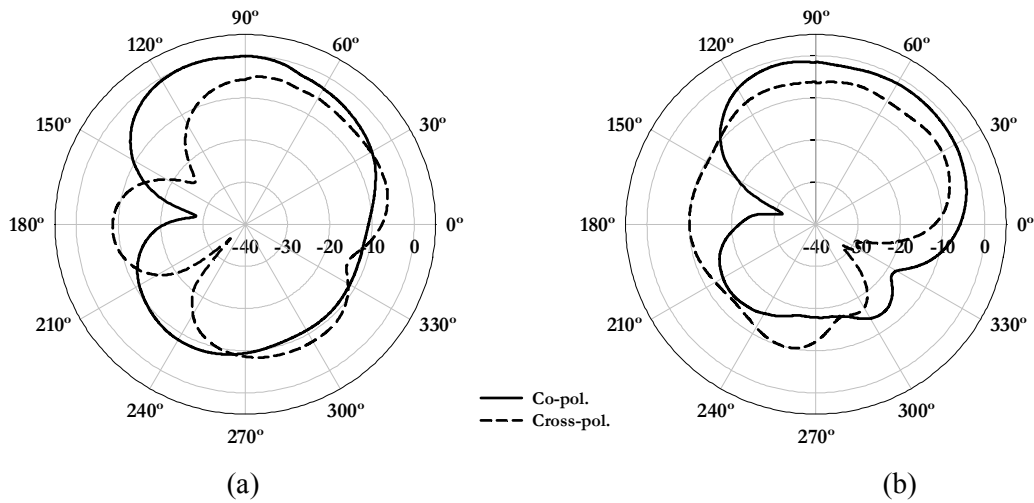


Figure 4.23 Measured radiation patterns of frequency and polarization reconfigurable cross patch antenna at 1.45GHz when biasing 10V (a) XZ-Plane and (b) YZ-Plane ($L=30.9\text{mm}$, $W=43.5\text{mm}$, $L_s=5.1\text{mm}$, $L_x=18.3\text{mm}$ and $W_x=2.3\text{mm}$).

The measured axial ratio of the antenna for different bias voltages is plotted in figure 4.25. The best axial ratio is 0.28dB at 1.43GHz. The CP operating frequency band follows the change of the pass band with respect to the bias voltage up to 5V. The antenna shows an axial ratio of 4.64dB at 1.45GHz when the reverse bias is increased to 10V. Further increase of the bias voltage causes a dramatic increase in the axial ratio which shows that the antenna is linearly polarized and the corresponding axial ratio value represents the cross polarization level of the LP antenna above 10V. The antenna shows a peak gain of 3.65dBi at 1.6GHz for LP and 1.65dBi at 1.42GHz for RHCP in the direction of maximum radiation. The low gain values are due to the opposing current on either side of the slot arm which cause field cancellation along the on-axis at the far-field and is comparable with regular and similar antennas reported in literature. A prototype of the fabricated antenna is given in figure 4.26.

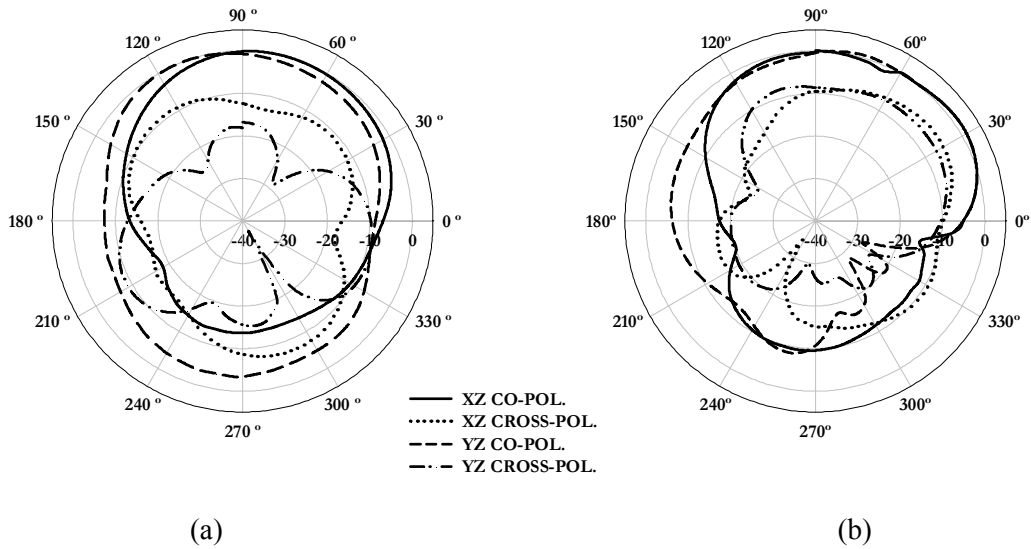


Figure 4.24 Radiation patterns of frequency and polarization reconfigurable cross patch antenna measured with biasing 15V at (a) 1.43GHz and (b) 1.527GHz ($L=30.9\text{mm}$, $W=43.5\text{mm}$, $L_s=5.1\text{mm}$, $L_x=18.3\text{mm}$ and $W_x=2.3\text{mm}$).

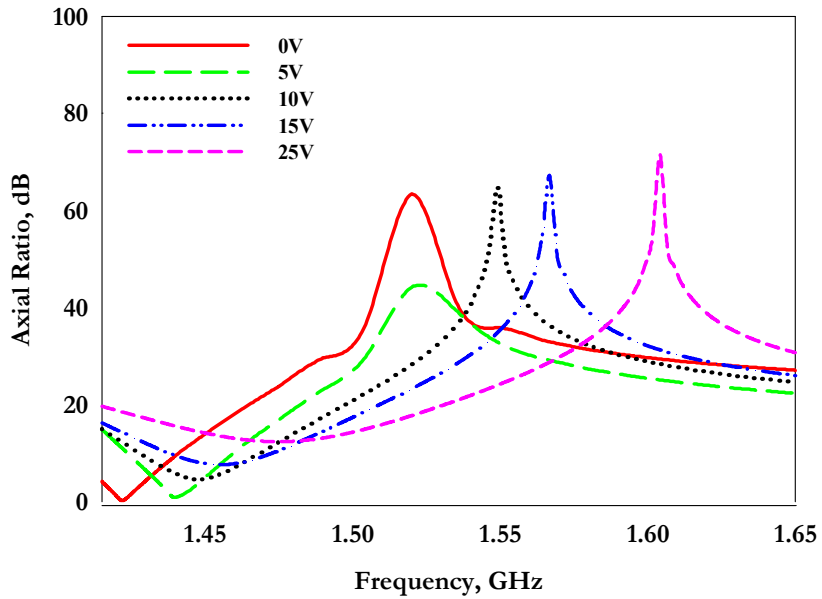


Figure 4.25 Measured axial ratio of the frequency and polarization reconfigurable cross patch antenna for different bias voltages ($L=30.9\text{mm}$, $W=43.5\text{mm}$, $L_s=5.1\text{mm}$, $L_x=18.3\text{mm}$ and $W_x=2.3\text{mm}$).

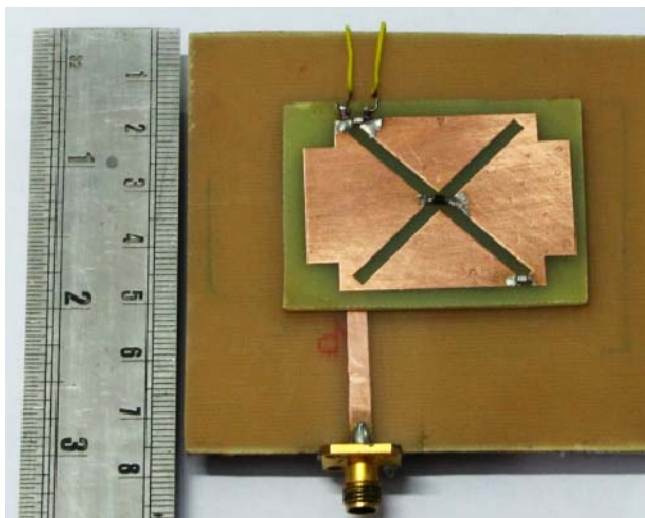


Figure 4.26 A prototype of the frequency and polarization reconfigurable cross patch antenna

A new design of single feed compact reconfigurable microstrip antenna with polarization diversity using single varactor is proposed. The prototype fabricated on inexpensive FR₄ laminate shows stable radiation characteristics and patterns of each frequency remain unchanged with respect to the voltage variation. Furthermore the antenna has an added advantage of reduced size with low levels of cross-polarized radiation in linear polarization state and a 10MHz axial ratio bandwidth in circular polarization state. In addition, the antenna is simple and requires less area to occupy the patch and dc-bias circuit compared to conventional polarization diversity antennas available in literature. The frequency and polarization diversities of this design provide some potential applications for wireless communications.

4.6 Summarized conjecture at a glance

Inferences obtained from the investigation of frequency and polarization reconfigurable cross shaped microstrip antenna using reactive loading is summarized in this section.

- A cross patch antenna with an embedded X-slot in the center excites compact orthogonal resonant modes.
- Mechanical tuning of the two orthogonal resonant modes can be varied by inserting a chip capacitor at the center of the X-slot.
- Frequency reconfigurable microstrip antenna with tunable frequency ratio is obtained when the chip capacitor is oriented parallel to the microstrip feed line.
- If the chip capacitor is positioned normal to the microstrip feed then the frequency reconfigurable microstrip antenna is useful for polarization diversity applications.
- Electronic control of the operating frequencies and the frequency ratio between two orthogonal resonant modes can be achieved with four varactors along the X-slot arms.
- Frequency reconfigurable polarization diversity operation is possible with a single varactor at the center of the X-slot.
- An electronically reconfigurable cross patch operates either in linear polarization or in circular polarization state with respect to the bias voltage applied across the varactor diode at the center of the X-slot.



Chapter 5

THEORETICAL ANALYSIS OF CROSS PATCH ANTENNA

Contents

- 5.1 Finite Difference Time Domain Technique (FDTD)
 - 5.2 Theoretical analysis of cross patch antenna
 - 5.3 Theoretical analysis of cross patch antenna with X-slot
 - 5.4 Theoretical analysis of Frequency reconfigurable polarization diversity microstrip antenna
 - 5.5 Chapter Summary
-

This chapter highlights a systematic approach to analyze a cross patch antenna using FDTD based numerical computation. The staircase approximation is employed to derive the slant edges of the X-slot. Various steps involved in the extraction of antenna parameters along with the assumptions taken in the implementation of the algorithm are also described. The predicted results are experimentally verified by developing and testing different printed cross patch antennas.

5.1 Finite Difference Time Domain Technique (FDTD)

Finite Difference Time Domain (FDTD) is a Computational Electro-Magnetic (CEM) technique that directly solves the differential form of Maxwell's curl equations, in the time domain using a discretized space-time grid. Field, voltage or current samples are taken from fixed points in the FDTD grid and Fast Fourier Transform (FFT) is employed to compute the frequency domain information. Finite Difference Time Domain (FDTD) method was introduced by Yee [1] in 1966 for solving Maxwell's curl equations directly in the time domain on a space grid. The algorithm was based on a central difference solution of Maxwell's equations with spatially staggered electric and magnetic fields placed alternatively at each time steps in a leap-frog algorithm. This method has been implemented by Teflove in 1975 for the solution of complex inhomogeneous problems.

The FDTD has been used by many investigators, because of its following advantages over other techniques:

- ❖ From the mathematical point of view, it is a direct implementation of Maxwell's curl equations.
- ❖ Broadband frequency response can be easily predicted since the analysis is carried out in the time domain.
- ❖ Arbitrary, irregular geometries, wires of any thickness can be easily modeled,
- ❖ It is capable of analyzing structures having different types of materials
- ❖ Time histories of electric and magnetic fields throughout the entire simulation domain are available
- ❖ Impedance and radiation pattern are easily obtainable
- ❖ Lumped loads can be easily included in the model

Formulation of the FDTD method begins by considering the differential form of Maxwell's two curl equations which govern the propagation of fields in

the structures. For simplicity, the media is assumed to be uniform, isotropic, homogeneous and lossless.

With these assumptions, Maxwell's equations can be written as

$$\mu \frac{\partial H}{\partial y} = -\nabla \times E \dots \dots \dots (1)$$

$$\varepsilon \frac{\partial E}{\partial t} = \nabla \times H \dots \dots \dots (2)$$

In order to find an approximate solution to these set of equations, the problem is discretized over a finite three dimensional computational domain with appropriate boundary conditions enforced on the source, conductors, and mesh walls. The divergence equations are automatically satisfied by the FDTD method.

To obtain discrete approximations to these continuous partial differential equations the centered difference approximation is used on both time and space. For convenience, the six field locations are considered to be interleaved in space as shown in Fig. 5.1 which is a drawing of the FDTD unit cell. The entire computational domain is obtained by stacking these Yee cubes into a larger rectangular volume. The x, y and z dimensions of the unit cell are Δx , Δy and Δz , respectively. The advantages of this field arrangement are that centered differences are realized in the calculation of each field component and that continuity of tangential field components is automatically satisfied.

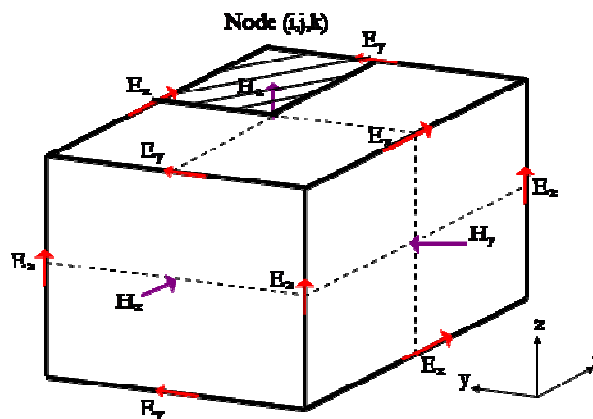


Figure 5. 1 Yee Cell using in FDTD with Electric and Magnetic field components

Because there are only six unique field components within the unit cell, the six field components touching the shaded upper eighth of the unit cell in figure 5.1 are considered to be a unit node with subscript indices i , j , and k corresponding to the node numbers in the x , y and z directions. The notation implicitly assumes the $\pm 1/2$ space indices and thus simplifies the notation, rendering the formulas directly implementable on the computer.

The time steps are indicated with the superscript n . Using this field component arrangement, the above notation, and the centered difference approximation, the explicit finite difference approximations to (1) and (2) are

$$H_{x,i,j,k}^{n+1/2} = H_{x,i,j,k}^{n-1/2} + \frac{\Delta t}{\mu\Delta z} (E_{y,i,j,k}^n - E_{y,i,j,k-1}^n) - \frac{\Delta t}{\mu\Delta y} (E_{z,i,j,k}^n - E_{z,i,j-1,k}^n) \dots \dots \dots (3)$$

$$H_{y,i,j,k}^{n+1/2} = H_{y,i,j,k}^{n-1/2} + \frac{\Delta t}{\mu\Delta x} (E_{z,i,j,k}^n - E_{z,i-1,j,k}^n) - \frac{\Delta t}{\mu\Delta z} (E_{x,i,j,k}^n - E_{x,i,j,k-1}^n) \dots \dots \dots (4)$$

$$H_{z,i,j,k}^{n+1/2} = H_{z,i,j,k}^{n-1/2} + \frac{\Delta t}{\mu\Delta y} (E_{x,i,j,k}^n - E_{x,i,j-1,k}^n) - \frac{\Delta t}{\mu\Delta x} (E_{y,i,j,k}^n - E_{y,i-1,j,k}^n) \dots \dots \dots (5)$$

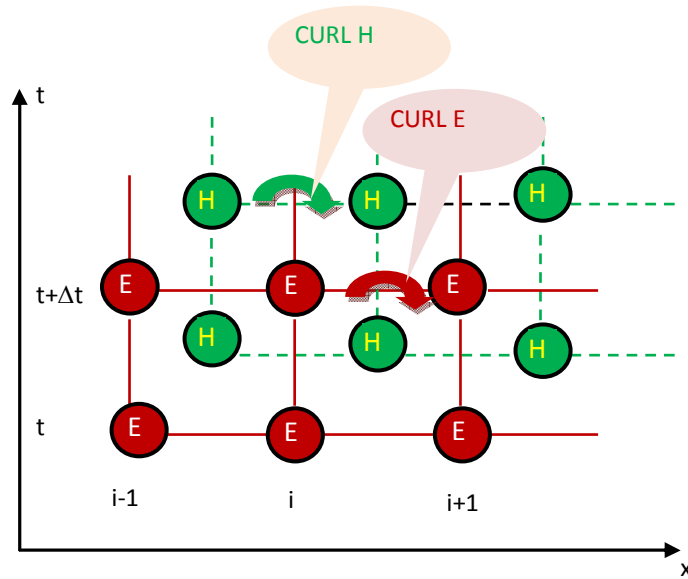
$$E_{x,i,j,k}^{n+1} = E_{x,i,j,k}^n + \frac{\Delta t}{\varepsilon\Delta y} (H_{z,i,j+1,k}^{n+1/2} - H_{z,i,j,k}^{n+1/2}) - \frac{\Delta t}{\varepsilon\Delta z} (H_{y,i,j,k+1}^{n+1/2} - H_{y,i,j,k}^{n+1/2}) \dots \dots \dots (6)$$

$$E_{y,i,j,k}^{n+1} = E_{y,i,j,k}^n + \frac{\Delta t}{\varepsilon\Delta z} (H_{x,i,j,k+1}^{n+1/2} - H_{x,i,j,k}^{n+1/2}) - \frac{\Delta t}{\varepsilon\Delta x} (H_{z,i+1,j,k}^{n+1/2} - H_{z,i,j,k}^{n+1/2}) \dots \dots \dots (7)$$

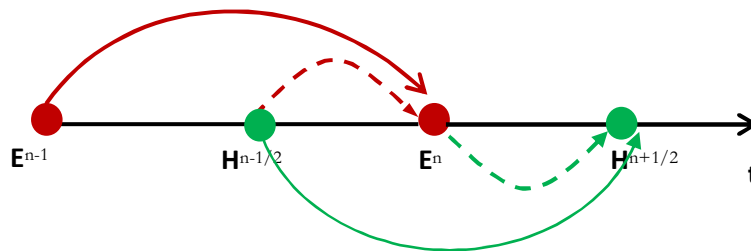
$$E_{z,i,j,k}^{n+1} = E_{z,i,j,k}^n + \frac{\Delta t}{\varepsilon\Delta x} (H_{y,i+1,j,k}^{n+1/2} - H_{y,i,j,k}^{n+1/2}) - \frac{\Delta t}{\varepsilon\Delta y} (H_{x,i,j+1,k}^{n+1/2} - H_{x,i,j,k}^{n+1/2}) \dots \dots \dots (8)$$

The half time steps indicate that E and H are alternately calculated in order to achieve centered differences for the time derivatives. In these equations, the permittivity and the permeability are set to the appropriate values, depending on the location of each field component. For the dielectric-air interface the average of the two permittivity $(\varepsilon_{r+1})/2$ is used [2].

The discretization in space and time and the calculation methodology of E and H granted the name leap frog algorithm to this method (figure 5.2).



(a) Discretization in space and time



(b) Leap frog time integration

Figure 5.2 Central differencing with Leapfrog method

5.1.1 Stability criteria

The numerical algorithm for Maxwell's curl equations derived requires the time increment Δt to have a specific upper bound relative to the space increments Δx , Δy and Δz . This bound is necessary to avoid numerical instability that can cause the computed results to increase spuriously without limit as time matching continues. The cause for numerical instability is the finite difference implementation of the derivative. The final expression for the upper bound on Δt can be written as,

$$\Delta t \leq \frac{1}{V_{\max}} \frac{1}{\sqrt{1/\Delta x^2 + 1/\Delta y^2 + 1/\Delta z^2}} \quad \text{-----} \quad (9)$$

Where V_{\max} is the maximum phase velocity of the signal in the problem being considered. Typically V_{\max} will be the velocity of light in free space unless the entire volume is filled with dielectric. These equations will allow the approximate solution of E and H in the volume of the computational domain or mesh. In practice, the maximum value of Δt used is about 90% of the value given by above equation.

5.1.2 Numerical Dispersion

Dispersion is defined as the variation of the phase constant of the propagating wave with frequency. The discretization of Maxwell's equations in space and time causes dispersion of the simulated wave in a dispersion-free structure. That is the phase velocity of the wave in an FDTD grid can differ from the analytical value. This dispersion is called numerical dispersion. The amount of dispersion depends on the wavelength, the direction of propagation in the grid, and the discretization size. Numerical dispersion can be reduced to any degree that is desired if one uses a fine enough FDTD mesh.

5.1.3 Absorbing Boundary Conditions

Absorbing boundary conditions are applied at the boundary mesh walls of finite difference to compute an unbounded space. A large number of electromagnetic problems have associated open space regions, where the spatial domain is unbounded in one or more directions. The solution of such a problem in this form will require an unlimited amount of computer resources. To avoid this, the domain must be truncated with minimum error. For this, the domain

can be divided into two regions: the interior region and the exterior region as shown in figure 5.3.

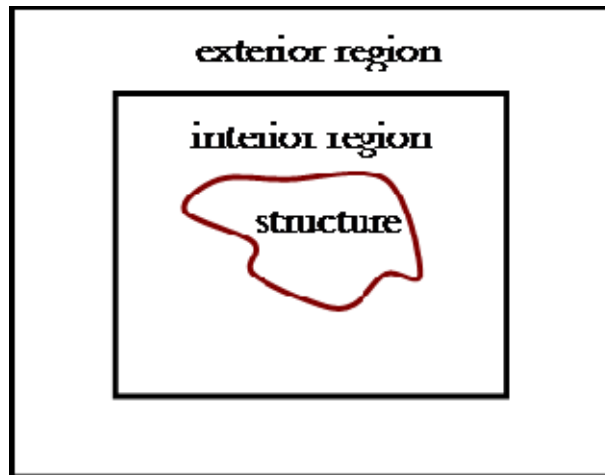


Figure 5.3 Truncation of the domain by the exterior region in FDTD algorithm

The interior region must be large enough to enclose the structure of interest. The exterior region simulates the infinite space. The FDTD algorithm is applied in the interior region. It simulates wave propagation in the forward and backward directions. However, only the propagation in the interior region is desired with minimum space without reflection from the truncated boundary. These reflections must be suppressed to an acceptable level so that the FDTD solution is valid for all time steps.

Two options are available to simulate the open region surrounding the problem space.

1. Terminate the interior region with equivalent currents on the surface of the interior region and use the Green's function to simulate the fields in the exterior region

2. Simulate the exterior region with absorbing boundary conditions in order to minimize reflections from the truncation of the mesh.

Simulation of the open region with the help of equivalent currents yields a solution whereby the radiation condition is satisfied exactly. But the values of fields on the surface enclosing the interior region are needed, for which CPU time and storage requirement increases rapidly with the surface size. On the other hand, the absorbing boundary concept truncates the computation domain and reduces the computational time and storage space. The absorbing boundary condition (ABC) can be simulated in a number of ways. These are classified as analytical (or differential) ABC and material ABC. The material ABC is realized from the physical absorption of the incident signal by means of a lossy medium [3], whereas analytical ABC is simulated by approximating the wave equation on the boundary [4].

Mur's first order ABC is the simple and optimal analytical ABC. In the thesis it is used as the boundary condition. Analysis of Mur's first-order ABC is based on the work of Enquist and Majda [4] and the optimal implementation given by Mur [5]. It provides satisfactory absorption for a great variety of problems and is extremely simple to implement. Mur's first order ABC looks back one step in time and one cell into the space location. An arbitrary wave can be expanded in terms of a spectrum of plane waves. If a plane wave is incident normally on a planar surface, and if the surface is perfectly absorbing, there will be no reflected wave. But while implementing the Mur's first order boundary conditions for printed microstrip antennas it should be noted that boundary walls are far enough from the radiating element to ensure the normal

incidence at the boundary walls. For the oblique incidence case the wave will be reflected from the boundary walls.

5.1.4 Source model

FDTD transient calculations are often excited by a hard voltage source, whose internal source resistance is zero ohms. These sources are very easy to implement in an FDTD code. The electric field at the mesh edge where the source is located is determined by some function of time rather than by the FDTD update equations. A common choice is a Gaussian pulse, but other functions may also be used. The Gaussian pulse is significantly greater than zero amplitude for only a very short fraction of the total computation time, and its Fourier Transform is also a pulse centered at zero frequency. This unique property makes it a perfect choice for investigating the frequency dependent characteristics especially for resonant geometries such as antennas and micro strip circuits.

When the pulse amplitude drops the source voltage, the source effectively becoming a short circuit, any reflections from the antenna or circuit which return to the source are totally reflected. The only way the energy introduced into the calculation space can be dissipated is through radiation or by absorption of lossy media or lumped loads. For resonant structures, there are frequencies for which this radiation or absorption process requires a relatively long time to dissipate the excitation energy. Using a source with an internal resistance to excite the FDTD calculation provides an additional loss mechanism for the calculations.

5.1.5 Staircase approximation

Microstrip patches with patch edges parallel to the grid lines can be accurately modeled using classical Yee FDTD approach. As there are four slant edges in an X-slot embedded in the patch, staircase approximation is employed to define the boundary between the patch and the slot. The microstrip surface edges which are not parallel to the FDTD cell edges are approximated as either completely covered by metal or as totally uncovered. The update equations for the grid will remain the same as the conventional one. Thus, the metallic patch edge being defined as a staircase boundary with steps of dimensions equal to that of the Yee cell dimension as shown in figure 5.4. In order to increase the accuracy of the results, very fine gridding is used throughout the study.

The antennas discussed in thesis uses a microstrip line as the feed. The microstrip excitation presented in the thesis is implemented by using Leubber's [7] approach of stair cased FDTD mesh transition from electric field sources location to the full width of the microstrip transmission line. In order to model the microstrip line, the substrate thickness is discretized as more than one Yee cell. The excitation field is to be applied to the cell between the top PEC of the strip line and the PEC ground plane. In order to obtain a gap feed model, a stair cased mesh transition as shown in the figure 5.5 is used in FDTD.

In the figure the darkened portions are treated as PEC. This stair cased configuration results a gap model between the top patch and ground plane. The excitation field is shown as arrow in the figure. The stair case model transition from the electric field feed to the microstrip line at the top is used to provide a relatively smooth connection from the single feed location to the microstrip.

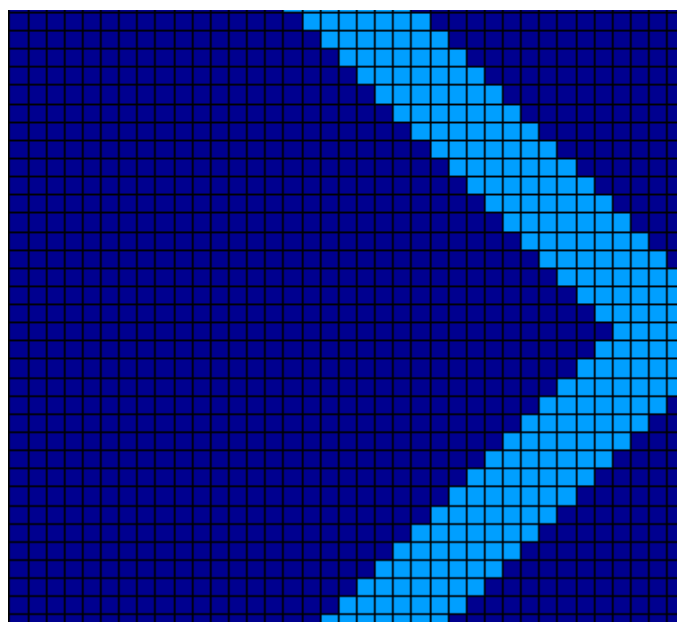


Figure 5.4 Staircase meshing employed in the X-slot boundary

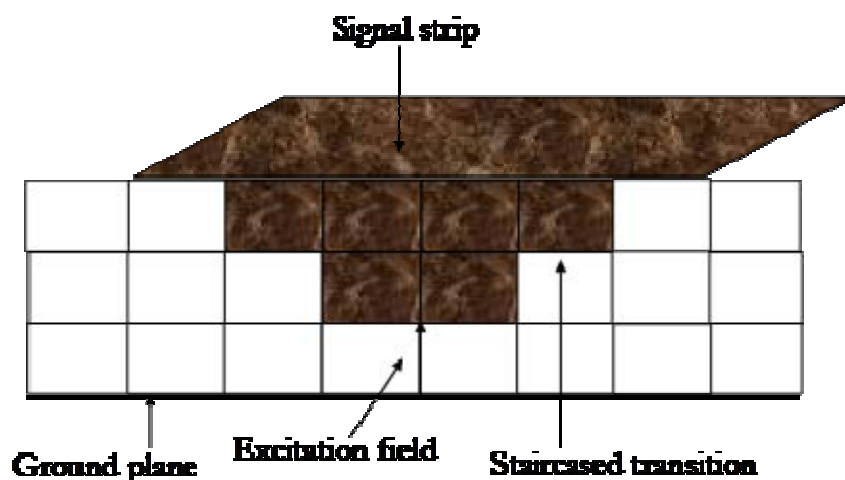


Figure 5.5 FDTD Staircase feed model for microstrip line in FDTD

5.1.6 General flow chart of FDTD algorithm

The MATLAB based computer codes were developed to study the resonant behavior of the proximity coupled printed cross patch antenna, cross patch antenna with X-slot and frequency reconfigurable polarization diversity

cross patch antenna. The general flow chart for the program to calculate the return loss characteristics is shown in figure 5.6.

5.1.7 Return loss calculation

The voltage at the input port location is computed from the E_z field components at the feed point over the entire simulation time interval. The current at the feed point is calculated from the H field values around the feed point using Ampere's circuital law. The input impedance of the antenna is computed as

$$Z_{in}(\omega) = \frac{FFT(V^n, P)}{FFT(I^{n-1}, P)} \dots \dots \dots (10)$$

Where P is the suitable Zero padding used for taking FFT, $V^n = E_z^n * \Delta z$ and I^{n-1} is the current through the source.

Since microstrip line is modeled using Leubber's staircase approach, the internal impedance of source resistance R_s is taken as the characteristic impedance (Z_0) of microstrip line.

Reflection coefficient is given as $\Gamma(\omega) = \frac{Z_{in} - Z_0}{Z_{in} + Z_0} \dots \dots \dots (11)$

Return loss in dB, $S_{11} = 20 \log_{10} |\Gamma(\omega)| \dots \dots \dots (12)$

The return loss computed in the above process is processed for extracting the fundamental resonant frequency and 2:1 VSWR bandwidth corresponding to the -10 dB return loss.

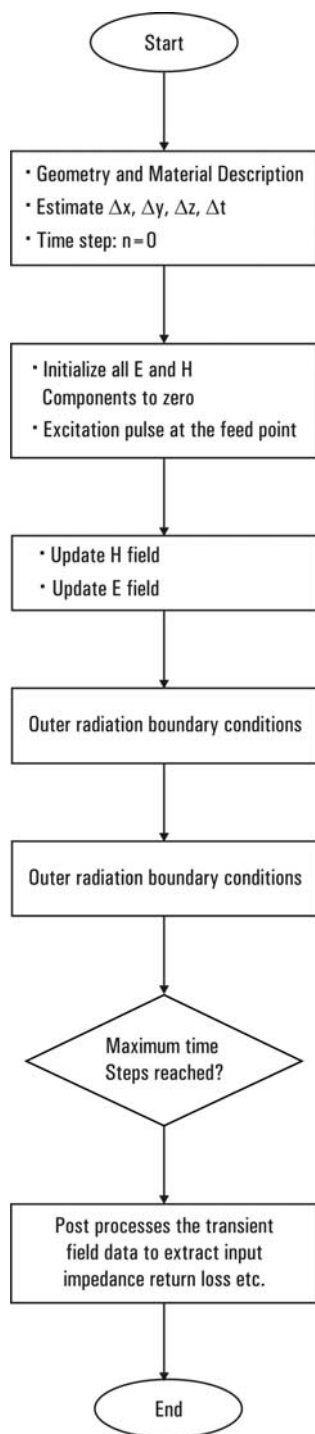


Figure 5.6 Flow chart for the computation of return loss

5.2 Theoretical analysis of cross patch antenna

The cross patch antenna configuration which is used as the primary design has been analyzed using FDTD technique. MATLAB based in-house codes were developed for simulation of the antenna. Figure 5.7 depicts the two dimensional view of the microstrip line feed used to excite the antenna. Two dimensional view of the FDTD computation domain generated plot of the patch geometry is shown in figure 5.8. The computational domain is divided in to Yee cells of dimension $\Delta x = \Delta y = 0.5\text{mm}$ and $\Delta z = 0.4\text{mm}$. Since substrate thickness is 3.2mm, 8 cells will exactly match substrate thickness. 10 cells on each of the 6 sides are used to model air cells. The total computation domain is discretized in to $220\Delta x * 220\Delta y * 28\Delta z$ cells. Luebber's feed model is employed to excite the microstrip line feed of the antenna and a Gaussian pulse is used as the source of excitation. Time step used for the computation is 0.95ps. The Gaussian half-width is $T = 20$ ps and the time delay t_0 is set to be $3T$.

The computed and measured reflection characteristics of the above configuration are illustrated in figure 5.9. The center fed cross patch antenna shows resonance at 2.3GHz with a bandwidth of 3.9%. As explained in the previous section, the feed line can be selected anywhere along the patch width, the feed line is centered with respect to the width of the patch so that the TM_{10} mode of the patch is excited. The resultant electric field distribution computed on the top layer using FDTD technique at the resonant frequency is given in figure 5.10. A half-wave variation of the electric field is observed along Y-direction on the patch.

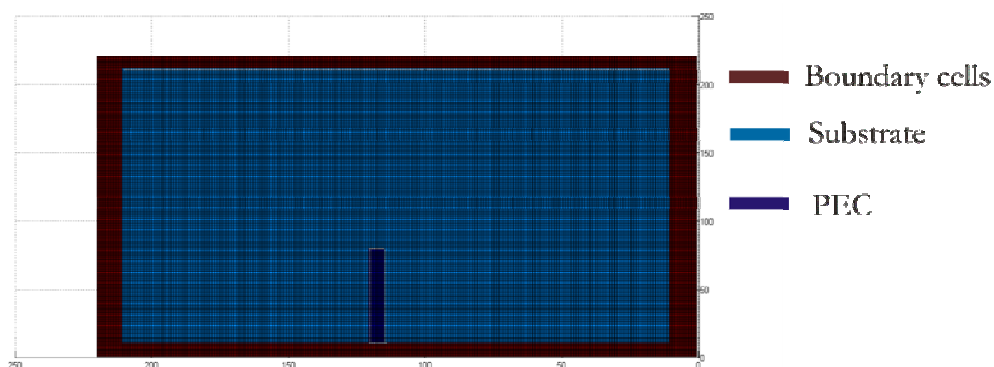


Figure 5.7 2D view of the FDTD computation domain of microstrip line feed

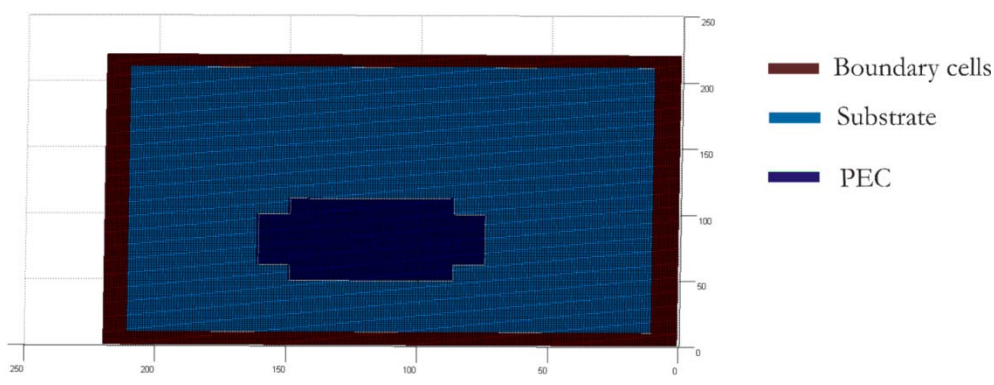


Figure 5.8 2D view of the FDTD computation domain of cross patch antenna

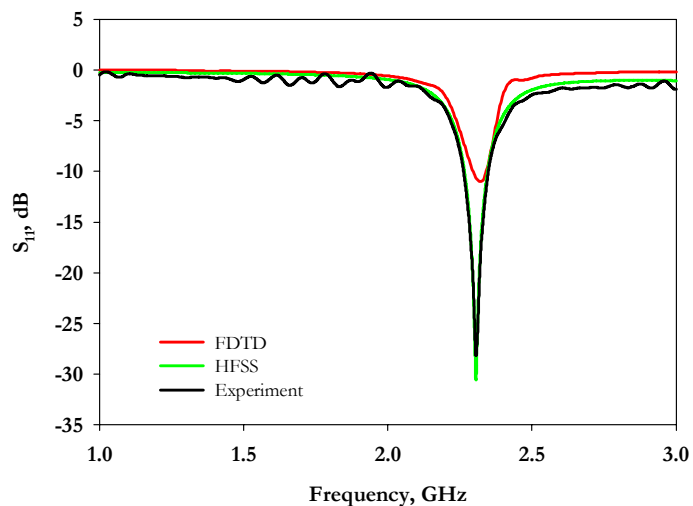


Figure 5.9 Reflection characteristics of center fed cross patch antenna ($L=30.9\text{mm}$, $W=43.5\text{mm}$ and $L_S=5.1\text{mm}$)

Although the feed line can be selected anywhere along the patch width, the feed line is moved along the width of the patch to operate at dual-frequencies using the first resonance of the two orthogonal dimensions of the patch, i.e. TM_{10} and TM_{01} modes. The reflection characteristics are plotted in figure 5.11. FDTD computed electric field distribution on the top layer illustrated in figure 5.12 reveals that the first resonance is directed along X-direction at 1.74GHz and the second resonance is directed along Y-direction at 2.3GHz.

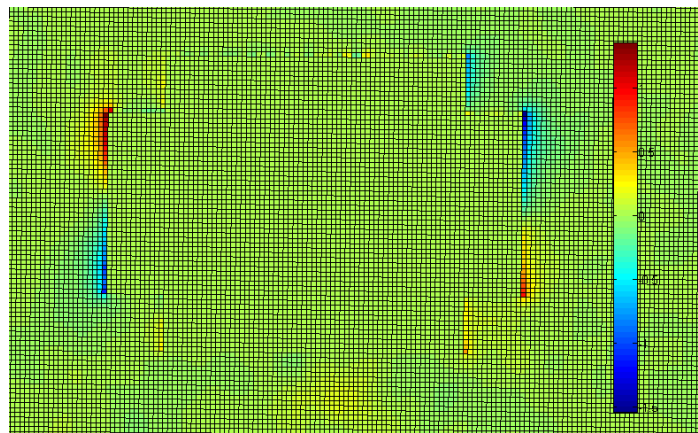


Figure 5.10 FDTD computed Electric field distribution of the center fed cross patch at 2.3GHz

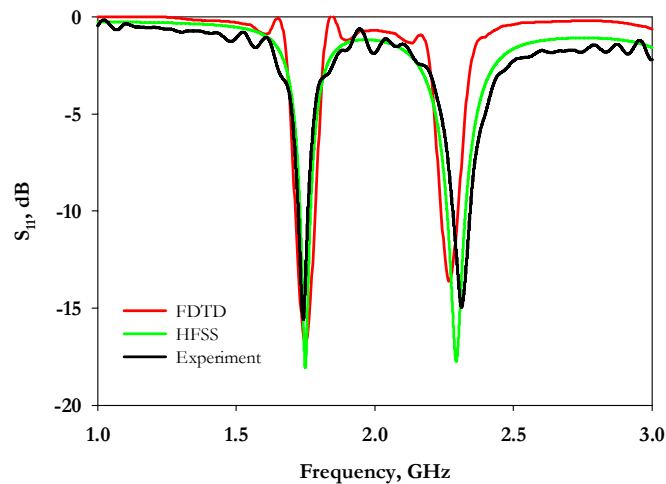


Figure 5.11 Reflection characteristics of dual-frequency dual-polarized cross patch antenna ($L=30.9\text{mm}$, $W=43.5\text{mm}$ and $L_s=5.1\text{mm}$)

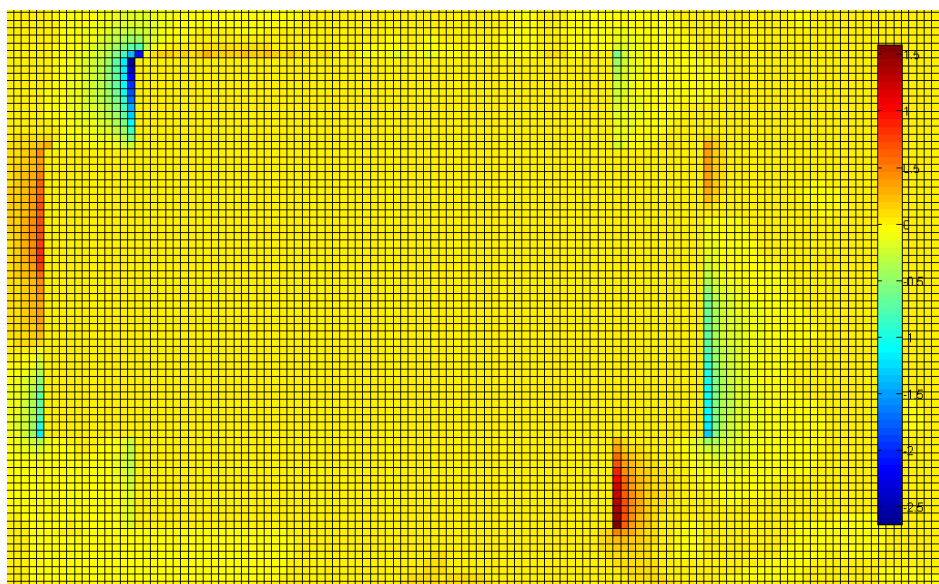


Figure 5. 12 FDTD computed Electric field distribution of the dual-frequency dual-polarized cross patch antenna

5.3 Theoretical analysis of cross patch antenna with X-slot

An X-slot is carved at the center of the cross patch and optimized the dimensions to induce symmetric current distributions and to achieve maximum area reduction for the TM_{01} and TM_{10} modes of the cross patch. This attempt reduces resonant frequencies to 1.1GHz and 1.4GHz from 1.74GHz and 2.3GHz respectively. Two dimensional view of FDTD computed configuration of the cross patch antenna with X-slot is shown in figure 5.13. The theoretical, simulated and experimental reflection coefficient of the cross patch antenna by the inclusion of the X-slot is plotted in figure 5.14. FDTD computed electric field distribution of the X-slot loaded cross patch antenna is given in figure 5.15.

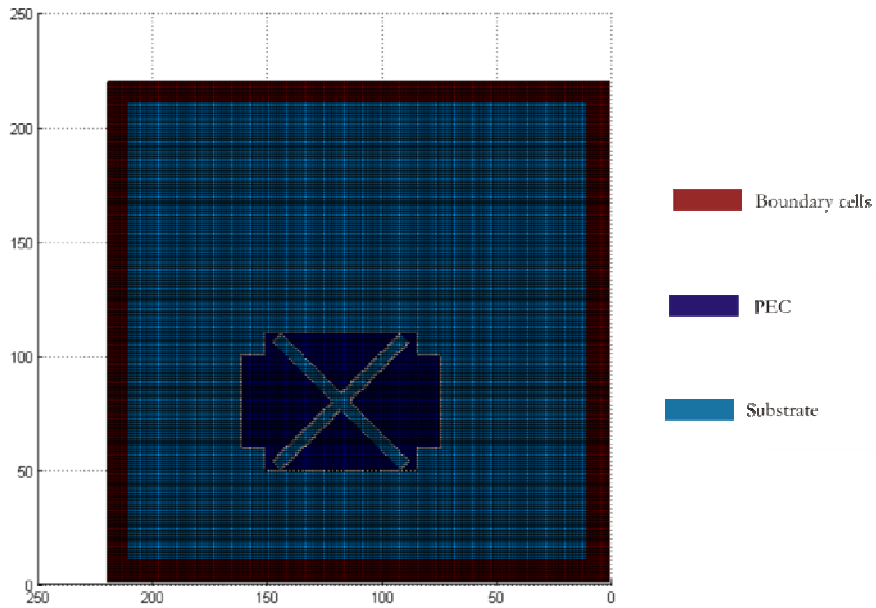


Figure 5.13 2D view of the FDTD computation domain of cross patch antenna with X-slot ($L=30.9\text{mm}$, $W=43.5\text{mm}$, $L_S=5.1\text{mm}$, $L_x=18.3\text{mm}$ and $W_x=2.3\text{mm}$)

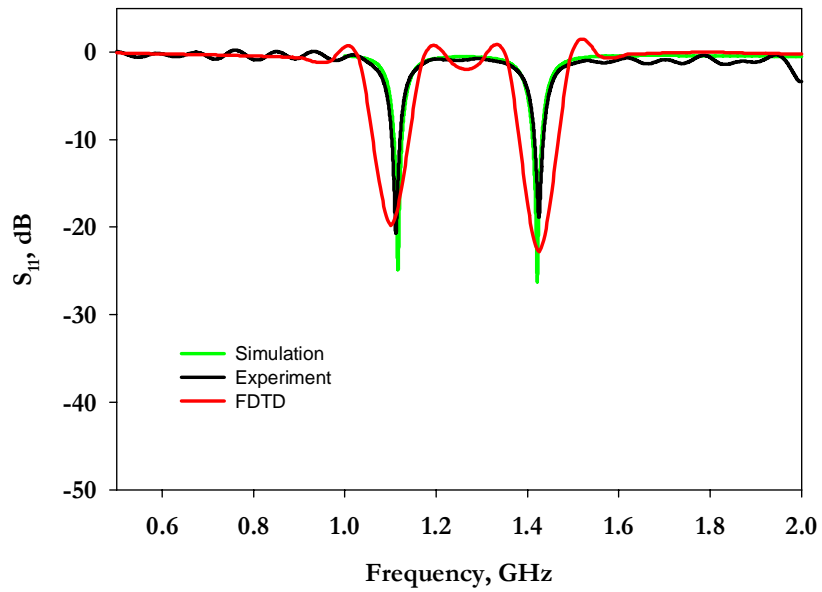


Figure 5.14 Reflection characteristics of dual-frequency dual-polarized cross patch antenna with X-slot ($L=30.9\text{mm}$, $W=43.5\text{mm}$, $L_S=5.1\text{mm}$, $L_x=18.3\text{mm}$ and $W_x=2.3\text{mm}$)

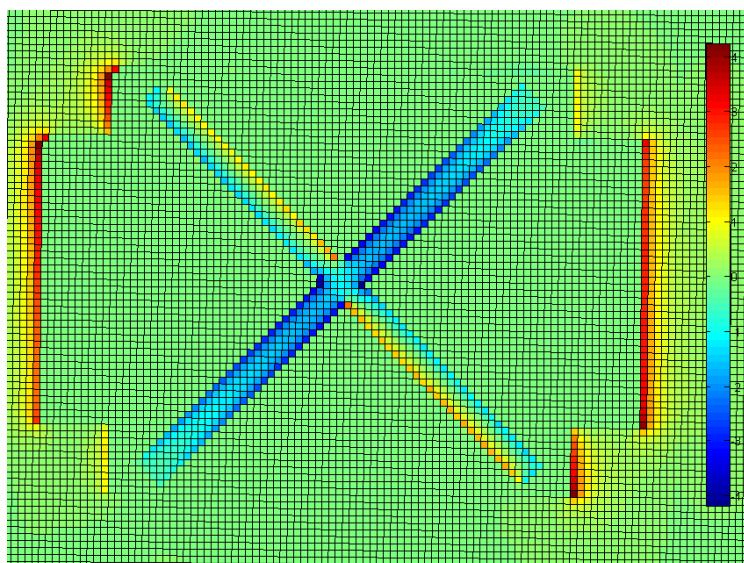


Figure 5.15 FDTD computed Electric field distribution of the X-slot loaded cross patch antenna ($L=30.9\text{mm}$, $W=43.5\text{mm}$, $L_S=5.1\text{mm}$, $L_x=18.3\text{mm}$ and $W_x=2.3\text{mm}$)

5.4 Theoretical analysis of Frequency reconfigurable polarization diversity microstrip antenna

Theoretical analysis of the PIN diode controlled frequency reconfigurable polarization diversity cross patch antenna is carried out using finite difference time domain method. Two PIN diodes are connected at the center of the X-slot to achieve frequency and polarization reconfigurability. The proposed antenna radiate linearly polarized waves when both PIN diodes on the cross patch should be biased either in the ON state (Antenna 1) or in the OFF state (Antenna 2). To radiate circularly polarized waves, one of the diodes on the patch (D_2) should be in the ON state while the other should be in the OFF state (antenna 3).

Fine meshing with cell size $\Delta x=\Delta y=0.5\text{mm}$ and $\Delta z=0.4\text{mm}$ are taken. The ON state of the PIN diode is modeled as metal contact and the OFF state is represented as an opening. Gaussian pulse 187,190,189,188,191,194,193,192 is then applied at the feed point and the boundary conditions are defined. Two

dimensional view of FDTD computed configuration of the Antenna 1 is shown in figure 5.16. A comparison between the theoretical, simulated and experimental reflection coefficient of the Antenna 1 is plotted in figure 5.17. FDTD computed electric field distribution of the Antenna 1 is given in figure 5.18.

Two dimensional view of FDTD computed configuration of the Antenna 2 is shown in figure 5.19. A comparison between the theoretical, simulated and experimental reflection coefficient of the Antenna 2 is plotted in figure 5.20. FDTD computed surface cur electric field rent distribution of the Antenna 2 is given in figure 5.21.

Two dimensional view of FDTD computed configuration of the Antenna 3 is shown in figure 5.22. A comparison between the theoretical, simulated and experimental reflection coefficient of the Antenna 3 is plotted in figure 5.23. FDTD computed electric field distribution of the Antenna 3 is given in figure 5.24. Comparison of the measured, simulated and FDTD computed results of the three different antennas are summarized in Table 5.1.

Table 5.1 Comparison between Measured, Simulated and FDTD computed resonant frequency of Frequency reconfigurable polarization diversity microstrip antenna

Antenna	Resonant Frequency, GHz		
	Experiment	HFSS	FDTD
1	1.474	1.475	1.484
2	1.54	1.54	1.55
3	1.45-1.536	1.45-1.53	1.44-1.53

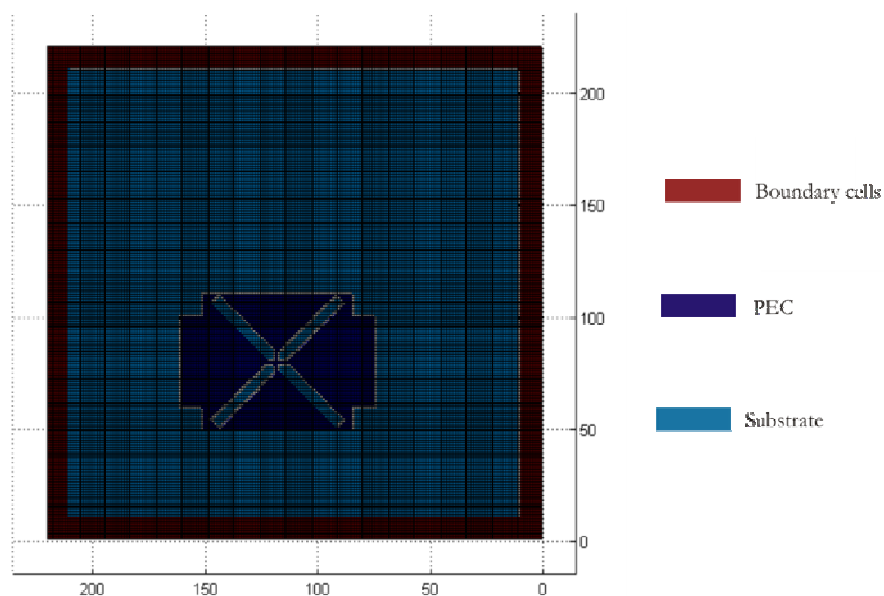


Figure 5. 16 2D view of the FDTD computation domain of Antenna 1 ($L=30.9\text{mm}$, $W=43.5\text{mm}$, $L_S=5.1\text{mm}$, $L_x= 18.3\text{mm}$ and $W_x=2.3\text{mm}$)

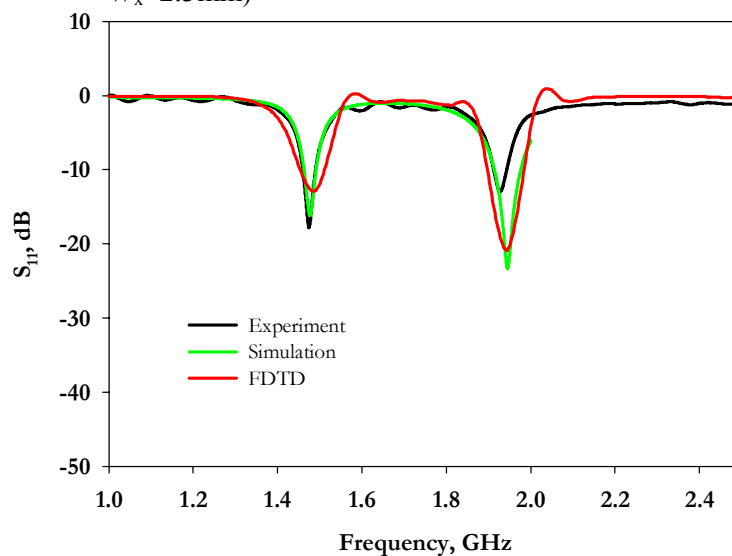


Figure 5. 17 Reflection characteristics of Antenna 1 ($L=30.9\text{mm}$, $W=43.5\text{mm}$, $L_S=5.1\text{mm}$, $L_x= 18.3\text{mm}$ and $W_x=2.3\text{mm}$)

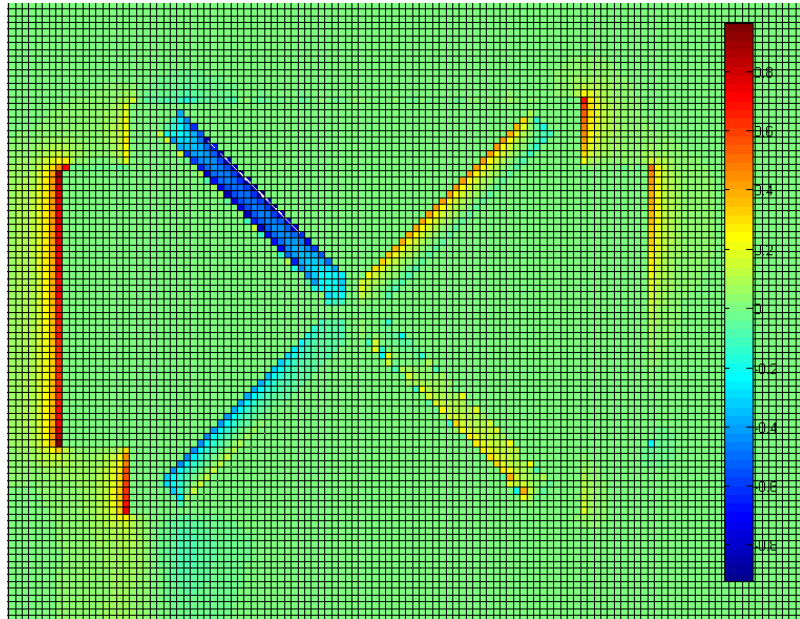


Figure 5.18 FDTD computed Electric field distribution of the Antenna 1 ($L=30.9\text{mm}$, $W=43.5\text{mm}$, $L_S=5.1\text{mm}$, $L_x= 18.3\text{mm}$ and $W_x=2.3\text{mm}$)

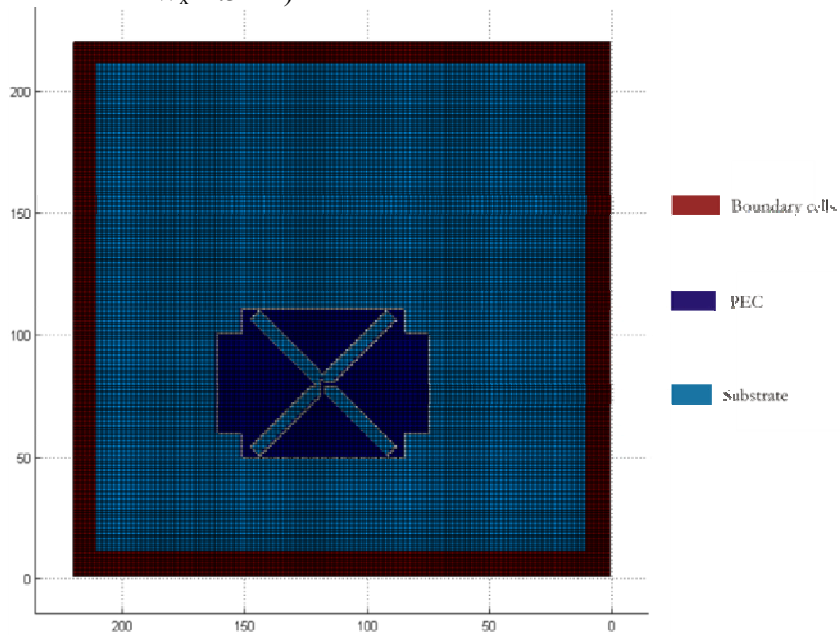


Figure 5.19 2D view of the FDTD computation domain of Antenna 2 ($L=30.9\text{mm}$, $W=43.5\text{mm}$, $L_S=5.1\text{mm}$, $L_x= 18.3\text{mm}$ and $W_x=2.3\text{mm}$)

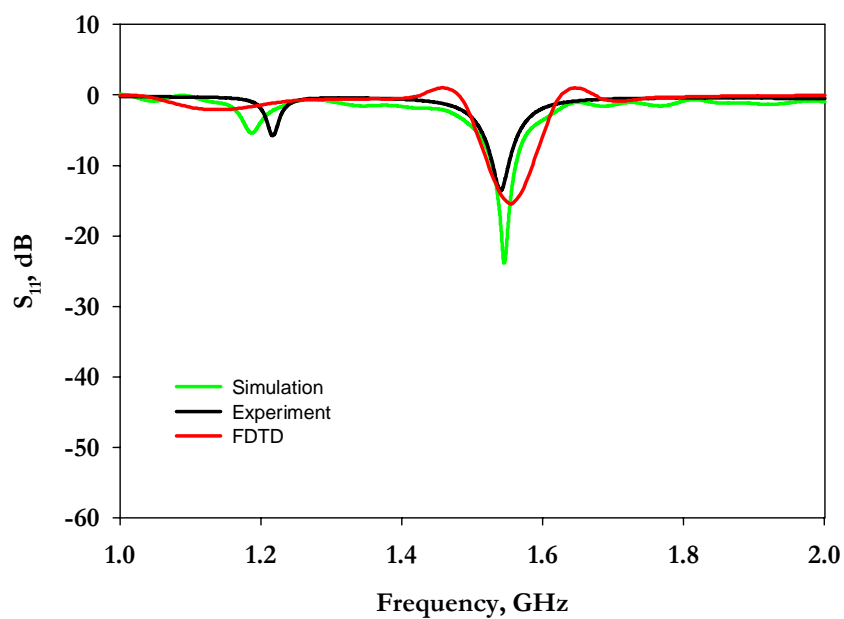


Figure 5.20 Reflection characteristics of Antenna 2 ($L=30.9\text{mm}$, $W=43.5\text{mm}$, $L_S=5.1\text{mm}$, $L_x=18.3\text{mm}$ and $W_x=2.3\text{mm}$)

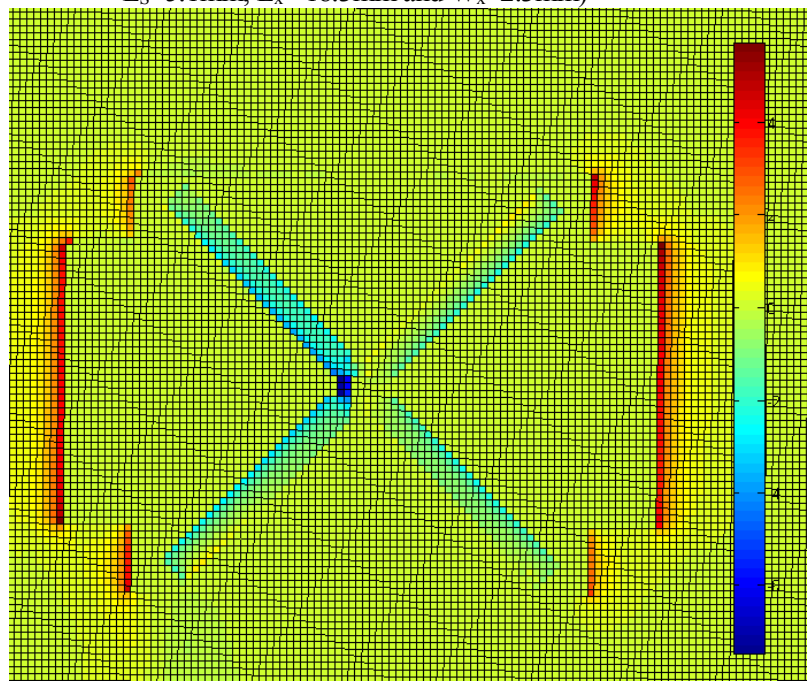


Figure 5.21 FDTD computed Electric field distribution of the Antenna 2 ($L=30.9\text{mm}$, $W=43.5\text{mm}$, $L_S=5.1\text{mm}$, $L_x=18.3\text{mm}$ and $W_x=2.3\text{mm}$)

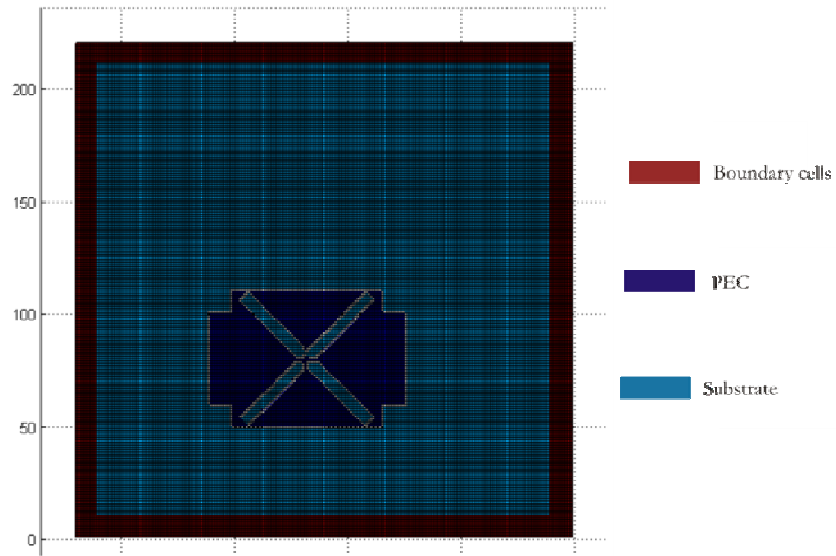


Figure 5. 22 2D view of the FDTD computation domain of Antenna 3 ($L=30.9\text{mm}$, $W=43.5\text{mm}$, $L_S=5.1\text{mm}$, $L_x= 18.3\text{mm}$ and $W_x=2.3\text{mm}$)

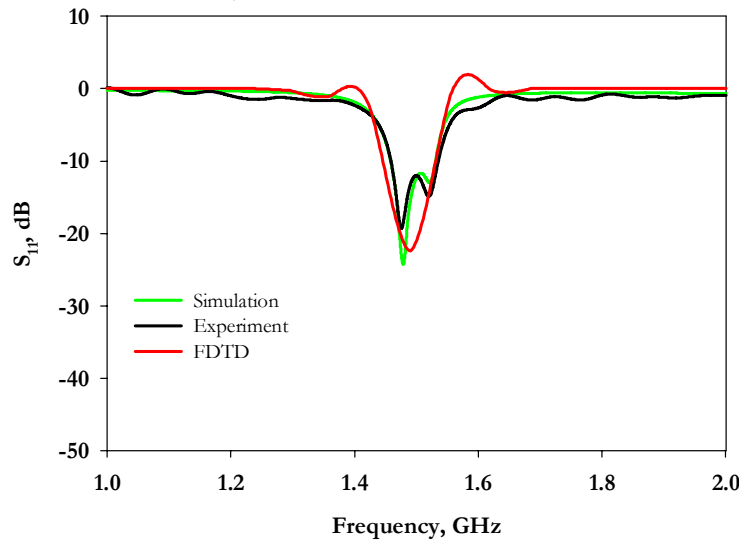


Figure 5. 23 Reflection characteristics of Antenna 3 ($L=30.9\text{mm}$, $W=43.5\text{mm}$, $L_S=5.1\text{mm}$, $L_x= 18.3\text{mm}$ and $W_x=2.3\text{mm}$)

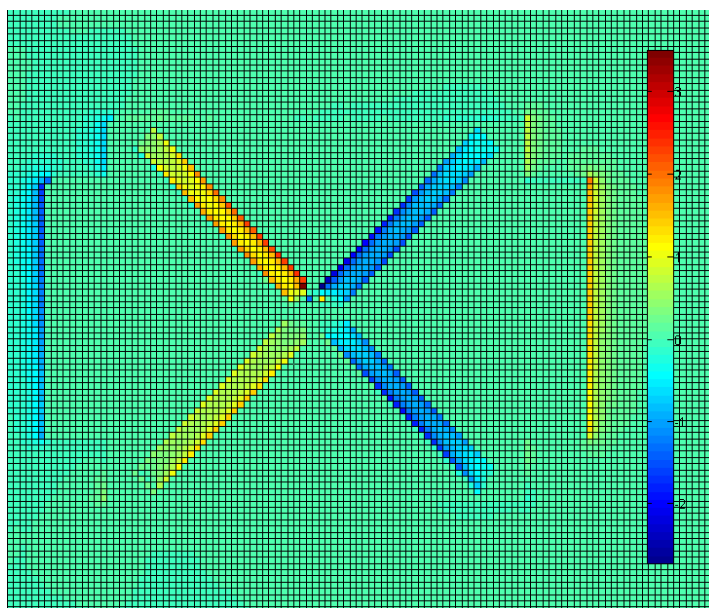


Figure 5.24 FDTD computed Electric field distribution of the Antenna 3 ($L=30.9\text{mm}$, $W=43.5\text{mm}$, $L_S=5.1\text{mm}$, $L_x= 18.3\text{mm}$ and $W_x=2.3\text{mm}$)

5.5 Chapter Summary

FDTD based numerical computation is used to analyze the performance of cross patch antenna with and without X-slot. PIN diode controlled frequency and polarization reconfigurable compact cross patch antenna is also analyzed using FDTD. The staircase approximation is employed to derive the slant edges of the X-slot. MATLAB based in-house codes were developed for simulation of the antenna. Luebber's feed model is employed to excite the microstrip line feed of the antenna and a Gaussian pulse is used as the source of excitation. Time step used for the computation is 0.95ps. The Gaussian half-width is $T = 20$ ps and the time delay t_0 is set to be $3T$. Various steps involved in the extraction of antenna parameters along with the assumptions taken in the implementation of the algorithm are also described. The predicted results are experimentally verified by fabricating and testing different printed cross patch antennas.

References

- 1 K. S. Yee, *Numerical solution of initial boundary value problems involving Maxwell's equations in isotropic media*, IEEE Transactions on Antennas and Propagation, Vol.14, No. 3, pp. 302-307, 1966.
- 2 X. Zhang and K. K. Mei, *Time domain finite difference approach to the calculation of the frequency dependent characteristics of microstrip discontinuities*, IEEE Trans. Microwave Theory Tech., Vol. 36, pp. 1775-1787, Dec. 1988.
- 3 Hallond, R, and J. W. Williams, *Total field versus scattered field finite difference codes: A comparative Assessment*, IEEE Transactions on Nuclear Science, Vol. 30, No.6, pp. 4583-4588, 1983.
- 4 Enquist and Majada, *Absorbing Boundary Conditions for the Numerical simulation of waves*, Mathematics of Computation, Vol. 31, pp. 629-651, 1977.
- 5 Mur G, *Absorbing boundary conditions for the Finite Difference Approximation of the Time domain Electromagnetic field equations*, IEEE Trans. Electromagn. Compat., Vol .EMC-23, pp. 377-382, Nov. 1981
- 6 V. Jandhyala, E. Michielssen, and R. Mittra, *FDTD signal extrapolation using the forward-backward autoregressive model*, IEEE Microwave and Guide Wave Letters, Vol. 4, pp. 163-165, June 1994.
- 7 R.J Leubbers and H.S Langdon., *A simple feed Model that reduces Time steps Needed for FDTD Antenna and Microstrip Calculations*, IEEE Trans. Antennas and Propogat., Vol.44,No.7, pp.1000-1005, July 1996.

- 8 R.J Leubbers, Karl s Kunz, Micheal Schneider and Forrest Hunsberger.,
A finite difference time Domain near zone to far zone transformation,
IEEE Trans. Antennas and Propagat., Vol.39,pp429-433, April 1991.
- 9 Martin L Zimmerman and Richard Q Lee, *Use of FDTD method in the
design of microstrip antenna arrays,* Int.Journal of Microwave and
Millimeter wave Comp. aided Engg., Vol.4, No.1,pp 58-66,1994.



CONCLUSION AND FUTURE PERSPECTIVE

- 6.1 Thesis Summary
 - 6.2 Inferences from PIN diode controlled frequency and polarization reconfigurable compact cross patch antenna
 - 6.3 Inferences from capacitor/varactor controlled compact cross patch antenna for frequency and polarization diversity applications
 - 6.4 Inferences from theoretical analysis of cross patch antenna
 - 6.5 Suggestions for future work
-

This chapter presents the conclusion drawn from the detailed investigations performed on the novel frequency and polarization reconfigurable compact cross patch antenna. Suggestions for future work are included in the following section. The results presented in the thesis have been published by the author in different international journals and conferences.

6.1 Thesis Summary

The aim of the thesis is to develop and optimize compact single feed dual frequency microstrip antenna that would facilitate frequency and polarization diversity without the use of any matching circuits and complicated biasing circuits. PIN diodes and varactors are used for switching or tuning mechanism. The antennas are designed to operate in the L-band where a large number of wireless communication applications exist.

The important design considerations throughout the study are compactness of the patch and tuning frequency and polarization effortlessly with simplified switching mechanism directly integrated into the radiating patch. This avoids the use of any matching networks or any transmission lines between non-linear components and patch. The design aspects, based on the geometrical parameters of the antenna, were first investigated. The simulation studies, in terms of their return loss and current distribution on the antenna at different resonances, reveal their dependence on the antenna dimensions. Dimensional parameters critically determine the resonances. Thus, the X-slot loaded cross patch antenna is brilliant because it not only provided a flexible tunability of operating frequency and polarization but also enhances the compactness of the design.

An introduction to the overview of state of the art of microstrip antenna technologies, with a special emphasis to reconfigurable antenna has been discussed in chapter 1. Previous reconfigurable antenna designs, their reconfiguration techniques and their applications are reviewed in chapter 2. The literature review presented clearly convinces the importance of the work in this direction and the novelty of work presented. The methodology employed for experimental investigations are also explained in chapter 2. The reconfigurable

antennas studied in this thesis are categorized into different groups based on their reconfiguration techniques and reconfigurability properties. Chapter 3 is devoted for the novel frequency and polarization reconfigurable compact cross patch antenna using PIN diodes. Investigations on radiation characteristics of compact cross patch antenna for frequency and polarization diversity applications using reactive loading were presented in chapter 4. Chapter 5 highlights a systematic approach to analyze a cross patch antenna using FDTD based numerical computation. A brief summary of the different antennas designed are discussed in the following sections.

6.2 Inferences from PIN diode controlled frequency and polarization reconfigurable compact cross patch antenna

A cross patch antenna with an embedded X-slot in the center excites compact orthogonal resonant modes. The X-slot induces symmetric current distributions for the orthogonal resonant modes with an area reduction of 79% and 66% for the two operating frequencies compared to standard rectangular patches. Mechanical tuning of the two orthogonal resonant modes can be varied by varying the length of the X-slot and can be easily modified to a compact reconfigurable antenna. Electronic control of the operating frequencies and the frequency ratio between two orthogonal resonant modes can be achieved with PIN diode switches along the X-slot arms. The proposed antenna can radiate four frequencies with stable radiation characteristics and considerable bandwidth and low operating frequency ratio in OFF and ON states of the PIN diodes. The antenna offers frequency shift of 190MHz for the first resonant frequency and 280MHz for the second resonant frequency.

Frequency reconfigurable polarization diversity operation is possible with two PIN diodes at the center of the X-slot. An electronically

reconfigurable cross patch operates either in linear polarization or in circular polarization state with respect to the proper biasing of the PIN diodes at the center of the X-slot. A good impedance matching performance for all polarization states is observed without any matching networks. The proposed design achieves a cross polar level better than -10dB in linear polarization and 0.85% CP bandwidth in circular polarization state with broadside radiation characteristics and moderate gain. In addition, the antenna is simple and compact because it uses only a few active and passive components and requires less area to occupy the patch and dc-bias circuit compared to conventional polarization diversity antennas. The frequency and polarization diversities of this design provide some potential applications for wireless communications.

6.3 Inferences from capacitor/varactor controlled compact cross patch antenna for frequency and polarization diversity applications

A single feed design of novel compact frequency reconfigurable microstrip antenna for tunable frequency ratio is based on the tuning of embedded slot in the patch antenna using a chip capacitor oriented along Y-direction at the center of the X-slot. This property of the antenna offers more flexibility in frequency tuning where the frequency ratio varies in a wider range from 1.84 to 1.68 when the capacitance is varied from 2.2pF to 82pF with linearly polarized radiation along Y-direction. Furthermore the proposed antenna has an added advantage of size reduction, moderate gain, low levels of cross-polarized radiation and the radiation patterns of each frequency remain unchanged as the capacitor value is changed.

Frequency and polarization reconfigurable microstrip antenna is obtained when the chip capacitor at the center of the X-slot is positioned along X-direction. A high tuning range of 34.48% and 14.3% is achieved for the first

and third resonant frequencies respectively by minimizing the variations of second resonant frequency. Measurement results of the antenna indicate that its frequency ratio can assume any value in the range $1.025 \leq f_R \leq 1.21$ with linear or circularly polarized radiation by changing the capacitor value from 1pF to 100pF. By replacing the chip capacitor with a varactor diode the proposed design can be extended to frequency agile polarization diversity antenna.

A compact electronically reconfigurable dual frequency microstrip antennas is proposed and experimentally verified. The concept is based on the electronic tuning of embedded slots in the patch antenna using varactor diodes. A high tuning range of 26.3% (1.02–1.299 GHz) and 15.3% (1.305–1.502 GHz) is achieved for the two operating frequencies respectively, when the bias voltage is varied from 0 to 16V. The salient feature of this design is that it uses no matching networks even though the resonant frequencies are tuned in a wide range with good matching below -10 dB. The antenna has an added advantage of size reduction up to 77% and 64% for the two operating frequencies compared to conventional rectangular patches. Another feature of this antenna is that the radiation characteristic is remaining essentially unaffected by the frequency tuning.

A new design of single feed compact reconfigurable microstrip antenna with polarization diversity using single varactor is proposed. The prototype shows stable radiation characteristics and patterns of each frequency remain unchanged with respect to the voltage variation. Furthermore the antenna has an added advantage of reduced size with low levels of cross-polarized radiation in linear polarization state and a 10MHz axial ratio bandwidth in circular polarization state.

6.4 Inferences from theoretical analysis of cross patch antenna

FDTD based numerical computation is used to analyze the performance of cross patch antenna with and without X-slot. PIN diode controlled frequency and polarization reconfigurable compact cross patch antenna is also analyzed using FDTD. The staircase approximation is employed to derive the slant edges of the X-slot. MATLAB based in-house codes were developed for simulation of the antenna. Luebber's feed model is employed to excite the microstrip line feed of the antenna and a Gaussian pulse is used as the source of excitation. Time step used for the computation is 0.95ps. The Gaussian half-width is $T = 20$ ps and the time delay t_0 is set to be $3T$. Various steps involved in the extraction of antenna parameters along with the assumptions taken in the implementation of the algorithm are also described. The predicted results are experimentally verified by fabricating and testing different printed cross patch antennas.

6.5 Suggestions for future work

The following are some of the prospects for future work:

A review of the research discussed here indicates that reconfigurable antenna concepts and prototypes have been in development for more than 40 years. However, there are still very few reconfigurable antennas in use today. Although reconfigurable antennas deliver expanded functionality over fixed antennas, they typically require extra parts, extra control lines, and extra infrastructure at one level or another. Antennas with all of these additional parts and connections may be devised in future.

The validation of RF-MEMS technology is being pushed to a certain degree by demands for low-cost, high-reliability reconfigurable circuits and antennas. Additionally, pursuit of new and novel tunable materials with improved loss and bias characteristics will make reconfiguration more practical and cost-effective. Finally, the development of new kinds of mechanical

actuators and electronic tuning methods is another area for future work with an even broader range of capabilities than those discussed here.

Reconfigurability is a demanding antenna design qualities in building multiple-in-1 antennas. The modifications in the design to achieve pattern and polarization reconfigurable microstrip antenna may be investigated in future.

The antennas designed in this thesis have been printed on lossy substrates. Instead, they may be designed on low temperature co-fired ceramic (LTCC) substrates in future which have the advantage of direct integration with monolithic microwave circuits.

The differential feeding structure has the ability to reconfigure the patch over a large frequency range. Therefore a differentially fed frequency and polarization reconfigure microstrip antenna may also be considered in future for wide tunability range.



DESIGN OF CIRCULARLY POLARIZED RECTANGULAR MICROSTRIP ANTENNA FOR GPS APPLICATIONS

Circularly polarized single feed microstrip patch antennas are widely employed in radar, GPS and mobile communication systems. Achieving 3dB axial ratio bandwidth along with the 2:1 VSWR bandwidth is a challenging task for designers. A compact design of a single feed microstrip antenna for circular polarization (CP) is proposed and studied in this section. Circular polarization is brought about by embedding slot in a cross shaped patch. Simulation and experimental results of the antenna are presented and discussed.

A.1 Circularly polarized microstrip antennas: Review

A microstrip antenna is a resonator type antenna usually designed for single-mode operation that radiates mainly linear polarization. For CP, a patch must support orthogonal fields of equal amplitude but in-phase quadrature. This requirement can be accomplished by a single patch with proper excitations or by an array of patches with an appropriate arrangement and phasing. A single patch antenna can be made to radiate CP using two types of feeding schemes. The first type is a dual-orthogonal feed, which employs an external power divider network. A single feed patch is very desirable in situations where it is difficult to accommodate dual-orthogonal feeds with a power divider network. Because a patch with a single point feed generally radiates linear polarization, CP radiation can be accomplished by perturbing a patch at appropriate locations with respect to the feed [1-5].

A nearly square patch with a single feed along the diagonal is one of the simplest microstrip antenna configurations to generate CP [6]. Instead of using a nearly square MSA to generate CP, the edges of the square MSA can be modified by adding stubs or by cutting notches [7]. CP can also be obtained by modifying corners of the square MSA. Small isosceles right angle triangular patches or small square patches are removed from the diagonally opposite corners of the square patch [8]. Instead of chopping the corners, small square patches could be added at the corners to obtain CP [9]. A square MSA with a rectangular slot along its diagonal and the feed along its central axis produces CP. The difference in the resonance frequencies of the orthogonal modes is caused by the rectangular slot, which makes the path lengths of the two diagonals unequal [10-11].

Instead of adding stubs or cutting slots or notches in the square patch shorting posts or chip resistors could be used to obtain CP [12-14]. Similar to the modified square microstrip antenna, modified circular and triangular microstrip antenna configurations with a single feed also generate CP. Circular microstrip antenna configurations include an elliptical patch, circular patch with notches or stubs and rectangular slot at the center of a circular patch to yield CP [15-19]. Many variations of the nearly square ring MSA with square slot are possible yielding similar performance. These are a square ring with a nearly square slot, a corner-chopped square ring with a square slot, and a square ring with a corner-chopped square slot [20-23].

It has been observed that the dual-feed microstrip antenna configurations yield a wider axial ratio bandwidth and narrower VSWR bandwidth as compared to the single-feed microstrip antenna configurations. The single-feed configurations have narrow axial ratio bandwidth on the order of 1%. These small axial ratio or VSWR bandwidths are not enough for many applications. Broadband CP is obtained by using planar multi-resonator microstrip antenna configurations. The fed patch and the parasitic patches could be gap-coupled or directly coupled [24-261]. Reddy and Kumar developed stacked rectangular and circular microstrip antenna configurations that yield broadband CP [27-29]. Several variations of apertures/slots, such as two orthogonal slots, single inclined slot, and inclined slot with V-slot loaded at both ends were proposed in literature [30–35].

The axial ratio bandwidth of the single-feed microstrip antennas can be significantly increased by using them in sequentially rotated array configuration [36-37]. The elements could be circularly or linearly polarized. Pozar demonstrated that a single fed square patch radiates both left-hand circularly polarized (LHCP) and right-hand circularly polarized (RHCP), however, LHCP

and RHCP have different resonant frequencies [38]. The sense of polarization can be reversed by reversing the polarity of the bias field with axial ratio bandwidth larger than the impedance bandwidth. Two linearly polarized patch antennas can be orthogonally arranged with one of the patches being fed 90^0 out of phase [39-41]. The disadvantages of this configuration are larger space requirements and rapid degradation of CP with angle off the boresight as a result of spatial phase delay due to different path lengths from the phase centers of the two radiating elements.

A.2 Single slot loaded circularly polarized cross patch antenna

In this section, a promising design of a proximity coupled circular polarized microstrip antenna is presented. A slot is embedded in to a cross shaped rectangular patch antenna. The insertion of the slot not only increases the impedance bandwidth, but also produces compact circular polarized radiation in the entire band. The above technique is simple and compact compared to the existing techniques. An area reduction of 46% as compared to a conventional rectangular microstrip antenna is obtained. Also the antenna exhibits broadside radiation characteristics with a beam width of 75° . The dimensions of the patch, feed point locations and slots are optimized for good performance. FEM based Ansoft HFSS is used for the simulation and analysis of the structure. The antenna is tested using HP 8510C vector network analyzer. The experimental results are in good agreement with the simulation results.

A.2.1 Antenna Geometry

The geometry of the proposed antenna is illustrated in figure A.1. It consists of a rectangular patch of size $L \times W \text{ mm}^2$ with two pairs of square slits at the corners of the rectangular patch having dimension $L_s \times L_s \text{ mm}^2$. A slot of dimension $(L_v + W_v + L_v) \times W_s \text{ mm}^2$ is etched at the centre of the patch. The

arms of the slot are tilted by α° along y . The antenna is symmetrical along the YZ- plane and is excited by a proximity feed of width W_f (mm).

A.2.2 Simulations

In this section, the performance of the antenna is investigated through simulations. Figure A.2 illustrates the simulated reflection coefficient of the antenna with parameters in Table A.1. The simulated -10dB bandwidth appears from 1.51GHz to 1.61GHz. In order to identify the resonant modes of the antenna, its input impedance is plotted against frequency in figure A.2 (a). This radiating geometry results two near orthogonal resonant modes at 1.53GHz and 1.59GHz respectively. The input impedance of first mode is inductive and the second mode is capacitive which in this case compares the best CP performance. Another way to recognize whether the given dimensions are optimum for the best AR is to look at the impedance plot of the antenna in figure A.2 (b). If there is a kink (extremely small loop) in the impedance plot corresponding to the excitation of the two orthogonal modes, it will yield the best AR at the kink frequency. Instead of a kink, a small loop or the absence of the loop in the impedance plot yields poor AR. In this antenna the best CP performance is achieved at 1.57GHz.

The return loss or the input impedance can only describe the behavior of an antenna as a lumped load at the end of a feeding line. The detailed EM behavior of the antenna is revealed by examining the radiation patterns. 3D radiation pattern of the antenna at 1.57GHz is given in figure A.3. There exists scattered radiation towards backward direction due to the finite ground plane; the antenna provides a broadside radiation characteristic with a sufficient front-to-back ratio. Figure A.4 shows the 2D radiation pattern of the antenna at 1.57GHz in two orthogonal planes.

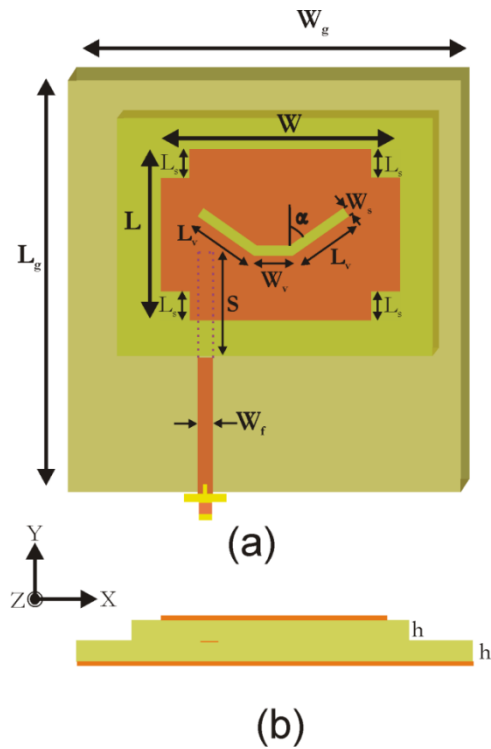


Figure A.1 Geometry of circularly polarized cross patch antenna (a) Front view (b) side view ($L=35\text{mm}$, $W=49\text{mm}$, $L_S=5.9\text{mm}$, $L_V=14\text{mm}$, $W_V=8\text{mm}$, $W_S=2\text{mm}$, $S=17\text{mm}$, $W_f=3\text{mm}$, $h=1.6\text{mm}$, $\alpha=55^\circ$ and $\epsilon_r=4.4$)

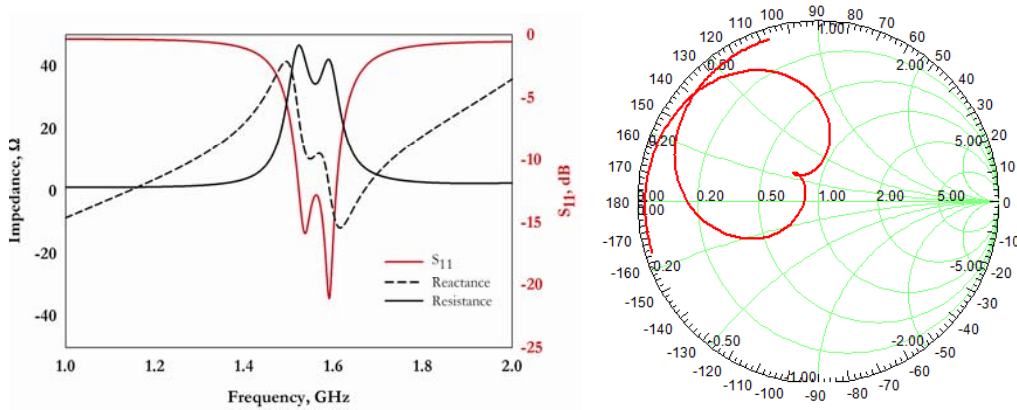


Figure A.2 Simulated reflection coefficient and input impedance curve of circularly polarized cross patch antenna ($L=35\text{mm}$, $W=49\text{mm}$, $L_S=5.9\text{mm}$, $L_V=14\text{mm}$, $W_V=8\text{mm}$, $W_S=2\text{mm}$ and $\alpha=55^\circ$)

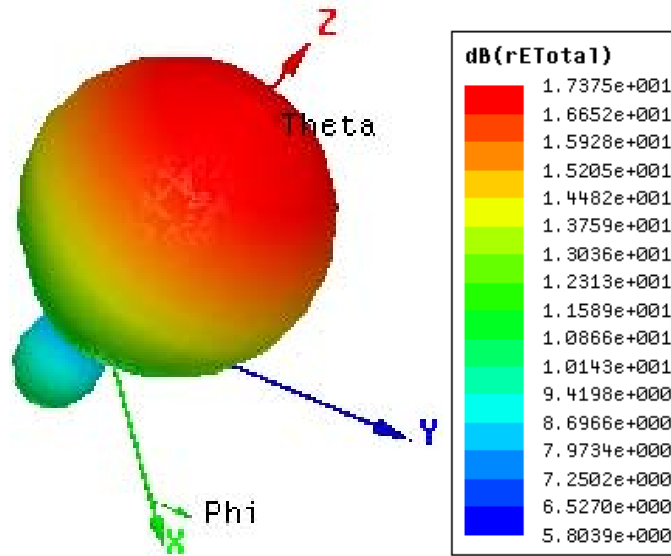


Figure A.3 Simulated 3D radiation pattern of circularly polarized cross patch antenna at 1.57GHz ($L=35\text{mm}$, $W=49\text{mm}$, $L_S=5.9\text{mm}$, $L_V=14\text{mm}$, $W_V=8\text{mm}$, $W_S=2\text{mm}$ and $\alpha=55^\circ$)

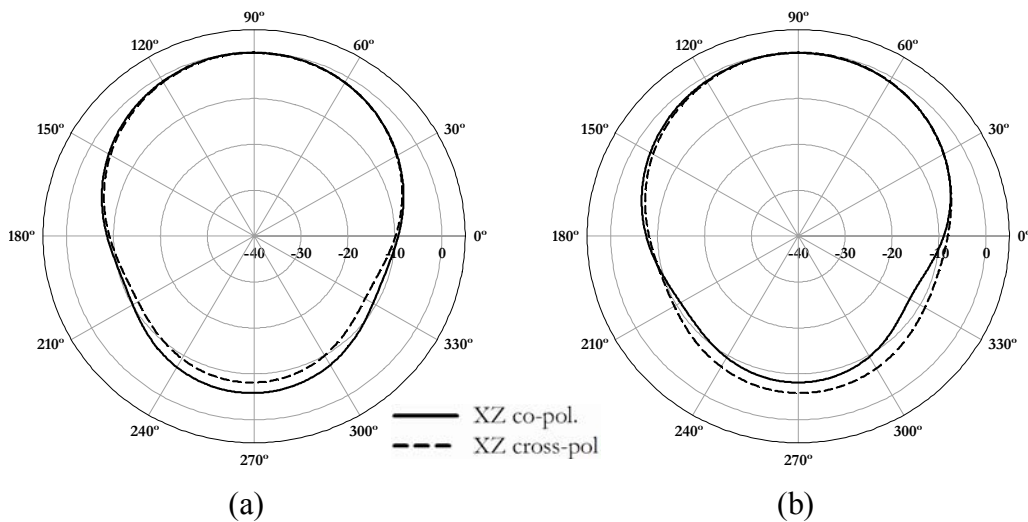


Figure A.4 Simulated 2D radiation pattern of circularly polarized cross patch antenna at 1.57GHz in (a) XZ-plane and (b) YZ- plane ($L=35\text{mm}$, $W=49\text{mm}$, $L_S=5.9\text{mm}$, $L_V=14\text{mm}$, $W_V=8\text{mm}$, $W_S=2\text{mm}$ and $\alpha=55^\circ$)

A.2.3 Parametric analysis

Further insight on the antenna performance is obtained by carrying out a detailed parametric analysis. The influence of the slot arm lengths (L_v) on the reflection characteristics is given in figure A.5. It is observed that the second resonance is more shifted towards lower frequency region than the first resonance with the increase in L_v . Also the CP performance is lost as L_v is increased. Therefore an optimum value of $L_v = 0.147 \lambda_g$ is selected which is a compromise between impedance matching and CP operation.

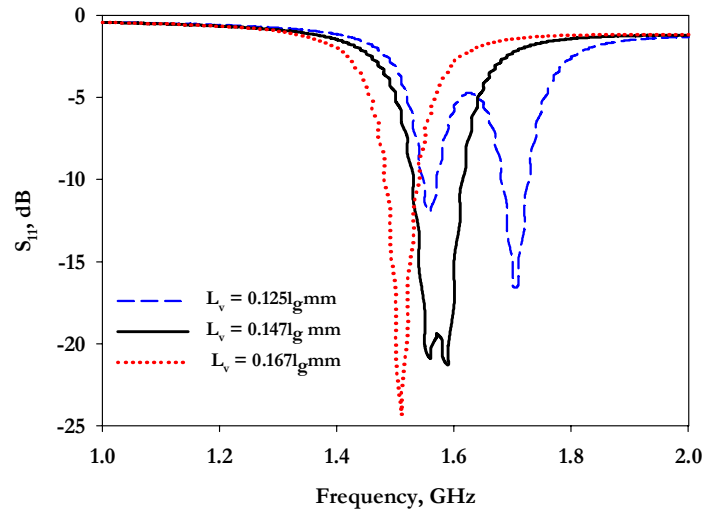


Figure A. 5. The influence of L_v on reflection characteristics of the antenna ($L=35\text{mm}$, $W=49\text{mm}$, $L_s=5.9\text{mm}$, $L_v=14\text{mm}$, $W_v=8\text{mm}$, $W_s=2\text{mm}$ and $\alpha=55^\circ$)

The tilt angle (α) has a crucial effect in the impedance matching of the antenna. From figure A.6, it can be seen that the centre frequency for CP operation is shifted to lower side with increasing α , but the impedance bandwidth get reduced. Smaller values of α excites two orthogonal resonant modes. Hence, an optimum value of $\alpha = 55^\circ$ is chosen for the proposed design.

The variation of axial ratio with W_s is presented in figure A.7. Impedance matching becomes poor as W_s are lowered. For larger values of W_s the centre frequency for CP operation is shifted to lower side of the resonant band. Also the resonant band is narrowed and the CP performance is lost.

Hence, an optimum value of $W_s = 2\text{mm}$ is selected as a compromise between impedance as well as 3dB axial ratio bandwidth.

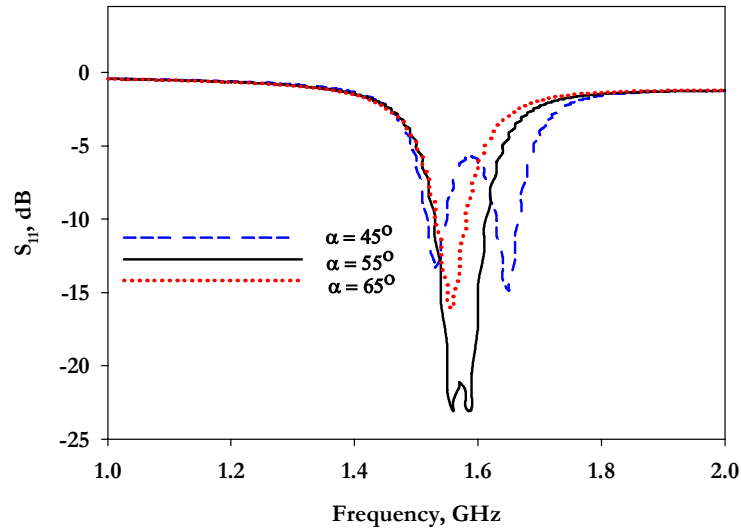


Figure A. 6. Reflection characteristics of the antenna for different α ($L=35\text{mm}$, $W=49\text{mm}$, $L_s=5.9\text{mm}$, $L_v= 14\text{mm}$, $W_v=8\text{mm}$, $W_s=2\text{mm}$ and $\alpha =55^\circ$)

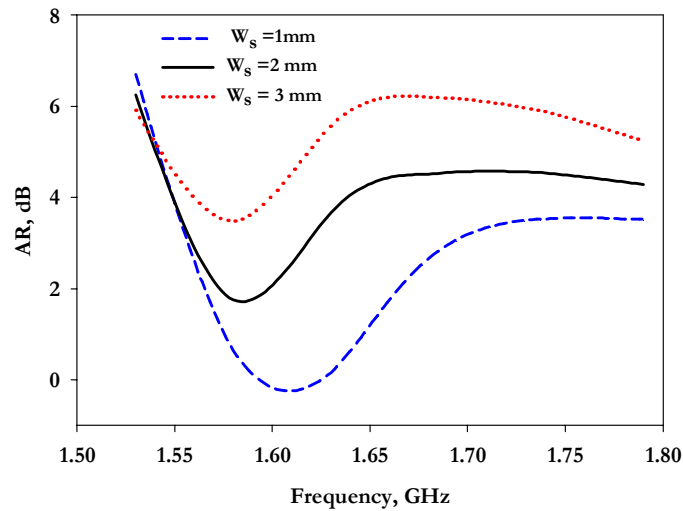


Figure A.7. Effect of w_s on CP operation of the antenna ($L=35\text{mm}$, $W=49\text{mm}$, $L_s=5.9\text{mm}$, $L_v= 14\text{mm}$, $W_v=8\text{mm}$, $W_s=2\text{mm}$ and $\alpha =55^\circ$)

Figure A.8 shows the effect of W_v on CP operation of the antenna. As W_v increases, the resonant band shifts to lower frequency. While the higher

values of W_v excites linearly polarized radiation. Therefore $W_v = 0.084 \lambda_g$ is a good selection which produces minimum reflection and better CP bandwidth in the resonant band.

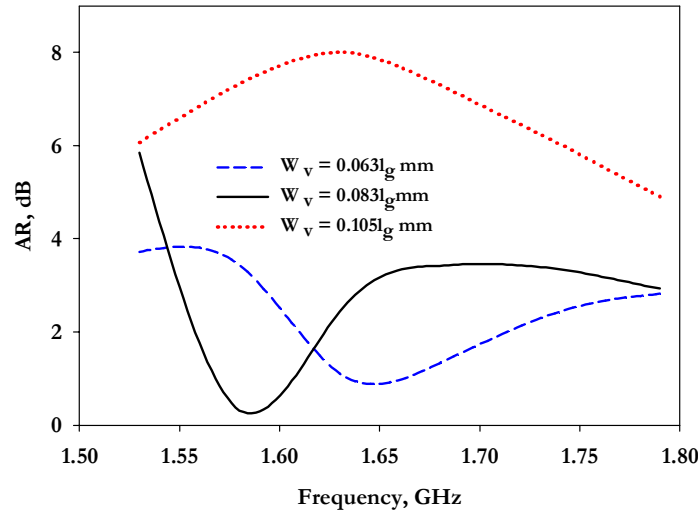


Figure A. 8. Axial ratio of the antenna against W_v ($L=35\text{mm}$, $W=49\text{mm}$, $L_s=5.9\text{mm}$, $L_v=14\text{mm}$, $W_v=8\text{mm}$, $W_s=2\text{mm}$ and $\alpha = 55^\circ$)

A.2.4 Design

The surface current distribution on the patch at the centre frequency (1.57GHz) simulated using HFSS is plotted in figure A.9. A half wavelength variation in current is observed along the patch boundary ($L+W$).

$$[L+W] / K = \lambda_g / 2 \quad (1)$$

Where K is an empirically derived parameter which includes the effect of the substrate and λ_g is the wavelength in the dielectric which is computed from the free space wavelength λ_0 as

$$\lambda_g = \lambda_0 / \sqrt{\epsilon_{re}} \quad (2)$$

and ϵ_{re} is the effective permittivity of the substrate.

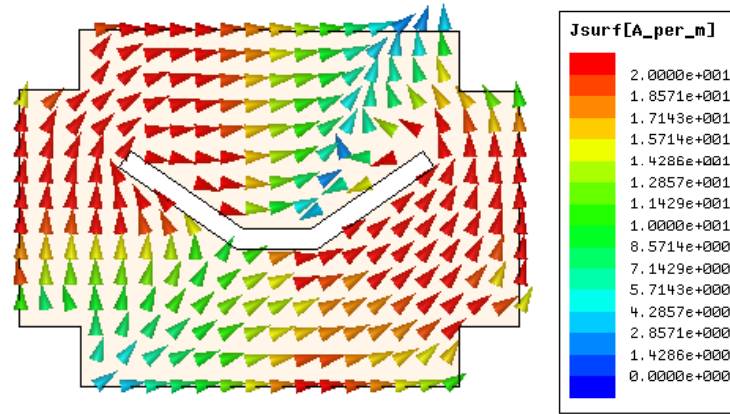


Figure A.9 Simulated surface current distribution of circularly polarized cross patch antenna at 1.57GHz ($L=35\text{mm}$, $W=49\text{mm}$, $L_s=5.9\text{mm}$, $L_v=14\text{mm}$, $W_v=8\text{mm}$, $W_s=2\text{mm}$ and $\alpha=55^\circ$)

Based on this, design equations are derived relating to the geometry and operating frequency band of the proposed antenna. The design procedure can be framed as

- 1) Design a 50Ω transmission line on a substrate with permittivity ϵ_r and thickness h . Calculate λ_g using equation (2).
- 2) Design the dimensions of the patch using

$$L = 0.33 \lambda_g \text{ and}$$

$$W = 0.47 \lambda_g$$

- 3) Design the dimensions of the slot using

$$L_v = 0.134 \lambda_g$$

$$W_v = 0.077 \lambda_g$$

$$W_s = 0.02 \lambda_g$$

$$\text{and } L_s = 0.056 \lambda_g$$

Using the parameters so computed, the antenna was studied on substrates with different permittivity, as described in Table A.1. Figure A.10 shows the reflection characteristics of the antennas with the computed geometric parameters given in Table A.2. Resonances of these antennas show slight deviation from the designed values but there is impedance match throughout the band. The reason for this is that the effective permittivity computed for the transmission line does not hold for the radiating part of the antenna.

Table A.1 Antenna Description

	Antenna 1	Antenna 2	Antenna 3	Antenna 4
Laminate	Rogers 5870	Neltec NH9338	FR4 Epoxy	Rogers R03006
h (mm)	1.59	1.57	1.6	1.28
ϵ_r	2.32	3.38	4.4	6.15
ϵ_{re}	1.969	2.686	3.345	4.428
w_f (mm)	4.72	3.62	3	1.87
K	1.56	1.59	1.6	1.52

Table A.2 Parameters of the antennas

Parameters	Antenna 1		Antenna 2		Antenna 3		Antenna 4	
	Computed	Optimized	Computed	Optimized	Computed	Optimized	Computed	Optimized
L_s (mm)	7.65	7.4	6.5	6.47	5.885	5.885	5.08	4.83
L_v (mm)	18.2	17.6	15.6	15.4	13.99	14	12	11.5
W_v (mm)	10.48	10.08	8.97	8.8	7.99	8	6.9	6.56
W_s (mm)	2.7	2.5	2.3	2.2	2.09	2	1.8	1.6
α (in degrees)	55°	55°	55°	55°	55°	55°	55°	55°
$L \times W$ (mm ²)	45.5x64	44x62	39x55	38.5x54	34.8x49	35x49	30x42.6	29x40.2

The simulated return loss of the antenna using a substrate of $\epsilon_r=4.4$ for different substrate height is shown in figure A.11. The increase in substrate thickness maximize the antenna bandwidth, but not so large as to the risk of surface wave excitation. The proposed antenna has an area reduction of 46% as compared to standard rectangular microstrip antennas.

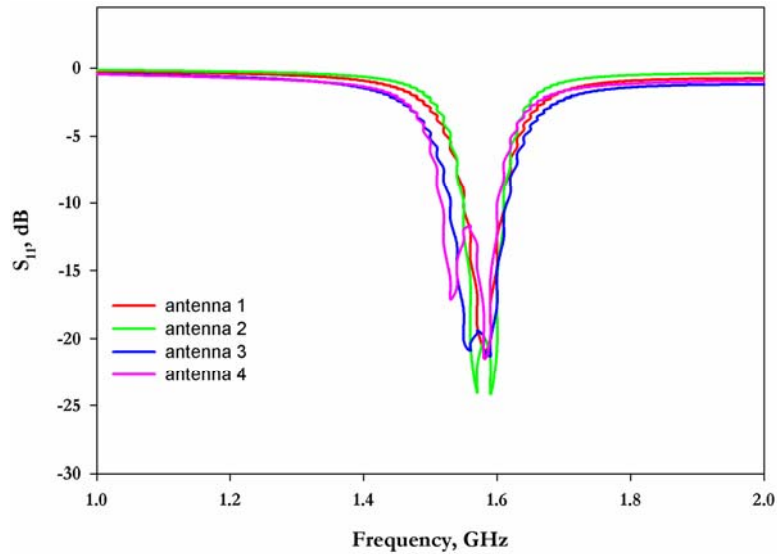


Figure A.10 Simulated reflection characteristics of circularly polarized cross patch antenna for dielectric substrate ($L=35\text{mm}$, $W=49\text{mm}$, $L_S=5.9\text{mm}$, $L_V=14\text{mm}$, $W_V=8\text{mm}$, $W_S=2\text{mm}$ and $\alpha=55^\circ$)

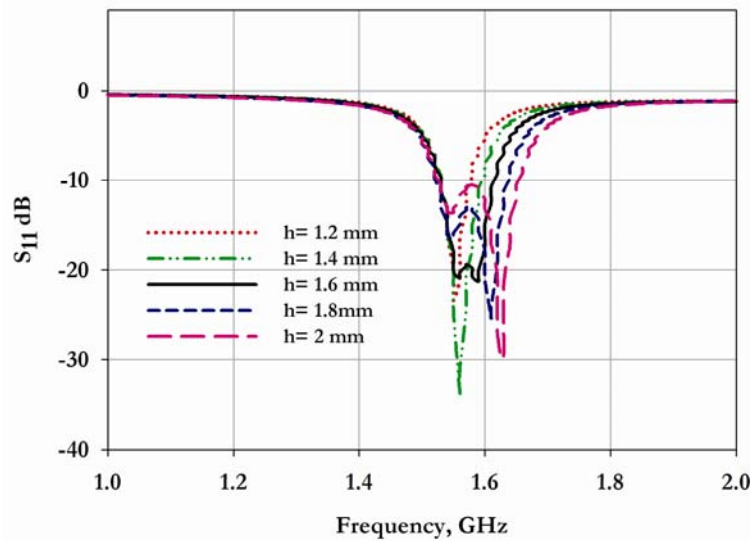


Figure A.11 Simulated reflection coefficient of the proposed antenna with substrate height h ($L=35\text{mm}$, $W=49\text{mm}$, $L_S=5.9\text{mm}$, $L_V=14\text{mm}$, $W_V=8\text{mm}$, $W_S=2\text{mm}$ and $\alpha=55^\circ$)

A.2.5 Measurements

A prototype of the antenna was fabricated on a substrate of $\epsilon_r=4.4$ and $h=1.6\text{mm}$ with the parameters as in Table A.2 and A.3. The measured reflection coefficient of the antenna given in figure A.12 is validated by simulations. The measured impedance bandwidth of the antenna is about 5% from 1.53 to 1.61GHz which covers GPS L1 band. A prototype of the proposed antenna is shown in figure A.13.

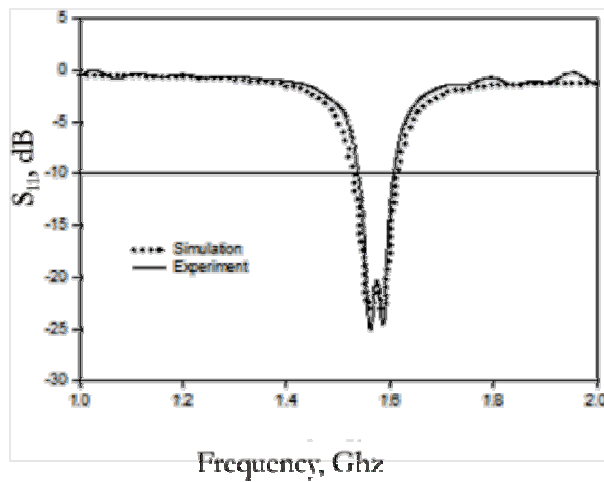


Figure A.12 Simulated and measured reflection coefficient of circularly polarized cross patch antenna ($L=35\text{mm}$, $W=49\text{mm}$, $L_S=5.9\text{mm}$, $L_V=14\text{mm}$, $W_V=8\text{mm}$, $W_S=2\text{mm}$ and $\alpha=55^\circ$)

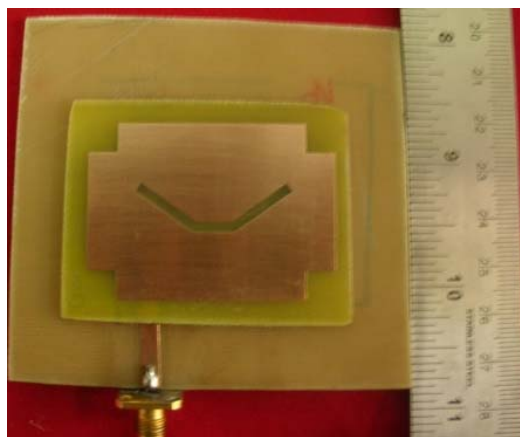


Figure A.13 Prototype of the fabricated antenna

The axial ratio graph of the antenna in the broadside direction is presented in figure A.14. It is observed that the circular polarization bandwidth determined from 3 dB axial ratio is 80MHz or about 5% from 1.55 to 1.63GHz.

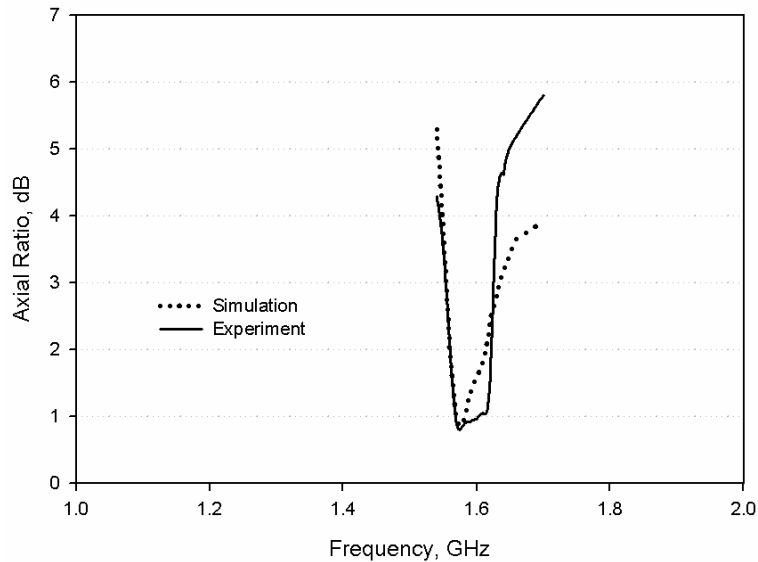


Figure A. 14 Simulated and measured axial-ratio along the on-axis ($L=35\text{mm}$, $W=49\text{mm}$, $L_S=5.9\text{mm}$, $L_V=14\text{mm}$, $W_V=8\text{mm}$, $W_S=2\text{mm}$ and $\alpha=55^\circ$)

The measured gain is plotted in figure A.15. The antenna exhibits an average gain of 5dBi in the entire band with stable broadside radiation characteristics. The radiation patterns of the proposed antenna in two orthogonal planes at 1.57GHz are shown in figure A.16 (a) and (b) respectively. The 3 dB beam widths of the antenna in both XZ and YZ plane are about 75° and a good left-hand CP radiation is observed.

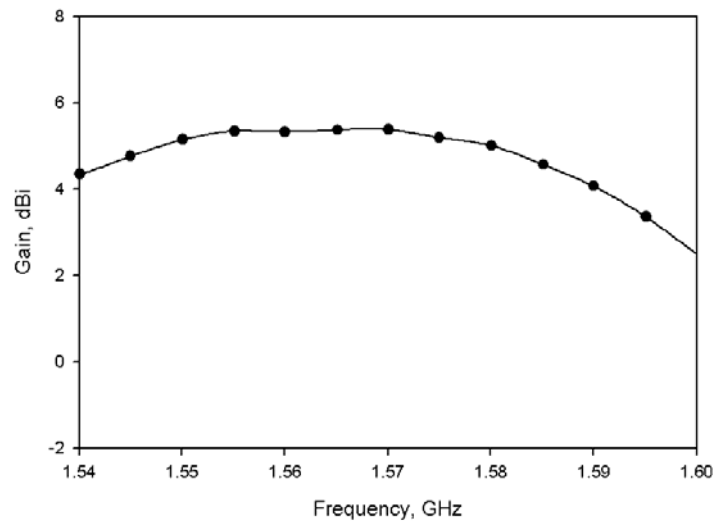


Figure A.15 Measured gain of circularly polarized cross patch antenna ($L=35\text{mm}$, $W=49\text{mm}$, $L_S=5.9\text{mm}$, $L_V=14\text{mm}$, $W_V=8\text{mm}$, $W_S=2\text{mm}$ and $\alpha=55^\circ$)

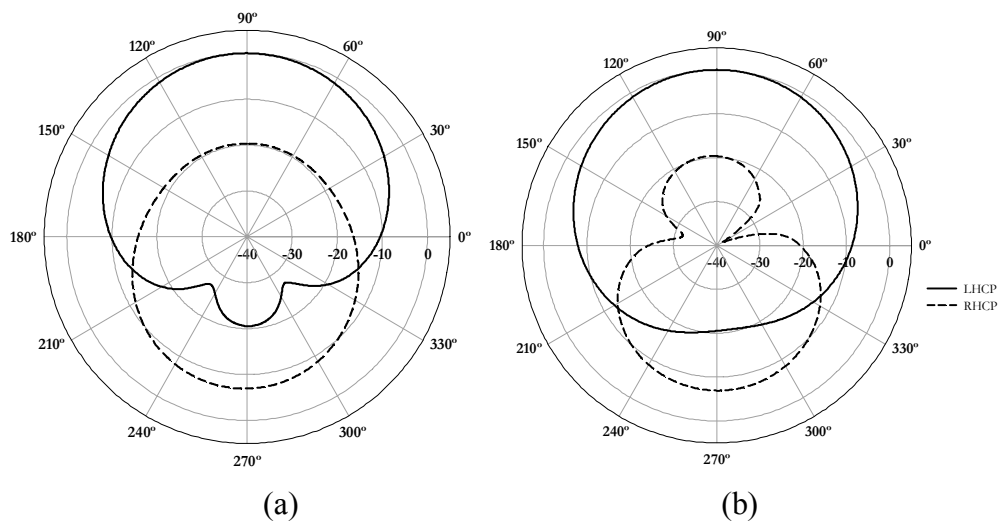


Figure A.16 Radiation patterns of circularly polarized cross patch antenna at 1.57GHz (a) XZ-plane and (b) YZ-plane ($L=35\text{mm}$, $W=49\text{mm}$, $L_S=5.9\text{mm}$, $L_V=14\text{mm}$, $W_V=8\text{mm}$, $W_S=2\text{mm}$ and $\alpha=55^\circ$)

A.2.6 Theoretical analysis of circularly polarized cross patch antenna

Circularly polarized cross patch antenna is analyzed theoretically using finite difference time domain method. Two dimensional view of the configuration computed theoretically is given in Fig. A.17. The computational domain is divided in to Yee cells of dimension $\Delta x = \Delta y = 0.5\text{mm}$ and $\Delta z = 0.4\text{mm}$. The antenna is electromagnetically coupled using a microstrip line fabricated on substrate of thickness 1.6mm, 4 cells will exactly match feed substrate and another 4 cells are used to model the patch substrate thickness. 10 cells on each of the 6 sides are used to model air cells. Thus the total computation domain is discretized in to $220\Delta x * 220\Delta y * 28\Delta z$ cells. Luebber's feed model is employed to excite the microstrip line feed of the antenna and a Gaussian pulse is used as the source of excitation. The measured, simulated and theoretically computed resonances of circularly polarized cross patch antenna plotted in Fig.A.18 show good agreement. FDTD computed electric field distribution is given in Fig. A. 19.

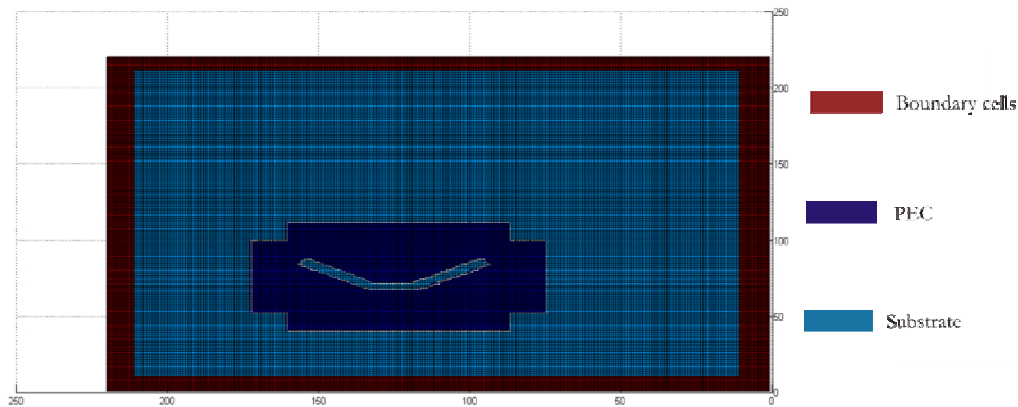


Figure A. 17 2D view of the FDTD computation domain of circularly polarized cross patch antenna ($L=35\text{mm}$, $W=49\text{mm}$, $L_S=5.9\text{mm}$, $L_V=14\text{mm}$, $W_V=8\text{mm}$, $W_S=2\text{mm}$ and $\alpha = 55^\circ$)

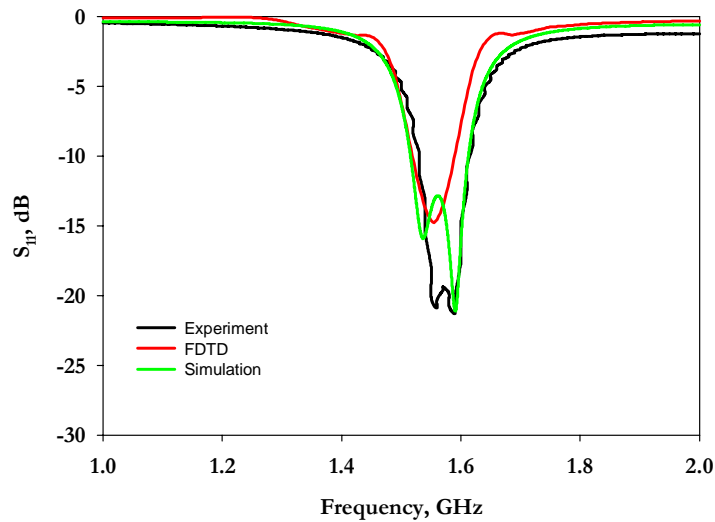


Figure A.18 Reflection characteristics of circularly polarized cross patch antenna ($L=35\text{mm}$, $W=49\text{mm}$, $L_S=5.9\text{mm}$, $L_V=14\text{mm}$, $W_V=8\text{mm}$, $W_S=2\text{mm}$ and $\alpha=55^\circ$)

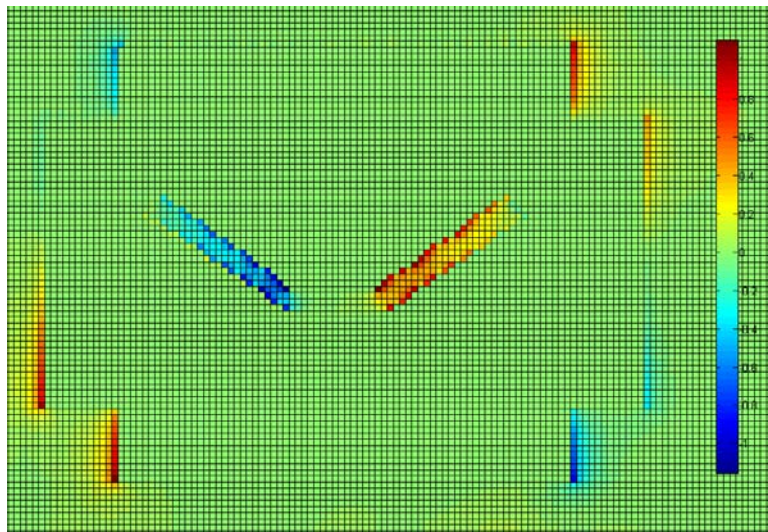


Figure A.19 FDTD computed Electric field distribution of circularly polarized cross patch antenna ($L=35\text{mm}$, $W=49\text{mm}$, $L_S=5.9\text{mm}$, $L_V=14\text{mm}$, $W_V=8\text{mm}$, $W_S=2\text{mm}$ and $\alpha=55^\circ$)

The slot inserted at the centre of the cross patch not only produces a compact circular polarized radiation but also increases the impedance bandwidth. The proposed antenna has an area reduction of 46% as compared to standard rectangular microstrip antennas. The prototype exhibits a 2:1 SWR

bandwidth of 5% from 1.53–1.61 GHz having 3dB axial ratio bandwidth of 5%. The antenna covers GPS L1 band giving broadside radiation characteristics with a beam width of 75° and an average gain of 5 dBi. The proposed design is validated for different frequencies.

A.3 Dual slot loaded circularly polarized cross patch antenna

By embedding an additional slot in such a way that two slots are connected back-to-back, the circular polarized radiation of the slotted cross shaped microstrip antenna can occur at a lower frequency. This implies that an even smaller antenna size for a fixed CP operation can be achieved, if one uses the present proposed compact circularly polarized rectangular microstrip antenna with a dual slot in place of the single slot CP design. The structure is giving an area reduction of 53% as compared to conventional rectangular microstrip antenna. The antenna offers a 2:1 VSWR bandwidth from 1.44 to 1.5GHz on a substrate of dielectric constant 4.4 and height 1.6mm with stable broadside radiation characteristics in the entire band. Simulation and experimental results show that the proposed antenna has moderate gain and good impedance bandwidth along with an axial ratio of less than 3dB. Design equations of the proposed antenna are developed and validated on different substrates.

A.3.1 Antenna Geometry

The geometry of a compact CP antenna is shown in figure A.20. Two slots of dimension $(L_v + W_v + L_v) \times W_s \text{ mm}^2$ are embedded back-to-back with a gap of V_g mm between them. The antenna is symmetrical along the YZ- plane and is excited by a proximity feed.

A.3.2 Design and simulations

Figure A.21 illustrates the simulated reflection coefficient of the antenna with parameters in Table A.4. The simulated -10dB bandwidth appears from 1.44GHz to 1.5GHz and it is found that by properly adjusting the slot lengths, two near-degenerate orthogonal resonant modes at 1.46GHz and 1.486GHz respectively with equal amplitudes and phase difference for CP operation are

excited at lower frequency compared to that of single slot antenna as shown in figure A.21. The center frequency is decreased to be 1.47 GHz and this lowering in the center operating frequency can correspond to an antenna size reduction of about 53%, when using the present compact CP design in place of the single slot CP design. There exists a kink at 1.467GHz in the impedance plot of the antenna in figure A.22 corresponding to the excitation of the two orthogonal modes. The design equations deduced for the single slot antenna continues to stand valid in this case as well. It is slightly modified in this case to take into account the dimensions of the slot and operating frequency. The simulated 3D radiation pattern and surface current distribution on the patch are shown in figure A.23 (a) and (b) respectively. It is then expected that due to the additional slot perturbation, both the surface current paths of the two orthogonal resonant modes can be lengthened, as compared to the design in Figure A.9, which lowers their corresponding resonant frequencies.

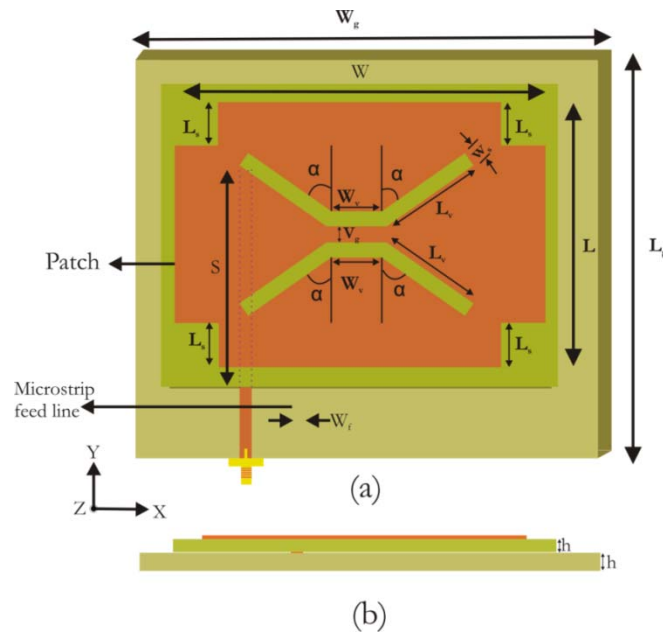


Figure A. 20 Geometry of circularly polarized dual slot cross Patch antenna (a) Front view (b) side view ($L=35\text{mm}$, $W=49\text{mm}$, $L_S=5.9\text{mm}$, $L_V= 12\text{mm}$, $W_V=8.7\text{mm}$, $W_S=2\text{mm}$ $S=27\text{mm}$, $W_f=3\text{mm}$, $V_g=3\text{mm}$, $h=1.6\text{mm}$, $\alpha =55^\circ$ and $\epsilon_r=4.4$)

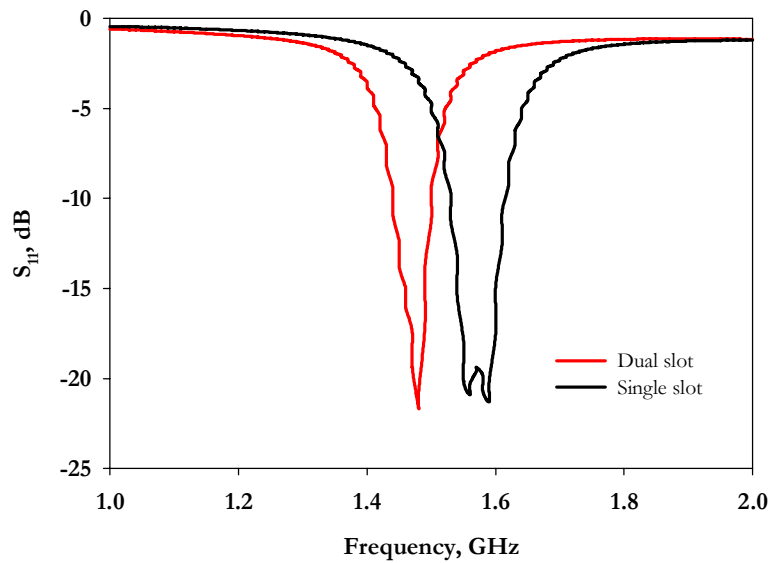


Figure A. 21 Simulated reflection coefficient of single and dual slot antenna

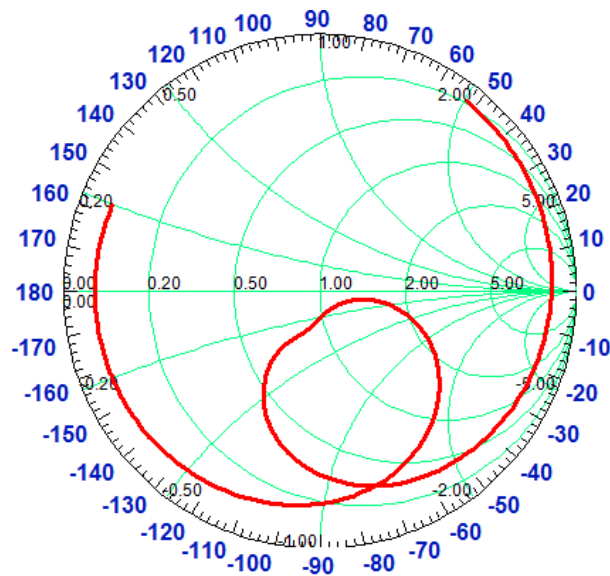


Figure A. 22 Simulated input impedance curve of dual slot loaded circularly polarized cross patch antenna ($L=35\text{mm}$, $W=49\text{mm}$, $L_s=5.9\text{mm}$, $L_v=12\text{mm}$, $W_v=8.7\text{mm}$, $W_s=2\text{mm}$, $V_g=3\text{mm}$ and $\alpha=55^\circ$)

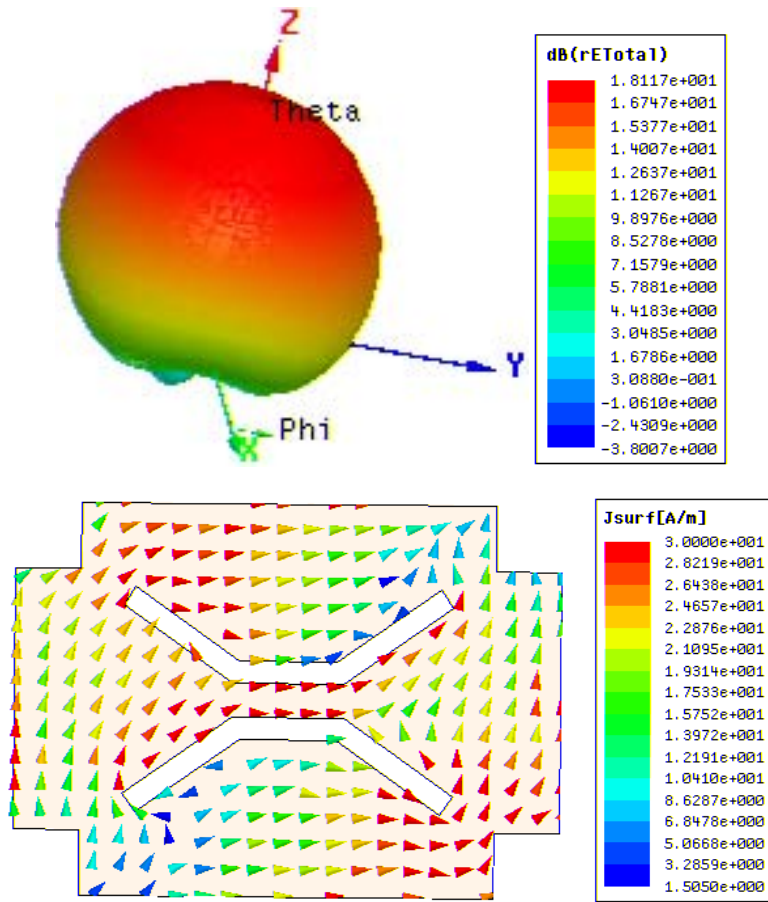


Figure A.23 3D radiation pattern and surface current distribution of dual slot loaded circularly polarized cross patch antenna at 1.46GHz ($L=35\text{mm}$, $W=49\text{mm}$, $L_s=5.9\text{mm}$, $L_v=12\text{mm}$, $W_v=8.7\text{mm}$, $W_s=2\text{mm}$, $V_g=3\text{mm}$ and $\alpha=55^\circ$)

The design procedure can be framed as

- 1) Design a 50Ω transmission line on a substrate with permittivity ϵ_r and thickness h . Calculate λ_g using equation (2).
- 2) Design the dimensions of the patch using

$$L = 0.314 \lambda_g \text{ and}$$

$$W = 0.439 \lambda_g$$

3) Design the dimensions of the slot using

$$L_v = 0.107 \lambda_g$$

$$W_v = 0.089 \lambda_g$$

$$W_s = 0.018 \lambda_g$$

$$L_s = 0.05 \lambda_g \text{ and}$$

$$V_g = 0.027 \lambda_g$$

Using the parameters so computed, the antenna was studied on substrates with different permittivity, as described in Table A.3. Figure A.24 shows the reflection characteristics of the antennas with the computed geometric parameters given in Table A.4. Resonances of these antennas show slight deviation from the designed values but there is impedance match throughout the band. The reason for this is that the effective permittivity computed for the transmission line does not hold for the radiating part of the antenna.

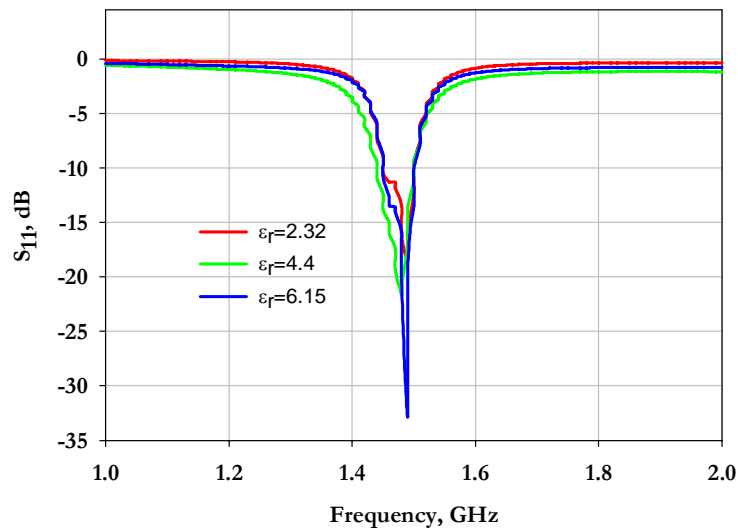


Figure A.24 Simulated reflection coefficient of dual slot loaded circularly polarized cross patch antenna for different substrate dielectric constant ($L=35\text{mm}$, $W=49\text{mm}$, $L_s=5.9\text{mm}$, $L_v=12\text{mm}$, $W_v=8.7\text{mm}$, $W_s=2\text{mm}$, $V_g=3\text{mm}$ and $\alpha=55^\circ$)

A.3.3 Measurements

A prototype of the antenna was fabricated on a substrate of $\epsilon_r=4.4$ and $h=1.6$ mm with the parameters as in Table A.3 and A.4. The measured reflection coefficient of the antenna given in figure A.25 is validated by simulations. The measured impedance bandwidth of the antenna is about 4% from 1.44 to 1.5GHz with an area reduction of 53% as compared to standard rectangular micro strip antennas.

Table A.3 Antenna description

	Antenna 1	Antenna 2	Antenna 3
Laminate	Rogers 5880	FR4 Epoxy	Rogers R03006
h (mm)	1.59	1.6	1.28
ϵ_r	2.32	4.4	6.15
ϵ_{re}	1.968	3.34	4.42
W_f (mm)	4.72	3	1.87
K	1.5	1.5	1.5

Table A.4 Parameters of the antennas

Parameters	Antenna 1		Antenna 2		Antenna 3	
	Computed	Optimized using HFSS	Computed	Optimized using HFSS	Computed	Optimized using HFSS
l_s (mm)	7.28	7.76	5.579	5.885	4.85	4.83
l_v (mm)	15.59	15.84	11.94	12	10.38	9.84
w_v (mm)	12.97	13.2	9.93	10	8.63	8.2
w_s (mm)	2.62	2.64	2	2	1.75	1.64
v_0 (mm)	3.93	3.96	3	3	2.62	2.46
L x W (mm ²)	45.75x63.96	46.2x64.68	35x48.99	35x49	30.46x42.58	28.7x40.18

The axial ratio graph of the antenna in the broadside direction is presented in figure A.26. The 3dB circular polarization bandwidth is 20MHz. The antenna exhibits an average gain of 4.5dBi in the entire band with stable broadside radiation characteristics. The bore sight radiation patterns of the proposed antenna in two orthogonal planes at 1.46GHz are shown in figure A.27 (a) and (b) respectively. The 3 dB beam widths of the antenna in both XZ- and YZ-planes are about 65°. The comparison of single and dual slot antennas is summarized in Table A.5.

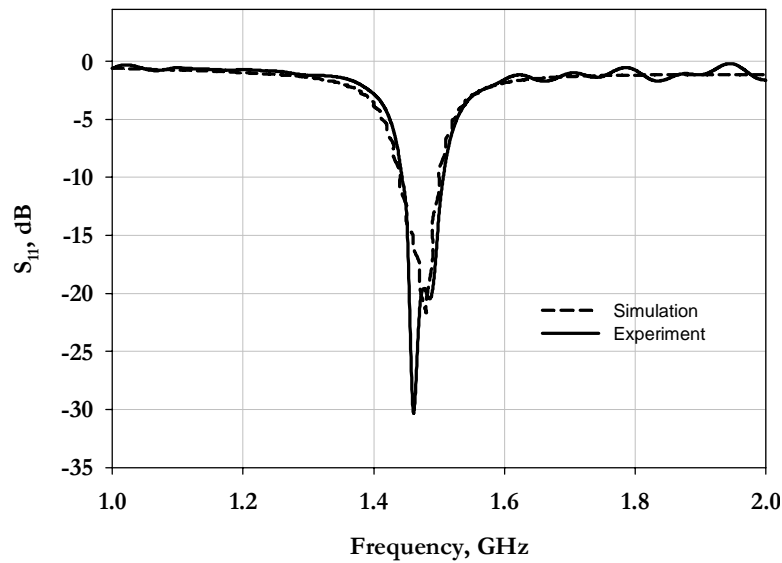


Figure A.25 Simulated and measured reflection coefficient of dual slot loaded circularly polarized cross patch antenna ($L=35\text{mm}$, $W=49\text{mm}$, $L_S=5.9\text{mm}$, $L_V=12\text{mm}$, $W_V=8.7\text{mm}$, $W_S=2\text{mm}$, $V_g=3\text{mm}$ and $\alpha=55^\circ$)

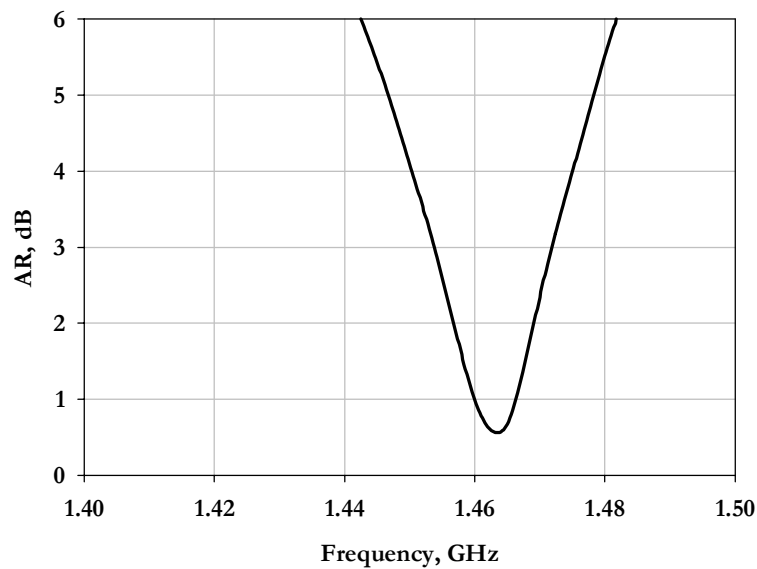


Figure A.26 Axial ratio of dual slot loaded circularly polarized cross patch antenna ($L=35\text{mm}$, $W=49\text{mm}$, $L_S=5.9\text{mm}$, $L_V=12\text{mm}$, $W_V=8.7\text{mm}$, $W_S=2\text{mm}$, $V_g=3\text{mm}$ and $\alpha=55^\circ$)

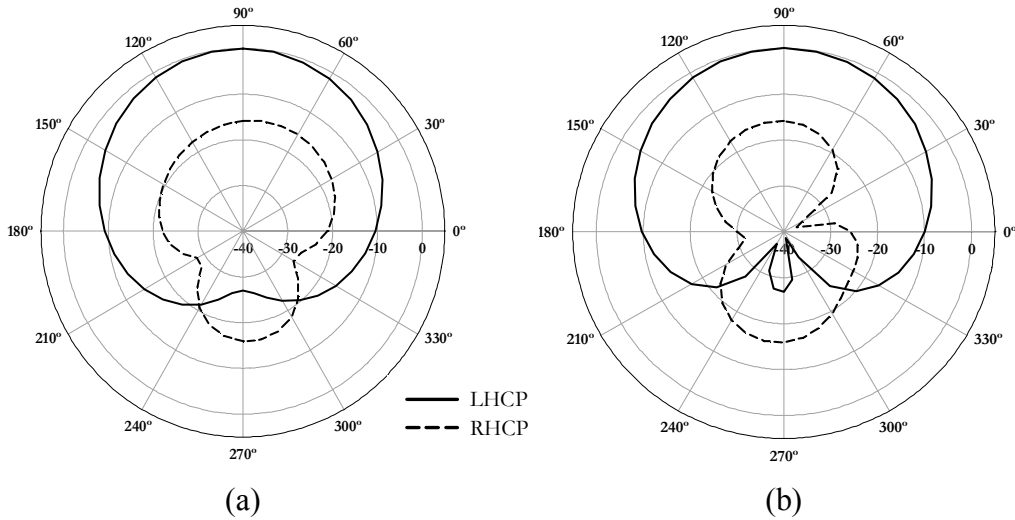


Figure A.27 Radiation patterns of dual slot loaded circularly polarized cross patch antenna at 1.46GHz ($L=35\text{mm}$, $W=49\text{mm}$, $L_S=5.9\text{mm}$, $L_V=12\text{mm}$, $W_V=8.7\text{mm}$, $W_S=2\text{mm}$, $V_g=3\text{mm}$ and $\alpha=55^\circ$)

Table A.5 Comparison of single and dual slot CP antenna

Parameters	Single slot	Dual slot
VSWR bandwidth	80MHz	60MHz
Center frequency	1.57GHz	1.47GHz
Axial ratio bandwidth	80MHz	20MHz
HPBW	75°	65°
Average Gain	5	4.5dBi
Area reduction	46%	53%

A.3.4 Theoretical analysis of circularly polarized dual-slot cross patch antenna

The circularly polarized dual-slot cross patch configuration has been analyzed using FDTD technique. MATLAB based in-house codes were

developed for simulation of the antenna. Two dimensional view of the configuration computed theoretically is given in figure A.28. The computational domain is divided in to Yee cells of dimension $\Delta x = \Delta y = 0.5\text{mm}$ and $\Delta z = 0.4\text{mm}$. $200\Delta x * 200\Delta y * 4\Delta z$ cells are used to model the microstrip line which is used to excite the antenna. 10 cells on each of the 6 sides are used to model air cells. Thus the total computation domain is discretized in to $220\Delta x * 220\Delta y * 28\Delta z$ cells. Luebber's feed model is employed to excite the microstrip line feed of the antenna and a Gaussian pulse is used as the source of excitation. The measured, simulated and theoretically computed resonances of circularly polarized cross patch antenna plotted in figure A.29 show good agreement. FDTD computed electric field distribution is given in figure A. 30.

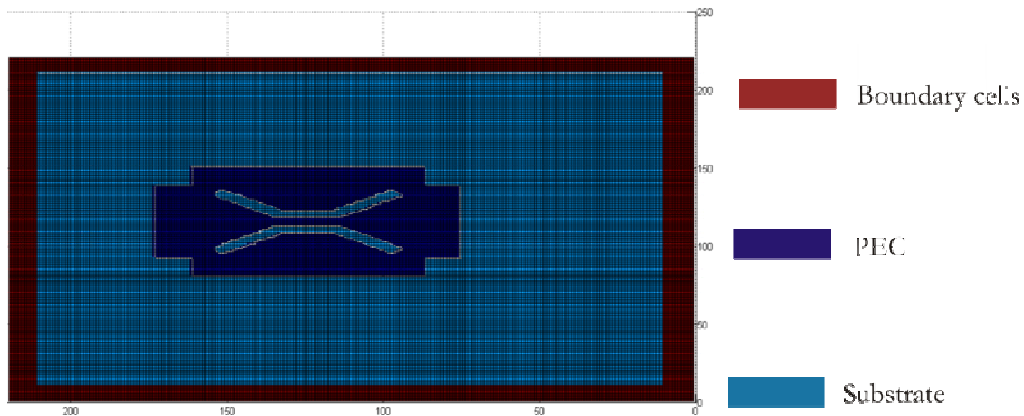


Figure A. 28 2D view of the FDTD computation domain of circularly polarized dual-slot cross patch antenna ($L=35\text{mm}$, $W=49\text{mm}$, $L_s=5.9\text{mm}$, $L_v= 12\text{mm}$, $W_v=8.7\text{mm}$, $V_g=3\text{mm}$, $W_g=2\text{mm}$ and $\alpha=55^\circ$)

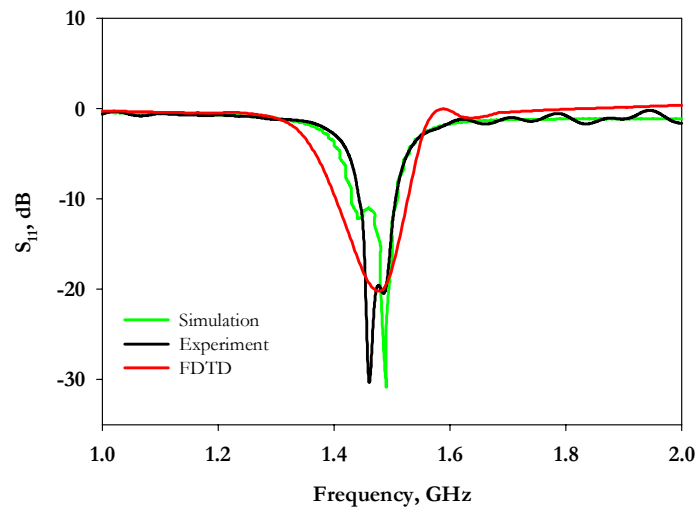


Figure A. 29 Reflection characteristics of circularly polarized dual-slot cross patch antenna ($L=35\text{mm}$, $W=49\text{mm}$, $L_S=5.9\text{mm}$, $L_V=12\text{mm}$, $W_V=8.7\text{mm}$, $V_g=3\text{mm}$, $W_S=2\text{mm}$ and $\alpha=55^\circ$)

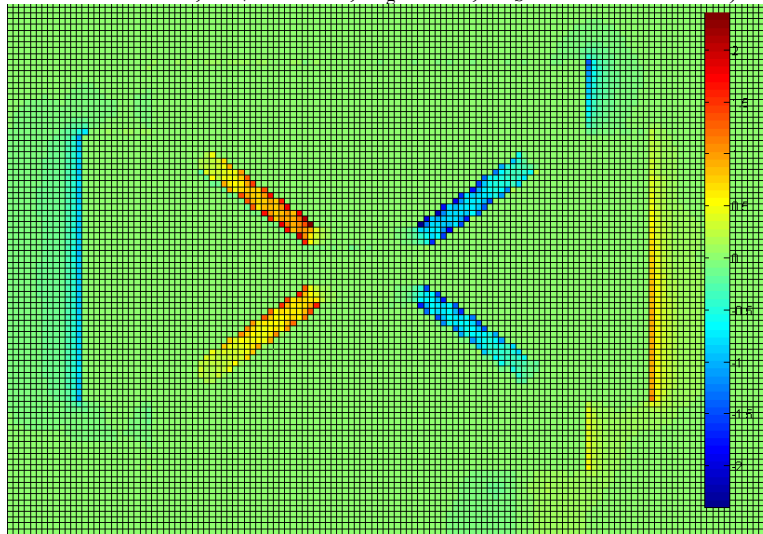


Figure A. 30 FDTD computed Electric field distribution of circularly polarized dual-slot cross patch antenna ($L=35\text{mm}$, $W=49\text{mm}$, $L_S=5.9\text{mm}$, $L_V=12\text{mm}$, $W_V=8.7\text{mm}$, $V_g=3\text{mm}$, $W_S=2\text{mm}$ and $\alpha=55^\circ$)

A cross patch antenna loaded with slots for circular polarization is proposed. The parameters affecting the antenna reflection and resonance performance are experimentally investigated and verified by simulation. The antenna design parameters are extracted from extensive simulation studies are validated on different substrates.

References

1. C. A. Balanis, *Antenna theory analysis and design*, John wiley and sons, Newyork, 1997.
2. W. L. Stutzman and G. A. Thiele, *Antenna theory and design*, John wiley and sons, Newyork, 1981.
3. K. K. Tsang and R. L. Langley, *Design of circular patch antennas on Ferrite substrate*, IEE pro. Microwave antennas propagation, vol.145, no.1, 1998, pp.49-55.
4. L. C. Shen, *The elliptical microstrip antenna with circular polarization*, IEEE Transactions on antennas and propagation, vol.AP-29, 1981, pp.90-94.
5. S. A. Long, L. C. Shen, D. H. Schaubert and F. G. Farrar, *An experimental study of the circular-polarized elliptical printed circuit antenna*, IEEE transactions on Antennas and propagation, Vol. AP-29, 1981, pp.95-99.
6. P. C. Sharma and K. C. Gupta, *Analysis and Optimized Design of Single Feed Circularly Polarized Microstrip Antennas*, IEEE Trans. Antennas Propagation, Vol. AP-31, No. 6, 1983, pp. 949–955.
7. M. D. Deshpande and N. K. Das, *Rectangular Microstrip Antenna for Circular Polarization*, IEEE Trans. Antennas Propagation, Vol. AP-34, No. 6, 1986, pp. 744–746.
8. Haneishi, M., et al., *A Design of Back Feed Type Circularly Polarized Microstrip Disk Antennas Having Symmetrical Perturbation Element by One Point Feed*, Electron. Commu. Japan, Vol. 64B, No. 7, 1981, pp. 52–60.

9. J. H. Lu *Single Feed Circularly Polarized Triangular Microstrip Antennas*, IEEE AP-S Int. Symp. Digest, 1999, pp. 264–267.
10. Y. Suzuki, N. Miyano, and T. Chiba, *Circularly Polarized Radiation from Single Fed Equilateral Microstrip Antenna*, IEE Proc. Microwaves, Antennas Propagation, Pt. H, Vol. 134, 1987, pp. 194–198.
11. K. L. Wong and J. Y. Wu, *Single Feed Small Circular Polarized Square Microstrip Antenna*, Electronics Letters, Vol. 33, No. 22, 1997, pp. 1833–1834.
12. K. L. Wong and Y. F. Lin, *Small Broadband Rectangular Microstrip Antenna with Chip Resistor Loading*, Electronics Letters, Vol. 33, No. 19, 1997, pp. 1593–1594.
13. K. L. Wong and J. Y. Wu, *Bandwidth Enhancement of Circularly Polarized Microstrip Antenna Using Chip Resistor Loading*, Electronics Letters, Vol. 33, No. 21, 1997, pp. 1749–1751.
14. C. Y. Huang, J. Y. Wu, and K. L. Wong, *Broadband Circularly Polarized Square Microstrip Antenna Using Chip-Resistor Loading*, IEE Proc. Microwaves, Antennas Propagation, Pt. H, Vol. 146, No. 1, 1999, pp. 94–96.
15. K. L. Wong and Y. F. Lin, *Circularly Polarized Microstrip Antenna with a Tuning Stub*, Electronics Letters, Vol. 34, No. 9, 1998, pp. 831–832.
16. A. K. Bhattacharya and L. Shafai, *Theoretical and Experimental Investigation of the Elliptical Annular Ring Antenna*, IEEE Trans. Antennas Propagation, Vol. AP-36, No. 11, 1988, pp. 1526–1530.
17. H. M. Chen and K. L. Wong, *On the Circular Polarization of Angular-Ring Microstrip Antennas*, IEEE Trans. Antennas Propagation, Vol. AP-47, No. 8, 1999, pp. 1289–1292.

18. W. S. Chen, C. K. Wu, and K. L. Wong, *Compact Circularly Polarized Microstrip Antenna with Cross-Slot and Peripheral Cuts*, Electronics Letters, Vol. 34, No. 11, 1998, pp. 1040–1041.
19. K. P. Yang and K. L. Wong, *Inclined Slot Coupled Compact Dual Frequency Microstrip Antenna with Cross Slot*, Electronics Letters, Vol. 34, February 1998, pp. 321–322.
20. W. H. Hsu and K. L. Wong, *Circularly Polarized Disk-Sector Microstrip Antenna*, Electronics Letters, Vol. 34, No. 23, 1998, pp. 2188–2190.
21. V. Palanisamy and R. Garg, *Analysis of Circularly Polarized Square Ring and Crossed Strip Microstrip Antennas*, IEEE Trans. Antennas Propagation, Vol. AP-34, No. 11, 1986, pp. 1340–1345.
22. W. S. Chen, C. K. Wu, and K. L. Wong, *Single Feed Ring Microstrip Antenna with Truncated Corners for Compact Circular Polarization*, Electronic Letters, Vol. 34, No. 11, 1998, pp. 1045–1047.
23. C. Y. Huang, C. Y. Wu, and K. L. Wong, *High-Gain Compact Circularly Polarized Microstrip Antenna*, Electronic Letters, Vol. 34, No. 8, 1998, pp. 712–713.
24. K. T. V. Reddy and G. Kumar, *Dual Feed Gap Coupled Square Microstrip Antennas for Broadband Circularly Polarization*, Microwave Optical Tech. Letters, Vol. 26, No. 6, 2000, pp. 399–402.
25. K. T. V. Reddy and G. Kumar, *Gap Coupled Broadband Circularly Polarized Square Microstrip Antennas*, Proc. Int. Conf. on Computers, Communication and Devices, ICCCD-2000, December 2000, pp. 365–368.
26. H. Legay and L. Shafai, *Analysis and Design of Circularly Polarized Series Fed Planar Subarray*, IEE Proc. Microwaves, Antennas Propagation, Pt. H, Vol. 142, No. 2, 1995, pp. 173–177.

27. K. T. V. Reddy and G. Kumar, *Stacked Square Microstrip Antennas for Wideband Circular Polarization*, Proc. National Conf. on Communications, NCC—2001, Indian Institute of Technology, Kanpur, January 2001, pp. 125–128.
28. K. T. V. Reddy and G. Kumar, *Stacked Microstrip Antennas for Broadband Circular Polarization*, IEEE AP-S Int. Symp. Digest, Boston, MA, July 2001, pp. 420–423.
29. K. T. V. Reddy and G. Kumar, *Stacked Circular Microstrip Antennas for Wideband Circular Polarization*, Proc. Symp. Antenna Propagation, Kochi, Japan, December 2000, pp. 47–50.
30. C. Y. Huang, J. Y. Wu, and K. L. Wong, *Cross-Slot-Coupled Microstrip Antenna and Dielectric Resonator Antenna for Circular Polarization*, IEEE Trans. Antennas Propagation, Vol. AP-47, No. 4, 1999, pp. 605–609.
31. T. Vlasits et al., *Performance of a Cross Aperture Coupled Single Feed Circularly Polarized Patch Antenna*, Electronic Letters, Vol. 32, No. 7, 1996, pp. 612–613.
32. S. D. Targonski and D. M. Pozar, *Design of Wideband Circularly Polarized Aperture Coupled Microstrip Antennas*, IEEE Trans. Antennas Propagation, Vol. 41, No. 2, 1993, pp. 214–220.
33. D. M. Pozar and S. M. Duffy, *A Dual-Band Circularly Polarized Aperture-Coupled Stacked Microstrip Antenna for Global Positioning Satellite*, IEEE Trans. Antennas Propagation, Vol. 45, No. 11, 1997, pp. 1618–1625.
34. M. I. Aksun, S. L. Chuang, and Y. T. Lo, *On Slot-Coupled Microstrip Antennas and Their Applications for Circular Polarization Operation*, IEEE Trans. Antennas Propagation, Vol. AP-38, 1990, pp. 1224–1230.

35. C. Y. Huang, C. Y. Wu, and K. L. Wong, *Slot-Coupled Microstrip Antenna for Broadband Circular Polarization*, *Electronic Letters*, Vol. 34, No. 9, 1998, pp. 835–836.
36. D. M. Pozar and D. H. Schaubert, *Microstrip Antennas: The Analysis and Design of Microstrip Antennas and Arrays*, New York: IEEE Press, 1995.
37. T. Teshirogi, M. Tanaka, and W. Chujo, *Wideband Circularly Polarized Antenna with Sequential Rotations and Phase Shift of Elements*, *Proc. ISAP*, 1985, pp. 117–120.
38. D. M. Pozar, *Microwave engineering*, John Wiley & Sons, New York, 1998.
39. D. M. Pozar, *Radiation and scattering characteristics of microstrip antennas on normally biased ferrite substrates*, *IEEE Transactions on antennas and propagation*, Vol. Ap-40, 1992, pp.1084-1092.
40. J. R. James, P. S. Hall and C. Wood, *Microstrip antenna: Theory and design*, Peter peregrines, London, UK, 1981.
41. J. Huang, *A technique for an array to generate circular polarization with linearly polarized elements*, *IEEE Transactions on antennas and propagation*, Vol. AP-34, 1986, pp. 1113-1124.



DESIGN AND DEVELOPMENT OF BROADBAND MICROSTRIP ANTENNAS

Experimental investigations on enhancing the bandwidth of a cross patch antenna are highlighted in this section. The slot resonators are engraved on the radiator to disable the antenna from functioning at the selected narrow band frequencies. Two novel designs of compact microstrip antennas are simulated and their resonant modes are identified. The performance of the fabricated antennas are then experimentally verified and are found to conform reasonably well with the simulated responses in all cases.

B.1 Broadband microstrip antennas: Review

The regular microstrip antenna configurations, such as rectangular and circular patches have been modified to rectangular ring [1] and circular ring [2], respectively, to enhance the bandwidth. The larger bandwidth is because of a reduction in the quality factor Q of the patch resonator, which is due to less energy stored beneath the patch and higher radiation. When a U-shaped slot is cut inside the rectangular patch, it gives a bandwidth of approximately 40% for $VSWR \leq 2$ [3]. Similar results are obtained when a U-slot is cut inside a circular or a triangular microstrip antenna [4-5]. The planar stagger-tuned coupled multiple resonators yield wide bandwidth in the same way as in the case of multistage tuned circuits. Several configurations are available yielding bandwidth of 5–25% [6-12].

In the multilayer configuration, two or more patches on different layers of the dielectric substrate are stacked on each other. Based on the coupling mechanism, these configurations are categorized as electromagnetically coupled or aperture-coupled microstrip antennas. In the electromagnetically coupled microstrip antenna, one or more patches at the different dielectric layers are electromagnetically coupled to the feed line located at the bottom dielectric layer [13-19]. In the aperture-coupled MSA, the field is coupled from the microstrip feed line placed on the other side of the ground plane to the radiating patch through an electrically small aperture/slot in the ground plane. Two patches of rectangular or circular shapes, which are stacked on each other in different dielectric layers, yield around 30% bandwidth [20-23]. A bandwidth of nearly 70% has been obtained by stacking patches with resonant apertures

[24]. The impedance-matching networks are used to increase the bandwidth of the microstrip antenna. Some examples that provide about 10% bandwidth are the rectangular microstrip antenna with a coplanar microstrip impedance-matching network and an electromagnetically coupled microstrip antenna with single-stub matching [25-27]. The concept of log-periodic antenna has been applied to obtain a multi-octave bandwidth. In this configuration, the patch dimensions are increased logarithmically and the subsequent patches are fed at 180° out of phase with respect to the previous patch [28-31].

A shorted $\lambda/4$ rectangular microstrip antenna has the same resonance frequency as that of a $\lambda/2$ rectangular microstrip antenna, with half the area. The resonance frequency reduces further as the width of the shorting plate decreases [32-33]. Similarly, compact microstrip antenna in circular and triangular configurations is realized by placing shorting posts at the zero potential lines [34-35]. A single shorting post yields a maximum reduction in the resonance frequency of the rectangular, circular, and triangular microstrip antennas [36-37]. The compact antennas have also been realized by cutting slots in regularly shaped antennas. The requirements of these compact broadband microstrip antennas will increase in the future due to the ever-growing miniaturization of communication systems. The bandwidth of the compact microstrip antenna has been increased in both planar as well as multilayer configurations [38-41].

Tunable microstrip antennas are of interest in many systems as they can be tuned over a large frequency range. These tunable antennas provide an alternative to large bandwidth antennas, especially when a large bandwidth is

required for encompassing several narrowband channels. The tunable microstrip antenna is realized by changing the length of the small stub attached to the regularly shaped microstrip antenna [42-43], or by changing the number of shorting posts used to make a compact configuration [32, 34-35]. Tunability is also achieved by integrating active devices such as varactor or PIN diodes along with the microstrip antenna [44].

B.2 Broadband Octagonal Ring Slot antenna

A simple electromagnetically coupled broadband printed microstrip antenna suitable for multi-functional wireless communication bands is presented. The geometry of the antenna fabricated on a substrate of height $h=1.6\text{mm}$ and dielectric constant $\epsilon_r=4.4$ is shown in figure B.1. The dual slot loaded circularly polarized microstrip antenna presented in section A.3, in which, the alignment of the slots are rearranged in face-to-face and combined together to form a octagonal ring slot of dimension $L_v \times W_v \times W_s \text{ mm}^3$. The antenna is electromagnetically coupled using a 50Ω transmission line fabricated on another FR-4 substrate. All the parameters have been optimized for best bandwidth performance. The overall dimension of the antenna is $L_g \times W_g \times 2h \text{ mm}^3$.

B.2.1 Simulations

A parametric study is investigated and it demonstrates that the following parameters influence the performance of the designed wide-slot antenna most effectively.

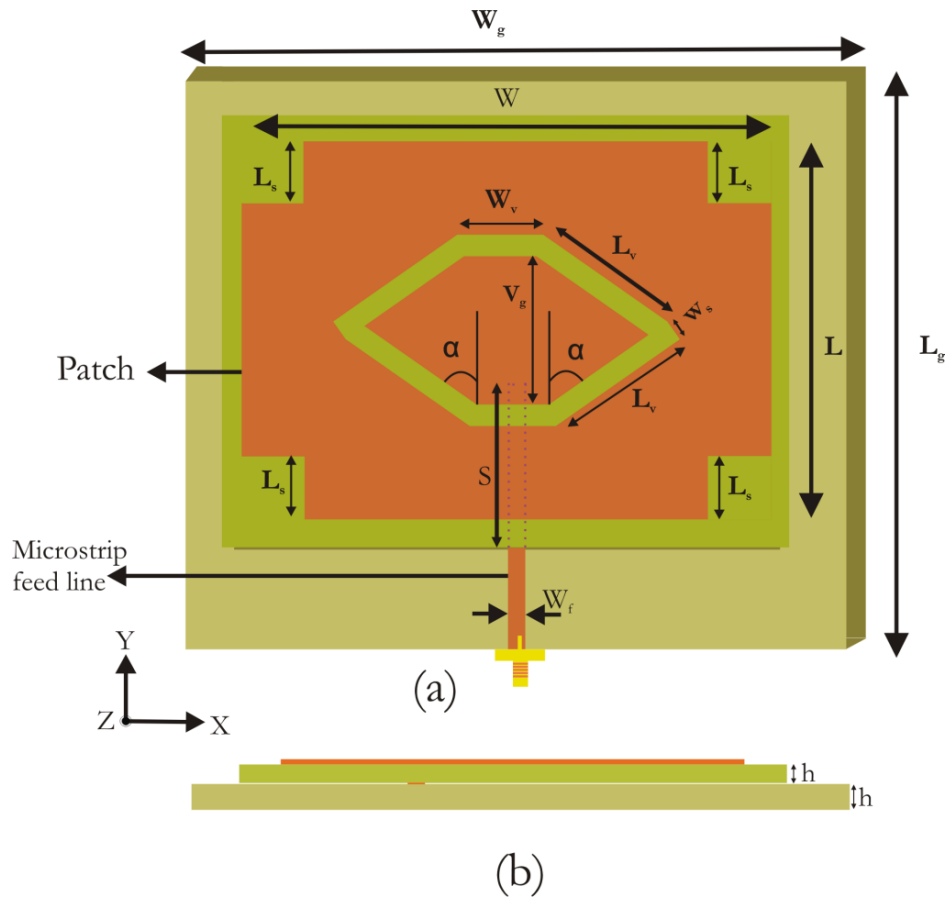


Figure B.1 Geometry of the broadband octagonal ring slot antenna (a) Front view (b) side view ($L=35\text{mm}$, $W=49\text{mm}$, $L_s=5.9\text{mm}$, $L_v=12\text{mm}$, $W_v=10\text{mm}$, $V_g=11.4\text{mm}$, $W_s=2\text{mm}$, $S=22\text{mm}$, $W_f=3\text{mm}$, $h=1.6\text{mm}$, $\alpha=55^\circ$ and $\epsilon_r=4.4$)

B.2.1 a Effect of slot size

To attain an insight on the effect of slot size on the antenna performance, the proposed antenna is designed with five different slot dimensions as tabulated in Table B.1. The lower edge of the operating frequency band is observed to be dependant on the slot and more specifically its perimeter. It is found that good impedance matching can be obtained for $L_v \times W_v \times W_s$ is $12 \times 10 \times 2\text{mm}^3$. Figure B.2 shows the simulated return losses of the antenna for various L_v and W_v keeping $W_s=2\text{mm}$.

B.2.1.b Effect of slot width (W_s)

The slot width also affects the performance of the proposed antenna most effectively. Figure B.3 shows the effect of W_s on the return loss characteristics of the antenna. As shown in the figure, the return loss deteriorates within the whole band as W_s changes. The best value for W_s in the designed antenna is 2mm.

Table B.1. Antenna details

Antenna	ϵ_r	h mm	L_v mm	W_v mm	W_s mm	L_s mm	LxW mm ²	Frequency band, GHz
1	4.4	1.6	10	8	2	5.885	35x49	6.15-11.2
2	4.4	1.6	12	10	2	5.885	35x49	5-6.95
3	4.4	1.6	14	12	2	5.885	35x49	4.5-6.1
4	4.4	1.6	16	14	2	5.885	35x49	3.68-4.84
5	4.4	1.6	18	16	2	5.885	35x49	3.53-4.23

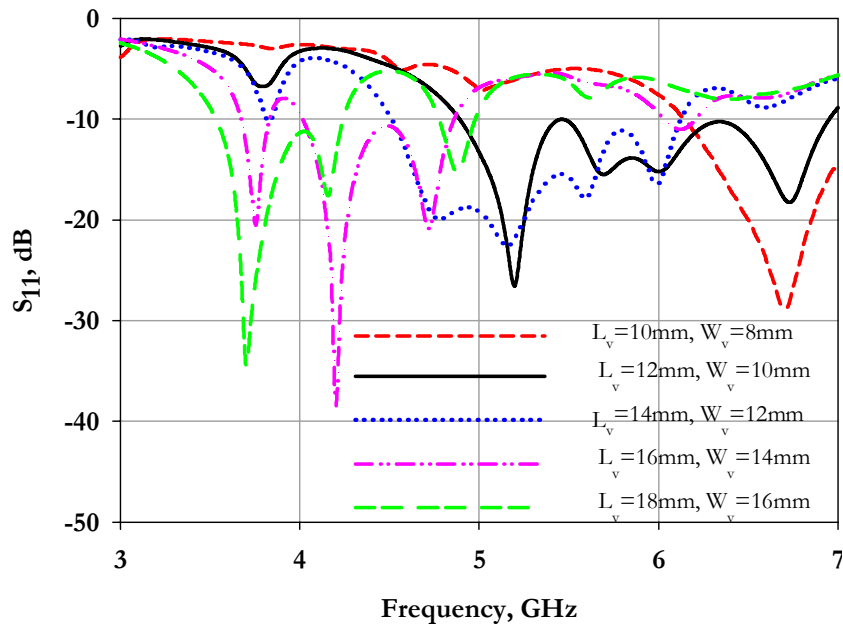


Figure B.2. Simulated return losses of the antenna for various L_v and W_v keeping $W_s=2$ mm. ($L=35$ mm, $W=49$ mm, $L_s=5.9$ mm, $L_v=12$ mm, $W_v=10$ mm, $V_g=11.4$ mm, $W_s=2$ mm and $\alpha=55^\circ$)

B.2.1.c Effect of corner slit length (L_s)

Figure B.4 shows the variation in reflection characteristics, centre frequency and percentage bandwidth with the corner slit length, L_s . It is observed from the plot that the center frequency and corresponding bandwidth remains almost stable with the slit length variation. Also, the resonances are shifted to lower frequency with the increase in slit length.

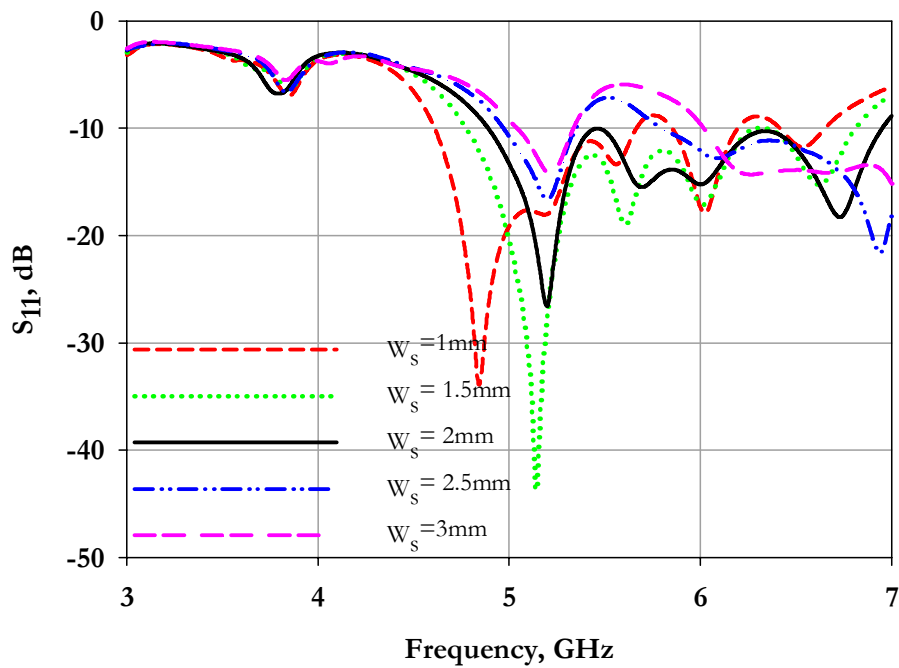


Figure B.3 Simulated return losses of the antenna for various w_s ($L=35\text{mm}$, $W=49\text{mm}$, $L_s=5.9\text{mm}$, $L_v=12\text{mm}$, $W_v=10\text{mm}$, $V_g=11.4\text{mm}$, $W_s=2\text{mm}$ and $\alpha=55^\circ$)

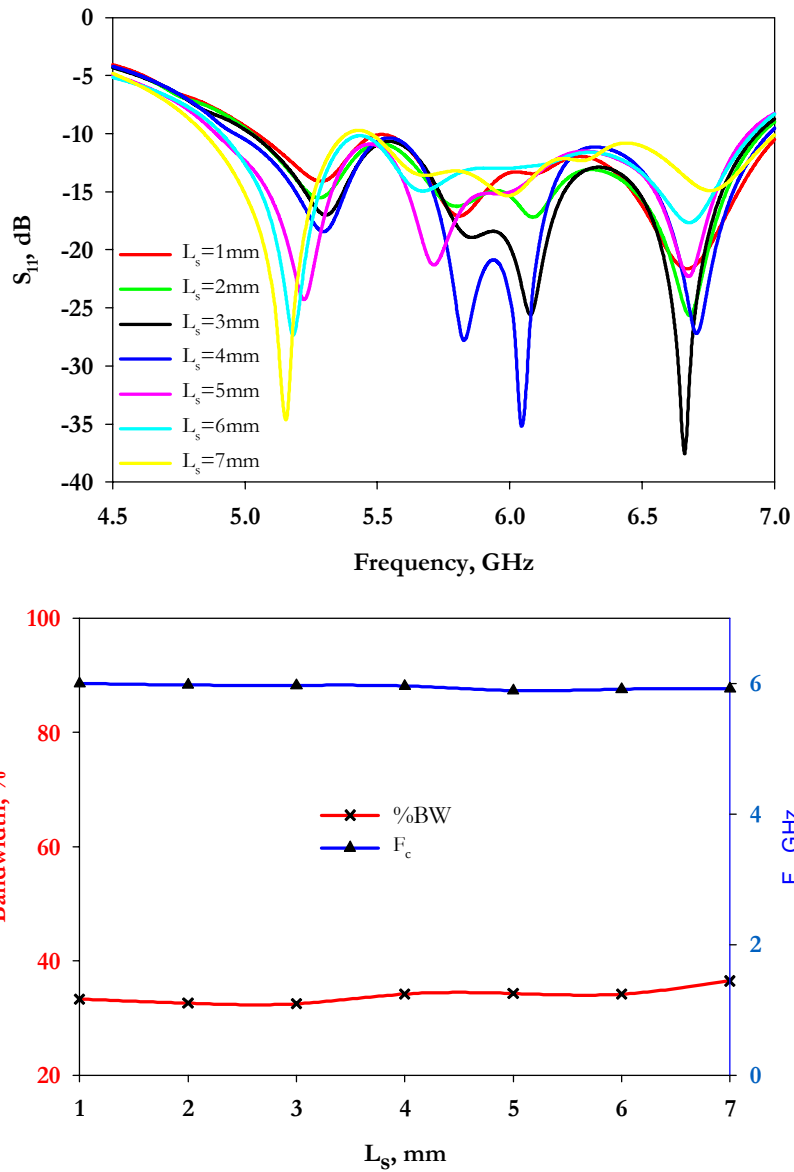


Figure B.4 Effect of corner slit length over the reflection characteristics, center frequency and bandwidth of broadband ring slot antenna ($L=35$ mm, $W=49$ mm, $L_s=5.9$ mm, $L_v=12$ mm, $W_v=10$ mm, $V_g=11.4$ mm, $W_s=2$ mm and $\alpha=55^\circ$)

Simulated 3D radiation patterns of the antenna plotted at 5.2GHz, 5.78GHz and 6.78GHz are shown in figure B.5 (a), (b) and (c) respectively.

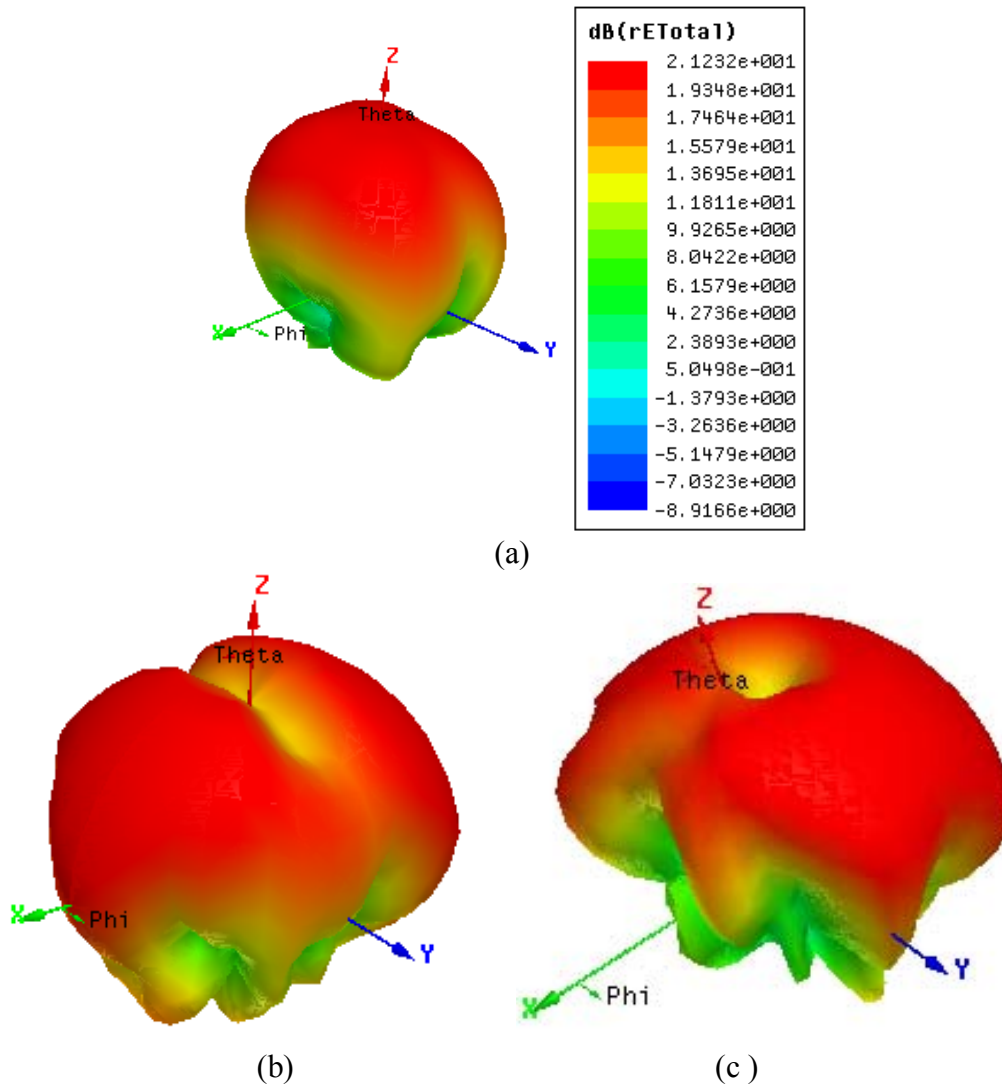


Figure B.5 Simulated 3D radiation pattern of broadband ring slot antenna at (a)5.2GHz (b)5.78GHz and (c) 6.78GHz ($L=35\text{mm}$, $W=49\text{mm}$, $L_S=5.9\text{mm}$, $L_V=12\text{mm}$, $W_V=10\text{mm}$, $V_g=11.4\text{mm}$, $W_S=2\text{mm}$ and $\alpha=55^\circ$)

B.2.2 Measurements

The photograph of the proposed antenna is given in figure B.6. The characteristics of the fabricated antenna have been measured using HP8510C vector network analyzer and a far field measurement system. The return loss

characteristics of the antenna are given in figure B.7. The proposed antenna offers a 2:1 VSWR bandwidth of 33% from 5GHz to 6.95GHz.

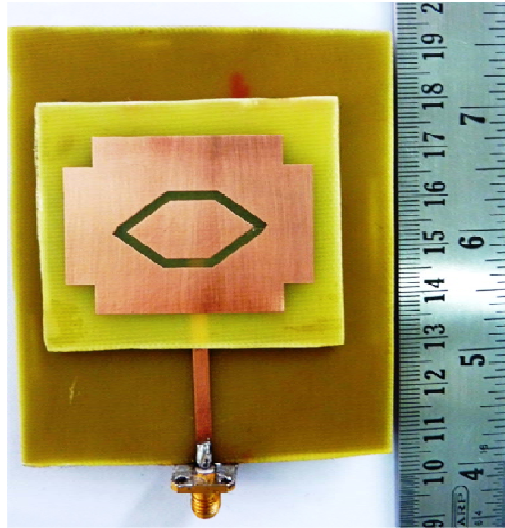


Figure B.6 Photograph of the ring slot loaded broadband cross patch antenna

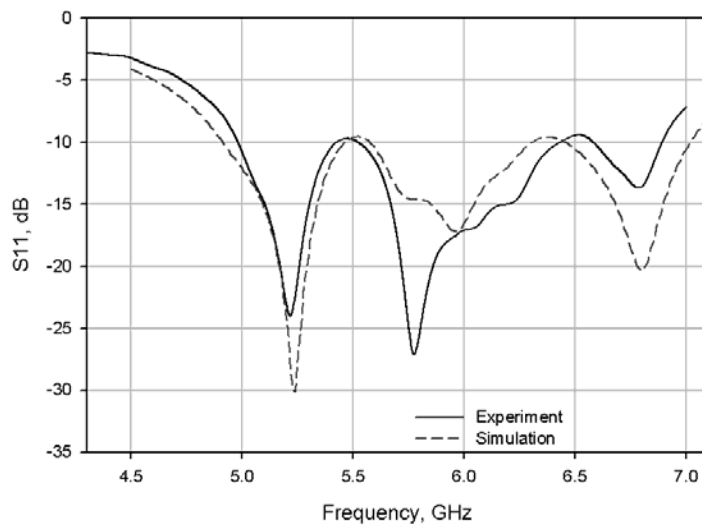


Figure B.7 Simulated and measured reflection characteristics of ring slot loaded broadband cross patch antenna ($L=35\text{mm}$, $W=49\text{mm}$, $L_S=5.9\text{mm}$, $L_V=12\text{mm}$, $W_V=10\text{mm}$, $V_g=11.4\text{mm}$, $W_S=2\text{mm}$ and $\alpha=55^\circ$)

Figure B.8 shows the measured YZ- and XZ- plane radiation patterns at 5.2GHz, 5.78GHz and 6.78 GHz respectively. Good cross polar isolation

greater than -10dB is observed for all the resonant frequencies. Although, a wide slot antenna provides wide operating bandwidth, generally its operating bandwidth is limited due to the degradation of radiation patterns at the upper edge of the impedance bandwidth. It is found that currents flowing on the edge of the slot will increase the cross polarization component in the YZ-plane and cause the main beam to tilt away from the broadside direction in the XZ-plane.

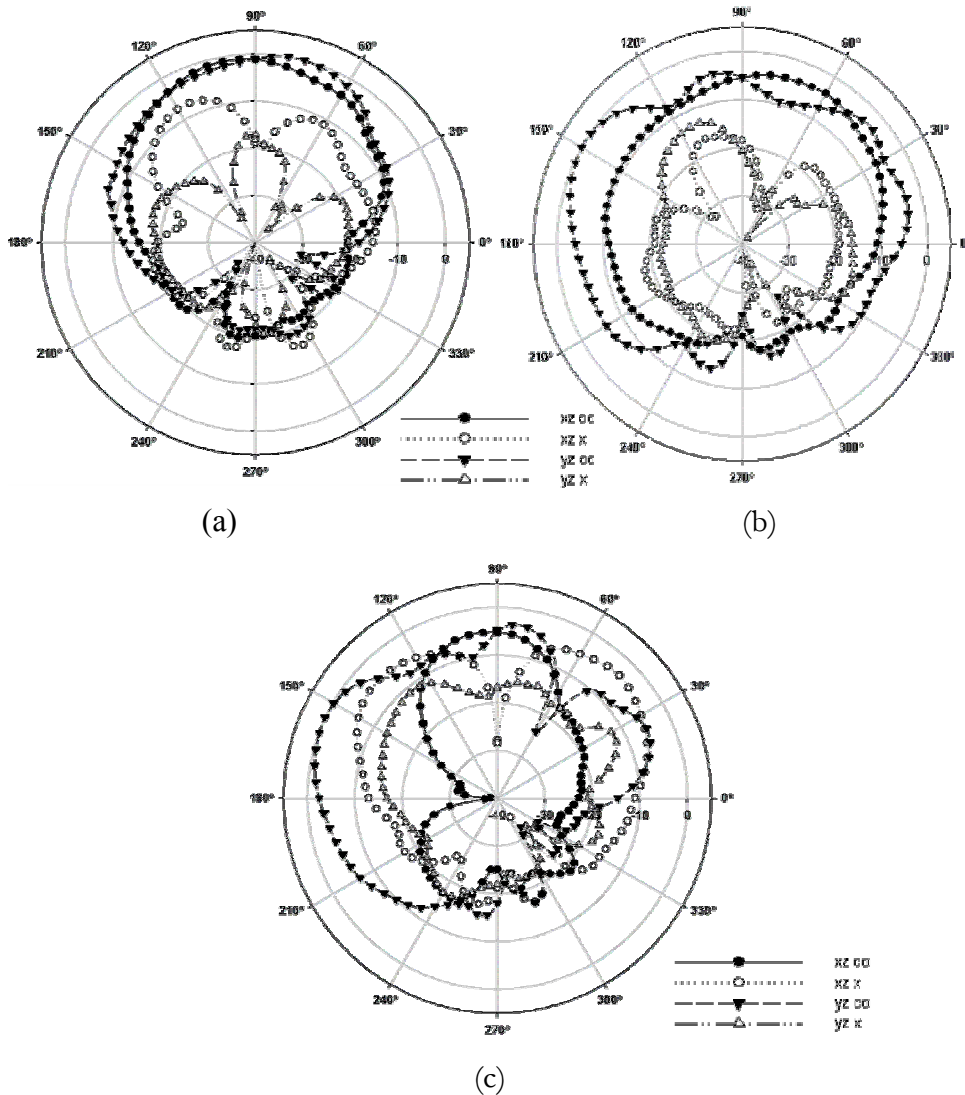


Figure B.8 Measured radiation patterns (a) at 5.2GHz (b) at 5.78GHz and (c) at 6.78GHz ($L=35\text{mm}$, $W=49\text{mm}$, $L_S=5.9\text{mm}$, $L_V=12\text{mm}$, $W_V=10\text{mm}$, $V_g=11.4\text{mm}$, $W_S=2\text{mm}$ and $\alpha=55^\circ$)

The measured gain of the antenna is given in figure B.9. Due to the excitation of higher order modes, the gain drops at higher frequency. At the centre frequency, the designed antenna has a maximum gain of 5.5dBi and has an average gain of 3.5dBi within the operating band.

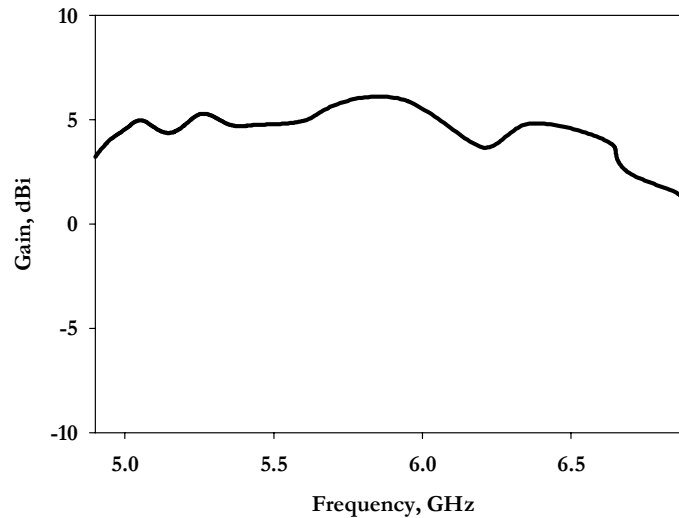


Figure B.9 Measured gain of the proposed antenna ($L=35\text{mm}$, $W=49\text{mm}$, $L_S=5.9\text{mm}$, $L_V=12\text{mm}$, $W_V=10\text{mm}$, $V_g=11.4\text{mm}$, $W_S=2\text{mm}$ and $\alpha=55^\circ$)

B.2.3 Theoretical analysis of broadband octagonal ring slot antenna

Two dimensional view of the FDTD computation domain of broadband octagonal ring slot antenna is given in figure B.10. The computational domain is divided into Yee cells of dimension $\Delta x=\Delta y=0.5\text{mm}$ and $\Delta z=0.4\text{mm}$. 10 cells are used to model air cells on each of the six sides. Microstrip feed line substrate is modeled by a computational volume of $200\Delta x * 200\Delta y * 4\Delta z$. The patch substrate is modeled by a computational volume of $120\Delta x * 100\Delta y * 4\Delta z$. Thus the total computation domain is discretized into $220\Delta x * 220\Delta y * 28\Delta z$ cells. Luebber's feed model is employed to excite the microstrip line feed of the antenna and a Gaussian pulse is used as the source of excitation. Mur's first order ABC is used as the boundary condition. Time step used for the computation is 0.95ps. The Gaussian half-width is $T = 20$ ps, and the time delay

t_0 is set to be $3T$. The theoretical, simulated and experimental reflection coefficient of the cross patch antenna by the inclusion of the octagonal ring slot is plotted in figure B.11. Also, FDTD computed electric field distribution of the broadband ring slot loaded cross patch antenna is given in figure B.12.

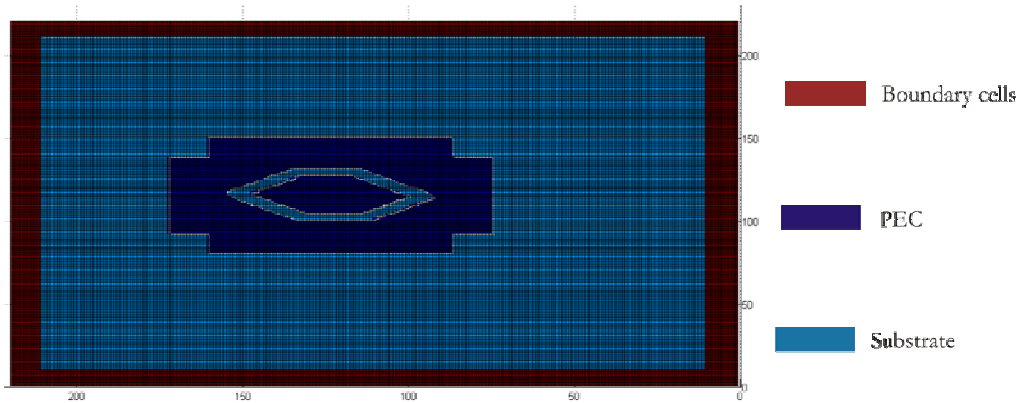


Figure B.10 2D view of the FDTD computation domain of broadband octagonal ring slot antenna ($L=35\text{mm}$, $W=49\text{mm}$, $L_S=5.9\text{mm}$, $L_V=12\text{mm}$, $W_V=10\text{mm}$, $V_g=11.4\text{mm}$, $W_S=2\text{mm}$ and $\alpha=55^\circ$)

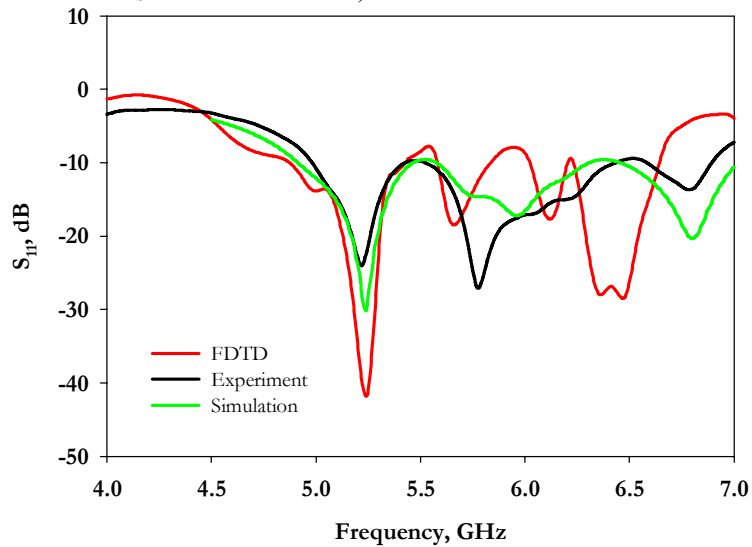


Figure B.11 Theoretical, simulated and experimental reflection coefficient of the broadband octagonal ring slot antenna ($L=35\text{mm}$, $W=49\text{mm}$, $L_S=5.9\text{mm}$, $L_V=12\text{mm}$, $W_V=10\text{mm}$, $V_g=11.4\text{mm}$, $W_S=2\text{mm}$ and $\alpha=55^\circ$)

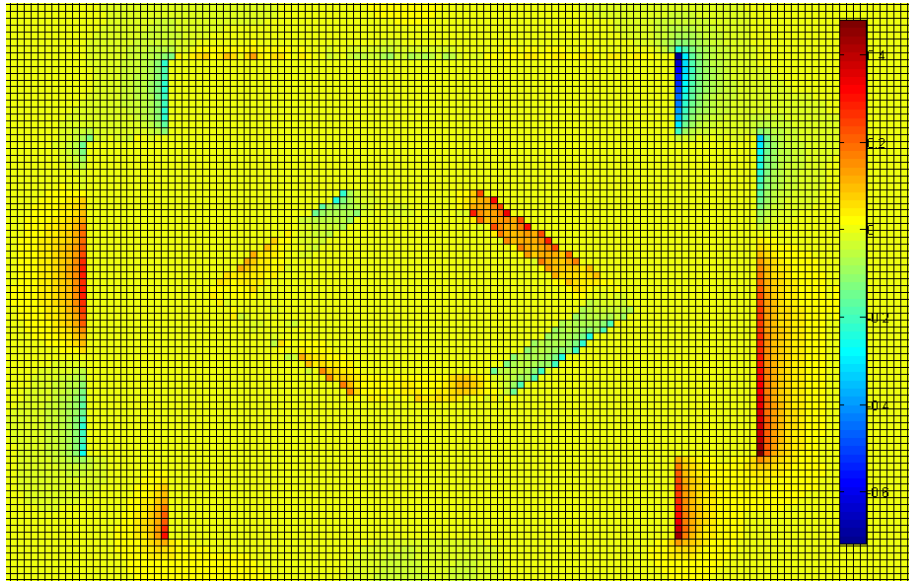


Figure B.12 FDTD computed electric field distribution of the broadband octagonal ring slot antenna ($L=35\text{mm}$, $W=49\text{mm}$, $L_S=5.9\text{mm}$, $L_V=12\text{mm}$, $W_V=10\text{mm}$, $V_g=11.4\text{mm}$, $W_S=2\text{mm}$ and $\alpha=55^\circ$)

B.3 A Broadband Microstrip Antenna for IEEE802.11.a/WiMAX/HiperLAN2 Applications

In recent years, the demand for broad-band antennas has increased for use in high-frequency and high speed data communication. In this section, a broadband proximity coupled microstrip patch antenna, loaded with two slots in which one slot is stacked over the other features an impedance bandwidth of 51% from 3.75GHz to 6.33GHz is presented. The proposed antenna is suitable for IEEE 802.11.a (5.15-5.35GHz, 5.725-5.825GHz), WiMAX (5.25-5.85GHz), HiperLAN2 (5.47-5.725 GHz) and HiSWaNa (5.15-5.25GHz) wireless application bands.

B.3.1 Antenna geometry

The geometry of the antenna fabricated on an FR-4 substrate of dielectric constant $\epsilon_r=4.4$ with loss tangent ($\tan \delta$) of 0.02 and height $h=1.6\text{mm}$

is shown in figure B.13. The antenna is electromagnetically coupled with a 50Ω transmission line ($L_f \times W_f \text{ mm}^2$) fabricated using the same substrate. It is observed that, without the slot, there exist three poorly matched resonances around 4GHz, 5.2GHz and 6.15GHz. With a single slot ($L_{v1} \times W_{v1} \times W_s \text{ mm}^3$), the resonance around 5.2GHz achieves impedance matching over the bandwidth of the antenna. When the second slot ($L_{v2} \times W_{v2} \times W_s \text{ mm}^3$) is placed at a distance v_g from the top of the first slot on the patch the resonance around 4GHz is split into two resonances at 3.8GHz and 4.2GHz over the bandwidth of the antenna and our aim is to change the parameters of the second slot in order to bring the resonances near to each other and have a broadband microstrip antenna. The height of the antenna is 2.67% of the free-space wavelength at the central operating frequency. The overall dimension of the antenna is $L_g \times W_g \times 2h \text{ mm}^3$.

B.3.2 Simulations

The proposed antenna is designed and optimized using a frequency domain three-dimensional full wave electromagnetic field solver (Ansoft HFSS). The simulated reflection coefficients of the antenna without slot, with single slot and with double slot are shown in figure B.14. It is observed that, without the slot, there exist two poorly matched resonances over the bandwidth of the antenna. These resonances are lowered by the introduction of the V-slots into the patch as seen in figure B.14 and improve the input impedance by effectively suppressing the excess reactance at these resonances as shown in figure B.15. The simulated 3D radiation pattern of the antenna at 3.75GHz, 5GHz and 6.33GHz are given in figure B.16 (a), (b) and (c) respectively. Further insight on the antenna performance is obtained from the detailed parametric analysis results discussed in the following section.

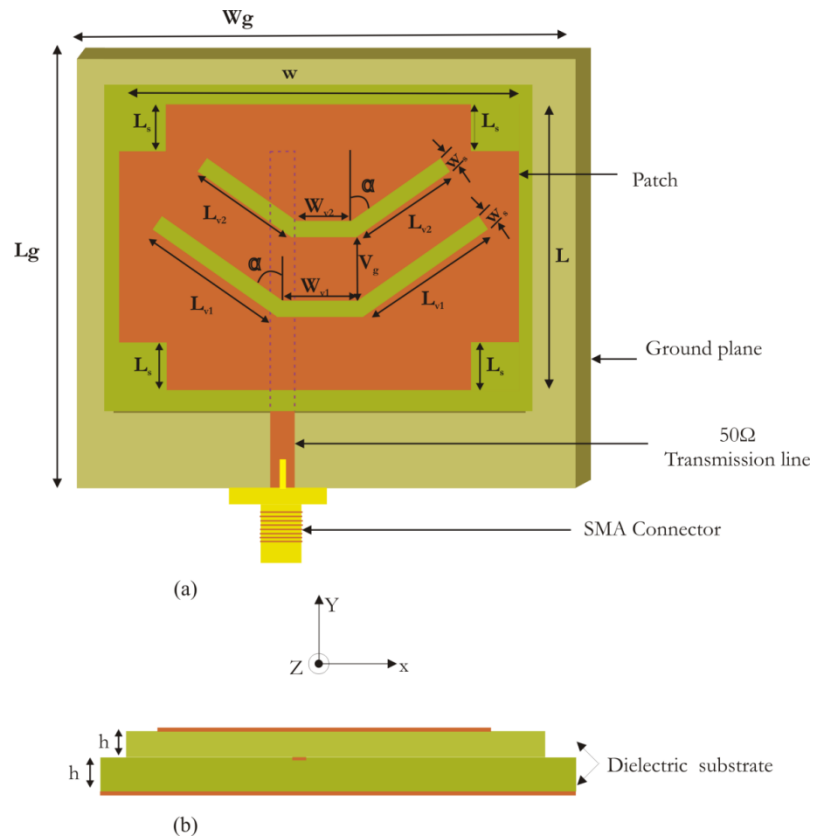


Figure B .13 Geometry of the broadband cross patch antenna ($L=35\text{mm}$, $W=49\text{mm}$, $L_s=5.9\text{mm}$, $L_{s1}=15\text{mm}$, $L_{s2}=12\text{mm}$, $W_{s1}=10.7\text{mm}$, $W_{s2}=8.7\text{mm}$, $V_g=7\text{mm}$, $W_s=2\text{mm}$, $S=31\text{mm}$, $W_f=3\text{mm}$, $h=1.6\text{mm}$, $\alpha=55^\circ$ and $\epsilon_r=4.4$)

B.3.2.a Effect of V_g

Figure B.17 shows the effect of V-slot gap on return loss characteristics of the antenna. There is only a slight variation in the bandwidth with V_g while the reflection coefficient in the mid- band region is more dependent on V_g . However, it is clear from the analysis that the antenna offers maximum bandwidth when $V_g=7\text{mm}$. It is also worth noting that the last resonant frequency is more affected by the V-slot gap than other resonances.

B.3.2.b Effect of L_s

The influence of the corner notches on the reflection characteristics of the optimized prototype is illustrated in figure B.18. It is observed that all the

resonances are shifted towards the higher frequency region with the increase in L_s . Also impedance matching becomes poor in low frequency region when L_s is lowered. Similarly increase in L_s degrades the impedance matching in the high frequency region. Therefore, $L_s=5.9\text{mm}$ is a compromise between impedance matching and bandwidth.

B.3.2.c Effect of tilt angle (α)

The tilt angle (α) has a crucial effect in the impedance matching of the antenna in the mid-band region over the bandwidth of the antenna. From figure B.19, it can be seen that the antenna offers maximum bandwidth when $\alpha=55^\circ$. It is also noted that the last two resonances are more affected to the change in tilt angle than other resonances.

B.3.2.d Influence of substrate parameters

It is observed from the analysis that as ϵ_r varies from 2.2 to 4.4 the bandwidth of the antenna is found to be reduced to a lower value due to the high Q of the substrate. The substrate height variation shown in figure B.20 indicate that the for higher substrate height the resonant band found to be broadened.

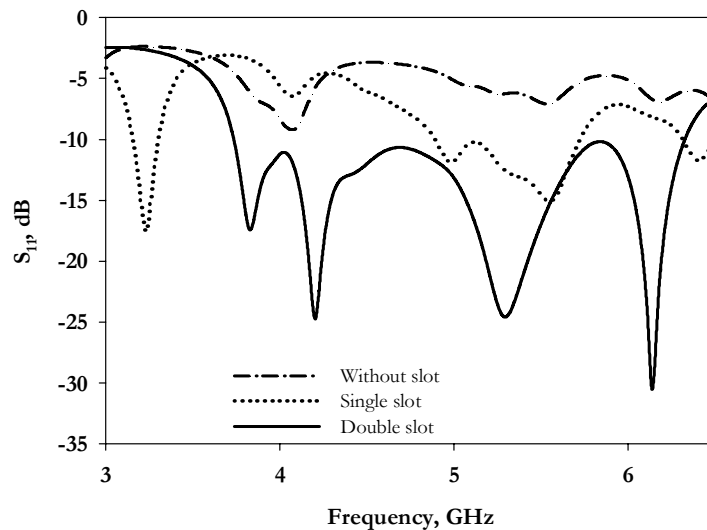


Figure B.14 Simulated reflection coefficient of cross patch antenna with and without slot ($L=35\text{mm}$, $W=49\text{mm}$, $L_s=5.9\text{mm}$, $L_{V1}=15\text{mm}$, $L_{V2}=12\text{mm}$, $W_{V1}=10.7\text{mm}$, $W_{V2}=8.7\text{mm}$, $V_g=7\text{mm}$, $W_s=2\text{mm}$ and $\alpha=55^\circ$)

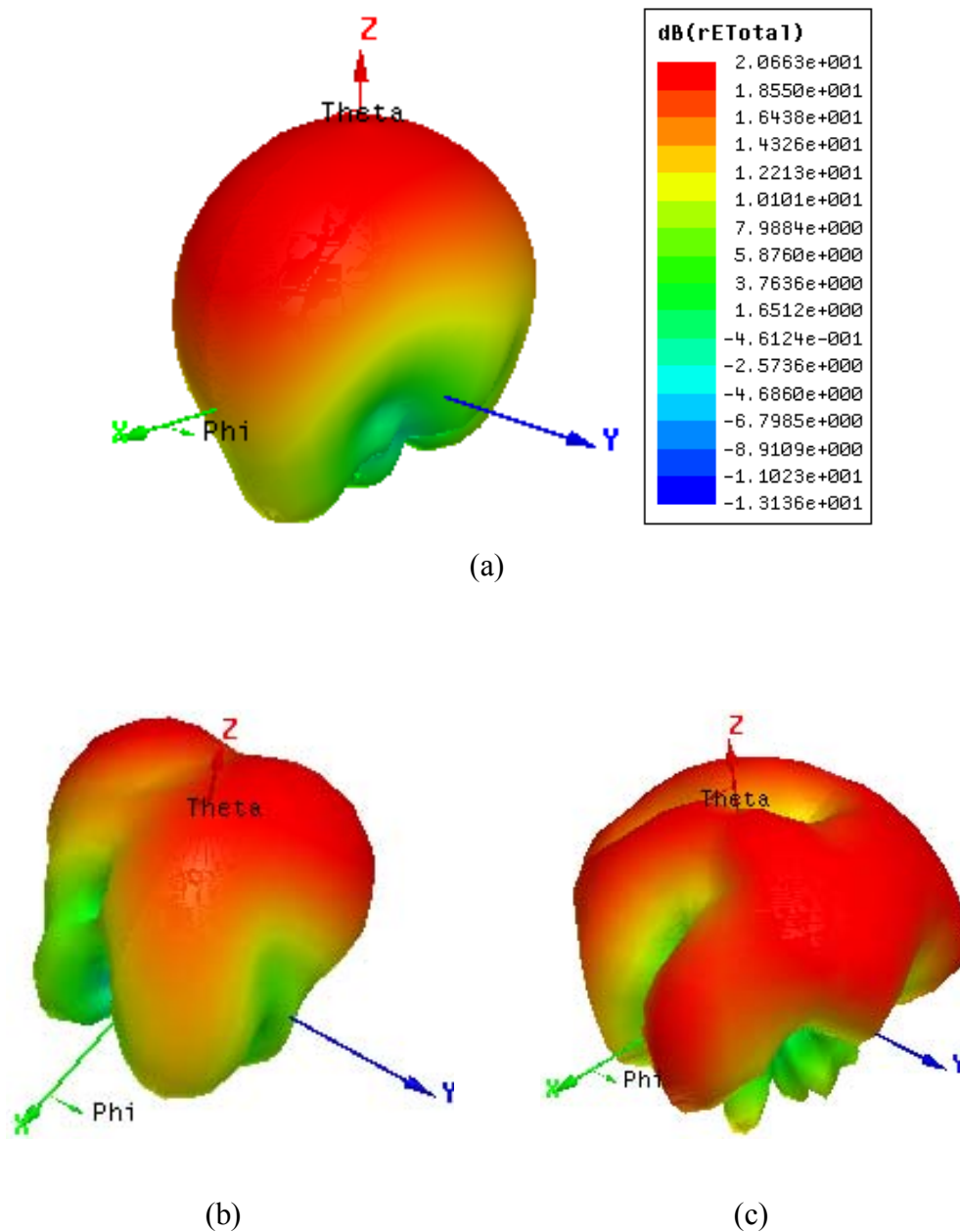


Figure B.15 3D radiation pattern of the antenna simulated at (a) 3.75GHz (b) 5GHz and (c) 6.33GHz ($L=35\text{mm}$, $W=49\text{mm}$, $L_S=5.9\text{mm}$, $L_{V1}=15\text{mm}$, $L_{V2}=12\text{mm}$, $W_{V1}=10.7\text{mm}$, $W_{V2}=8.7\text{mm}$, $V_g=7\text{mm}$, $W_S=2\text{mm}$ and $\alpha=55^\circ$)

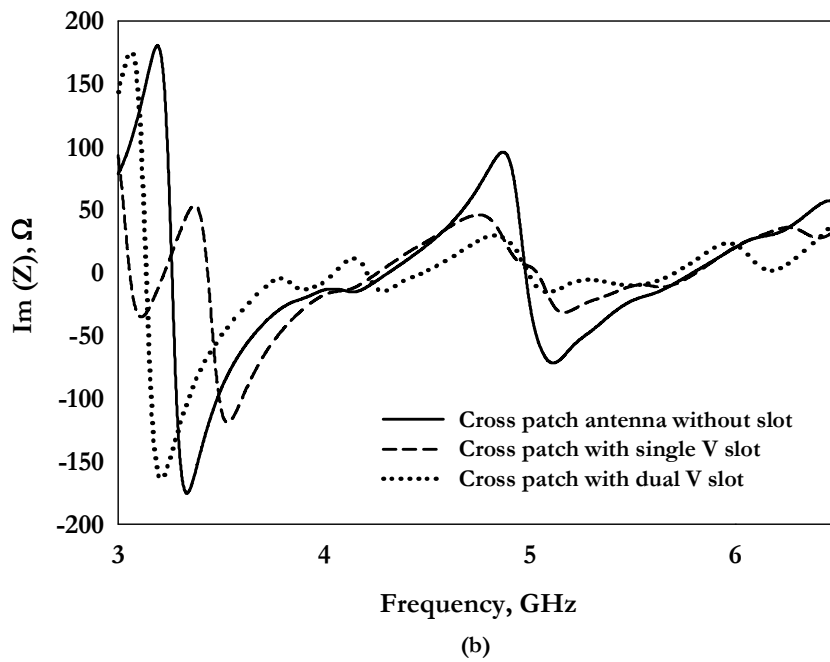
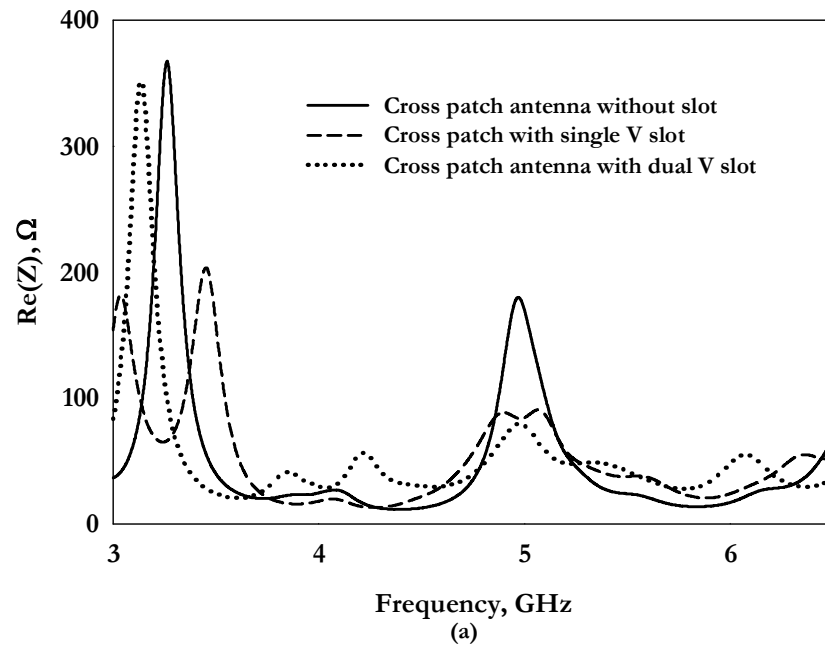


Figure B.16 Input impedance of the antenna with and without slot (a) real part and (b) imaginary part ($L=35\text{mm}$, $W=49\text{mm}$, $L_S=5.9\text{mm}$, $L_{V1}=15\text{mm}$, $L_{V2}=12\text{mm}$, $W_{V1}=10.7\text{mm}$, $W_{V2}=8.7\text{mm}$, $V_g=7\text{mm}$, $W_S=2\text{mm}$ and $\alpha=55^\circ$)

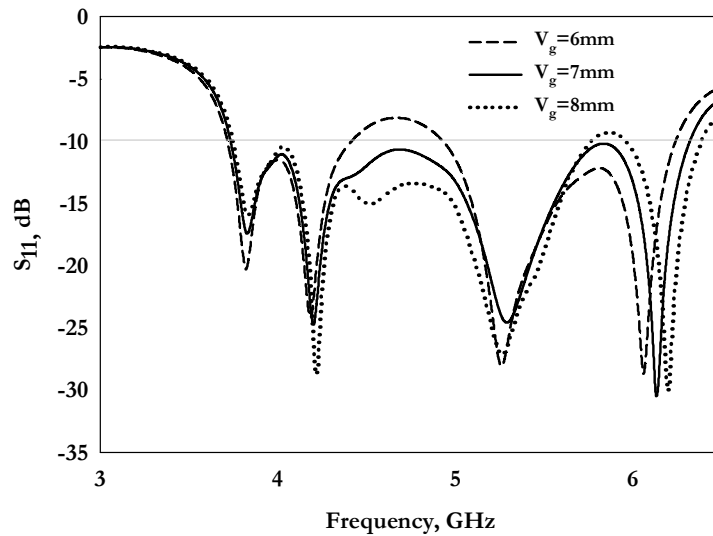


Figure B.17 Effect of V-slot gap V_g on the reflection characteristics of the antenna ($L=35\text{mm}$, $W=49\text{mm}$, $L_s=5.9\text{mm}$, $L_{V1}=15\text{mm}$, $L_{V2}=12\text{mm}$, $W_{V1}=10.7\text{mm}$, $W_{V2}=8.7\text{mm}$, $W_s=2\text{mm}$ and $\alpha=55^\circ$)

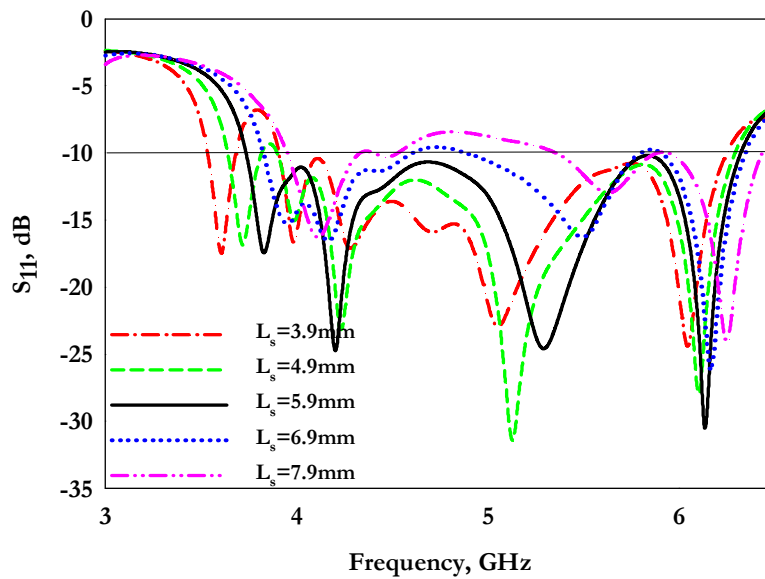


Figure B.18 Variation of reflection characteristics with corner notch dimension L_s of the antenna ($L=35\text{mm}$, $W=49\text{mm}$, $L_{V1}=15\text{mm}$, $L_{V2}=12\text{mm}$, $W_{V1}=10.7\text{mm}$, $W_{V2}=8.7\text{mm}$, $V_g=11.4\text{mm}$, $W_s=2\text{mm}$ and $\alpha=55^\circ$)

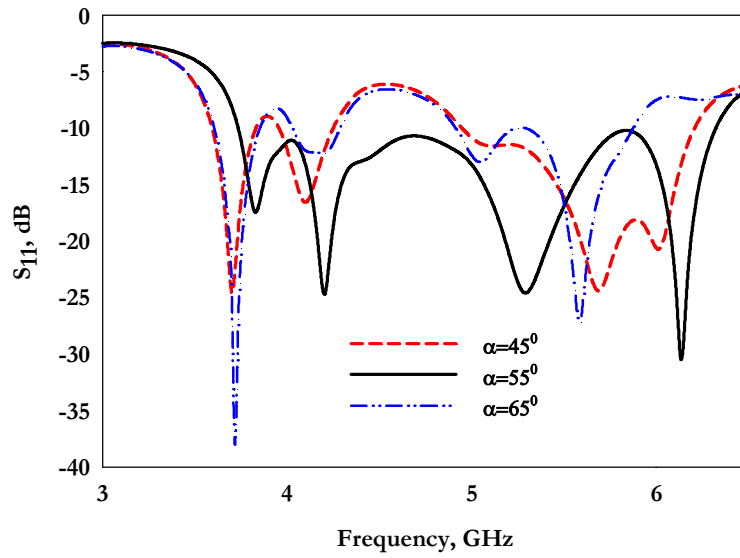
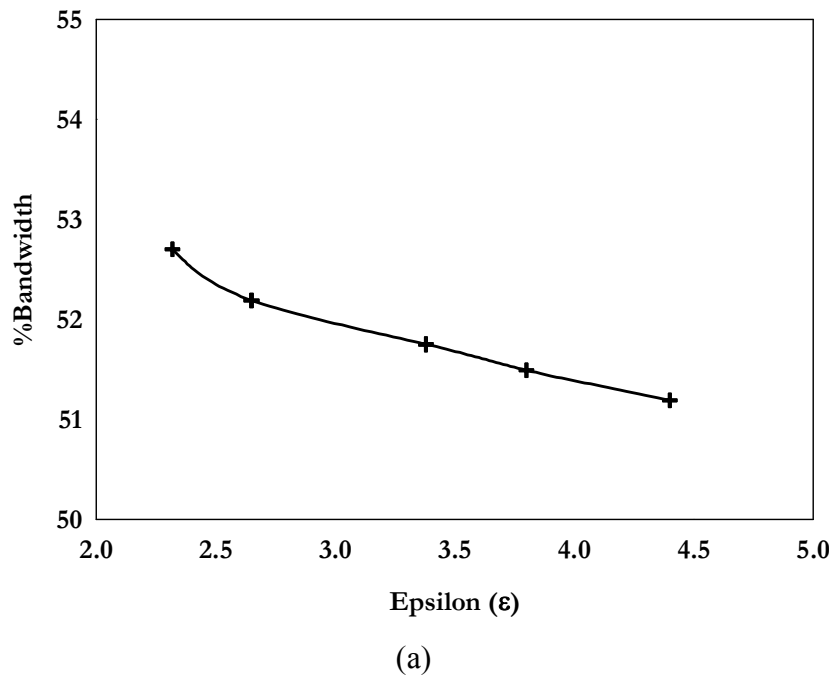


Figure B .19 Influence of tilt angle on the reflection coefficient of broadband cross patch antenna ($L=35\text{mm}$, $W=49\text{mm}$, $L_{V1}=15\text{mm}$, $L_{V2}= 12\text{mm}$, $W_{V1}=10.7\text{mm}$, $W_{V2}=8.7\text{mm}$, $V_g=11.4\text{mm}$ and $W_s=2\text{mm}$)



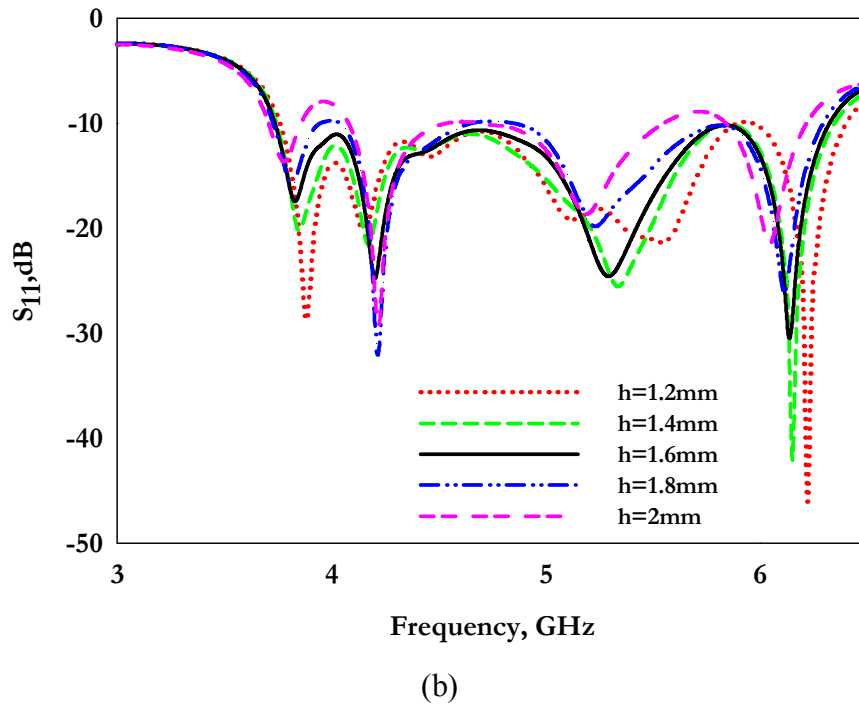


Figure B.20 Influence of substrate parameters on the reflection coefficient of the broadband cross patch antenna (a) Substrate dielectric constant (b) substrate height ($L=35\text{mm}$, $W=49\text{mm}$, $L_S=5.9\text{mm}$, $L_{V1}=15\text{mm}$, $L_{V2}=12\text{mm}$, $W_{V1}=10.7\text{mm}$, $W_{V2}=8.7\text{mm}$, $V_g=7\text{mm}$, $W_S=2\text{mm}$ and $\alpha=55^\circ$)

B.3.3 Measurements

A prototype of the antenna was fabricated on a substrate of $\epsilon_r=4.4$ with loss tangent ($\tan\delta$) of 0.02 and height $h=1.6\text{mm}$. The characteristics of the fabricated antenna have been measured using HP8510C vector network analyzer. The simulated and measured reflection coefficient of the antenna is given in figure B.21. Corresponding to the resonance around 3.82 GHz, a full-wave variation of current is noted on the top and bottom edges of the patch along the X-direction in figure B.22 (a). At 4.2GHz and 5.29GHz, three half-wave variations are observed along the sides of the patch and the edges of the slot as shown in figure B.22 (b) and (c) respectively. The resonance around

6.13GHz are due to four half-wave variations on the top and bottom edges of the patch along the X-direction. At the optimum design, these resonances are merged together to achieve the maximum bandwidth as shown in figure B.21. The small discrepancies between simulated and measured return loss characteristics of the antenna are due to the tolerance errors in antenna fabrication. From both results, the proposed antenna offers a 2:1 VSWR bandwidth of 51% from 3.75GHz to 6.33 GHz.

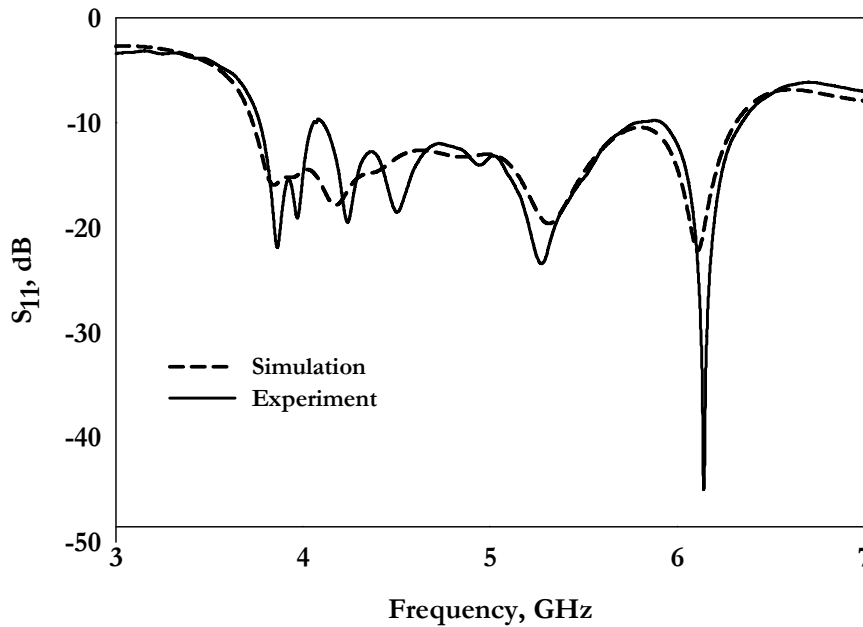


Figure B.21 Measured and simulated reflection characteristics of the antenna ($L=35\text{mm}$, $W=49\text{mm}$, $L_S=5.9\text{mm}$, $L_{V1}=15\text{mm}$, $L_{V2}=12\text{mm}$, $W_{V1}=10.7\text{mm}$, $W_{V2}=8.7\text{mm}$, $V_g=7\text{mm}$, $W_S=2\text{mm}$ and $\alpha=55^\circ$)

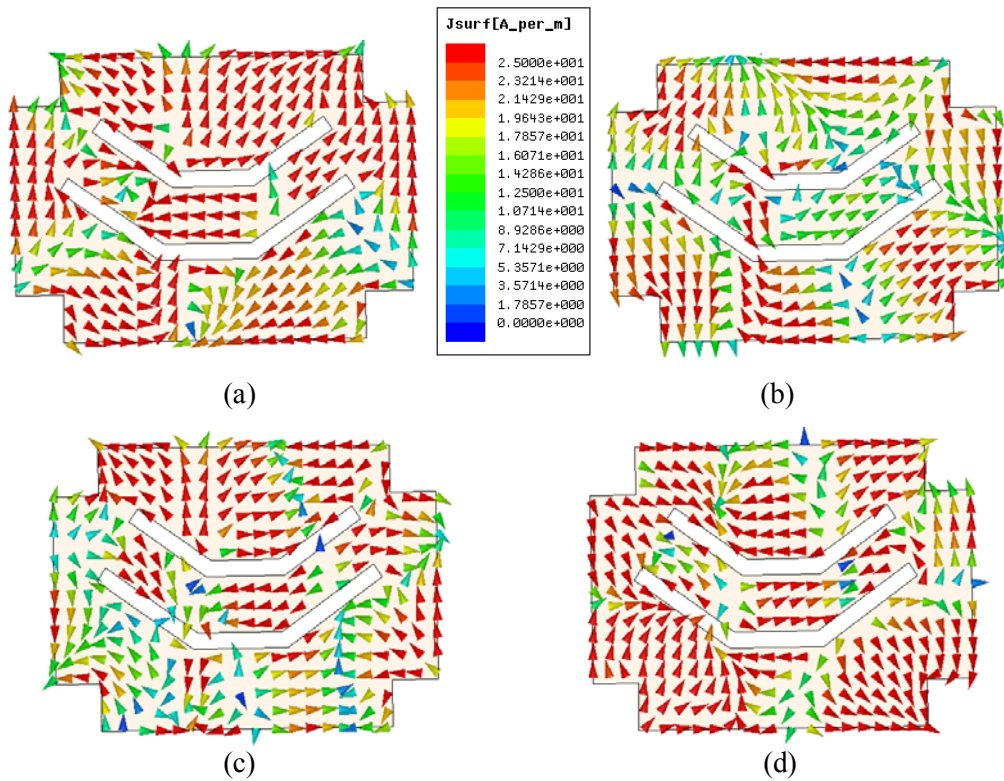


Figure B.22 Simulated surface current distribution of broadband cross patch antenna at (a) 3.82GHz (b) 4.2GHz(c) 5.29GHz and (d) 6.13GHz ($L=35\text{mm}$, $W=49\text{mm}$, $L_S=5.9\text{mm}$, $L_{V1}=15\text{mm}$, $L_{V2}=12\text{mm}$, $W_{V1}=10.7\text{mm}$, $W_{V2}=8.7\text{mm}$, $V_g=7\text{mm}$, $W_S=2\text{mm}$ and $\alpha=55^\circ$)

Figure B.23 shows the normalized YZ- and XZ-plane radiation patterns at 3.75GHz, 5GHz and 6.33 GHz respectively. The main beams of the radiation pattern are tilted similar to other wideband U or V-slotted patch antennas which also increase with frequency due to the excitation of higher order modes. The measured gain of the antenna is given in figure B.24. The designed antenna has a maximum gain of 7dBi in the mid-band region and has an average gain of 5dBi within the operating band. It can be seen that the opposing currents on either sides of the slot cause field cancellation along the on axis at the far field

giving a reduced gain at the higher frequency. The polarization of the antenna is also verified. The antenna is linearly polarized along the X – axis.

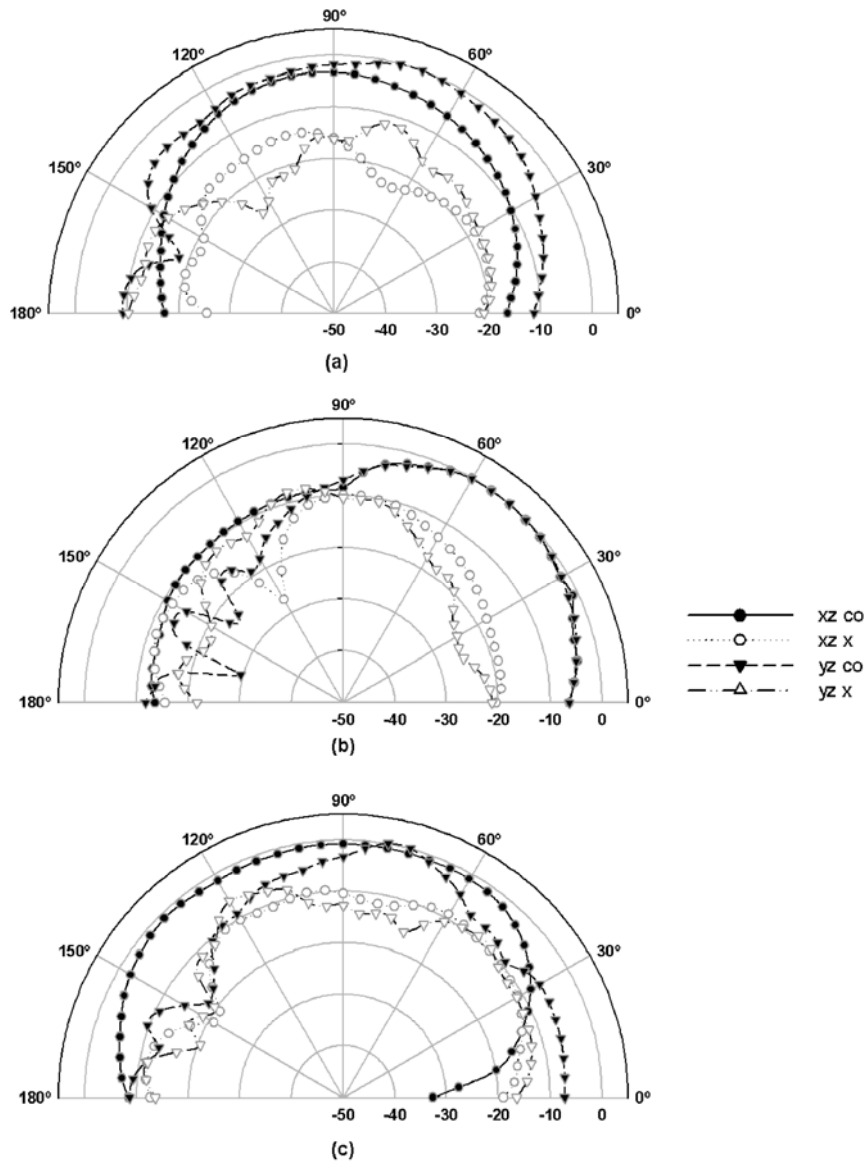


Figure B.23 Measured radiation patterns (a) at 3.75 GHz (b) at 5GHz (c) at 6.33GHz ($L=35\text{mm}$, $W=49\text{mm}$, $L_S=5.9\text{mm}$, $L_{V1}=15\text{mm}$, $L_{V2}=12\text{mm}$, $W_{V1}=10.7\text{mm}$, $W_{V2}=8.7\text{mm}$, $V_g=7\text{mm}$, $W_S=2\text{mm}$ and $\alpha=55^\circ$)

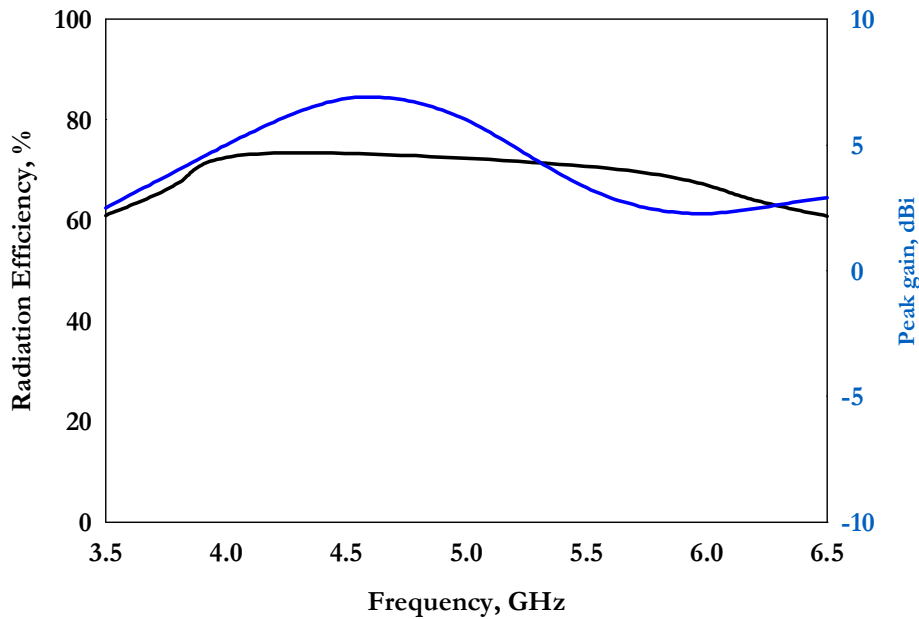


Figure B.24 Measured gain of the antenna ($L=35\text{mm}$, $W=49\text{mm}$, $L_S=5.9\text{mm}$, $L_{V1}=15\text{mm}$, $L_{V2}=12\text{mm}$, $W_{V1}=10.7\text{mm}$, $W_{V2}=8.7\text{mm}$, $V_g=7\text{mm}$, $W_S=2\text{mm}$ and $\alpha=55^\circ$)

Maximum radiation efficiency of the antenna is found to be 73% at 4.93 GHz with an average efficiency of 65%. Small antenna design is always a compromise between size, bandwidth, and efficiency. This configuration delivers broader bandwidth and acceptable gain although the efficiency of the total system will suffer due to dielectric losses.

B.3.4 Theoretical analysis of broadband microstrip antenna

Theoretical analysis of the broadband cross patch antenna is done using finite difference time domain method. Figure B.25 shows the two dimensional view of FDTD computed configuration of the broadband microstrip antenna. The measured, simulated and theoretically computed resonances plotted in figure B.26 show almost close agreement. Theoretically computed electric field distribution is illustrated in figure B.27.

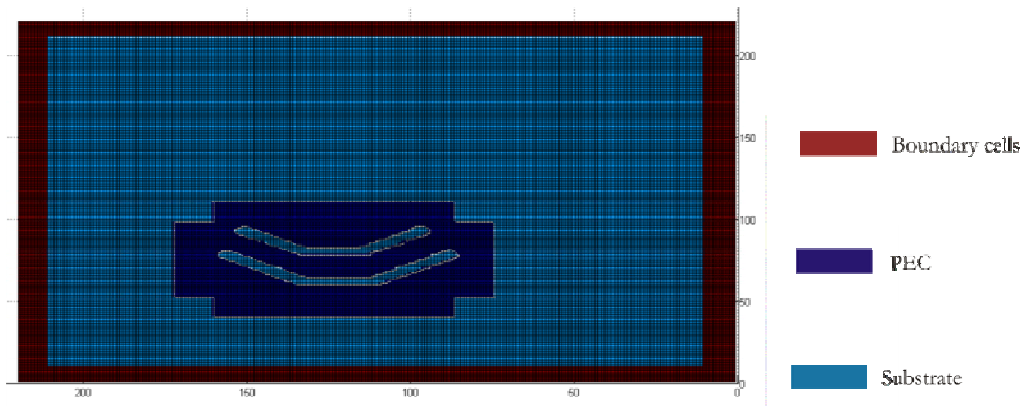


Figure B.25 2D view of the FDTD computation domain of broadband microstrip antenna ($L=35\text{mm}$, $W=49\text{mm}$, $L_S=5.9\text{mm}$, $L_{V1}=15\text{mm}$, $L_{V2}=12\text{mm}$, $W_{V1}=10.7\text{mm}$, $W_{V2}=8.7\text{mm}$, $V_g=7\text{mm}$, $W_S=2\text{mm}$ and $\alpha=55^\circ$)

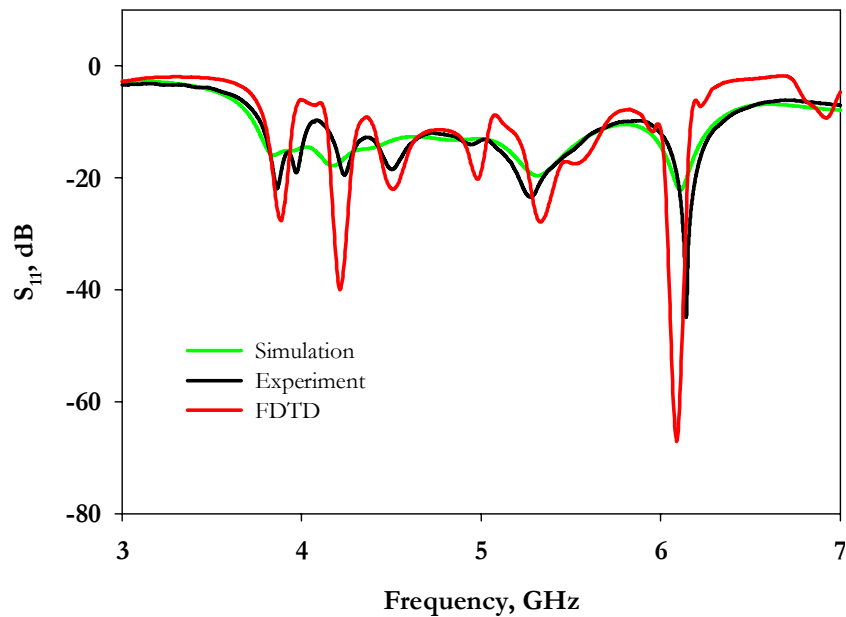


Figure B.26 Theoretical, measured and simulated reflection characteristics of broadband microstrip antenna ($L=35\text{mm}$, $W=49\text{mm}$, $L_S=5.9\text{mm}$, $L_{V1}=15\text{mm}$, $L_{V2}=12\text{mm}$, $W_{V1}=10.7\text{mm}$, $W_{V2}=8.7\text{mm}$, $V_g=7\text{mm}$, $W_S=2\text{mm}$ and $\alpha=55^\circ$)

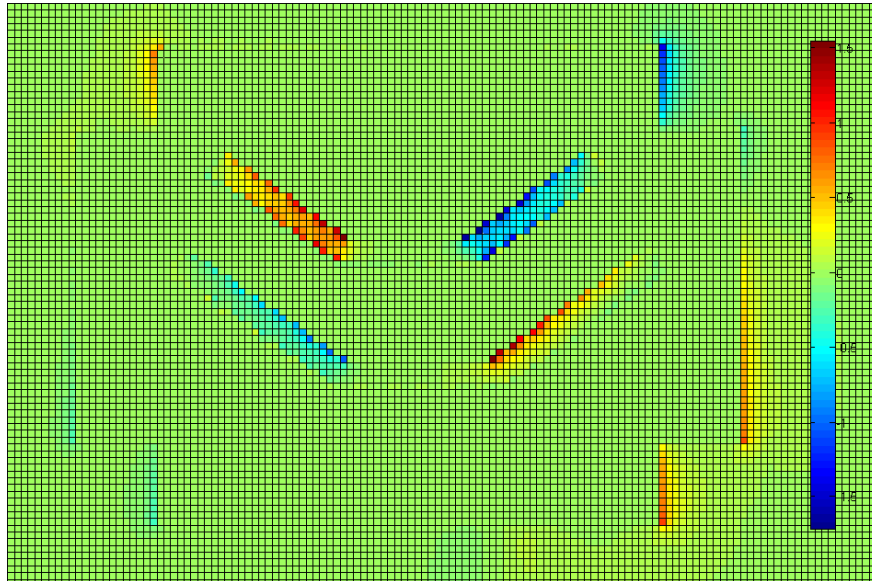


Figure B .27 FDTD computed electric field distribution of broadband microstrip antenna ($L=35\text{mm}$, $W=49\text{mm}$, $L_S=5.9\text{mm}$, $L_{V1}=15\text{mm}$, $L_{V2}=12\text{mm}$, $W_{V1}=10.7\text{mm}$, $W_{V2}=8.7\text{mm}$, $V_g=7\text{mm}$, $W_S=2\text{mm}$ and $\alpha =55^\circ$)

A cross patch antenna loaded with slots for broadband operation is proposed. The parameters affecting the antenna reflection and resonance performance are experimentally investigated and verified by simulation. The antenna is compact, occupies less volume and simple structure compared to other antenna designs.

References

1. V. Palanisamy and R. Garg, *Rectangular Ring and H-Shaped Microstrip Antennas Alternative to Rectangular Patch Antennas*, Electronics Letters, Vol. 21, No. 19, 1985, pp. 874–876.
2. W. C. Chew, *A Broadband Annular Ring Microstrip Antennas*, IEEE Trans. Antennas Propagation, Vol. AP-30, September 1982, pp. 918–922.
3. T. Huynh and K. F. Lee, *Single-Layer Single-Patch Wideband Microstrip Antenna*, Electronics Letters, Vol. 31, No. 16, 1995, pp. 1310–1312.
4. K. M. Luk, K. F. Lee, and W. L. Tam, *Circular U-Slot Patch with Dielectric Superstrate*, Electronics Letters, Vol. 33, No. 12, 1997, pp. 1001–1002.
5. K. L. Wong and Hsu W. H., *Broadband Triangular Microstrip Antenna with U-Shaped Slot*, Electronics Letters, Vol. 33, No. 25, 1997, pp. 2085–2087.
6. C. Wood, *Improved Bandwidth of Microstrip Antennas Using Parasitic Elements*, Proc. IEE, Pt. H, Vol. 127, 1980, pp. 231–234.
7. G. Kumar and K. C. Gupta, *Broadband Microstrip Antennas Using Additional Resonators Gap-Coupled to the Radiating Edges*, IEEE Trans. Antennas Propagation, Vol. AP-32, December 1984, pp. 1375–1379.
8. G. Kumar and K. C. Gupta, *Non-radiating Edges and Four Edges Gap-Coupled Multiple Resonator, Broadband Microstrip Antennas*, IEEE Trans. Antennas Propagation, Vol. AP-33, February 1985, pp. 173–178.

9. G. Kumar and K. C. Gupta, *Directly Coupled Multiple Resonator Wideband Microstrip Antennas*, IEEE Trans. Antennas Propagation, Vol. AP-33, June 1985, pp. 588–593.
10. K. P. Ray and G. Kumar, *Multi-frequency and Broadband Hybrid-Coupled Circular Microstrip Antennas*, Electronics Letters, Vol. 33, No. 6, 1997, pp. 437–438.
11. P. S. Bhatnagar et al., *Hybrid Edge Gap and Directly Coupled Triangular Microstrip Antenna*, Electronics Letters, Vol. 22, No. 16, 1986, pp. 853–855.
12. C. K. Anandan and K. G. Nair, *Compact Broadband Microstrip Antennas*, Electronics Letters, Vol. 22, No. 20, 1986, pp. 1064–1065.
13. P. S. Hall, C. Wood, and C. Garrett, *Wide Bandwidth Microstrip Antennas for Circuit Integration*, Electronics Letters, Vol. 15, July 1979, pp. 458–460.
14. A. Sabban., *A New Broadband Stacked Two-Layer Microstrip Antenna*, IEEE AP-S Int. Symp. Digest, June 1983, pp. 63–66.
15. A.H. Chen, A. Tulintseff, and R. M. Sorbello, *Broadband Two-Layer Microstrip Antenna*, IEEE AP-S Int. Symp. Digest, Vol. 2, June 1984, pp. 251–254.
16. P. S. Bhatnagar et al., *Experimental Study of Stacked Triangular Microstrip Antenna*, Electronics Letters, Vol. 22, No. 16, 1986, pp. 864–865.
17. K. Araki, K. et al., *Numerical Analysis of Circular Disc Microstrip Antennas with Parasitic Elements*, IEEE Trans. Antennas Propagation, Vol. AP-34, December 1986, pp. 1390–1394.

18. R. Q. Lee, K. F. Lee, and J. Bobinchak, *Characteristics of a Two-Layer Electromagnetically Coupled Rectangular Patch Antenna*, Electronics Letters, Vol. 23, No. 20, 1987, pp. 1070–1072.
19. J. S. Roy, *A Broadband Microstrip Antenna*, Microwave Optical Tech. Letters, Vol. 19, No. 4, 1998, pp. 307–308.
20. F. Croq, A. Papiernik, and P. Brachart, *Wideband Aperture-Coupled Microstrip Subarray*, IEEE AP-S Int. Symp. Digest, May 1990, pp. 1128–1131.
21. C. Baumer, *Analysis of Slot Coupled Circular Microstrip Patch Antennas*, Electronics Letters, Vol. 28, No. 15, 1992, pp. 1454–1455.
22. M. El Yazidi, *Analysis of Aperture-Coupled Circular Microstrip Antenna*, Electronics Letters, Vol. 29, No. 11, 1993, pp. 1021–1022.
23. K. M. Luk, K. F. Tong, and T. M. Au, *Offset Dual Patch Microstrip Antenna*, Electronics Letters, Vol. 29, No. 18, 1993, pp. 1635–1636.
24. S. D. Targonski, R. B. Waterhouse, and D. M. Pozar, *Design of Wideband Aperture Stacked Patch Microstrip Antenna*, IEEE Trans. Antennas Propagation, Vol. AP-46, No. 9, 1998, pp. 1245–1251.
25. H. G. Pues and A. R. Van De Capelle, *An Impedance Matching Technique for Increasing the Bandwidth of Microstrip Antennas*, IEEE Trans. Antennas Propagation, Vol. AP-37, No. 11, 1989, pp. 1345–1354.
26. H. G. Pues and A. R. Van De Capelle, *Wideband Impedance Matching Microstrip Resonator Antennas*, Proc. IEE 2nd Int. Conf. Antennas Propagation, Pt. 1, 1981, pp. 402–405.

27. K. S. Fong, H. F. Pues, and M. J. Withers, *Wideband Multilayer Coaxial-Fed Microstrip Antenna Element*, Electronics Letters, Vol. 21, May 1985, pp. 497–498.
28. P. S. Hall, *Multi-Octave Bandwidth Log-Periodic Microstrip Antenna Array*, IEE Proc. Microwaves, Antennas Propagation, Pt. H, Vol. 133, No. 2, April 1986, pp. 127–138.
29. R. Kakkar and G. Kumar, *Stagger Tuned Microstrip Log-Periodic Antennas*, IEEE AP-S Int. Symp. Digest, July 1996, pp. 1262–1265.
30. B. D. Popovic et al., *Broadband Quasi-Microstrip Antenna*, IEEE Trans. Antennas Propagation, Vol. AP-43, No. 10, 1995, pp. 1148–1152.
31. M. M. Gitin et al., *Broadband Characterization of Millimeter-Wave Log-Periodic Antennas by Photoconductive Sampling*, IEEE Trans. Antennas Propagation, Vol. AP-42, No. 3, 1994, pp. 335–339.
32. K. Hirasawa and M. Haneishi, *Analysis, Design, and Measurement of Small and Low-Profile Antennas*, Norwood, MA: Artech House, 1992.
33. M. Sanad, *Effect of the Shorting Posts on Short Circuit Microstrip Antennas*, IEEE AP-S Int. Symp. Digest, 1994, pp. 794–797.
34. S. Satpathy, K. P. Ray, and G. Kumar, *Compact Shorted Variations of Circular Microstrip Antennas*, Electronics Letters, Vol. 34, No. 2, 1998, pp. 137–138.
35. S. Satpathy, G. Kumar, and K. P. Ray, *Compact Shorted Variations of Triangular Microstrip Antennas*, Electronics Letters, Vol. 34, No. 8, 1998, pp. 709–711.
36. R. Waterhouse, *Small Microstrip Patch Antenna*, Electronics Letters, Vol. 31, No. 8, 1995, pp. 604–605.

37. K. L. Wong and S. C. Pan, *Compact Triangular Microstrip Antenna*, Electronics Letters, Vol. 33, No. 6, 1997, pp. 433–434.
38. S. Satpathy, K. P. Ray, and G. Kumar, *Compact Microstrip Antennas Using a Single Post*, Proc. NSAML, New Delhi, India, March 1998, pp. 69–72.
39. K. P. Ray and G. Kumar, *Wideband Gap-Coupled Compact Sectoral Microstrip Antennas*, Proc. ISAP–2000, August 2000.
40. K. P. Ray and G. Kumar, *Compact Gap-Coupled Shorted 90° Sectoral Microstrip Antennas for Broadband and Dual Band Operations*, Microwave Optical Tech. Letters, Vol. 26, No. 3, 2000, pp. 143–145.
41. R. B. Waterhouse, *Broadband Stacked Shorted Patch*, Electronics Letters, Vol. 35, No. 2, 1999, pp. 98–99.
42. M. Du. Plessis and J. H. Cloete, *Tuning Stub for Microstrip Patch Antenna*, IEEE AP-S Int. Symp. Digest, June 1993, pp. 964–967.
43. K. P. Ray and G. Kumar, *Tunable and Dual-Band Circular Microstrip Antenna with Stubs*, IEEE Trans. Antennas Propagation, Vol. 48, July 2000, pp. 1036–1039.
44. P. Bhartia and I. J. Bahl, *A Frequency Agile Microstrip Antenna*, IEEE AP-S Int. Symp. Digest, May 1982, pp. 304–307.



LIST OF PUBLICATIONS

1. **Nishamol M S**, Sarin V P , G ijo Augustine, D eepu V, C K Aa nandan, P Mohanan a nd K Vasudevan “ Compact du al f requency dual p olarized cross patch antenna with an X-slot”, Microwave and optical technology letters, vol. 50, No.12, pp. 3198-3201, December 2008.
2. **Nishamol M S**, Sarin V P , T ony D , C K Aa nandan, P M ohanan a nd K Vasudevan “ Broadband p rinted V- s lotted c ross p atch a ntenna f or IEEE802.11a/WiMAX/HiperLAN2 applications”, Progress In Electromagnetic Research Letters, Vol. 19, pp. 155-161, 2010.
3. **Nishamol M S**, Sarin V P , T ony D , C K Aa nandan, P M ohanan a nd K Vasudevan “ Design of F requency a nd P olarization T unable M icrostrip Antenna” Microwave Review, vol.16, No.2, pp.22-28, December 2010.
4. **Nishamol M S**, Sarin V P , Tony D , C K Aa nandan, P M ohanan a nd K Vasudevan “Design of a circularly polarized r ectangular microstrip a ntenna for GPS applications” Microwave and optical technology letters, vol. 53, No.2, pp.468-470, February 2011.
5. **Nishamol M S**, Sarin V P , Tony D , C K Aa nandan, P M ohanan a nd K Vasudevan “ An E lectronically R econfigurable M icrostrip Ant enna wit h Switchable Slots for Polarization Diversity” IEEE Transactions on Antennas and Propagation, Vol.59, No.9, pp.3424-3427, September 2011.
6. **Nishamol M S** , Sarin V P , T ony D , C K Aa nandan, P M ohanan a nd K Vasudevan “ Varactor C ontrolled F requency a nd P olarization R econfigurable

List of Publications

- Microstrip Antenna” RF and microwave computer-aided engineering, Vol.21, pp.680-686, November 2011.
7. Sarin V P, **Nishamol M S**, Tony D, C K Aanandan, P Mohanan and K Vasudevan “ A broadband L -strip fed printed microstrip antenna” *IEEE Transactions on Antennas and Propagation*, Vol.59, No .1, pp. 281-284, January 2011.
 8. Sarin V P, **Nishamol M S**, Tony D, C K Aanandan, P Mohanan and K Vasudevan “A Wideband stacked offset microstrip antenna with improved gain and low cross polarization” *IEEE Transactions on Antennas and Propagation* Vol.59, No.4, pp.1376-1379, April 2011.
 9. Sarin V P, **Nishamol M S**, Deepu V, C K Aanandan, P Mohanan and K Vasudevan “ Wideband printed microstrip antenna for wireless communications” *IEEE Antennas and Wireless Propagation Letters*, Vol.8, pp.779-781, 2009.
 10. Sarin V P, **Nishamol M S**, Gijo Augustine, C K Aanandan, P Mohanan and K Vasudevan “ An Electromagnetically coupled dual band dual polarized microstrip antenna for WLAN applications”, *Microwave and optical technology letters*, Vol. 50, No.7, pp. 1867-1870, July 2008.
 11. Tony D, Sarin V P, **Nishamol M S**, C K Aanandan, P Mohanan and K Vasudevan “ CPW fed slotted planar antenna for wireless communications ” *Microwave and optical technology letters*, Vol .53, No.11, pp. 2501-2504, November 2011.
 12. **Nishamol M S**, C K Aanandan, P Mohanan and K Vasudevan, “ dual frequency reconfigurable microstrip antenna using varactor diodes” 30th URSI General assembly and symposium (URSI G ASS), August 2011, Istanbul, Turkey.

13. **Nishamol M S**, Sarin V P, Tony D, P Mohanan, C K Aanandan and K Vasudevan “Frequency and polarization tuning of a cross patch antenna using capacitive loading” International conference on Communications and signal processing (ICCSP 2011), February 2011, NIT, Calicut, Kerala, India.
14. **Nishamol M S**, Sarin V P, Tony D, P Mohanan, C K Aanandan and K Vasudevan “ Broadband printed cross-shaped microstrip antenna for multifunctional wireless applications” 4th European conference on Antennas and propagation (EuCAP 2010) April 2010, Barcelona, Spain.
15. **Nishamol M S**, Sarin V P, Tony D, P Mohanan, C K Aanandan and K Vasudevan, “Single feed circularly polarized cross patch antenna” IEEE Applied Electromagnetics Conference(AEMC-2009), December 2009, Kolkata, India.
16. **Nishamol M S**, Sarin V P, P Mohanan, C K Aanandan and K Vasudevan “ Single feed miniaturized cross patch antenna” International conference on Recent advances in microwave theory and applications (Microwave 2008) , November 2008,Jaipur, Rajasthan.
17. Sarin V P, **Nishamol M S**, Tony D, P Mohanan, C K Aanandan and K Vasudevan, “ Strip loaded slotted patch antenna for wireless applications” IEEE Applied Electromagnetics Conference(AEMC-2009), December 2009, Kolkata, India.
18. Sarin V P, **Nishamol M S**, Gijo Augustine, P Mohanan, C K Aanandan and K Vasudevan, “ A Dual band dual polarized electromagnetically coupled microstrip antenna for WLAN 5.2/5.8GHz applications” IEEE Antennas and Propagation society International Symposium(APS-2008), San Diego, USA.
19. Gijo Augustine, Bybi P C, Sarin V P, **Nishamol M S**, P Mohanan, C K Aanandan and K Vasudevan, “ Compact dual band antenna for handheld

- wireless communication gadgets” IEEE Antennas and Propagation society International Symposium(APS-2008), San Diego, USA.
20. Gijo Augustine, Bybi P C, Sarin V P, **Nishamol M S**, P Mohanan, C K Aanandan and K Vasudevan, “compact dual band planar antenna for IMT-2000 application” International conference on microwave antenna propagation and remote sensing (ICMARS-2008).
 21. Gijo Augustine, Bybi P C, Sarin V P, **Nishamol M S**, P Mohanan, C K Aanandan and K Vasudevan, “A compact dual band planar antenna for IMT-2000 and WLAN applications” Proceedings of IEEE Applied Electromagnetic conference, December 2007, Kolkata, India.
 22. **Nishamol M S**, Sarin V P, Deepu V, Sujith R, P Mohanan, C K Aanandan and K Vasudevan ‘Cross patch antenna with an X slot for polarization switching’ National symposium on Antennas and Propagation(APSYM 2008) , 29- 31 December 2008,CUSAT, KERALA, INDIA.
 23. Sarin V P, **Nishamol M S**, Tony D , Sreejith M . Nair, P Mohanan, C K Aanandan and K Vasudevan, ‘A Broadband microstrip antenna for wireless applications’ National Conference on Electronics, February 2011, BPC College, Piravom, Kerala
 24. Sarin V P, **Nishamol M S** , Deepu V, Sujith R, P Mohanan, C K Aanandan and K Vasudevan, ‘Broadband microstrip antenna for wireless applications’ National symposium on Antennas and Propagation(APSYM 2008) , 29- 31 December 2008,CUSAT, KERALA, INDIA.
 25. Tony D , Sarin V P, **Nishamol M S**, P Mohanan, C K Aanandan and K Vasudevan ‘CPW fed slotted planar antenna for WLAN applications” National symposium on Antennas and Propagation(APSYM 2010), 14- 16 December 2010,CUSAT, KERALA, INDIA.

RESUME

M. S. NISHAMOL

Senior Research Scholar
Department of Electronics
Cochin University of Science and Technology
Cochin-22, Kerala, India.
E-mail: nishanassar@gmail.com

Objective:

To be a part of an organization to pursue research activities in the field of Electromagnetics and antennas and to do something that is innovative and beneficial to mankind.

Education:

M.Sc Electronics Science (2001)

Specialization: Microwave Electronics

Cochin University of Science and Technology, Cochin, India.

Awards and Honours received:

- Student author award in IEEE Applied Electromagnetics Conference (AEMC), 14-16 December 2009, Kolkata, India.
- Research Fellowship Scheme for Meritorious Students (RFSMS) by University Grants Commission (UGC) Government of India from 2008 to till date.
- Awarded second rank in the M. Sc. Program in Cochin University of Science and Technology, Cochin, India in the year 2001.

EXPERIENCE

Research

- Project Fellow in the UGC sponsored Project entitled 'Development of electronically reconfigurable microstrip antennas for mobile and satellite communication systems', at the Department of Electronics, Cochin University of Science and Technology, Cochin, India from April 2007 to April 2008.
- Research scholar with the center for Research in Electro-Magnetics and Antennas (CREMA), Department of Electronics, Cochin University of Science and Technology, Cochin, India from May 2008 to September 2011.

Teaching

- Lecturer in Electronics, M. E. S. College, Marampally, Aluva, Kerala, India (October 2002 – March 2007).
- Assistant Professor, Department of Electronics, Government College, Chittur, Palakkad, Kerala, India (October 2011 onwards).

Publications:

International Journal	: 11
International Conference	: 09
National Conference	: 04
Citation in international journal	: 02

Scientific meetings attended:

Month (Year)	Organising Body	Title and Purpose of Events
August 2011	International Union of Radio Science(URSI)	URSIGASS-2011, Istanbul, Turkey. To receive young scientist Award and to present a research paper.
February 2011	National Institute of Technology, CALICUT, Kerala	ICCSP 2011- To present a research paper
March, 2011	University Grants Commission(UGC) and Cochin University of Science and Technology	National Seminar on Frontier Technologies in RF Engineering. As a Participant
December 2010	Department of Electronics, Cochin University of Science and Technology	Antennas and Propagation Symposium -2010 Organizing committee member
December 2009	AP-MTT Joint Chapter IEEE Calcutta section in association with the Institute of Radio Physics and Electronics, University of Calcutta and Webel, India.	Applied Electromagnetic Conference -09 (AEMC-09) To present a research paper
November 2009	Department of Electronics, Cochin University of Science and Technology	International conference on Ocean Electronics- SYMPOL-09 Organizing committee member
December 2008	Department of Electronics, Cochin University of Science and Technology	Antennas and Propagation Symposium -2008 Organizing committee member and Presented a research paper

Citation

- a) **Nishamol M S**, Sarin V P, Tony D, C K Aanandan, P Mohanan and K Vasudevan "Broadband printed V-slotted cross patch antenna for IEEE802.11a/WiMAX/HiperLAN2 applications", Progress In Electromagnetic Research Letters, Vol. 19, pp. 155-161, 2010.
1. H. H. Wang, K. Yang, Z. Y. Lei and C. L. Li, "Broadband microstrip antennas using coplanar feed line", Progress In Electromagnetic Research Letters, Vol. 20, pp. 129-136, 2011.
 2. V. G. Kasabegoudar, "Low profile suspended microstrip antennas for wideband applications", Journal of Electromagnetic Waves and Applications, Vol.25, pp. 1795-1806, 2011.

INDEX

A

Analysis of antennas, 1, 15
Aperture coupling, 10, 14, 43
Array,
40,41,44,45,47,48,49,53,83,105,
196,206,207

B

Broadside,10,
41,44,47,48,110,119,123,141,153,163
,200,208,209,219,223

C

Cavity model, 15,17,18,42
Cellular phones, 3,29
Circular polarization, 6, 22,
26,30,42,49, 114,123,125, 126,127,
138, 167, 168, 200,202, 228,232
Coaxial probe, 10,43
Coplanar waveguide feed, 14, 43,
54,72
Cross-polar radiation, 9
Current distribution, 50, 57, 87, 88,
90, 91, 97, 117, 118, 119, 120, 127,
132, 134, 136, 144, 186, 198, 262

D

Dielectric substrate, 5, 6, 7, 8, 11, 12,
13, 15, 17, 40, 130, 240
Dielectric/lens antennas, 3
Dipole, 8, 9, 10, 50, 76
Dual-frequency, 23, 24, 37, 46, 55, 64,
198, 201

E

Effective dielectric constant, 5, 28, 98
Efficiency, 6, 7, 40, 48, 49, 58, 64,
125,129, 130

Electromagnetic field, 2, 10, 17, 57,
195, 253

F

FDTD, 15, 19, 32, 46, 48, 221, 230,
231, 250
Feeding Techniques, 10, 16, 31
Finite-element method, 18, 19, 56
Fourier transform, 19, 20
Free-space wavelength, 5, 214
Frequency-independent antennas, 3
Fringing fields, 4, 5, 16, 17, 18, 98

G

Global positioning system (GPS), 48
Global system for mobile
communication (GSM), 8, 29, 46
Green's function, 17, 175

H

Helical antennas, 3
HFSS, 31, 57, 91, 98, 115, 157, 208,
214
Homogeneous boundary condition, 19

I

Impedance matching, 11, 16, 45, 63,
83, 91, 94, 108, 125, 133, 159, 200,
212, 243, 256

L

Length-to-width ratio, 9
Linear polarization, 26, 200, 201, 206
Log periodic antennas, 3

M

Maxwell, 2, 46, 170, 171, 173, 174
Meandering, 21
Mechanical tuning, 26, 27, 127, 130,
168

Method of moments, 15, 18
Microstrip antennas, 40, 59, 84, 114, 130, 157, 176, 222, 241
Microstrip line, 12, 43, 59, 131, 147, 149, 178, 182, 193, 202, 231
Microwave integrated circuit (MIC), 7
Mobile communication, 4, 8, 23, 43, 46, 205
Multiport Network Model, 15, 17
Mur, 176, 252

N

Numerical dispersion, 174
Numerical techniques, 18, 20

O

Orthogonal polarization, 21, 24, 46, 91, 94, 104, 115

P

Photolithographic technology, 5
PIN diodes, 27, 84, 106, 110, 115, 119, 127, 187, 200
Planar antennas, 4, 43, 44
Polarization, 206, 208, 219, 232, 250
Propagation, 16
Proximity coupling, 10, 59

Q

quality factor, 7, 22, 43, 149

R

Radar systems, 1, 3
RF-MEMS, 27
Reconfigurable antennas, 199, 202
Reconfiguration mechanisms, 27
Reflector antennas, 3

Resistive source model, 190

Return loss, 65, 68, 119, 180

S

Satellite communication, 6, 8, 29, 113
Slot antennas, 7, 8, 9, 25, 40
SMA connector, 12
Spectral domain technique, 15, 19
Standing waves, 10
Switches, 26, 56, 82, 83, 84, 105, 116, 127, 148

T

TE mode, 9
Transmission line model, 15, 16
THRU calibration, 66, 68
TM₁₀ mode, 5, 91, 117, 118, 125, 133, 139, 151, 159, 161, 182, 185
Travelling-wave antennas, 8, 9

V

Varactor diode, 32, 52, 129, 130, 146, 148, 149, 151, 156, 157
Variable reactive loading, 27
VNA, 61, 65
VSWR, 43, 64, 65

W

Wireless communication, 3, 29, 49
WLAN, 44

Y

Yee, 171, 178, 182
YIG, 61